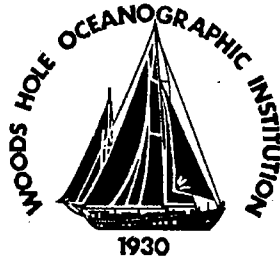# Woods Hole
Oceanographic
Institution

1930

Double Diffusion in Oceanography:
Proceedings of a Meeting
September 26-29, 1989

compiled by

Raymond W. Schmitt

July 1991

Technical Report

Double Diffusion in Oceanography: Proceedings of a Meeting
September 26-29, 1989

compiled by

Raymond W. Schmitt

Woods Hole Oceanographic Institution
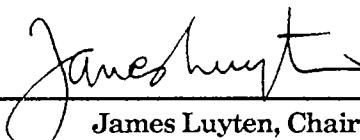Woods Hole, Massachusetts 02543

July 1991

Technical Report

Approved for Distribution:

James Luyten, Chairman
Department of Physical Oceanography

Abstract

A meeting to review research progress on double-diffusive phenomena in the ocean was held September 26–29, 1989, at the Woods Hole Oceanographic Institution. Twenty-five oral presentations were made and a number of discussion session were held. This report contains manuscripts provided by meeting participants, summaries of the discussion sessions and an extensive bibliography on oceanic double-diffusion. Since double-diffusive processes appear to play an important role in ocean mixing, further research in this field should have high priority. It is hoped that this update on the status of our current understanding will facilitate planning of additional research.

Table of Contents

Forward

This report provides a summary of a meeting held in Woods Hole in late September, 1989, that focussed on the topic of Double Diffusion in Oceanography. This is a field which has seen rapid progress and growth in the past decade and which seems poised for significantly more progress in the nineties. The report consists of papers submitted by meeting speakers in "camera ready" form, reports on discussion sessions which identify areas ripe for future work, and a bibliography on ocean double diffusion.

The meeting was motivated by a number of factors. These include:

1. A markedly improved data base on ocean double diffusion resulting from recent field programs in tropical and high latitude regions which has advanced understanding of the phenomena.

2. Emerging evidence which indicates that double diffusion is an important ocean mixing mechanism, clearly dominant in some regions and significant in much of the main thermocline of the subtropical gyre.

3. A perceived need to promote interactions among observationalists, experimentalists, theoreticians and modelers.

4. The significant growth in the field as reflected in the volume of literature on the topic (Figure 1).

5. The obvious needs for: more quantitative laboratory experiments, additional numerical modeling, new observational tools, well-designed, process-oriented field programs and development of double diffusive parameterizations for application to large scale models.

6. Finally, it was felt that the identification of major problems and possible solution paths would help to foster future progress.

The meeting was open to all interested parties and was promoted by letters of invitation and announcements on electronic mail and in *EOS*, the Transactions of the American Geophysical Union. There were 25 prepared talks and 4 discussion sessions. Several films and videos were shown of laboratory and model results. Social functions consisting of a reception hosted by WHOI Director Dr. Craig Dorman at Meteor House and a New England Clam Bake at Fenno House were well attended.

An additional feature of this report is the bibliography on double diffusion. It was compiled from bibliographies by Janice Boyd, Nick Fofonoff, and Jiro Yoshida and was augmented by contributions from a number of others. Its purpose is to bring together in one place all the references on double diffusion which have particular oceanographic relevance. In addition, a small number of references on other aspects of ocean mixing or double diffusion in other media are included to provide connection to a broader range of literature. An attempt was made to be all inclusive with respect to oceanographic double diffusion; the choices of related papers were subjective. References for the last two or three years are probably less complete than earlier years. Hopefully, the compilation will simplify the work of students and researchers of ocean mixing.

The bibliography also serves an additional purpose; it illustrates the dramatic growth in this area of research in the past several decades. If the double diffusive references alone are summed in five year groups, the change from one or two papers/year to nearly 20 papers/year from the '60s to the '80s is readily seen (Figure 1). If references from the double diffusive literature in geology, astrophysics and materials science had been included, the growth would be even more dramatic, especially in the last decade. This growth has occurred mostly by the efforts of individual investigators. It is felt that there now exists sufficient "critical mass" to warrant more coordinated and systematic research programs. Some ideas for the focus of such efforts are given in the discussion session summaries on Salt Fingers, Diffusive Convection and Thermohaline Intrusions.

Acknowledgments
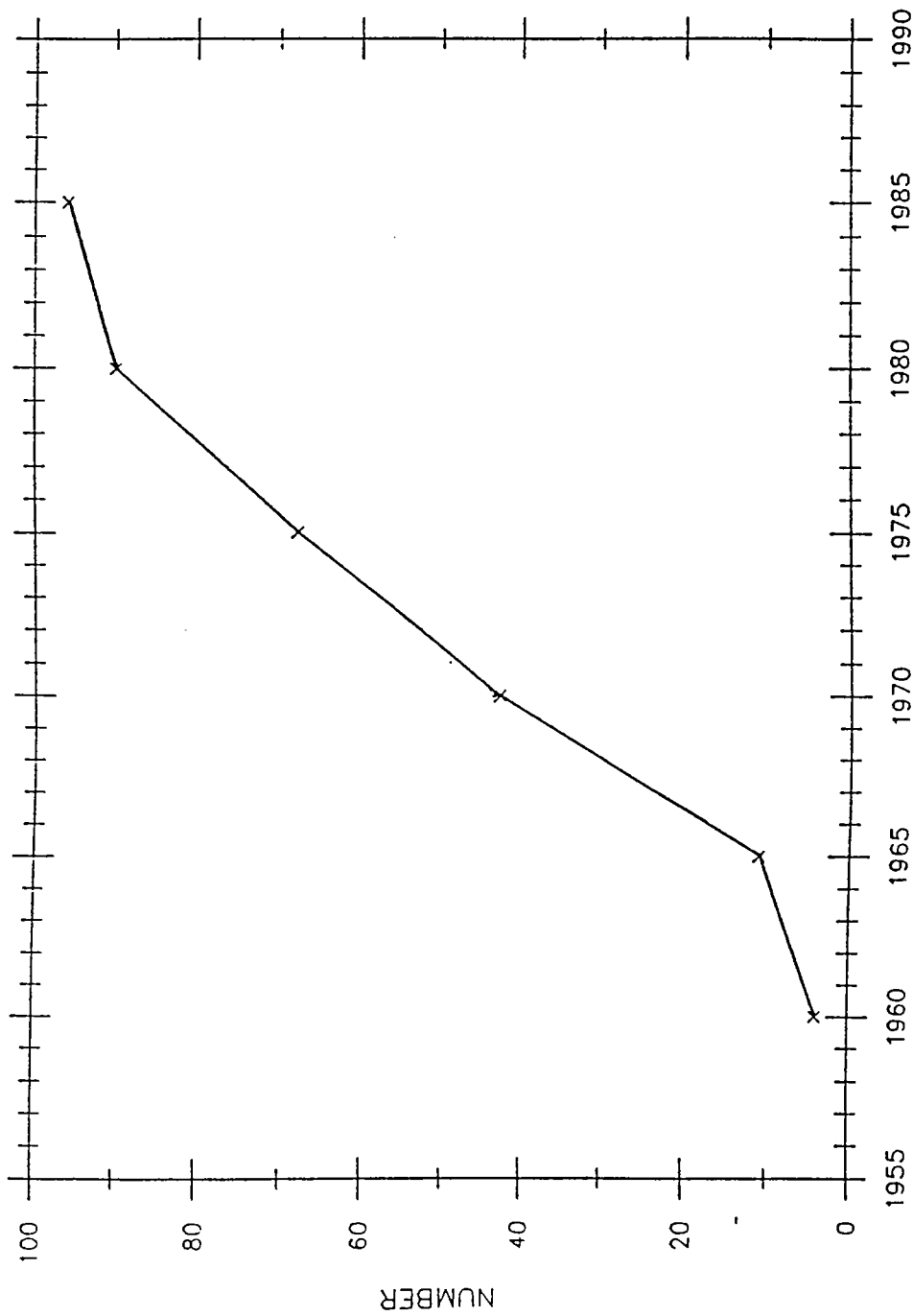
Figure 1: Numbers of papers on oceanic double-diffusion published in five-year intervals. Each point represents a sum over the previous five-years of a selected subset of publications from the bibliography.

DOUBLE DIFFUSION IN OCEANOGRAPHY

Woods Hole Oceanographic Institution
Woods Hole, MA
September 26-29, 1989

A meeting to survey recent progress in understanding double-diffusive mixing in the ocean and to identify areas where future work might profitably focus.

Schedule:
Monday, September 25: Meteor House

  6:00 pm   Reception with the Director

Tuesday, September 26: Redfield Auditorium

  8:30 am   Welcome

Science Session 1, Salt Fingers: Results from C-SALT
Moderator: Trevor McDougall

  9:00   Ray Schmitt, WHOI
          "Overview of C-SALT"

  9:45   Mike Gregg and Tom Sanford, Univ. of Washington
          "Some observational puzzles about double-diffusion"

  10:30   Coffee Break

  10:45   Marc Fleury, Chesapeake Bay Institute
          "Horizontal variation of dissipation and characteristics of a single interface"

  11:30   Rolf Lueck, Chesapeake Bay Institute
          "Vertical coherence of horizontal temperature gradients"

  12:15   Lunch

Science Session 2, Salt Fingers: Models
Moderator: Barry Ruddick

1:30 pm   Eric Kunze, Univ. of Washington
             "Behavior of salt fingers in shear"

2:15   Colin Shen, Naval Research Laboratory
             "An overview of numerical salt finger experiments"

3:00   Break

3:15   George Veronis, Yale University
             "Inversion of C-SALT data"

4:00   Trevor McDougall, CSIRO, Tasmania
             "Interpretation of C-SALT layers"

Wednesday, September 27: Redfield Auditorium
Science Session 3, Salt Fingers: Other Observations
Moderator: Eric Kunze

8:30am   Tom Osborn, Chesapeake Bay Institute
             "The Salt Fountain"

9:15   Steve Mack and Howard Schoeberlien, Applied
             Physics Lab
             "Observation of salt fingering from a towed
             conductivity array"

10:00   Break

10:15   James Hamilton and Neil Oakey, Bedford Institute of
             Oceanography
             "Double-diffusion and turbulence in the Canary
             Basin"

11:00   Dave Hebert, Oregon State Univ.
             "Salt finger fluxes in a Meddy"

11:45   John Taylor, Univ. of Western Australia
             "The growth of salt fingers after disruption
             by turbulence

12:30   Lunch

Science Session 4, Diffusive Convection
Moderator: Barry Ruddick

1:30 pm   Harindra J. Fernando, Arizona State University
"Laboratory experiments on mixing across double-diffusive interfaces"

2:15   Ruby Krishnamurti, Florida State University
"Laboratory experimental studies on subcritical double-diffusive convection"

3:00   Break

3:15   Laurie Padman, Oregon State University
"Arctic double-diffusive steps"

4:00   Ray Schmitt, W.H.O.I.
"Mean shear and the density ratio in the Central Water"

Thursday, September 28: Redfield Auditorium
Science Session 5, Thermohaline Intrusions
Moderator: Ray Schmitt

8:30am   Barry Ruddick, Dalhousie University
"Thermohaline Intrusions"

9:15   Jiro Yoshida, Tokyo University
"The behavior of double-diffusively induced secondary currents"

10:00   Hideki Nagashima, Institute of Physical and Chemical Research, Japan
"Numerical models of double-diffusive density currents"

10:15   Break

10:30   Ellen Thomas, Stanford University
"Intrusions into a thermohaline stratification I: Experiments"

11:15   Jeff Koseff, Stanford University
        "Intrusions into a thermohaline stratification II:
        numerical simulations"

12:00   Lunch

Open period

5:30 pm   New England Clam Bake, Fenno House, Quisset Campus

Friday, September 29: Redfield Auditorium
Discussion Session 1: Prospects for Future Work:
What are the primary areas where additional observations, analysis,
laboratory experimentation, numerical modelling, or technical
developments can advance our understanding of double diffusion in the ocean?

8:30 am   Salt fingers
          Moderator: R. Schmitt

9:30   Break

9:45   Diffusive Convection
          Moderator: B. Ruddick

10:45   Thermohaline Intrusions
          Moderator: T. McDougall

11:45   Lunch

Discussion Session 2: A mixing experiment in the Central Water

1:15 pm   Jim Ledwell, Lamont-Doherty Geo. Observatory
          "NATRE: The North Atlantic Tracer Release
          Experiment"

2:00   Open discussion, with contributions from:
          M. Gregg, E. Kunze, R. Lueck, N. Oakey,
          B. Ruddick, R. Schmitt, A. Williams
          and Others.

4:00   Close of Meeting

Overview of C-SALT

R. W. Schmitt
Woods Hole Oceanographic Institution
Woods Hole, MA 02543

Abstract

The Caribbean Sheets And Layers Transects (C-SALT) field program was organized to survey the prominent thermohaline staircases found in the western tropical North Atlantic. In addition to two hydrographic occupations of the step region there were large area AXBT surveys, a current meter mooring and intensive microstructure measurements. One striking result of the survey work was a very large horizontal coherence length to the layers and systematic trends in the temperature and salinity of individual layers. The spatial trends in T-S are quite similar to the temporal trends observed in laboratory salt finger experiments, where salt is transported at a greater rate than heat. The numerical value of the heat/salt flux ratio is slightly larger than expected from salt fingers alone. Several mechanisms are considered to explain this; all of them require significant salt fingering. The actual rates of mixing are difficult to establish from the large scale surveys because of eddy variability, but the microstructure measurements suggest a vertical salt diffusivity of order 10^{-4} m^2/s. This indicates that the C-SALT region is a "hot spot" for vertical transport in the thermocline.

1. Introduction

The C-SALT field program was carried out in the spring and fall of 1985 in the tropical North Atlantic east of Barbados. An extensive thermohaline staircase consisting of approximately 10 well mixed layers between 150-600 m depth was found. The layers were 5-40 m thick; high gradient interfaces between them were 0.5-5 m thick. Temperature contrasts of order 0.5 to 1. °C existed across the interfaces (Figure 1). The layers were found over an area of about 1 million square kilometers and some layers appeared to be traceable for 3-400 kilometers. Temperature data from the current meter mooring indicated that the layers were present continuously from March
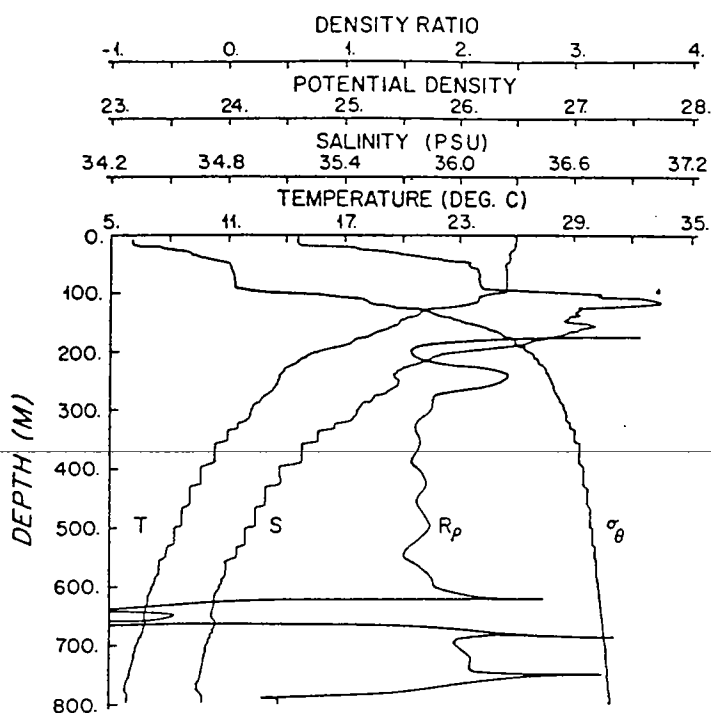
Figure 1. A thermohaline staircase from Station 49 during the spring cruise from the C-SALT survey area. Profiles of temperature, salinity, potential density (σ_θ) and density ratio (R_ρ) are shown. The density ratio was computed using least squares fits over a sliding 40 m vertical interval. The layers only appear when the density ratio is less than 1.7.

through November 1985. The currents were weak and variable within the steps (350–450 m) and in the core of the underlying Antarctic Intermediate Water (850 m) where current meters were deployed. A project overview is given in Schmitt (1987) and various results are presented in the October 1987 issue of *Deep Sea Research*, 34 and in Boyd (1989); Kunze (1987); Marmorino (1989); Schmitt (1988) etc,.

One of the most interesting results of the C-SALT hydrographic surveys was the discovery that the layers displayed distinct patterns on a T-S diagram (Schmitt *et al.*, 1987). This is readily seen on a T-S scatter plot because of the higher density of points from the mixed layers (Figure 2.a) or in a volumetric T-S diagram (Figure 2.b). Layer temperature - salinity values are grouped in well defined lines. Examination of closely spaced tow-yo casts (Schmitt *et al.*, 1987) and towed thermistor chain data (Marmorino *et al.*, 1987) reveals that changes within layers are often gradual,
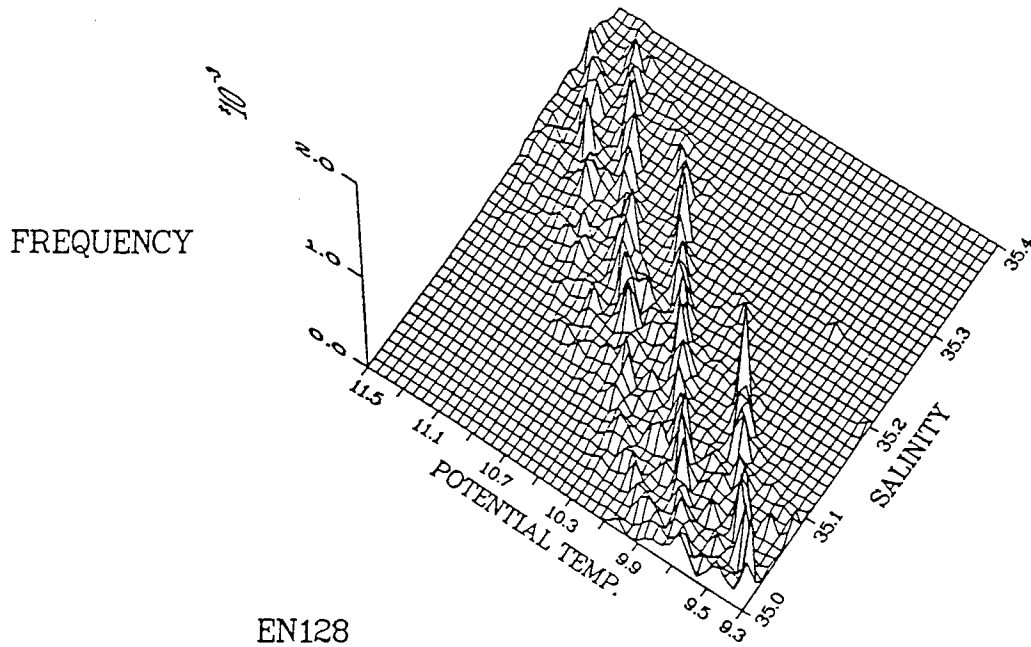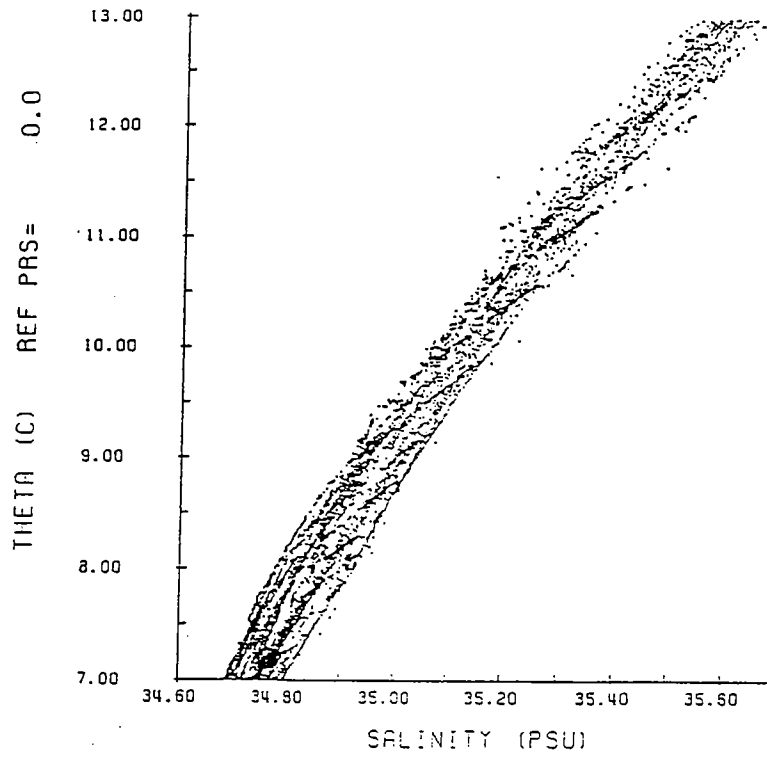
Figure 2.a. (Top) Scatter plot of $\theta - S$ values from C-SALT CTD casts during the spring cruise.

Figure 2.b. (Bottom) Volumetric projection of $\theta - S$ points from spring CTD data.
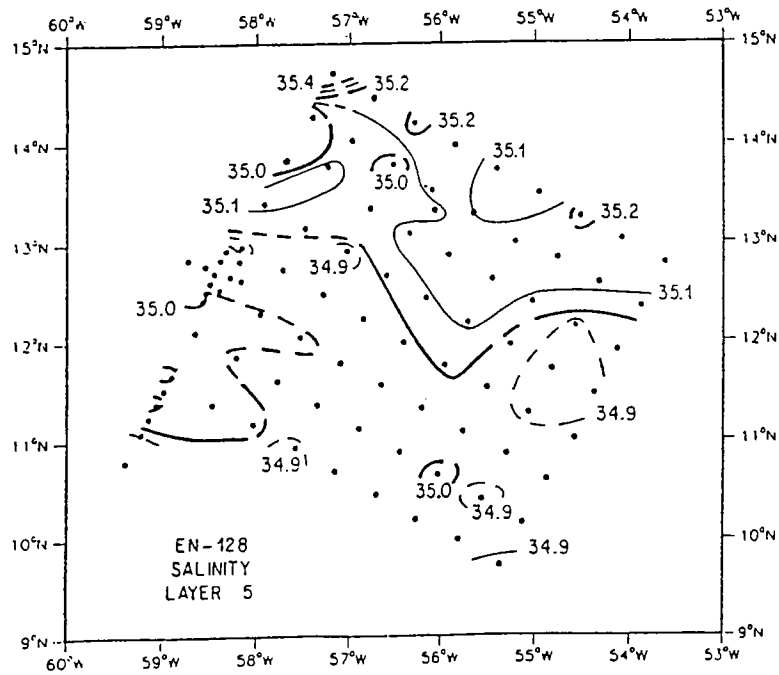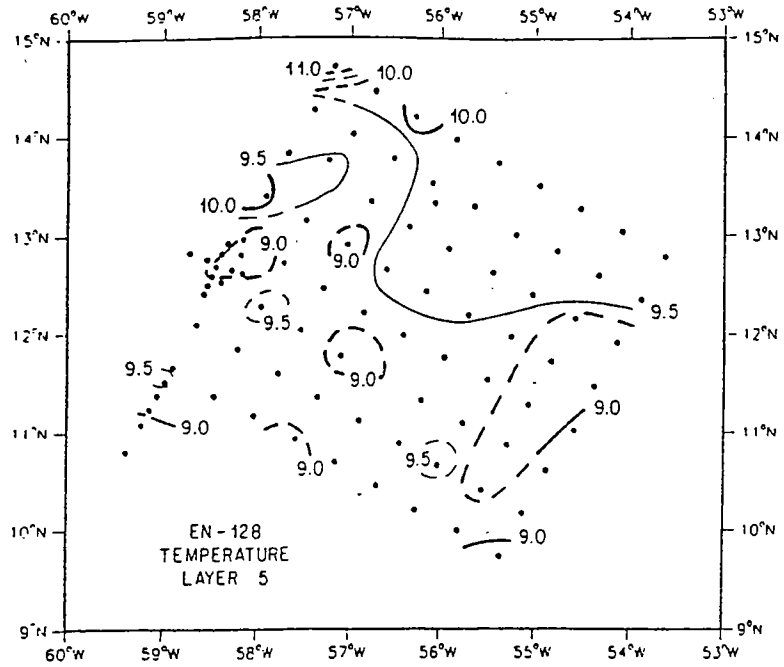
Figure 3.a.   (Top) Temperature within layer 5 from the spring survey.

Figure 3.b.   (Bottom) Salinity within layer 5 from the spring survey.

but occasionally punctuated by more abrupt transitions involving a temperature inversion within the layer. T-S points falling on the same line serve to identify individual layers over horizontal separations of hundreds of kilometers. This permits mapping of temperature and salinity variations within layers over the survey area (Figure 3.a, 3.b). The pattern of spatial variations in T-S properties of the layers is a rather direct confirmation of differential heat and salt transport. That is, strikingly similar groupings of T-S points are seen in the temporal evolution of laboratory salt finger experiments (Lambert and Demenkow, 1972). The horizontal density ratio within layers,

$$R_H = \frac{\alpha \nabla_\ell T}{\beta \nabla_\ell S} \tag{1}$$

where $\alpha = -\frac{1}{\rho}\frac{\partial \rho}{\partial T}$, $\beta = \frac{1}{\rho}\frac{\partial \rho}{\partial s}$ and ∇_ℓ = lateral gradient within a layer, showed no systematic variation with depth or time, being about 0.85 in the spring data set, 0.84 in the fall (Table 1). This number is well below the local vertical density ratio (1.6) which means that mechanical turbulence cannot be responsible for the layers. It is also less than one, which means that isopycnal mixing is not a primary cause of the layers. However, it is close to what would be expected for a vertically divergent salt finger field. Specific interpretations of this ratio will be the topic of the following section (2). Section 3 will discuss the estimation of mixing rates for the staircase from the microstructure data. A brief summary is given in section 4.

Table I

Horizontal density ratio of the C-SALT layers, $\alpha \nabla T / \beta \nabla S$

Layer	Spring	Fall
1	0.837	0.843
2	0.860	0.875
3	0.866	0.889
4	0.872	0.864
5	0.873	0.847
6	0.853	0.833
7	0.828	0.834
8	0.846	0.807
9	0.871	0.820
10	0.817	0.772
Average	0.852±0.019	0.839±0.032

2. Effects of Mixing in T-S Space

A very useful approach to problems in thermohaline mixing is to consider the action of the various mixing mechanisms in a space defined by the separate contributions of temperature and salinity to density. That is, the axis are given by $\alpha\delta T$ and $\beta\delta S$ where δ represents the deviation away from a mean state (Figure 4). On such a diagram, different mixing and advection processes are represented by vectors having different slopes (assuming α and β are locally constant. See McDougall's article in this collection for elaboration on cases where the flux ratio is not equal to the flux divergence ratio.) Isopycnal mixing or advection has a slope of unity. Simple vertical mixing and advection are represented by a vector with a slope equal to the local vertical density ratio, about 1.6 for the C-SALT area. Salt fingers transport more salt than heat and have an expected slope of 0.5–0.8, which is equal to the flux ratio of the fingers. No other known mixing process has a slope below unity; cabelling for instance, leads to vertical entrainment which has a slope of 1.6. Thus, the observed horizontal density ratio of 0.85 seems a decisive indicator of a significant salt finger presence. However, this ratio is somewhat above that expected for fingers alone, which is an issue worth exploring in some detail.
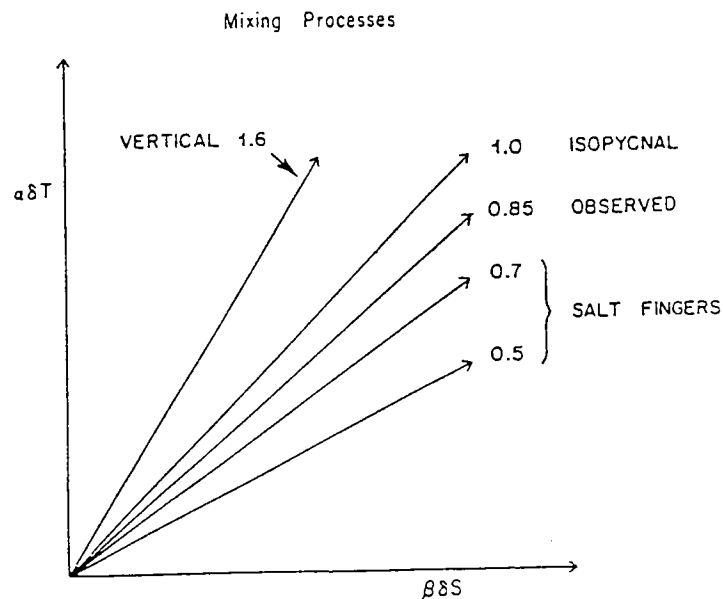
Mixing Processes

Figure 4. $T - S$ density perturbation diagram. The slopes representing various mixing processes are shown.

The heat/salt flux ratio for salt fingers is determined by two components: the advective flux carried within the fingers and the conductive fluxes across the interface. The advective flux ratio is simply given by the ratio of the heat and salt density perturbations within the fingers, since both components are subject to the same velocity field. The diffusive flux of salt across an interface is negligible compared to the conductive heat flux, which is simply determined by the mean vertical temperature gradient within the interface. That is, the density fluxes are given by:

$$\alpha \, F_T \;=\; \alpha \, \overline{w'T'} + \alpha K_T \, \overline{T}_z$$

$$\beta F_s \;=\; \beta \, \overline{w'S'} \tag{2}$$

where w', T', S' are the velocity, temperature and salinity perturbations within the fingers, K_T is the thermal conductivity, and $\overline{T}_z$ is the mean vertical temperature gradient.

The total flux ratio (γ) is:

$$\gamma \;=\; \frac{\alpha F_T}{\beta F_s} = \frac{\alpha \, T'}{\beta S'} + \frac{\alpha K_T \overline{T}_z}{\beta F_s} \tag{3}$$

The diffusive correction (second term) to the flux ratio can be expressed in terms of the Stern number (Stern, 1969), defined by:

$$A \;=\; \frac{\beta F_s(1 - \gamma_0)}{\nu \beta S_z(R_\rho - 1)} = \frac{\epsilon}{\nu N^2} \tag{4}$$

The Stern number (A) is found to be about one in most low density ratio laboratory experiments (Schmitt, 1979; McDougall and Taylor, 1984). The conductive correction to the flux ratio is thus:

$$\frac{K_T}{\nu}(1 - \gamma_0) \, R_\rho / A(R_\rho - 1) \tag{5}$$

Since the Prandtl number (ν/K_T) is about ten at these temperatures, the conductive correction is typically 0.1.

The advective flux ratio (γ_0) is what is normally reported from laboratory studies. Turner (1967) reported $\gamma_0 = 0.56$ for $R_\rho > 2$; Schmitt (1979a) estimated $\gamma_0 = 0.72$ for $R_\rho < 2$. and

McDougall and Taylor (1984) quote a value of γ_0 0.5 for $R_\rho < 2.0$. In principal, any value of γ_0 less than one is a viable salt finger flux ratio. Some theoretical values are available from the flux maximization theory of Stern (1976) ($\gamma_0 = 0.25$) and the growth rate maximization theory of Schmitt (1979) ($\gamma_0 = 0.62$ at $R_\rho = 1.6$). The Schmitt (1979) model works well at explaining the higher experimental flux ratio of the sugar/salt finger system and yields accurate predictions of the salt finger wavenumber spectrum (Gargett and Schmitt, 1982), so we are partial to it. If we accept this number and add the conductive correction, we would predict a total flux ratio for oceanic fingers of about 0.72. If we use the experimental value of Schmitt (1979b) and add in the conductive correction we get an expected value of 0.82, in reasonable agreement with the observations. However, the Schmitt experiments have a rather high value compared to other experiments and we must question their generality. Thus, we wish to explore several alternative mechanisms. The first involves a modified salt finger model, the others involve various combinations of salt fingers and other processes.

2.a Broadband Salt Fingers

The width of salt fingers bears a very close relationship to the flux ratio. This is because a thin finger more rapidly looses its temperature anomaly, and thus has a lower flux ratio than a thick finger. This dependence is readily seen in Figure 5, where the flux ratio - wavenumber relationship is plotted for the similarity solutions of Schmitt (1979a) at a density ratio of 1.6 and for the "equilibrium" salt finger (Huppert and Manins, 1973; Lambert and Demenkow 1972) for $1 < R_\rho < 100$. The closeness of the curves despite very different growthrates indicates that this is a robust relationship which should hold nearly independent of the dynamic state of the fingers. If the finger field were composed of only the fastest growing finger (or sheet in the presence of shear) then the expected flux ratio is 0.62 as noted above. However, if the spectrum is rich in high wavenumber fingers, which carry salt but not much heat and are highly dissipative, then the flux ratio will be low. If the spectrum is red, containing fingers with nearly equal T and S anomalies and being weakly dissipative, then the flux ratio will be high. Gargett and Schmitt (1982) considered the evolution of

salt finger spectra grown from 2 different red seed spectra using the Schmitt (1979a) model, which used a white seed spectra. Here we reexamine such spectral calculations for the effect on the flux ratio. That is, the flux ratio will be determined by flux contributions at all wavenumbers, not just the fastest growing, and we must sum the fluxes from the whole finger spectrum.
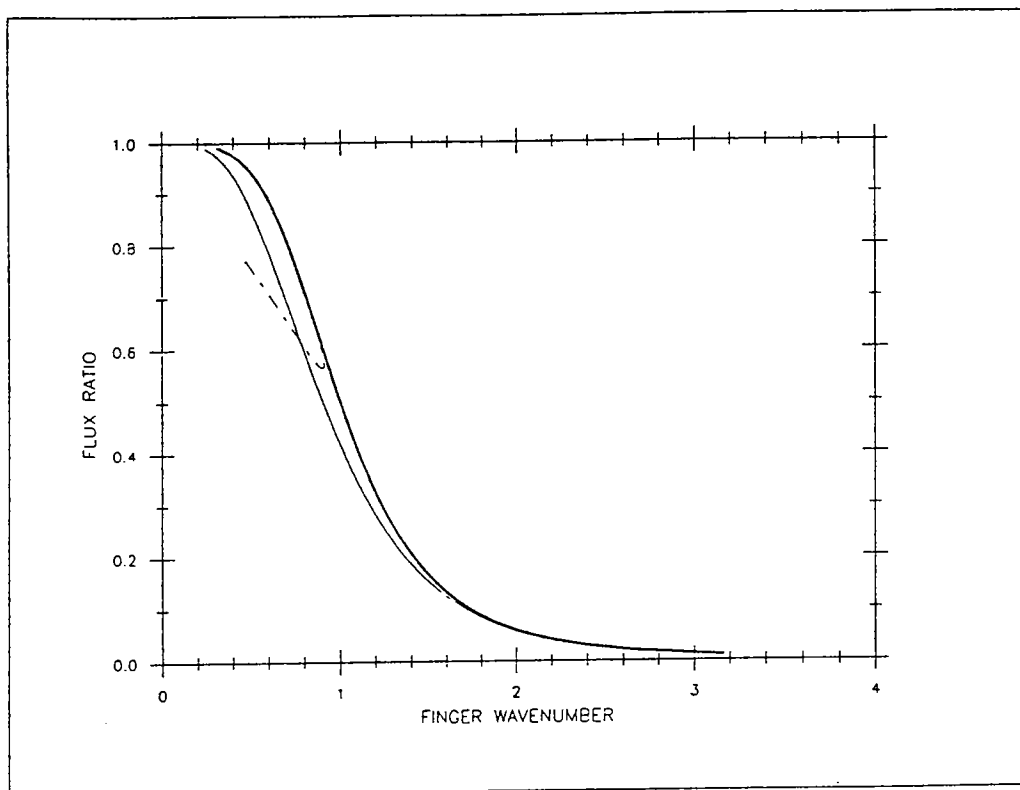
Figure 5.   Salt finger flux ratio versus non-dimensional wavenumber for three cases: Equilibrium fingers for $1 < R_\rho < 100$ (—), fastest growing fingers for $1 < R_\rho < 100$ (— · —), and the whole spectrum of salt fingers at $R_\rho = 1.6$, (—)

This has been done for several different seed spectra using relationships given in Schmitt (1979a). Figure 6 displays the evolution of the flux ratio with time for fingers grown from salinity seed spectra having slopes of −4, −2, −1 and 0. Also shown is the (invariant) flux ratio for the fastest growing finger. All the curves tend toward the fastest growing flux ratio, as this wavenumber comes to dominate the flux. However, it is somewhat surprising that only the reddest seed spectrum causes much elevation of the flux ratio.

It is illuminating to consider the causes of this decreased flux ratio for the less red seed spectra. The essential element is the fact the salt anomalies are the driving force for the convection. The salt also has a richer high wavenumber spectrum (no matter what the seed spectrum) than the temperature, because of the factor of 1/100 smaller diffusivity. Despite the viscosity being 1000 times larger than the salt diffusivity, the velocity spectrum is also relatively enriched at higher wavenumbers because it is driven by the salt anomalies. The temperature spectrum falls off most sharply of the three spectra at wavenumbers greater than the fastest growing. The fact that the low wavenumber portion of the spectrum has relatively high flux ratio and thus nearly canceling T and S anomalies also means that this portion of the spectrum has weaker gravitational forcing of the velocity field. Thus, the wavenumbers greater than the fastest growing make a tangible contri-
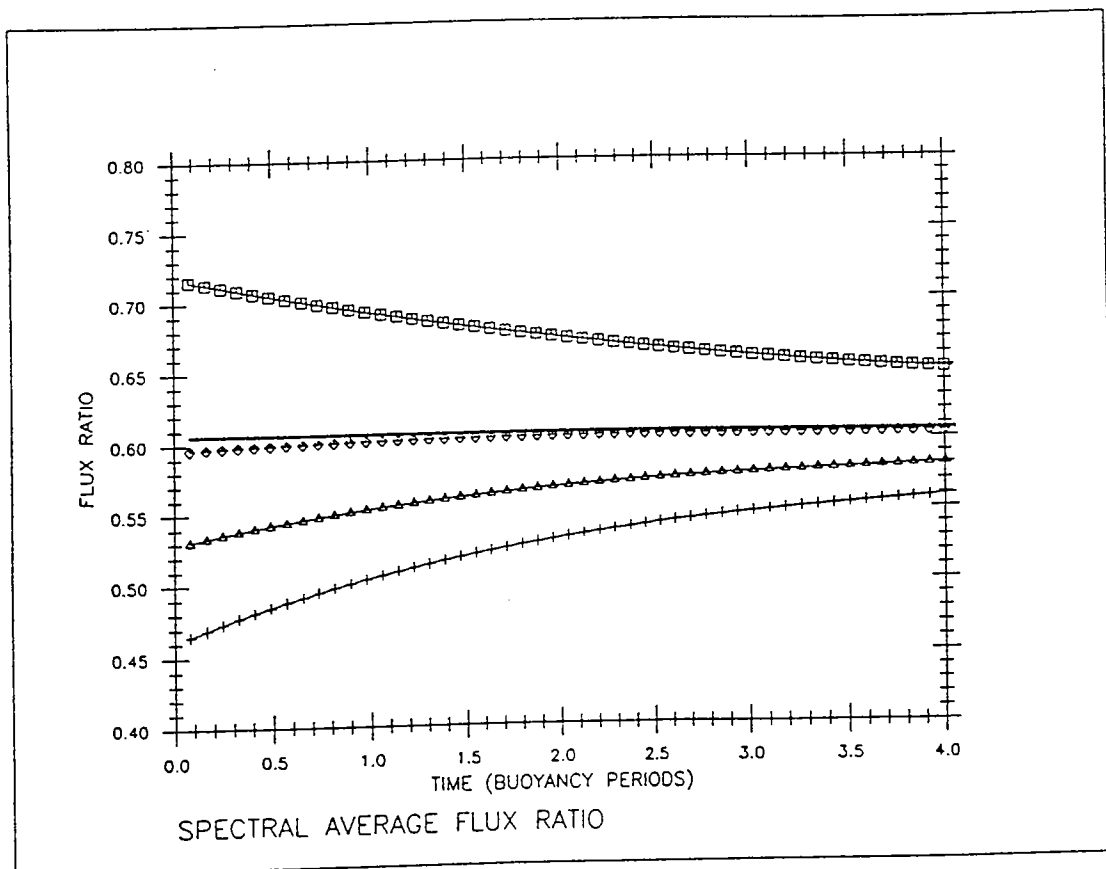
Figure 6.   The evolution of the net flux ratio for salt finger spectra growing from initial salinity seed spectra having slopes of −4(□), −2(◇), −1(△), and 0(+). The constant flux ratio of the fastest growing finger is also shown (—).

tribution to the salt flux, though not to the heat flux, and lower the overall flux ratio to a value less than that of the fastest growing alone unless the seed spectrum is very red. The spectra of shear, temperature and salinity gradient for salt fingers is in stark contrast to ordinary turbulence, which is forced by larger scale velocity gradients. For turbulence, we expect the shear, T and S spectra to peak at successively higher wavenumbers, which are quite distinct from one another. For salt fingers we expect them all to peak at the same wavenumber (the fastest growing) with salt and velocity shear having relatively more high wavenumber variance than temperature. This poses some interesting questions for microscale observations. In particular: 1. Can we develop probes to resolve the salinity gradient spectrum? and 2. Is the 2 cm resolution of the typical shear probe adequate to resolve all the shear variance in salt fingers? Higher resolution probes operated from a low noise platform might provide information on the dynamic state of the fingers.

In summary, unless the forcing spectrum for salt fingers is very red, a broadbanded salt finger spectrum is more likely to lower the flux ratio than raise it. Thus, broadbandedness is not particularly promising to explain the elevated "flux ratio" observed in the C-SALT layers. However, consideration of the effect does raise possibilities for understanding the dynamical state of the fingers through higher resolution measurements.

2.b   Salt Fingers Plus Turbulence

One mechanism that could elevate the net flux ratio is turbulence. Assuming that turbulent patches are sufficiently intense to completely mix the temperature and salinity gradients then the flux ratio due to turbulence is simply equal to the vertical density ratio, about 1.6. Occasional turbulent events that augment the more continuous salt fingering could raise the net flux ratio by the appropriate amount.

This can be roughly quantified by assuming that "horizontal" advection within the layers balances the vertical flux divergence due to the salt fingers and the turbulence. That is, the

temperature and salinity balances are given by:

$$U \cdot \alpha \nabla_\ell T = \gamma K_{SF} \beta S_{zz} + K_{Tu} \alpha\, T_{zz}$$

$$(6)$$

$$U \cdot \beta \nabla_\ell S = K_{SF} \beta S_{zz} + K_{Tu} \beta\, S_{zz}$$

where K_{SF} is the effective salt finger diffusivity and K_{Tu} is the turbulent diffusivity. Since within the layers, T and S are well correlated, we can write:

$$U \cdot \alpha \nabla_\ell T = R_H\, U \cdot \beta \nabla_\ell S \qquad (7)$$

where R_H is the horizontal density ratio in the layers (0.85). Using the foregoing substitution we find:

$$R_H = \frac{\gamma K_{SF} + R_\rho K_{Tu}}{K_{SF} + K_{Tu}}$$

or

$$K_{SF} = \left(\frac{R_\rho - R_H}{R_H - \gamma} \right) K_{Tu} \qquad (8)$$

For $R_\rho = 1.6$, $R_H = 0.85$, and taking $\gamma = 0.72$, I estimate that the salt finger diffusivity is 5-6 times the turbulent diffusivity. If the finger diffusivity is O 10^{-4} m^2/s then $K_{Tu} = 2$ x 10^{-5} m^2/s, which seems a bit high considering that Gregg (1989) estimates a diffusivity of this order in a number of stronger shear regions (C-SALT had anomalously low internal wave shears). However, Marmorino (1990) finds evidence for occasional shear instabilities in C-SALT which may be sufficient to explain the elevated flux ratio. Another possibility is that the layer convection was sufficiently intense that turbulent entrainment across the interfaces occurred. Some of the laboratory experiments of Schmitt (1979) displayed elevated flux ratios due to entrainment. We conclude that turbulent mixing of unknown origin is a possible explanation for an elevated "flux ratio" in the C-SALT layers. If it is primarily turbulence it must be modulated in a way that is proportional to the salt finger flux, since there is no systematic variation of the apparent flux ratio with depth in the staircase.

2.c Salt Fingers and Vertical Advection

Here we consider the effect of a cross-interface velocity, which might be due to upward or downward entrainment of fluid across the interface. The effective heat/salt ratio for such advection is given by the vertical density ratio R_ρ. Formulated as in the simple model above we obtain:

$$U \cdot \alpha \nabla_\ell T + W \alpha T_z = \gamma K_{SF} \beta S_{zz}$$

$$(9)$$

$$U \cdot \beta \nabla_\ell S + W \beta S_z = K_{SF} \beta S_{zz}$$

This leads to the relation for the vertical velocity:

$$W = \frac{K_{SF} \; S_{zz}}{S_z} \frac{(R_H - \gamma)}{(R_H - R_\rho)} \tag{10}$$

Evaluated for the observed vertical and horizontal density ratios, a diffusivity of $1 \times 10^{-4} \; \mathrm{m^2/s}$, and a halocline scale height of 200 m, we obtain a vertical velocity of -1×10^{-7} m/s. This magnitude is typical of thermocline upwelling rates and an order of magnitude smaller than Ekman pumping rates. We have to emphasis though, that this is a "dia-interface" velocity, not strictly diapycnal or vertical. A specific mechanism to produce such a velocity would have to be identified. One candidate is the asymmetric entrainment observed in the salt finger experiments of Schmitt (1979). The observed upward migration of the interface would correspond to the downward flow required here.

2.d Salt Fingers and Isopycnal Mixing

Since processes which lead to exchange and mixing of water parcels along density surfaces influence temperature and salinity in the proportion α/β, or with a "flux ratio" of 1, it is possible to combine fingering with isopycnal mixing to match the observed horizontal density ratio in the layers. Here we model the isopycnal mixing as being due to flux divergences caused by an "eddy" diffusivity acting on the Laplacian of T and S on isopycnal surfaces. That is:

$$U \cdot \alpha \nabla_l T = \gamma K_{SF} \beta S_{zz} + K_i \beta \nabla_i^2 S \tag{11}$$

$$U \cdot \beta \nabla_t S = \gamma K_{SF} \beta S_{zz} + K_i \beta \nabla_i^2 S \qquad (12)$$

Where K_i is the isopycnal diffusivity.

This leads to the relation:

$$K_i = K_{SF} \frac{S_{zz}}{\nabla_i^2 S} \frac{(R_H - \gamma)}{(1 - R_H)} \qquad (13)$$

For the eddy resolving C-SALT hydrographic data we find strong isopycnal gradients of T and S but also find that it is difficult to pick out a particular length to characterize a convergence scale. The eddy field is sufficiently robust that the sign of the isopycnal gradients changes over 10s of kilometers. In this situation, the above relation cannot be applied quantitatively. If we assume a vertical scale height of 200 m and a horizontal length scale of 200 km then we find that K_H must be 10^6 x K_{SF}, a plausible number. However, since the isopycnal mixing would again have to maintain a strength that was proportional to salt fingers in order to preserve depth independence of the layer density ratio, it seems somewhat unlikely that isopycnal mixing is an important factor in establishing the value 0.85 for the horizontal density ratio, though we cannot rule it out.

One could interpret the temperature inversions within layers as evidence of horizontal stirring. But they could merely reflect an occasional concentration of the horizontal temperature and salinity variations within layers. That is, the large scale hydrographic surveys reveal changing T, S and density over scales of 200-400 km within the layers. The finer scale towyos and towed chain data of Marmorino (1989) showed that these changes could be concentrated in certain regions where inversions within the layers would appear. The density ratio of the inversions is necessarily the same as the large scale horizontal density ratio, 0.85. Thus, they are capable of supporting diffusive convection. Whether these intrusions are actively generated and driven by double-diffusive flux convergence, occur simply because of horizontal variability in the vertical flux convergence, or are passive concentrations of the large scale gradients by mesoscale eddy stirring, is beyond the scope of our present data.

2.e   Salt Fingers and Cabelling

Because seawater has an equation of state which has a nonlinear dependence on temperature, any process which destroys thermal variance will lead to "densification" of the participating fluid. This includes vertical mixing processes as well as the traditional scheme in which seawater parcels of identical density but different T and S are mixed to produce a mass of higher density than the original parcels. McDougall (1981a,b,c) and Schmitt (1979) have noted an asymmetrical entrainment effect in double-diffusive experiments. In the fingering case the lower mixed layer erodes the interface and expands while the top of the interface grows into the upper mixed layer. This leads to an upward migration of the interface of the sense required to explain the variations in the C-SALT layer properties. McDougall (this volume) explores this mechanism in some detail and concludes that it is a viable candidate. Here we note that the vertical advection case considered in 2.c above is relevant.

2.f   Summary of Mechanisms

Of all the above processes two seem more probable than the others, those are the scenarios involving turbulence and cabelling in addition to salt fingers. Marmorino (1989) and Fleury and Lueck (this volume) cite evidence of a turbulence incidence of order 1% which would contribute to raising the effective flux ratio above the theoretical salt finger value of 0.62. McDougall (this volume) provides arguments indicating that the effect of a nonlinear equation of state may account for half to all of the required flux ratio elevation. Thus, plausible explanations exist for the observed horizontal density ratio in the layers. Proof that these particular mechanisms do indeed operate in the C-SALT layers would probably require time series measurements of microstructure (Lagrangian and/or moored). Such capabilities are at a very preliminary stage of development.

3. Mixing Rates

In the aftermath of the C-SALT field work Lueck (1987) and Gregg and Sanford (1987) emphasized the smallness of the turbulent dissipation and the disagreement with one particular laboratory data set to conclude that the fingers were not particularly vigorous. This is understandable if approached from the perspective of conventional turbulence. However, this is quite misleading, as has been noted by Schmitt *et al.* (1987) and Schmitt (1988), since double-diffusion differs from turbulence in fundamental ways. Here we reiterate the issues to discourage further propagation of such misinterpretations.

3.a Salt Finger Efficiency

Turbulence derived from internal wave breaking in the thermocline is a rather inefficient process from the standpoint of mixing. Only a small fraction (10-20%) of the kinetic energy derived from the shear is converted to a change in potential energy of the stratified fluid and the rest is dissipated. Thus, the turbulent dissipation is the largest energy sink in a mixing event and relatively easy to monitor. In contrast, salt fingers are expected to convert over 70% of the energy derived from the salt field into a change in potential energy for the temperature field. The turbulent dissipation is a small energy sink for salt fingers; they are much more efficient at mixing than shear driven turbulence. The buoyancy flux, which is equal to the dissipation, is the difference between the heat and salt fluxes, and is thus rather small for salt fingers. This dichotomy between the processes is reflected in the expressions relating the dissipation rate to vertical diffusivity. For turbulence the Osborn (1980) equation holds:

$$K_\rho \simeq \left[\frac{R_f}{1 - R_f} \right] \frac{\epsilon}{N^2} \simeq (0.1 \to 0.2) \frac{\epsilon}{N^2} \qquad (14)$$

where R_F is the flux Richardson number, usually taken to be 0.15.

In contrast, for salt fingers the relevant relation (derived by McDougall (1987 personal communication) and given by Hamilton, Lewis and Ruddick (1989) and Schmitt (1988)) is:

$$K_{SF} = \left[\frac{R_\rho - 1}{1 - \gamma}\right] \frac{\epsilon}{N^2} \simeq (1 \rightarrow 4)\frac{\epsilon}{N^2} \tag{15}$$

Thus, there is a difference of a factor of 5 to 40 in the estimated vertical eddy diffusivity depending on whether the dissipation is due to turbulence or double diffusion!

There are also reasons to suspect that conventional shear probes cannot resolve the full shear spectrum of salt fingers. In turbulence the shear spectrum peaks at a lower wavenumber than the temperature and salinity gradient spectra. As noted in 2.a above, for salt fingers the shear, temperature and salinity gradient spectra all peak at about the same wavenumber, and the salinity and shear fall off more slowly than the temperature at higher wavenumbers. This is because it is the small scale salt anomalies that are driving the flow. Given the very small structure seen in the shadowgraph images, it is possible that a significant portion of the dissipation spectrum is unresolved by shear probes with a 2 cm scale cutoff. Similarly, data processing procedures which assume the shear should follow empirical turbulence spectra would underestimate the dissipation.

Using the Lueck (1987) and Gregg and Sanford (1987) estimates of dissipations in the range of 2 to 5 x 10^{-10} W/kg and relation (15) above, yields vertical salt diffusivities in the range of 0.2 to 2.5 x 10^{-4} m^2/s (Schmitt, 1988). In contrast, diffusivities estimated for shear instability of internal waves are one to two orders of magnitude smaller, in much more strongly sheared regions (Gregg, 1989). Thus, the thermohaline staircase may have one of the largest vertical transfer rates in the main thermocline, despite a relatively low turbulent dissipation.

3.b Interface microstructure

Marmorino (1987) and Lueck (1987) reported on the narrow band thermal microstructure found within the interfaces of the staircase. The wavelength of the dominant structure is 5–10 cm, in excellent agreement with the theoretical finger size. The predicted $-1/4$ power dependence of the wavelength on the vertical temperature gradient is supported by Marmorino's data. His data

also indicate that the amplitude of the fingers scales with the 3/4 power of the vertical temperature gradient, as predicted by the model of Kunze. Also, on average, the thermal cox number is near ten, in excellent agreement with the model of Kunze (1987) (and that of Stern (1969) as shown by Schmitt (1988)). The buoyancy flux (assumed equal to the dissipation) also appears to be consistent with the collective instability model of Stern (1969, 1975) in that the "Stern number" (or nondimensional dissipation) is about 1 for the C-SALT interfaces.

However, in several respects the interfacial microstructure differed from expectations. These include the following points:

i. The interface thicknesses were greater than expected from laboratory experiments and highly variable. A typical interface thickness of 2 m (Boyd, 1988) with excursions to 10 m contrasts with the 20–50 cm thickness obtained by application of laboratory results (Kunze, 1987; Schmitt, 1988).

ii. There was low vertical coherence of temperature microstructure over a few centimeters (Lueck, 1987).

iii. The shadowgraph imagery revealed nearly horizontal lamina rather than the vertical structure seen in salt finger experiments and other ocean regions (Kunze, et al., 1987)

iv. The Cox number of the interface varied inversely with interfacial temperature gradient (Marmorino, 1989; Lueck and Fleury, 1990). No model has predicted such dependence.

Point i must be related to the low dissipation measured in the staircase. That is, if the fluxes had been as large as predicted by application of the laboratory "4/3" power laws, then the interface should have been thinner to maintain a Stern number of order unity. It is not unreasonable to expect that interfacial internal waves and other processes could vary the interface thickness, and thus modulate the strength of the fingers.

Lueck (1987) suggested that the low vertical coherence indicated that the fingers were not vertical pipes as seen in the laboratory. However, such vertical structure only becomes apparent

in the later stages of the typical lab experiment. The early fingering interface can be rather non-uniform and display a more isotropic microstructure. Similar isotropic structure is seen in the numerical model of Shen (1989). Another explanation for low vertical coherence is that the fingers are bent over by shear. This would also explain the shadowgraph results, which consistently displayed horizontal lamina in all of the interfaces; no isotropic structures were seen except in rare turbulent patches outside the step interval. Thus, shear-tilted fingers seems to be the most probable explanation of points ii and iii.

Point iv is an intriguing result which should motivate development of finger models which take into account the temporal evolution of the interface. Internal waves or other external influences may have to be incorporated into the models. The inverse relation between Cox number and temperature gradient means that the integral of thermal dissipation (χ) within an interface depends only on the temperature difference from layer to layer and not the interface thickness. Thus, a simple linear flux law may be applicable.

4. Summary

The C-SALT field program provided the first detailed look at a thermohaline staircase. The system of about ten layers was found to cover a large area (1 million kilometer^2) and to be surprisingly coherent in the horizontal. Historical data and an 8 month mooring record suggest that the staircase is a permanent feature of the western tropical North Atlantic. Water mass changes within the layers are consistent with the expected difference in vertical mixing rates for heat and salt due to salt fingers.

Similarly, there was strong evidence for salt fingers in the small scale data. Narrow band, limited amplitude thermal microstructure was observed on the interfaces at the predicted wavenumber and amplitude. The interfaces were generally thicker than expected from laboratory experiments and fluxes were modestly lower, perhaps due to modulation by internal wave strain or shear. Also, the vertical coherence of temperature microstructure was small and shadowgraph images showed

nearly horizontal lamina. Both these effects are probably due to weak vertical shear across the interfaces. A vertical salt diffusivity of order 1×10^{-4} m^2/s is estimated for the staircase from the microstructure data. This indicates that the C-SALT region has enhanced vertical transport in the main thermocline, which is most likely one or two orders of magnitude smaller in nonstaircase regimes.

References are given in the Double-Diffusive Bibliography in this volume.

Horizontal Variations of a Thermohaline Interface

M. Fleury and R.G. Lueck

The Johns Hopkins University
Chesapeake Bay Institute
Baltimore, Maryland 21211

Abstract

Measurements of velocity and temperature microstructure and hydrography made over a distance of 40 km, along a single interface in a double-diffusive staircase, reveal strong horizontal variations in the characteristics of the interface. The thickness of the interface varied from 0.2 to 12 m while the temperature and salinity difference across the interface remained nearly constant. The thermal Cox number C was small, with most values falling between 1 and 10, and varied with the mean vertical temperature gradient according to $C=0.91<T_z>^{-1}$, making the local vertical heat flux independent of the interfacial thickness. The interface was turbulent in one 500 m long section where the average dissipation rate was 3.4×10^{-8} W kg^{-1}. The rate of dissipation was low in the remaining 39.5 km, averaging 10×10^{-10} W kg^{-1} in the interface and 3×10^{-10} W kg^{-1} in the adjoining mixed layers. The flux ratio deduced from the average heat flux and the average rate of dissipation in the mixed layers is 0.56.

Introduction

The results presented here come from data collected in and around a single interface during the C-SALT experiment in November 1985 (Schmitt et al. 1987). The interface was located in the central region of the C-SALT site (12° 06′ N, 56° 30′ W) and at mid depth (450 m) where the staircase like structure of the thermo-halocline was well established. The measurements were made from a towed vehicle that repeatedly crossed the interface in a saw-tooth pattern for a total of 220 crossings over a distance of 40 km. The profiles provide a picture of the horizontal variations of the characteristics of the interface (thickness, vertical gradients, heat flux and dissipation rates). We will briefly describe our instrumentation and data processing, present the results and discuss their implication.

Instrumentation and Data-Processing

The data reported here were collected with the towed body *HOTDAD* (Lueck, 1987). Two fast thermometers (FP-07 thermistors) and two airfoil type velocity probes were mounted at the nose of the vehicle. The thermometers were separated vertically by 0.035 m and produced signals proportional to temperature and its along-path gradient ($\approx \partial T/\partial x$). The two velocity sensors were separated horizontally and athwartship by 0.035 m and produced signals proportional to the along-path gradient of athwartship velocity ($\approx \partial v/\partial x$) and an orthogonal velocity ($\approx \partial w/\partial x$). With the help of some signal correction, the spatial resolution of the thermometers is 0 to 100 cpm while the resolution of the velocity sensors is 1.5 to 100 cpm. Also aboard the towed body were a Sea-

Bird temperature and conductivity sensor, a strain-gauge pressure transducer, a tri-axial accelerometer and a two-component electro-magnetic velocity sensor.

The fast thermometers resolves the temperature gradient variances satisfactorily because the temperature gradient spectra due to double-diffusion are band-limited. The spectra have been corrected for the speed dependent frequency response of the sensors (Vachon and Lueck, 1984) and were integrated from 1 to 60 Hz when $U < 1$ m s^{-1} and 1 to 80 Hz when $U > 1$ m s^{-1} where U is the speed of the body. The thermometers did not resolve the entire gradient spectrum in the turbulent region of the interface.

Two estimates of the rate of dissipation of kinetic energy, ϵ_w and ϵ_v, are available from the velocity probes, assuming isotropy. For reasons which are not yet understood, the noise level of the $\partial v/\partial x$ probe increased with speed while the noise from the $\partial w/\partial x$ probe decreased with speed. We estimated the rate of dissipation of kinetic energy with the data collected in the mixed layer in the following manner:

    (1) all shear data were high-pass filtered at 1.5 Hz with a 5 pole elliptic filter,

    (2) power spectra were computed for each one-second block of data and the rates of dissipation, ϵ_v and ϵ_w were estimated by integration from 1 cpm to 60% of the Kolmogorov wavenumber,

    (3) we retain the lower of the two dissipation estimates from (2) and the spectra associated with them, and, for each crossing of the interface, we average these spectra in wavenumber space,

    (4) the average wavenumber spectrum was then integrated from 1 cpm to 60% of the Kolmogorov wavenumber to produce a mean dissipation estimate and this mean was adjusted for the missing data from below 1 cpm and above 60% of the Kolmogorov wavenumber using the Nasmyth empirical spectrum (Oakey 1982).

At a level of about 2×10^{-10} W kg^{-1} (1 W kg$^{-1} \equiv 10^{3}$ W m^{-3}) the fit to the empirical spectrum is poor and we took this to be the noise level of our instrumentation.

Our method for estimating the rate of dissipation in the interfaces was similar to the technique used on the data from the mixed layers except that we only used ϵ_v. The interface was highly stratified and the assumption of isotropy in the dissipation range of the wavenumber spectrum may be incorrect. Yamazaki and Osborn (1989) showed that ϵ_v is correct to within better than 35%, whereas ϵ_w may be too low by more than an order of magnitude. The spectra from the interface contain more energy at low frequencies than the spectra from the mixed layer and this may have resulted from the small but, not insignificant, temperature sensitivity of the velocity sensors. Spectral leakage from low frequencies is reduced by the 1.5 Hz low-pass filter. The average difference between the upward ($U > 1$ m s^{-1}) and downward ($U < 1$ m s^{-1}) profiles is 5×10^{-10} W kg^{-1}. If we take the noise level in the interface (2×10^{-10} W kg^{-1}) to be the base noise level in the absence of temperature contamination, then the average noise level in the interface is 4.5×10^{-10} W kg^{-1}.

Results

The towed body crossed the interface 220 times during its 40 km trip and its presence in the interface accounted for 20% of the total distance travelled. Isotherms constructed with the temperature data from each crossing (figure 1) show that the depth of the interface had a peak-to-peak amplitude of 30 m and an apparent wavelength of 15 km in addition to smaller amplitude displacements at shorter scales. The thickness varied widely and the interface was bifurcated over the last 8 km of our observations. The bifurcation split the interface into two thin interfaces separated by a mixed layer approximately 3 m thick. The isotherms leaving the interface represent horizontal inhomogeneities in the surrounding mixed layers.

Upper and lower mixed layers characteristics

The potential temperature and density, salinity and density ratio of the mixed layers adjacent to the interface were not horizontally uniform (figure 2a). Anomalously cold, fresh and light water was observed over 8 km simultaneously above and below the interface (km 21 to 29). The magnitude of this anomaly was slightly stronger below than above the interface and resulted in a lowering of the density ratio from 1.6 to 1.3. The intermediate points in figure 2a represent the characteristics of thin mixed layers inside of the interface. When main mixed layer values are plotted in a θ-S diagram (figure 2b) the points follow a curve of constant density ratio equal to 0.85 (0.82 and 0.87 respectively for the lower and upper mixed-layer). The spread of the data points and the slope of the curve is mainly determined by the 8 km long anomaly. A similar result was obtained by Schmitt et al. (1987) for data covering 300 km and was interpreted as a measure of the flux ratio. The 8 km long anomaly is associated with thermohaline inversions in the mixed layers, probably caused by an intrusion (Marmorino et al. 1987) and, because the horizontal scale of the anomaly was only 8 km, we prefer to interpret the slope in θ-S space as a measure of the density ratio of the inversions.

Interface thickness

We define the thickness of an interface as the vertical distance in which the temperature in an interface changes by 95%. Because the body intersects the interface at an angle $\theta_b \simeq \pm 10°$, our estimates of the thickness are biased if the interface is not horizontal. Our estimate of the thickness of a sloping interface is wrong by a factor of $\sin(\theta_i \pm \theta_b)/\sin(\theta_b)$, where θ_i is the interface slope. Because internal wave motions produce only small values of θ_i ($\theta_i < 3°$ at most from figure 1) this error is limited to 10%. We did not observe any significant difference between up and down going profiles which would have led us to suspect an error in our estimates.

The thickness of the interface ranged from 0.2 to 12 m (figure 3), nearly two orders of magnitude. The interface was very thin at km 11 where we measured values between 0.25 m and 0.5 m at 7 consecutive crossings in 400 m. The mean vertical temperature gradients were 1.4 to 2.6 °C m^{-1}. The interfaces were also very thin in the bifurcation region (as low as 0.22 m) but, since these interfaces

support only half of the temperature difference between the upper and lower mixed layer, the gradients were only 1 °C m^{-1}. According to Kunze's model (1987) fingers cannot extend through the entire interface if its thickness t is greater than $t_{max} = 0.27 <\partial T/\partial z>^{-1/4} \approx 0.25$ m where we took Kunze's parameter $C_w = 1/2$. The interface was thinner than Kunze's criterium in three observations, only 20% thicker in 4 observations and 20 to 50% thicker on 7 crossings.

Heat flux

The thermal Cox number, defined by

$$C = <(\nabla T)^2 > <\partial T/\partial z >^{-2},$$

is estimated using

$$<(\nabla T)^2> = 3<(\partial T/\partial x)^2> \text{ and } <\partial T/\partial z> = \Delta T/t$$

where < > denotes the ensemble average from a crossing of the interface, the variance is estimated from the integral of the wavenumber spectra and ΔT is the temperature difference across the interface of thickness t. We used a factor of 3 which is appropriate for isotropic conditions because the numerical simulations of Shen (personal communication) and the microstructure analysis of Lueck and Fleury (1989) indicate that the temperature gradient is close to isotropic in a double-diffusive interface. The average Cox number was 8.2 with most estimates lying between 1 and 10 (figure 4a). The largest values come from the region where the interface was thickest, which is seen by comparing figures 3 and 4a. For the 7 crossings where the interface was thinner than 0.5 m, the average Cox number was 2 (0.05 to 8.5) and stands in sharp contrast to the value of several hundred predicted by Kunze's model for contiguous fingers across an interface. The Cox number was also close to 1 where the interface was bifurcated (km 37 to 42). The Cox number clearly decreased with increasing mean temperature gradient and a regression (figure 4b) yields

$$C = 0.91 <\partial T/\partial z>^{-1.08}$$

which agrees with Marmorino (1989). The points associated with shear-induced turbulence (figure 4a) have been excluded from the regression. The large range of temperature gradients was essentially provided by the variations of thickness of the interface but, plotting the Cox number against thickness, does not reduce the scatter from our regression. The average Cox number is close to the value of 7 ($R_\rho = 1.5$) predicted by Kunze (1987,1989) but, his model does not portend a dependence on the mean temperature gradient.

The average contribution of the heat flux towards the buoyancy flux was estimated by averaging the product of the Cox number and the mean vertical gradient at each crossing of the interface. This method introduced a slight bias because thin interfaces are sampled more quickly (hence, more frequently) per unit distance travelled than are thick interfaces. No correction was made for this

possible bias. Our flux estimate excludes the molecular conductive flux by the definition of the Cox number. The average buoyancy flux by heat was

$$F_T = g\kappa<\alpha C<\partial T/\partial z>> = 3.8\times10^{-10} \text{ W kg}^{-1}$$

and will later be compared to the dissipation rate in the mixed layer to deduce the flux ratio.

Dissipation rates

Estimates of the rate of dissipation of kinetic energy (figure 5) revealed low values in both the mixed layers and the interface as well as the presence of shear-induced turbulence. A 500 m long section (at km 13) of the interface was turbulent. At one crossing in this section, the density structure had a 4 m vertical overturn implicating a Kelvin-Helmholtz instability. The dissipation rate in this overturn was 7.4×10^{-8} W kg^{-1} (average of the two velocity probes). The non-dimensional dissipation rate, $\epsilon/\nu N^2=572$, is much larger than the minimum value of 16 required to support a buoyancy flux (Rohr et al. 1988) and also larger than the minimum value for isotropy in the dissipation range of the velocity wavenumber spectrum (Garget et al. 1984). The average rate of dissipation in the turbulent section was 3.4×10^{-8} W kg^{-1} and the length of this section represents 1.3% of the total length of our observations. The frequency of occurrence of turbulence is consistent with the estimate of 1% by Marmorino (1989) based on overturns of the isotherms. Although a relatively high value of ϵ occurred at some places (in particular in the bifurcation region) the remaining 39.5 km of the interface cannot be considered turbulent because $\epsilon/\nu N^2$ was less than 10 and frequently as low as 1. Excluding the region of shear induced turbulence, the mean rate of dissipation in the interface was

$$\epsilon = 9.5\times10^{-10} \text{ W kg}^{-1}$$

after we subtracted a noise level of 4.5×10^{-10} W kg^{-1}.

An examination of the dissipation rates in the mixed layers (figure 5) reveals 12 large estimates. Two of the large values are associated with the turbulent section near km 13 and these are probably real. However, the remaining 10 large values are artifacts of our instrumentation. They all occurred in the lower mixed layer and just after the towed body turned around and started its ascent (figure 5). During the previous descent and at the same depth no turbulence was observed. Furthermore, the large values were only observed for a narrow range of amplitude and frequency in the depth cycle of the towed body. We believe that the remaining 10 large dissipation values are the result of crossing the wake of the tow line which is impossible in a steady ascent and descent but can occur if the trajectory is cyclic. Excluding the 10 spurious peaks, all of which are larger than 2×10^{-9} W kg^{-1}, the mean rate of dissipation in mixed layers was:

$$\epsilon = 3\times10^{-10} \text{ W kg}^{-1}$$

after subtracting a noise level of 2×10^{-10} W kg^{-1}. The mean value rises to 13×10^{-10} W kg^{-1} if we include the 10 spurious values. The mean rate of dissipation in the mixed layer agrees with Kunze's (1987; 1989) model.

The dissipation rate in the interface was 3.2 times larger than in the mixed layers. Gregg and Sanford (1987) reported a ratio of 3.5. These authors found an average value of 1.4×10^{-10} W kg^{-1} for mixed layers between 300 and 600 m depth. However, all layers did not have the same dissipation rates. Layer 5 (our lower layer) of Gregg (1988, figure 7) had a relatively high dissipation rate (2.5×10^{-10} W kg^{-1}) in agreement with our results, whereas layer 4 (our upper layer) was below their noise level of 1.0×10^{-10} W kg^{-1}.

Discussion

If we assume that the dissipation in the mixed layers is exclusively produced by the buoyancy flux generated by double-diffusion in the interfaces, then the buoyancy flux produced by the heat flux and the dissipation rate can be used to estimate the flux ratio with

$$R_f = F_T/F_S = (1 + \epsilon/F_T)^{-1} = 0.56,$$

where $\epsilon = 3\times10^{-10}$ W kg^{-1} and $F_T = 3.8\times10^{-10}$ W kg^{-1} (considered as a positive number). Our estimate falls between the laboratory based estimates of Schmitt (1979, $R_\rho \simeq 0.72$) and Turner (1967, $R_\rho \simeq 0.6$) and those of McDougall and Taylor (1984, $R_\rho \simeq 0.45$). The theoretical prediction (Kunze, 1987) is 0.63. If we do not subtract the noise level, we get 0.43 and if we take the dissipation rate measured by Gregg and Sanford (1987) ($\epsilon = 1.4\times10^{-10}$ W kg^{-1}), we get 0.73. The deduced flux ratio is very sensitive to the measured dissipation rate and because our mean dissipation rate is very close to the noise level of our instrumentation, our flux ratio should be considered a lower bound.

Our estimates of the oceanic dissipation rates, heat flux and the flux ratio of a double-diffusive interface agrees quit well with the theoretical predictions of Kunze (1987; 1989) but, they all also differ from his model in one crucial way — the heat flux is independent of the mean vertical gradient. The flux is limited by some mechanism internal to the interface even when the interface is thinner than the maximum thickness for contiguous fingers in Kunze's model. Also at variance with all models of double-diffusion is that the microstructure temperature gradient is isotropic Shen 1989; Lueck and Fleury 1989). Therefor, considerable progress has been made towards predicting the fluxes in oceanic double-diffusion but, the physics of oceanic double-diffusion is still not fully understood or modelled.

Bibliography

Gargett, A.E., T.R. Osborn and P.W. Nasmyth, 1984, Local isotropy and the decay of turbulence in a stratified fluid, *J. Fluid. Mech.*, **144**, 231-280.

Gregg M.C. and T.B. Sanford, 1987, Shear and turbulence in thermohaline staircases, *Deep-Sea Res.*, **34**, 1689-1696.

Gregg M.C., 1988, Mixing in the thermohaline staircase east of Barbados, *Small scale turbulence and Mixing in the Ocean*, J.C.J. Nihoul and B.M. Jamart (Editors), 453-470.

Kunze, E., 1987, Limits on growing, finite-length salt fingers: a Richardson number constraint, *J. Mar. Res.*, **45**, 533-556.

Kunze, E., 1989, The evolution of salt fingers in shear, *J. Mar. Res.*, submitted.

Lueck, R.G. and M. Fleury, 1989, Fine and microstructure of a thermohaline interface, in these proceedings.

Lueck, R.G., 1987, Microstructure measurements in a thermohaline staircase, *Deep-Sea Res.*, **34**, 1677-1688.

Marmorino, G.O., W.K. Brown and W.D. Morris, 1987, Two-dimensional temperature structure in the C-SALT thermohaline staircase, *Deep-Sea Res.*, **34**, 1667-1676.

Marmorino G.O., 1989, Substructure of oceanic salt finger interfaces, *J. Geophys.. Res.*, **94**, 4891-4904.

McDougall, T.J. and J.R. Taylor, 1984, Flux measurements across a finger interface at low values of the stability ratio, *J. Mar. Res.*, **42**, 1-14.

Oakey, N.S., 1982, Determination of the rate of dissipation of turbulent energy from simultaneous temperature and velocity shear microstructure measurements, *J. Phys. Oceanogr.*, **12**, 256-271.

Schmitt R. W. 1979, Flux measurements on salt fingers at an interface, *J. Mar. Res.*, **37**, 419-436.

Schmitt R. W., H. Perkins, J.D. Boyd and M.C. Stalcup, 1987, C-SALT: an investigation of the thermohaline staircase in the western tropical North Atlantic, *Deep-Sea Res.*, **34**, 1655-1665.

Shen C. Y., 1989, The evolution of the double-diffusive instability: Salt fingers, *Phys. Fluids*, **5**, 829-844.

Rohr, J.J., E.C. Itsweire, K.N. Helland and C.W. Van Atta, 1988, Growth and decay of turbulence in a stably stratified shear flow, *J. Fluid. Mech.*, **195**, 77-111.

Turner J.S., 1967, Salt fingers across a density interface, *Deep-Sea Res.*, **14**, 599-611.

Vachon P. and R.G. Lueck, 1984, A small combined temperature and conductivity probe. Proceedings of the 1984 STD Conference and Workshop, sponsored by the Marine Technology Society and the MPS Oceanic Instrumentation Committee, San Diego section.

Yamazaki, H. and T. Osborn, 1989, Dissipation estimates for stratified turbulence, *J. Geophys.. Res.*, submitted.

Dive 7

Isotherms:9.05 to 9.55
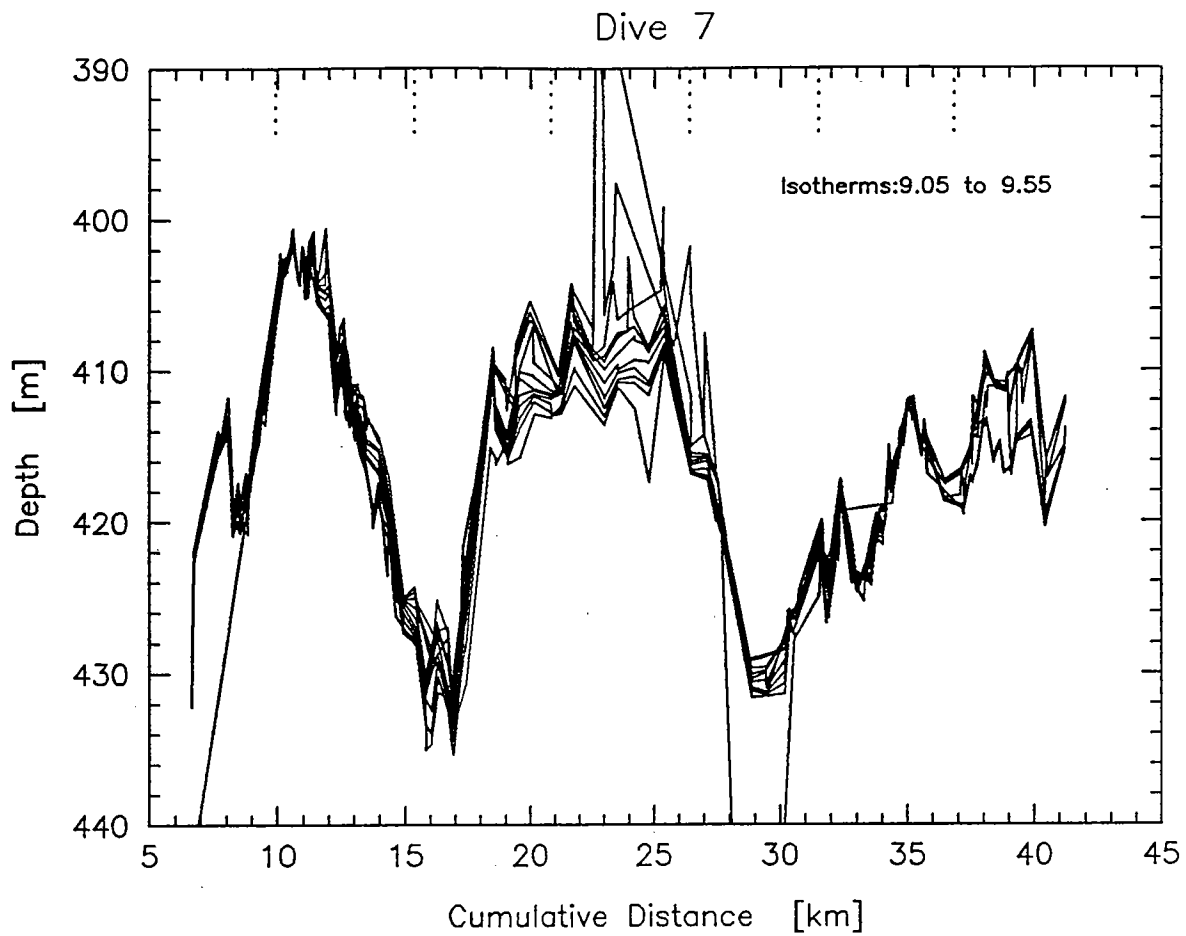
1. Isotherms in intervals of 0.05 °C using the temperature measured at each crossing of the interface. The intersection of some isotherms is an artifact of the plotting algorithm and does not necessarily represent inversions.

Dive 7
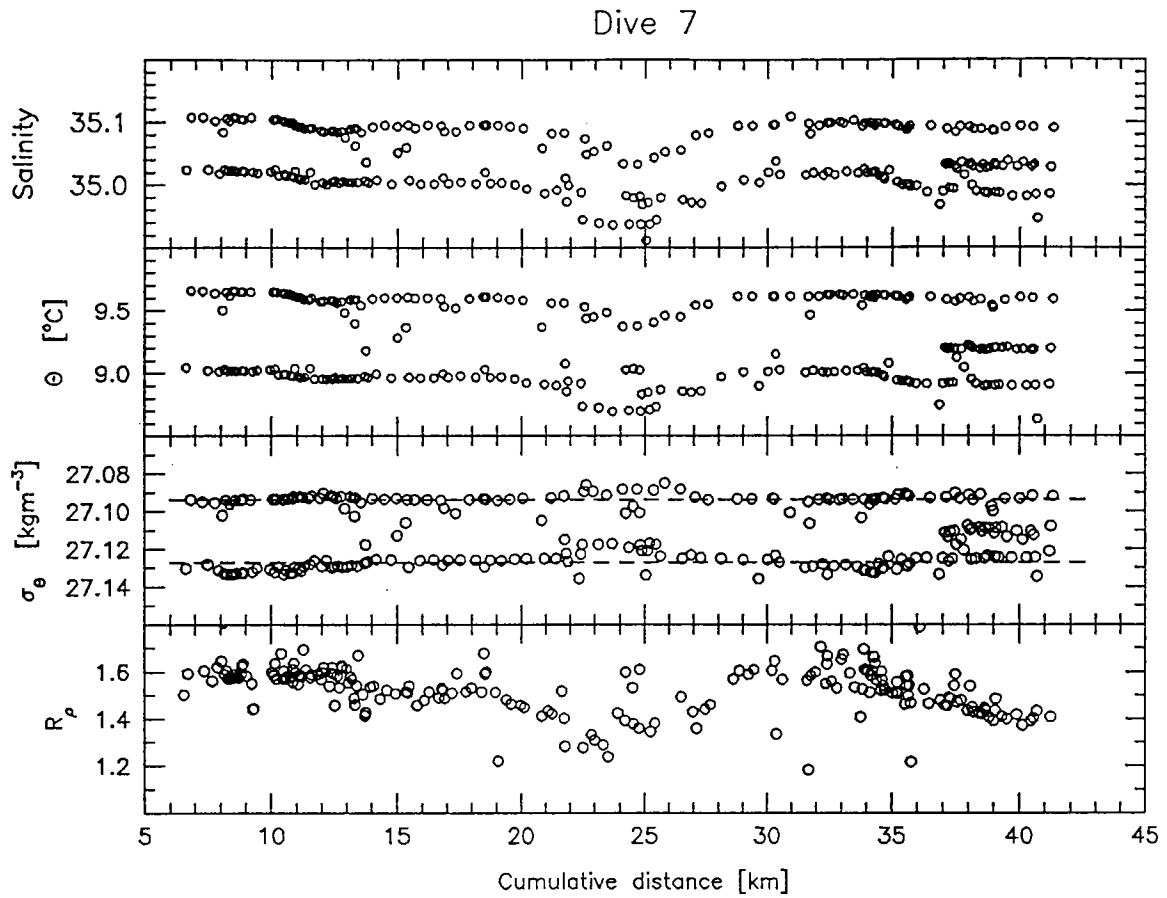
2a. Salinity, potential temperature and density of the upper and lower mixed layers as well as the density ratio of the property differences across the interface. Each point is the average from one-half of each depth cycle of the towed body.

Dive 7
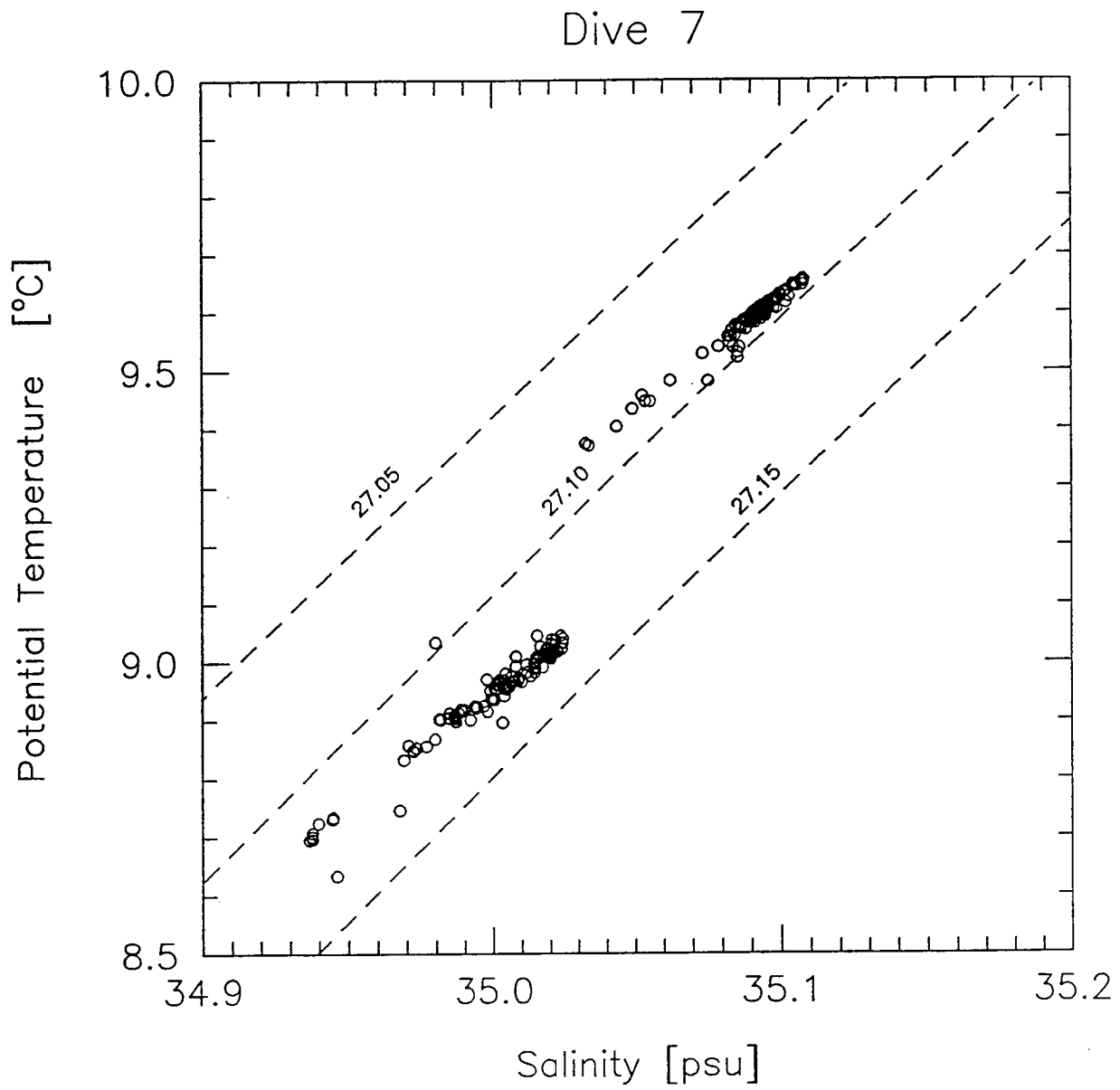
2b. θ-S diagram for the upper and lower mixed layers. The dashed lines are isopycnals. For the upper layer, $\alpha\Delta T \simeq 0.87\beta\Delta S$, and for the lower layer, $\alpha\Delta T \simeq 0.82\beta\Delta S$.

Dive 7
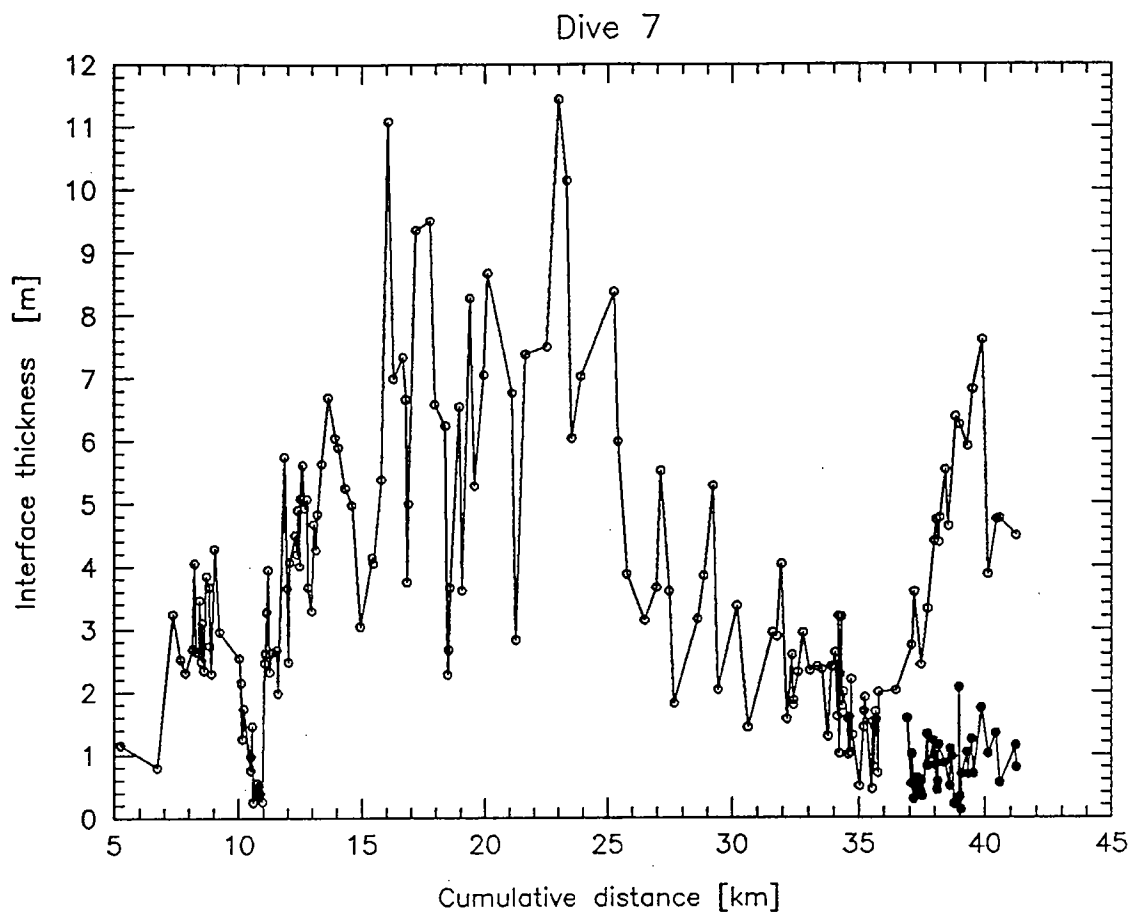
3. Interface thickness. Open circles represent the thickness based on the temperature difference between the upper and lower mixed layers. Filled circles represent the interfaces in the bifurcated region.

Dive 7
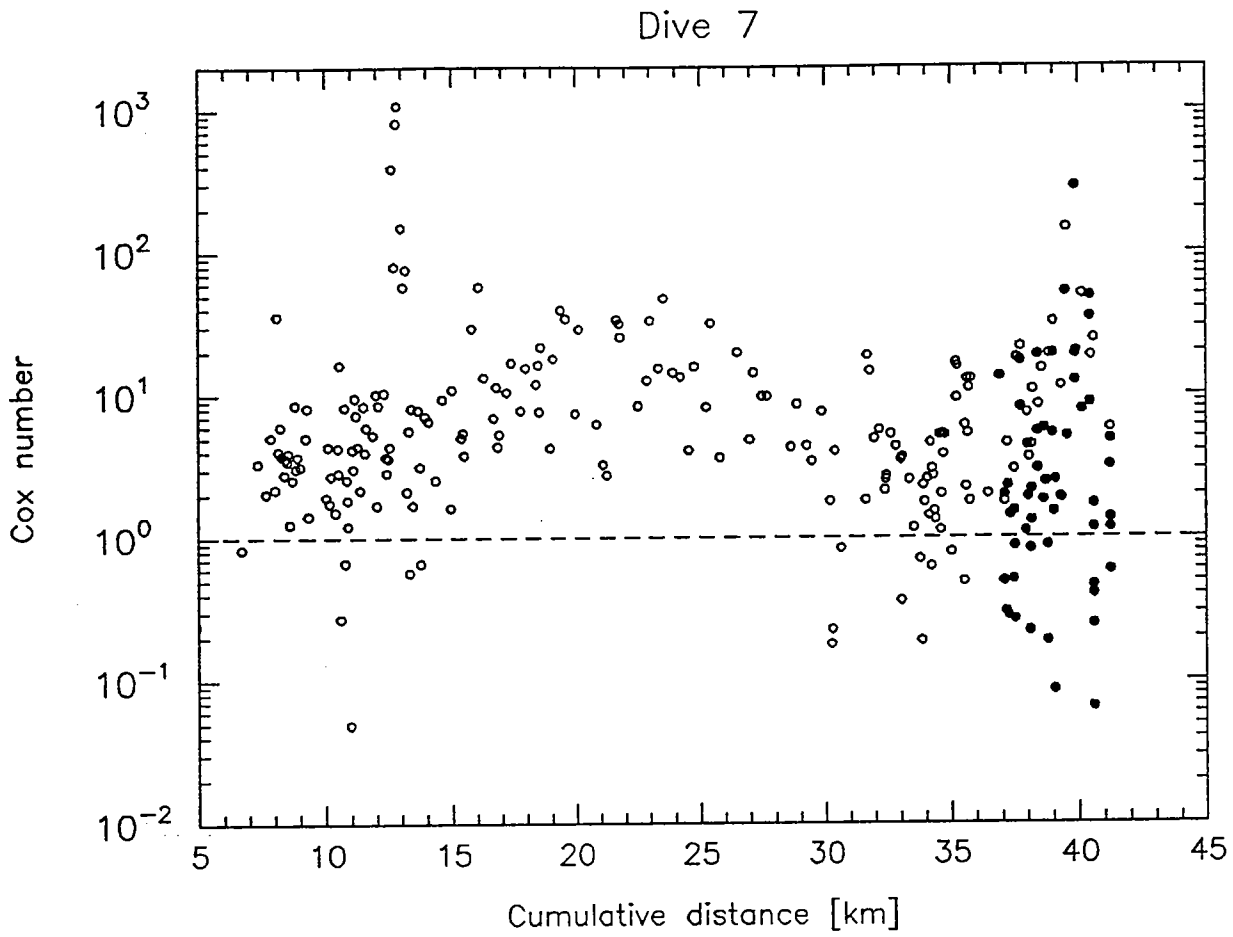
4a. The Cox number, defined by $3<(\partial T/\partial x)^2><\Delta T/t>^{-2}$. The large values (>80) at km 13 come from the turbulent portion of the interface. Filled circles represent the interfaces in the bifurcated region.
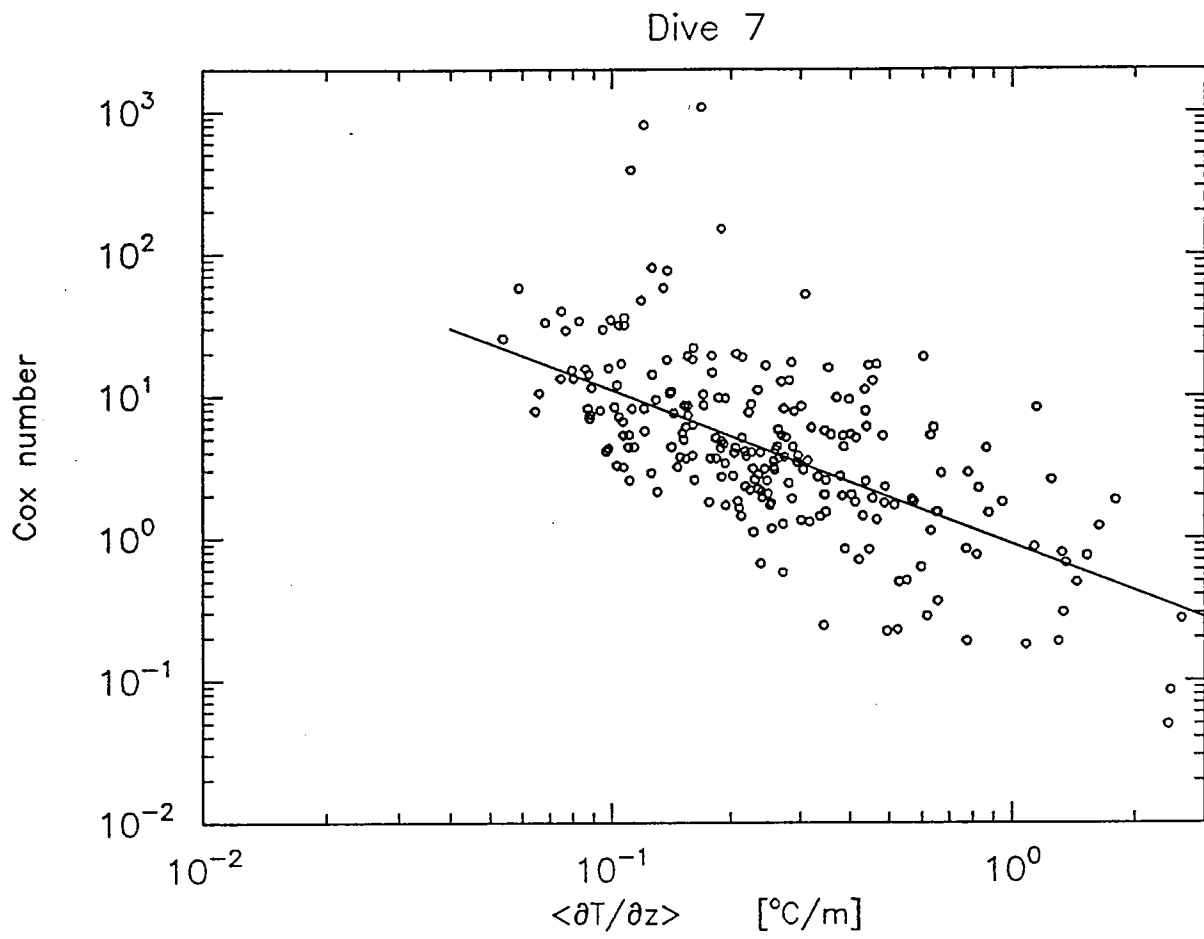
4b. Cox number versus mean vertical temperature gradient. The solid line represents the least-square fit $C = 0.91 \; <\partial T / \partial z>^{-1.08}$.
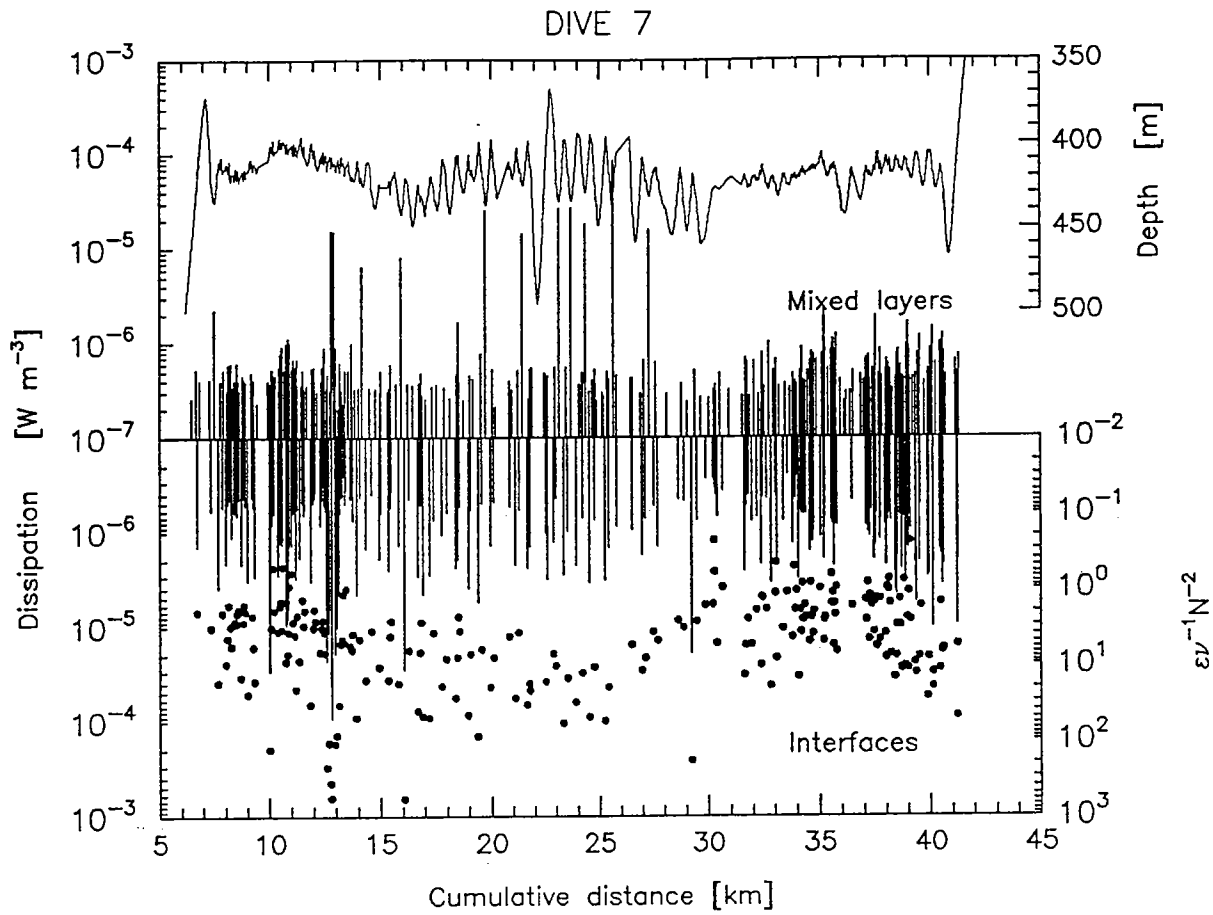
5. The depth profile of the towed body (solid line, upper panel). The mean rate of dissipation from each half cycle of the profile (mixed layers, upper panel; interface, lower panel). The non-dimensional dissipation rate in the interface (dots, lower panel).

Fine and Microstructure of a Thermohaline Interface

R.G. Lueck and M. Fleury
The Johns Hopkins University
Chesapeake Bay Institute
The Rotunda, Suite 315
Baltimore, Maryland 21211
(301) 338-6328

Introduction

The structure of a single double-diffusive interface was examined using data collected during the C-SALT experiment in November 1985 (Schmitt et al. 1987). The interface was located in the central region of the C-SALT site (12° 06′ N, 56° 30′ W) and at mid depth (450 m) where the staircase-like structure of the thermohalocline was well established. The measurements were made from a towed vehicle that repeatedly crossed the interface in a saw-tooth pattern for a total of 220 crossings over a distance of 40 km. The path of the body, while it traversed the interface, was never more than 15° from horizontal. The ship towing our instrument headed north-east at a speed of 2 knots. The thermal structure of the interface was revealed with two thermometers mounted at the nose of the towed body and separated vertically by 0.035 m. Lueck (1987) provided a more detailed description of the instrumentation.

The thickness of the interface varied from 0.2 to 12 m (Fleury and Lueck, 1990) while the temperature difference between the adjacent mixed layers bounding the interface remained nearly constant. The heat flux across the interface was also nearly uniform in contradiction with the models of Kunze (1987, 1989). In the view of Kunze's and other models of double-diffusive interfaces, we have examined the data for evidence of a finger or sheet structure. We will present first the coherence and phase of the transfer function of the temperature gradients measured by the two thermometers. These two signals should be very coherent in a finger and sheet structure. We have also estimated the isotropy of the local temperature gradient because the variance of the horizontal component should be much larger than the vertical component in a structure dominated by sheets or fingers. Finally, we will show some samples of the two-dimensional temperature gradient microstructure observed in the interface.

Coherence of the Temperature Gradients

Evidence for coherence between the signals from our two thermometers was first sought by examining their time series (figure 1). We interpret the time series as a space series because the speed of the body was fairly uniform while it traversed the interface. In the example (figure 1), which

is typical of our observations, the interface was 0.25 m thick, its mean vertical temperature gradient was 2.6 °C m^{-1} and the density ratio was 1.6. The vehicle traversed the interface in a horizontal distance of 3 m. The edges of the interface are clearly defined by the absence of temperature gradients in the adjacent mixed layers (figure 1, $x < 0.3$ m and $x > 3.4$). The value of the thickness is slightly larger than the maximum finger length of 0.21 m predicted by Kunze (1987) when using Kunze's parameter $C_w = 1/2$. Thus, according to his model, the interfacial structure should consist largely of vertical cells with a typical width 0.025-0.05 m. In the presence of shear, cells should transform into sheets aligned with the direction of the shear (Kunze, 1989). Consequently, with or without shear, the signals from the two thermometers should be correlated during most of the crossing of the interface. The signals were indeed dominated by features with wavelength less than 0.1 m, but there is no evidence for a relation between them although some isolated peaks (at $x=2.5$ m and $x=0.5$ m for example) occur simultaneously. Shifting one signal relative to the other does not improve the correlation.

We computed the coherence function Γ and the phase Φ of the transfer function using

$$\Gamma(f) = S_{12}^{2}(f)\, S_{11}^{-1}(f)\, S_{22}^{-1}(f) \tag{1}$$

where C_i is the complex Fourier coefficient computed from a one-second section of the temperature gradient $\partial T_i/\partial x$, $S_{ij} = <C_i C_j^{*}>$ is an ensemble average of these one-second estimates and the subscript identify the sensor. The phase of the transfer function $H(f) = S_{12}(f)\, S_{22}^{-1}(f)$ was computed using

$$\Phi(f) = \tan^{-1}[\mathrm{Im}(H)/\mathrm{Re}(H)] \tag{2}$$

where the functions Re and Im extract the real and imaginary parts of their arguments. Figure 2 shows the coherence and phase for a 400-meter section where the vehicle crossed the interface 6 times and where the thickness of the interface was less than 0.55 m (the section shown in figure 1 is included). The coherence decreases above 1 Hz and approaches zero for frequencies above 4 Hz (or 4 cpm with an average speed of 1 m s^{-1}). The spectra do peak between 10 and 20 cpm, as also noted by Lueck (1987), and this is consistent with the predicted width of fingers. However, no coherence is observed in this spectral range. The phase of the transfer function (figure 2, lower panel) also indicates that the two temperature gradient signals are uncorrelated — the phase is randomly distributed between $\pm\pi$ at frequencies above 4 Hz. Thus, the coherence and the phase show that, over a vertical distance of 0.035 m, the two temperature gradients are not vertically correlated for horizontal wavelength smaller than 0.25 m. This result is not specific to the 400 m long section shown in figure 1. We have

examined various sections for coherence, and even made an estimate for the entire set of observation. None of these efforts revealed any correlation between the two temperature gradient signals.

Isotropy

In a finger or sheet structure, local vertical gradients should be much smaller than horizontal gradients and the ratio of the variance of these two gradients should be small compared to 1. We have estimated the local vertical gradient of temperature using

$$\Delta T_V(x) = [T_1(x) - T_2(x)]/d \tag{3}$$

where $d=0.035$ m is the vertical distance between the upper and lower thermometer. By definition, $\Delta T_V(x)$ is the local mean vertical gradient over the vertical distance d. In order to obtain an estimate of the local horizontal temperature gradient with a spatial smoothing identical to (3), we have estimated the horizontal gradient using

$$\Delta T_{H1}(x) = [T_1(x) - T_1(x+d)]/d \tag{4a}$$

$$\Delta T_{H2}(x) = [T_2(x) - T_2(x+d)]/d. \tag{4b}$$

The two thermometers provide two independent estimates and using $\partial T/\partial x$ directly is incompatible with (3). Three caveats apply to equations 3 and 4. The gradients are not exactly horizontal and vertical, they are not precisely orthogonal and there is some attenuation of variance near the peak of the spectrum. The path of the body deviated from horizontal by as much as 15°. The gradient in (3) is not exactly orthogonal to the vector in (4). The line joining the sensitive tip of the two thermometers was exactly orthogonal to the longitudinal axis of the towed body. However, the direction of travel was not exactly parallel to the axis of the body because of hydrodynamic lift. A comparison of the direction of travel, deduced from the speed and pressure records, against the inclination of the body, inferred from the record of the axial accelerometer, indicates that these two directions differed by as much as 6°. The finite difference applied in equation (3) and (4) acts like a low-pass filter with a null response at $1/0.035 = 28.6$ cpm and a half-power response at 13 cpm. Thus, variance near the peak of the gradient spectrum was attenuated, but the amount of attenuation was the same for both components of the gradient.

For each crossing of the interface we computed the mean variance of ΔT_{H1}, ΔT_{H2} and ΔT_V between the wavenumbers of 1 and 50 cpm. The ratio $<\Delta T_V^2>/<\Delta T_{H1}^2>$ (figure 3) contradicts the notion that the interface was largely composed of fingers or sheets. Instead of being small compared to unity,

the ratio of the variance was generally near 1 and ranged from 0.5 to 6. On average, the variance of the vertical gradient was larger than that of the horizontal gradient and the mean ratio was 1.54. The average of the ratio $<T_V^2>/<T_{H2}^2>$, computed with the gradient measured by the second thermometer, was 10% higher. Spectra of the vertical and horizontal temperature gradients indicate that vertical gradients are larger between 1 and 10 cpm and that the two components are comparable at higher wavenumbers. Thus, the gradients with long length scales (0.1 to 1 m) were somewhat flattened into the horizontal plane while gradients with shorter length scales were close to isotropic. This picture is consistent with the numerical models of Shen (1989) and laboratory observations of Taylor (1990).

Microstructure

The thermal microstructure in the interface is shown by plotting the instantaneous temperature gradient along the path of the vehicle (figure 4a). Sticks are plotted with a density of 64 per meter and represent the orientation and magnitude of the temperature gradient. Because we are interested in the local structure and not merely the variance, equations 3 and 4 are inadequate because the horizontal gradient is displaced by half of one data point. To bring the two components into coincidence, we calculated the horizontal and vertical temperature gradients using

$$[\Delta T_V(x) + \Delta T_V(x+d)]/2 \qquad (5a)$$

$$[\Delta T_{H1}(x) + \Delta T_{H2}(x)]/2 \qquad (5b)$$

where the variables are given in (3) and (4). Thus, the sticks (in figure 4a) show the local gradient smoothed equally in the vertical and horizontal direction over a distance of 0.035 m. In the first example considered, the temperature from one sensor and the two components of the gradient are plotted against depth (figure 4b). The interface was 0.56 m thick and had fairly sharp edges. Its mean vertical temperature gradient was 1.15 °C m^{-1} and the density ratio was 1.6. The profile (figure 4b indicates that the temperature stratification was weakly disturbed — the mean vertical gradient was comparable to the rms fluctuations. The local gradient was directed upwards with only small variations in its orientation. When the interface was thicker, the structure was different. A stick diagram of a subsection of a crossing is shown in figure 5. The interface was well defined, was 0.75 m thick, had a mean temperature gradient of 0.9 °C m^{-1} and a density ratio of 1.6. The sticks are orientated randomly with numerous inversions (sticks pointing downward) and this structure was frequently observed when the interface was about 1 to 2 meters thick. Vertical cells and sheets should produce horizontal gradients (horizontal sticks) alternating in directions over length scales of

0.025-0.05 m. This was not observed and figure 5 suggests an eddy-like structure. The last example selected was relatively rare (figure 6). The interface was 2.0 m thick, its mean gradient was 0.3 °C m^{-1} and the density ratio was 1.6. The portion between $x=7.8$ and 9 m contained a contiguous inversion with a vertical scale of 0.5 m. The sticks veered towards a normal orientation above depth 404.0 m and the structure below 404.8 m was eddy-like. There was no enhanced dissipation of kinetic energy associated with the temperature inversion, in fact, the non-dimensional dissipation rate $\epsilon(\nu N^2)^{-1}$ was 2, much too small for a turbulent mixing process (Rohr et al. 1988). Thus, it appears likely that the structure revealed by figure 6 represents a density compensated intrusion *inside* an interface.

Conclusion

A finger- or sheet-like structure was not observed in the thermohaline interface although the conditions were favorable to the formation of such a structure — a density ratio of 1.6 and a well defined staircase. Two temperature sensors separated vertically by 0.035 m and moving nearly horizontally showed no coherence at wavelengths shorter than 0.25 m. Thus, although the peak of the gradient spectra (10-20 cpm) is in agreement with the theoretical width of the "fingers", no coherence was observed at this scale and fingers do not appear to be present. An eddy-like structure describes the interface more appropriately. A comparison between the vertical and horizontal temperature gradients indicates that the structures were isotropic at length scales shorter than 0.1 and that it was slightly flattened into the horizontal plane at length scales 0.1 to 1 m. The average variance of the vertical gradient exceeded the variance of the horizontal gradient. Stick diagrams of the temperature gradient vector also suggest an eddy-like structure, although some parts of the interface were hardly disturbed away from a layered pattern.

The observed structures undoubtedly represent the result of double diffusion because the heat flux across the interface could not have been generated by shear induced turbulence (Fleury and Lueck, 1990). The wide variety of microstructure observed may be related to the large (1 decade) scatter of the heat flux estimated by Fleury and Lueck. Our observations agree qualitatively with the numerical simulation of Shen (1989) and the laboratory experiments of Taylor (1990). The buoyancy driven motions that would otherwise lead to the formation of sheets and fingers appear to be suppressed before these motions form structures with vertical length scales exceeding their horizontal scales. This may account for the absence of coherence at a vertical separation of 0.035 m, and Kunze's (1987) Richardson number constraint may not be the first factor limiting the growth of fingers and the flux associated with them.

Bibliography

Kunze, E., 1987: Limits on growing, finite-length salt fingers: a Richardson number constraint. *J. Mar. Res.*, **45**, 533-556.

Kunze, E., 1989: The evolution of salt fingers in shear. *J. Mar. Res.*, submitted.

Fleury, M. and R.G. Lueck, 1990: Horizontal variations of a thermohaline interface. In these proceedings.

Lueck, R.G., 1987: Microstructure measurements in a thermohaline staircase. *Deep-Sea Res.*, **34**, 1677-1688.

Schmitt, R.W., H. Perkins, J.D. Boyd and M.C. Stalcup, 1987: C-SALT: an investigation of the thermohaline staircase in the western tropical North Atlantic. *Deep-Sea Res.*, **34**, 1655-1665.

Shen, C.Y., 1989: The evolution of the double-diffusive instability: Salt fingers. *Phys. Fluids*, **5**, 829-844.

Rohr, J.J., E.C. Itsweire, K.N. Helland and C.W. van Atta, 1988: Growth and decay of turbulence in a stably stratified shear flow. *J. Fluid. Mech.*, **195**, 77-111.

Taylor, J., 1990: Laboratory investigation of the effect of initial interface thickness on the evolution of salt fingers. In these proceedings.
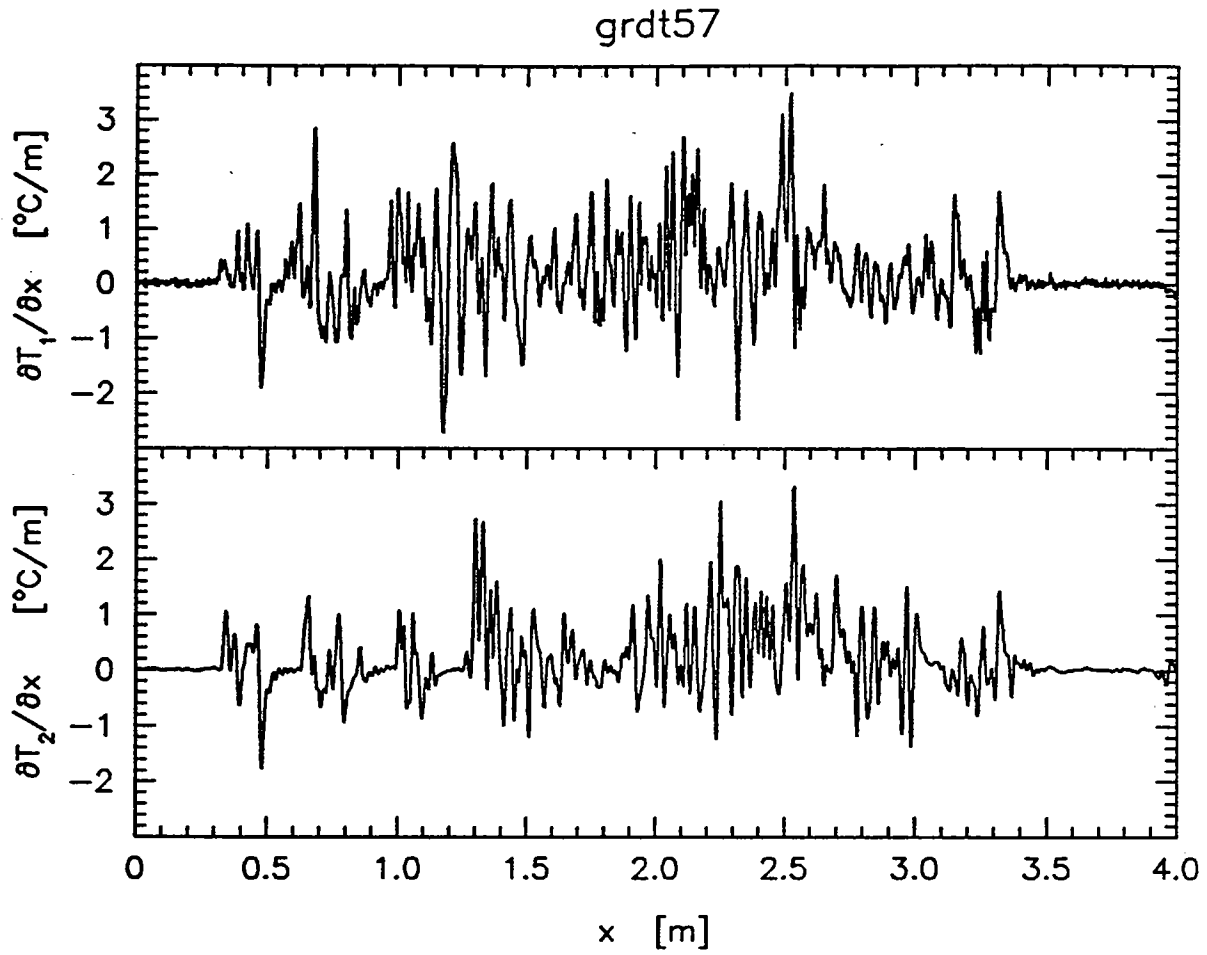
Figure 1. Temperature gradients in an interface from the two sensors separated vertically by 0.035 m. The interface was 0.25 m thick.
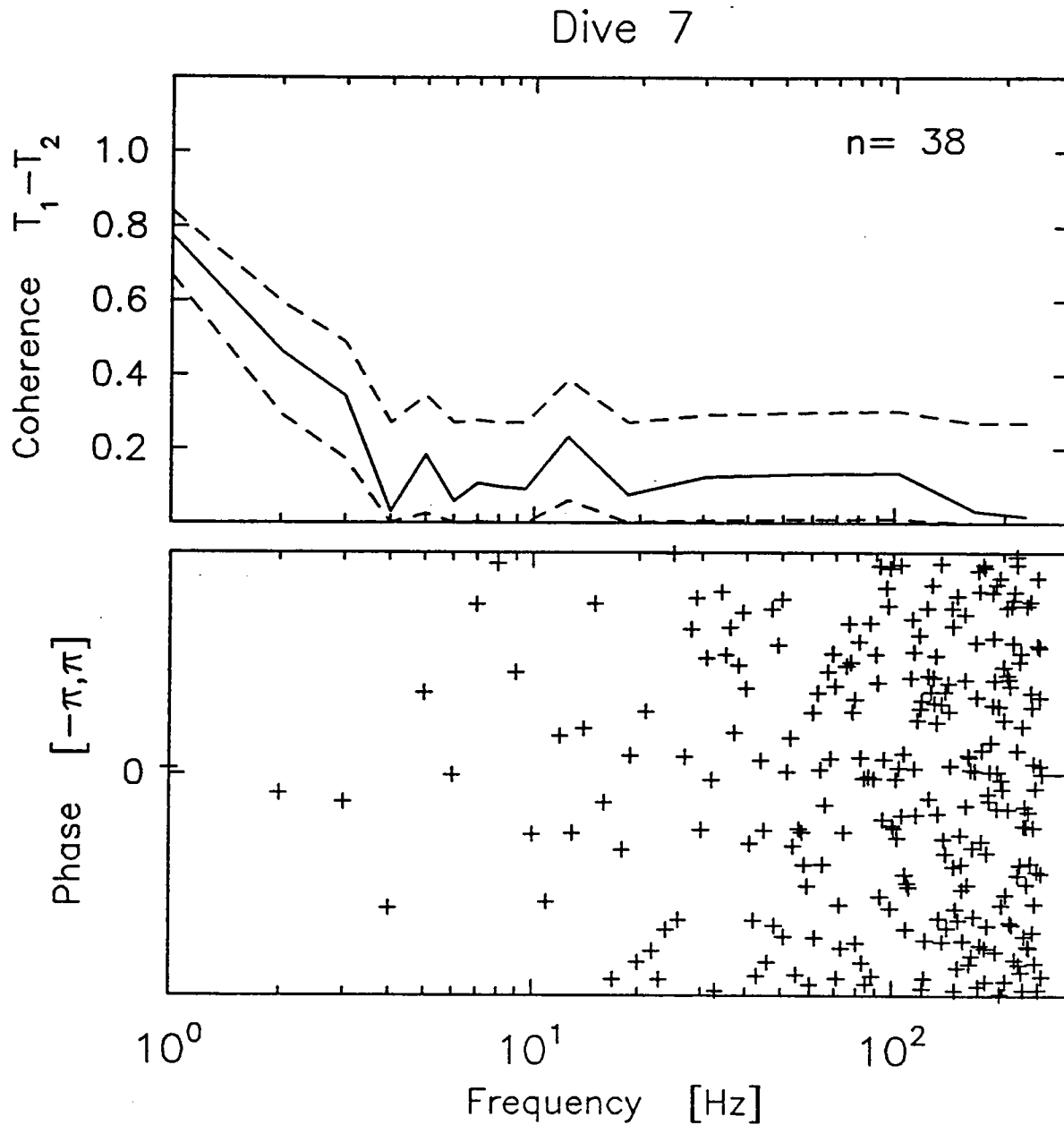
Figure 2. Coherence function (upper panel, solid line) and phase of the transfer function (lower panel) between the two thermometers separated vertically by 0.035 m. Dashed lines show the 90% confidence interval. The data were collected on 6 successive crossings of the interface where its thickness ranged from 0.25 to 0.55 m.
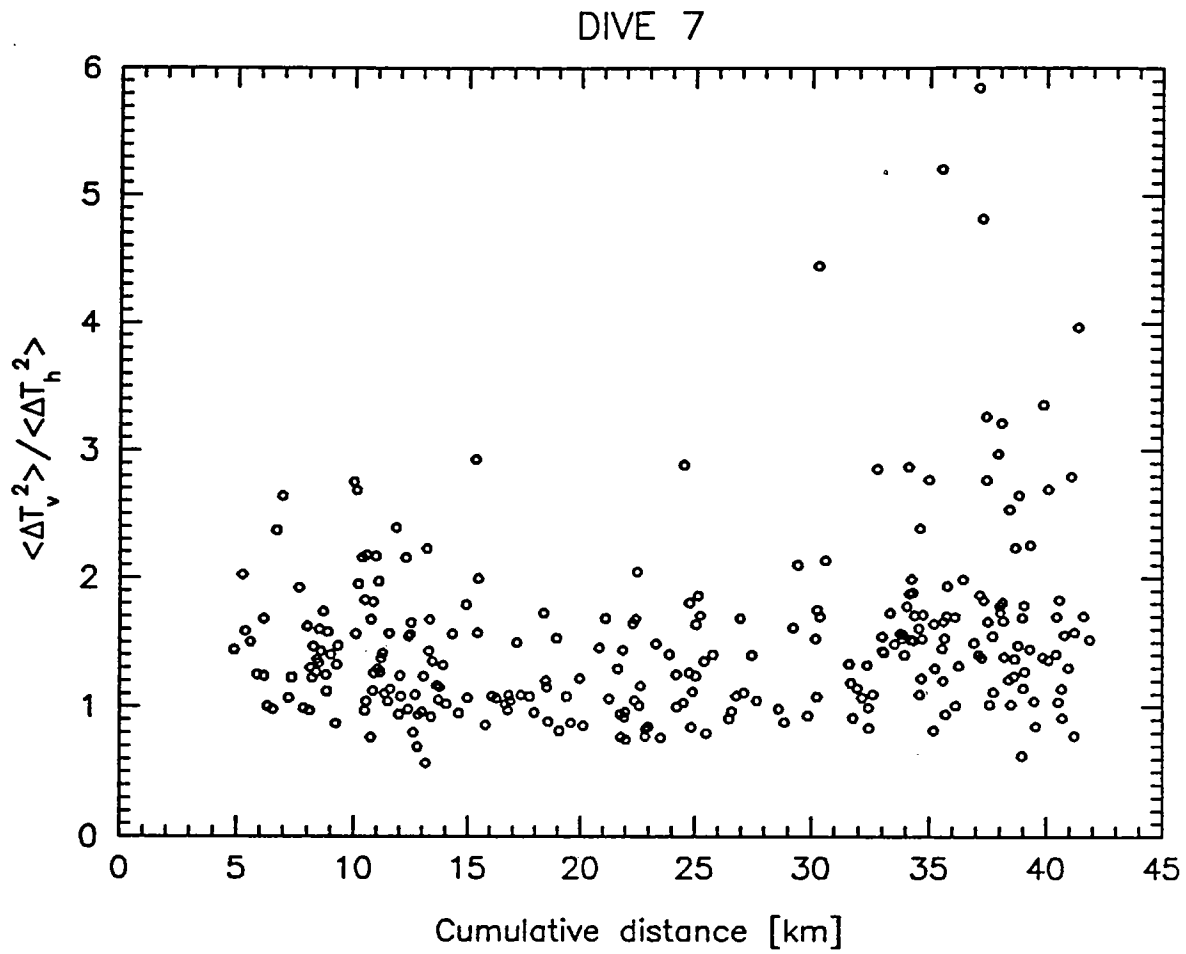
Figure 3. Ratio of the variance of the vertical temperature gradient and the variance of the horizontal temperature gradient at each crossing of the interface.
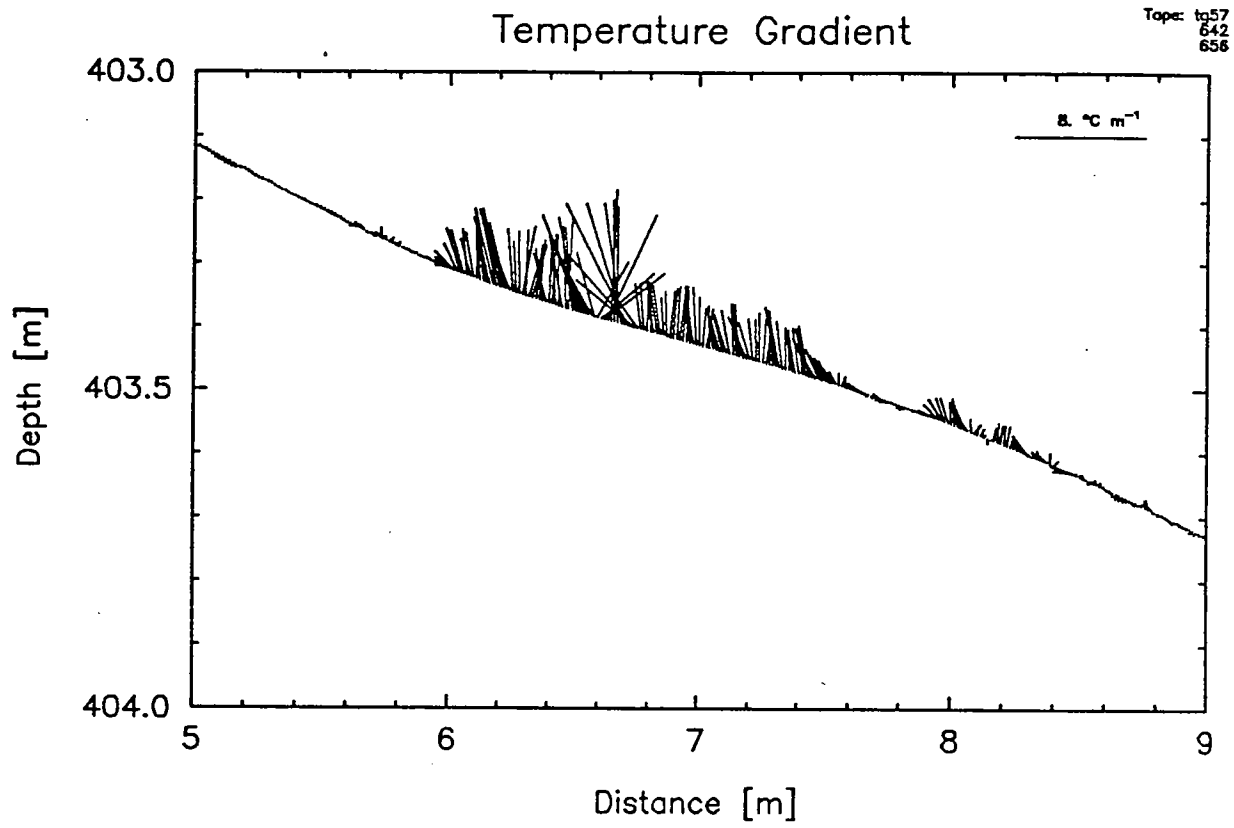
Figure 4a.   Stick diagram of the temperature gradient vector smoothed over 0.035 m in the interface while it was 0.56 m thick. The density ratio was 1.6 and mean vertical gradient was 1.15 °C m^{-1}.
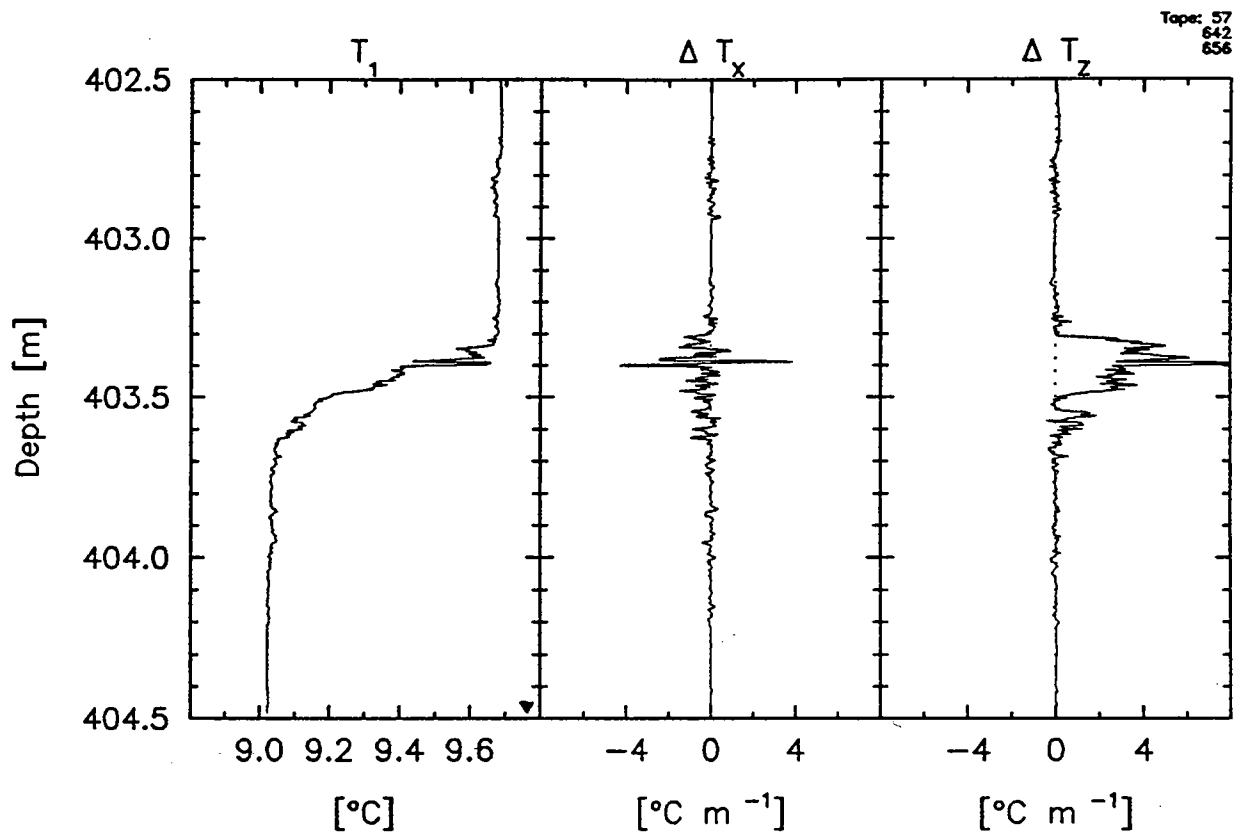
Figure 4b.   Vertical profile of temperature from one of the sensors and the two components of the local gradient.
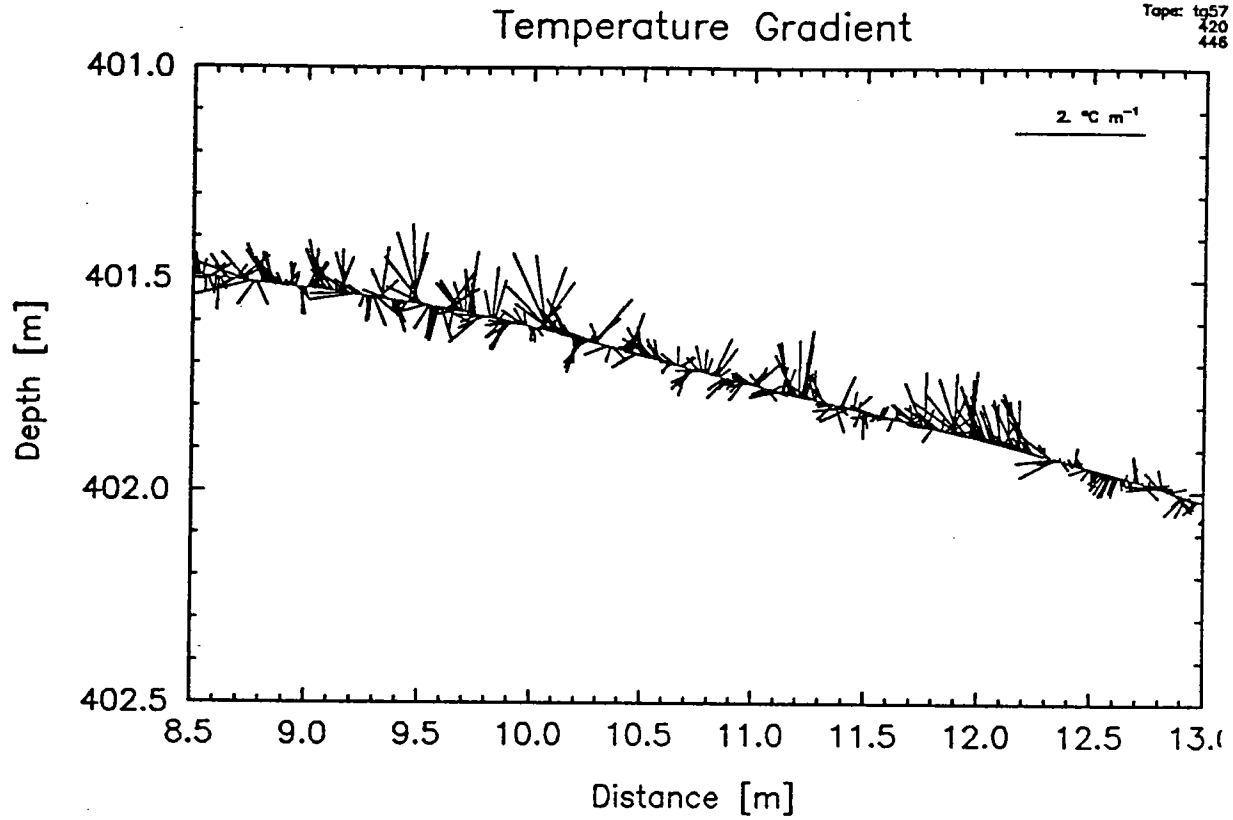
Figure 5. Stick diagram of the temperature gradient in a portion of the interface where it was 0.75 m thick. The density ratio was 1.6 and mean vertical gradient was 0.9 °C m^{-1}.
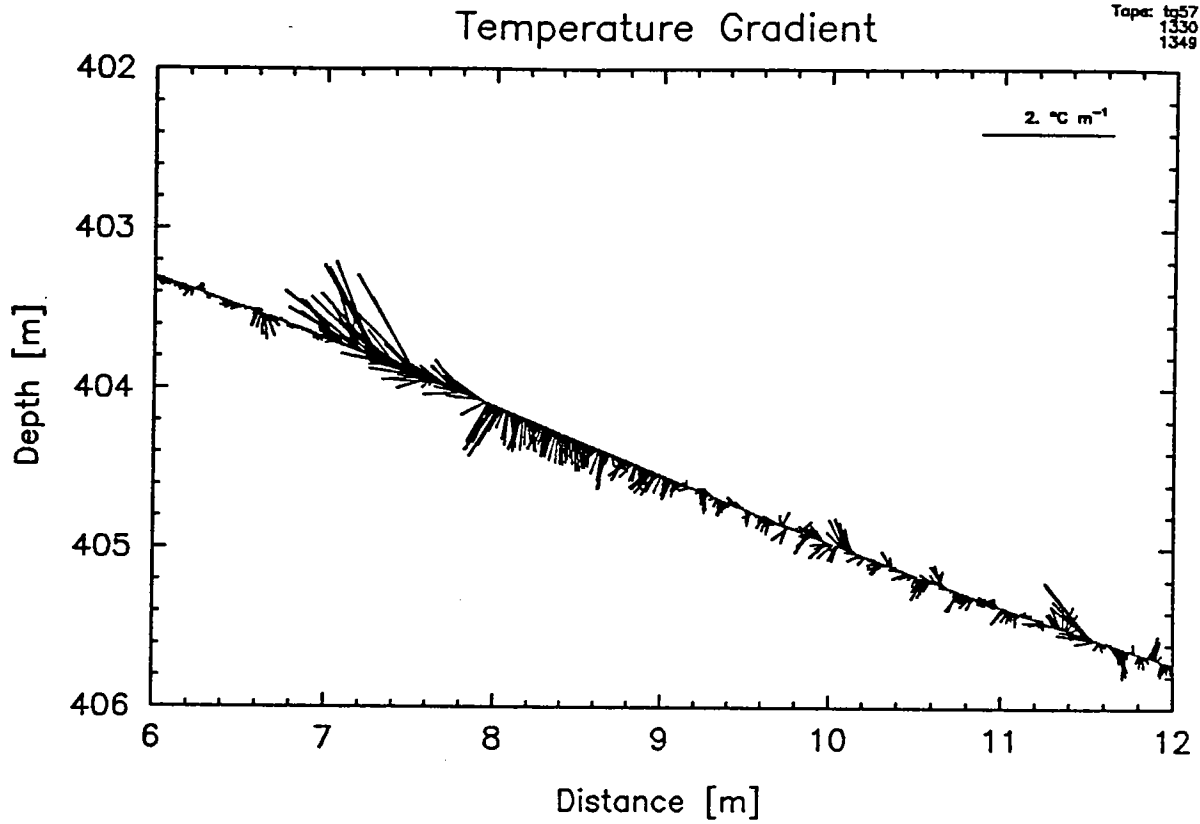
Figure 6. Stick diagram of the temperature gradient where the interface was 2.0 m thick. The density ratio was 1.6 and mean vertical gradient was 0.3 °C m^{-1}.

THE BEHAVIOR OF SALT FINGERS IN SHEAR

Eric Kunze
School of Oceanography, WB-10, University of Washington, Seattle, WA 98195

ABSTRACT

Shadowgraph profiles collected in the thermohaline staircase east of Barbados reveal nearly-horizontal banding -- unlike the vertical banding found in other fingering-favorable parts of the ocean. A plausible interpretation of this optical microstructure is that vertical shear is tilting over the fingers. This paper sketches results from a model for shear-tilting of fingers (to appear described in greater detail in Kunze, *J. Mar. Res.*, 1989). The $0.4N$ inertial wave shear observed during C-SALT would tilt over and damp out square planform $(k_x=k_y)$ fingers so rapidly that they could not produce significant fluxes. Vertical *sheets* aligned with the shear $(k_y=0)$ will behave like unsheared fingers provided the shear is steady. But because oceanic shear is dominantly near-inertial, turning with time to produce a component of shear normal to sheet crests, sheets will ultimately be tilted over. This happens slowly enough that they can grow to significant lengths. When such growing, tilting sheets are limited by a critical inverse finger Richardson number, $(\nabla x V)^2/N^2 \sim 3\text{-}8$, the model is able to reproduce the observed microstructure and inferred fluxes in C-SALT within our uncertainty. However, this constraint does not explain the density ratio dependence in laboratory studies and numerical simulations. What constrains the growth of fingers needs to be better understood.

INTRODUCTION

This note describes the effect of vertical shear on salt fingers to try to explain the nearly-horizontal laminae observed with a shadowgraph profiler in the fingering-favorable thermohaline staircase east of Barbados (Kunze et al., 1987). The strong correlation between the presence of laminae and fingering-favorable conditions in the profiles suggests that they are in some way connected with the salt-fingering form of double-diffusive instability.

A model for salt sheets in an inertially-rotating shear can reproduce the spatial structure of temperature and salinity inferred from the C-SALT microstructure measurements (Lueck, 1987; Marmorino et al., 1987; Gregg and Sanford, 1987; Kunze et al., 1987). The inferred fluxes (Gregg and Sanford, 1987) and flux ratio (Schmitt, 1988; McDougall, 1989) can be reproduced by a combination of growing, tilting sheets and molecular diffusion if it is assumed that the growth of the sheets is disrupted at a critical inverse finger Richardson number, $(\nabla x V)^2/N^2 \sim 3\text{-}8$. The Schmitt flux ratio deduced from the layer density ratio (0.85) would constrain the dissipation rates, fluxes and Cox numbers to the lower bounds allowed by the measurements. Smaller finger flux ratios imply larger finger fluxes in this model. McDougall's inferences from the nonlinearity of the equation of state suggest that the layer density ratio cannot be used as a constraint on the flux ratio, and that interface migration $(R_F=R_\rho=1.6)$ must be making a contribution. If this is true, then all that can be said about the combined finger/molecular flux ratio is that it must be less than one to produce a staircase.

EQUATIONS OF MOTION

The equations of motion for tilted salt fingers in a uniform shear U_z are

$$\frac{\partial u}{\partial t} + \boxed{U\,\frac{\partial u}{\partial x}} - \nu\nabla^2 u + U_z w = -\frac{\partial p}{\partial x}$$

$$\frac{\partial w}{\partial t} + \boxed{U\,\frac{\partial w}{\partial x}} - \nu\nabla^2 w = \boxed{-\frac{\partial p}{\partial z}} + g(\alpha\delta T - \beta\delta S)$$

$$\frac{\partial \delta T}{\partial t} + \boxed{U\,\frac{\partial \delta T}{\partial x}} - \kappa_T\nabla^2\delta T + T_z w = 0 \tag{1}$$

$$\frac{\partial \delta S}{\partial t} + \boxed{U\,\frac{\partial \delta S}{\partial x}} - \kappa_S\nabla^2\delta S + S_z w = 0$$

$$\boxed{\frac{\partial u}{\partial x} + \frac{\partial w}{\partial z} = 0}$$

(Kunze, 1989). The terms in boxes are those not found for unsheared salt fingers (Stern, 1960). These include (i) the u-momentum equation, (ii) a pressure term in the w-momentum equation , (iii) conservation of mass and (iv) advection $U\partial/\partial x$ by the background flow [in double boxes]. Looking for solutions proportional to $exp[i(k_x x + k_y y + k_z z)]$, Kunze (1989) showed that (1) could be reduced to a diagnostic equation for w and two evolution equations

$$w = \frac{g(\alpha\delta T - \beta\delta S)}{\nu k^2(1+s^2) - sU_z}$$

$$\frac{D\delta T}{Dt} = -\kappa_T k^2 \delta T - T_z w \tag{2}$$

$$\frac{D\delta S}{Dt} = -\kappa_S k^2 \delta S - S_z w.$$

In a shear field, the finger wavevector will be continuously-deformed just as with internal waves in shear (e.g., Lighthill, 1978; Phillips, 1966). From WKB theory (e.g., Frankignoul, 1970; Olbers, 1981), the fingers preserve their horizontal wavenumber but their vertical wavenumber changes continuously

$$\boxed{\frac{dk_z}{dt} = -k_x U_z}\,. \tag{3}$$

A NUMERICAL MODEL

In this section, the evolution of fingers in shear is examined numerically. Equations (2)-(3) were solved with a Runge-Kutta routine (Press *et al.*, 1986) using a time-step of $2\pi/(200N)$. Environmental parameters were set to values typical of the interfaces in the thermohaline staircase east of Barbados (Kunze, 1989) and the fingers given initial seed heights $h_o=2w_o/\sigma_o=\pi/(2k_o)$, where k_o is the total wavenumber and σ_o is the associated growth rate at $t=0$ (see Kunze, 1989).

Linden's (1974) laboratory experiments demonstrated that the dominant double-diffusive instability in steady shear was vertical sheets aligned with the shear $(k_x=0)$. However, the shear in the C-SALT staircase is not steady but near-inertial (Gregg and Sanford, 1987). Therefore, if fingers start growing as sheets aligned with the shear $(k_x, k_y)=(k_H, 0)$, where the shear is in the y-direction initially, then as time progresses the shear will rotate, $(U_z,V_z)=|V_z|(sin(ft),cos(ft))$, introducing a slowly-growing component of the shear normal to the sheets which will cause them to tilt over.

Fig. 1 displays the normalized (by their initial values) vertical finger gradients of temperature and salinity, $T_z/|\nabla_o T_o|$ and $S_z/|\nabla_o S_o|$ as functions of vertical wavelength. Recall that the vertical wavenumber is increasing in magnitude in time (3). Thus, the vertical wavelength diminishes in time and time increases to the left. As the sheets grow, the temperature- and salinity-gradients increase until molecular diffusion smooths out their structure. This occurs at a wavelength of *3 cm* for temperature and *1 cm* for salt. The salt wavelength is identical to that of the optical striations in the shadowgraph images, supporting the hypothesis that the observed laminae are due to salt. The temperature scale is larger than the salt scale, but not as large as the *6-cm* temperature vertical wavelength reported by Gregg and Sanford (1987). This may be the scale at which the sheets go unstable.

FLUXES

Replicating the scales of the observed microstructure does not guarantee that the model can reproduce the observed fluxes. If the model is appropriate, it should also be able to provide the flux ratio, $R_F\sim0.85$ (Schmitt *et al.*, 1987) or $R_F<1.0$ (McDougall, 1989), dissipation rates $(\varepsilon\sim5\times10^{-10}$ *W/kg* in the interfaces and *1.4×10^{-10} W/kg* in the layers; Gregg and Sanford, 1987) and Cox numbers (*6-30*; Gregg and Sanford, 1987; Marmorino *et al.*, 1987; Lueck, 1987) deduced from the C-SALT measurements.

McDougall (1989) deduced a flux ratio of *1.4* from the layer density ratio (0.85) and the nonlinearity of the equation of state. He argued that this was made up of a contribution from fingers and molecular diffusion $(R_F<1)$, and interface migration $(R_F=R_\rho=1.6)$; the combined finger/diffusion flux must have a flux ratio less than one to produce and maintain a staircase (Kelley, 1988). Internal wave-generated turbulence appears to be too weak to produce significant interface fluxes.

Allowing sheets to grow unrestricted by any amplitude constraint produces average dissipation rates and buoyancy-fluxes two orders of magnitude greater than observed. Therefore, some constraint must limit the growth of sheets.

What limits the magnitude of salt-fingering fluxes in the laboratory and ocean has been a longstanding question in the field, and is still unresolved. Stern (1969) proposed that
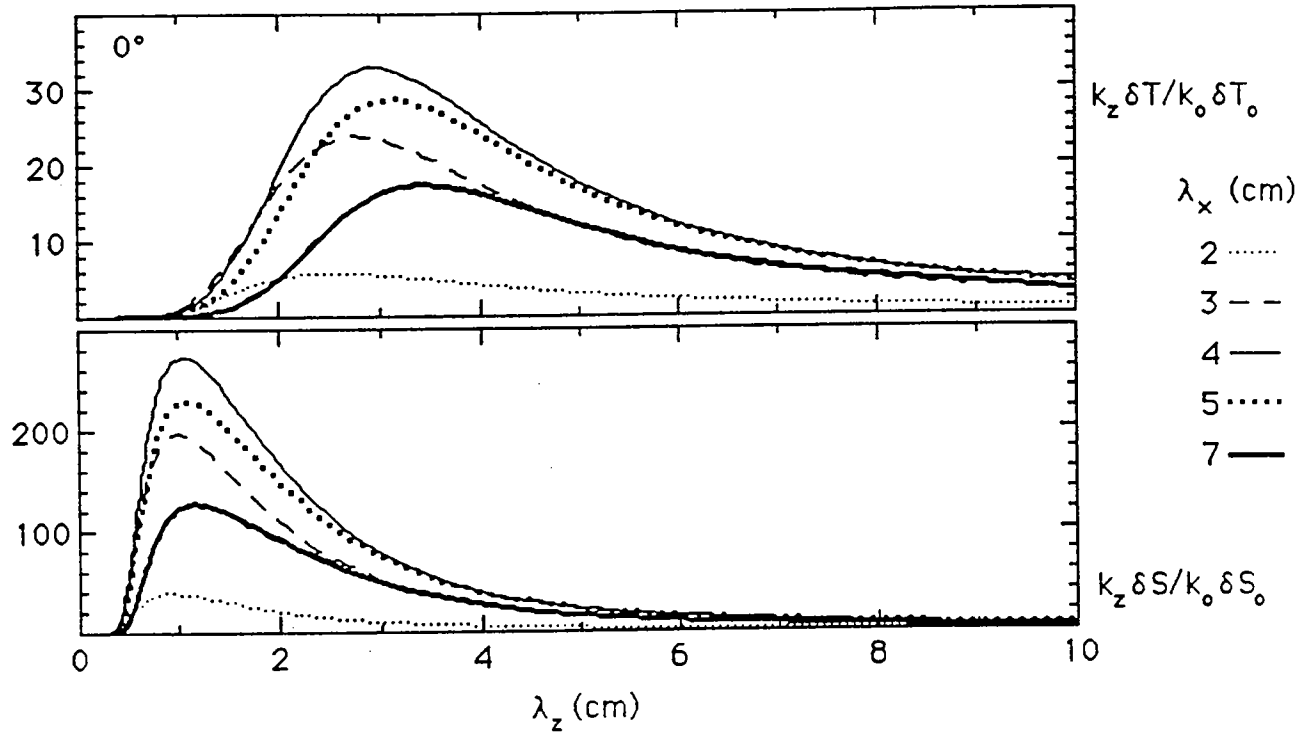
Figure 1: Normalized vertical temperature- (upper panel) and salinity-gradients (lower panel) *vs* vertical wavelength for horizontal wavelengths of *2-7 cm*. The vertical wavelength decreases in time, so time increases to the left. As fingers grow, their vertical gradients increase until the wavelength becomes sufficiently small that molecular diffusion eradicates the signature. This occurs at a vertical wavelength of *3 cm* for temperature and *1 cm* for salt.

fingers grow until their normalized buoyancy-flux, $F_b/\nu N^2$ (henceforth referred to as the Stern number, A), exceeds a critical value $\sim O(1)$. Then their fluxes are disrupted by (collective) instability of the fingers. Holyer (1981) showed that the Stern number should be 1/3, however, in a later paper (1984) identified a different instability which arose at Stern numbers $\sim O(10^{-2})$.

For vertical fingers, the Stern number is identical to an inverse *finger* Richardson number, $Ri_f^{-1} = (\nabla x V)^2/N^2 = (\nabla_H w)^2/N^2$ (Kunze, 1987), where the horizontally-sheared vertical velocity replaces the vertically-sheared horizontal velocity of the more familiar Richardson number. Fig. 2 displays laboratory (Schmitt, 1979; McDougall and Taylor, 1984; Taylor and Bucens, 1989) and computer simulation (Shen, 1989; Whitfield *et al.*, 1989) estimates of the *average approximate* Stern number $\beta\langle F_S\rangle/(\nu \overline{a T_z})$ as a function of density ratio R_ρ along with model curves of this quantity (Kunze, 1987) for *critical* $A = Ri_f^{-1} = 4$, 8 and 16 (assuming fastest-growing fingers). Neither the lab nor numerical results support fingers being disrupted at Stern numbers $\sim O(10^{-2})$ although Whitfield *et al.* (1989) report that perturbations on fingers grew at growth rates consistent with Holyer (1984). The numerical values (Shen 1989; Whitfield *et al.*, 1989) might be questioned because the simulations are two-dimensional and correspond to Prandtl and Lewis numbers much closer to one than appropriate for heat-salt fingers. Taylor and Bucens (1989) suggest that the very high values found at very low R_ρ by McDougall and Taylor (1984) may be due to their unique initial conditions. Nevertheless, the fact that numerical simulations and laboratory measurements independently give very high Stern numbers at low R_ρ raises doubts about the applicability of the Stern number constraint.

This constraint will be used all the same. For the constant density ratio found in C-SALT, the density ratio dependence in Fig. 2 is not a serious concern. It will be assumed that new sheets are initiated immediately after the old sheets go critical (unstable). Therefore, averaging is carried out from $t=0$ to the time t_c when the critical inverse finger Richardson number is exceeded.

The first fingers to become critical for $Ri_f^{-1}_c = 4$ (at $Nt_c/2\pi = 5.5$, lowermost panel in Fig. 3) correspond to fastest-growing vertical fingers initially ($\lambda = \lambda_x \sim 3$ cm, $\theta_0 \sim 0°$). They have the Schmitt (1988) flux ratio but average dissipation rates, buoyancy-fluxes and Cox numbers a factor of three smaller than the C-SALT observations. Choosing a larger critical inverse finger Richardson number will reproduce the C-SALT dissipation rate, buoyancy-flux and Cox number as well as be more consistent with Fig. 2, but then the flux ratio will be lower than the Schmitt value. This is not a concern if we believe McDougall's (1989) arguments that the layer density ratio is not identical to the flux ratio and that interface migration must be contributing to the layer properties. Alternatively, all the C-SALT microstructure investigators assumed isotropy and therefore multiplied their measured variances by a factor of three. Reducing their values by the same amount also reconciles them with the first sheets to go critical in Fig. 3. Arguing against this alternative, Lueck (1989) presents evidence for near-isotropy in the interface microstructure.

The sensitivity of the fluxes is examined assuming that when the fastest-growing sheets go unstable, they disrupt the fluxes associated with other sheets and so dominate the overall fluxes. Fig. 4 displays the average flux ratio, dissipation rate, buoyancy-flux, Cox number, and final tilt angle as functions of initial conditions and critical inverse finger Richardson number. The range of values inferred from the C-SALT measurements is stippled (with account taken for anisotropy). There is little or no sensitivity to the initial conditions as a consequence of nearly exponential growth but there *is* dependence on the
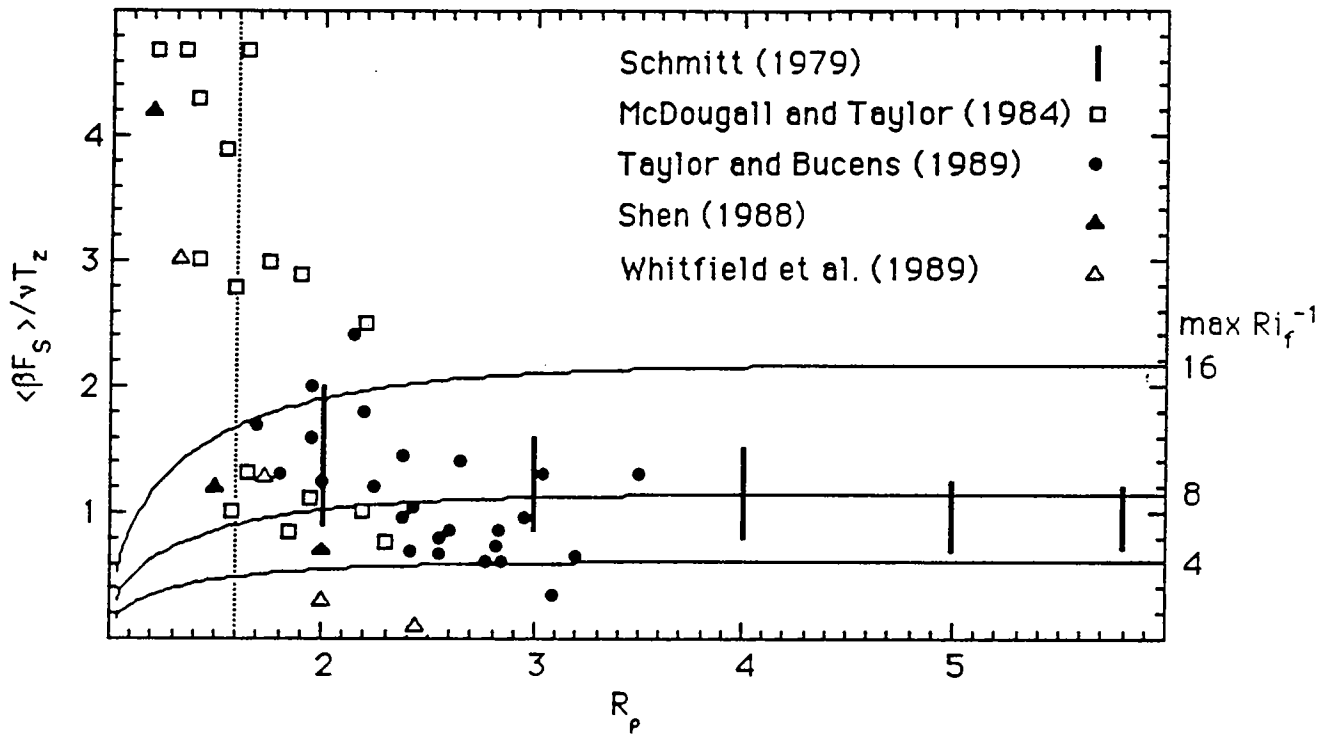
Figure 2: *Average* approximate Stern number $\beta\!<\!F_S\!>\!/\nu\overline{\alpha T}_z$ vs density ratio R_ρ from laboratory measurements and numerical simulations. The solid curves are model (Kunze, 1987) values for various *critical Ri_f^{-1}* (numbers along right axis). For $R_\rho\!>\!1.5$, most of the data are consistent with critical $Ri_f^{-1}\!=\!4\text{-}16$. Taylor and Bucens (1989) suggest that the very high values at low R_ρ found by McDougall and Taylor (1984) may be due to their unique initial conditions. However, similar values are found in numerical simulations.

Figure 3: The *average* flux ratio R_F, dissipation rate $<\varepsilon>$, buoyancy-flux $<F_b>$, Cox number $<C_T>$ and time $Nt_c/2\pi$ the sheets take to reach critical inverse finger Richardson number of *4* as a function of horizontal wavelength and initial tilt angle. The first sheets to go unstable are marked by the patch of stippling ($Nt_c/2\pi=5.5$). They have wavelengths and initial tilts corresponding to fastest-growing fingers ($\lambda_x=3$ *cm*, $\theta_0=0°$). Their flux ratios are ~0.8-0.85, dissipations ~$13x10^{-11}$ *W/kg*, buoyancy-fluxes ~$5-6x10^{-11}$ *W/kg* and Cox numbers *2*. The ridge of high dissipation $<\varepsilon>$ and buoyancy-flux $<F_b>$ running from $\lambda_x=3$ *cm*, $\theta_0=0°$ to ~*8 cm*, *60°* corresponds to sheets which initially have *total* wavelengths equal to the fastest-growing wavelength. Thus, for a given tilt, sheets with the fastest-growing wavelength ultimately grow more than sheets of higher or lower wavenumber.

$(Ri_f^{-1} = 4)$
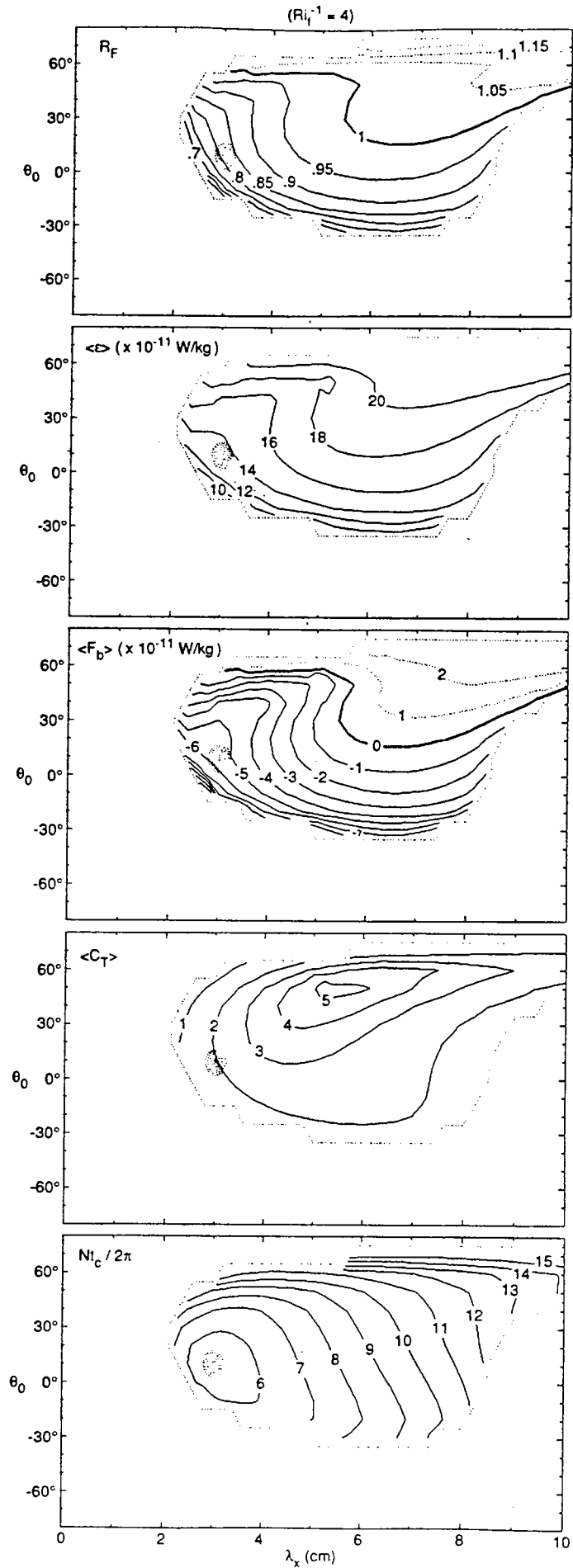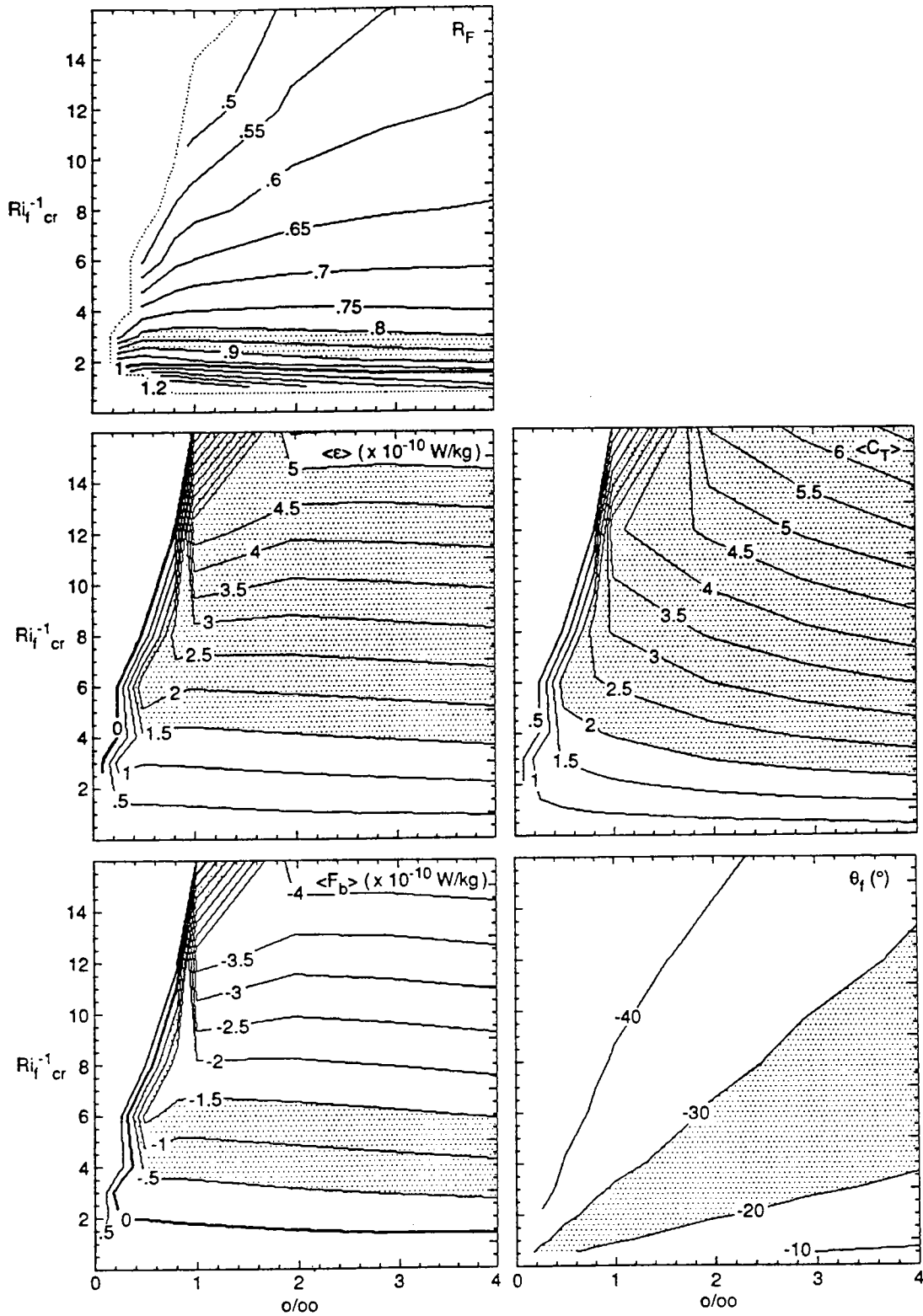
Figure 4: Contours of average flux ratio R_F, dissipation rate $<\varepsilon>$, buoyancy-flux $<F_b>$, Cox number $<C_T>$ and final tilt angle θ_f for the first sheets to go critical ($\lambda_x=3$ cm, $\theta_o=0°$) as a function of critical inverse finger Richardson number Ri_f^{-1} and initial conditions. Stippling indicates the range of C-SALT observations. These are consistent with a critical inverse finger Richardson number of 3-8.

critical inverse finger Richardson number. The Schmitt flux ratio provides the strongest constraint on R_{if}^{-1}, limiting it to a range of 2-3. On the other hand, the C-SALT layer buoyancy-flux implies a critical R_{if}^{-1} of 3-6 and the interface Cox number and dissipation rates imply critical values of 4-16. McDougall's (1989) arguments indicate that the flux ratio is not a useful constraint. The remaining measured quantities allow critical Richardson numbers between 4-6. This is commensurate with the laboratory and numerical estimates (Fig. 2) at $R_p=1.6$.

But if the sheets go unstable before being fully tilted over, the question arises of how the optical microstructure is produced. This is easily addressed. Instability of the sheets will disrupt fluxes and smooth both velocity and temperature microstructure because of the higher molecular diffusivities associated with these quantities. But passive salinity microstructure will remain on scales too small to drive vertical motions and will continue to be sheared until it reaches the 1-cm wavelength where molecular diffusion can eradicate it.

CONCLUSIONS

To summarize, the model results will be reviewed to see how they fare against the C-SALT observations. The 1-cm limiting wavelength for salt is identical to the wavelength of the optical shadowgraph microstructure (Kunze et al., 1987), supporting the hypothesis that the Laplacian of the index of refraction emphasizes the smallest scales which will be dominated by salt because of its very low molecular diffusivity.

Constraining finger growth with a critical inverse finger Richardson number $(\nabla \times V)^2/N^2$ of ~3-8 reproduces the C-SALT microstructure (Fig. 3) within our present uncertainty. Initially vertical sheets with horizontal wavelengths of ~3 cm are the first to go unstable. This is consistent with the ~6 cm observed with towed thermistors and conductivity sensors (Marmorino et al., 1987; Lueck, 1987) when account is taken that towed sensors cross the finger crests at random orientations which leads to a overestimate bias of ~1.5. At maximum amplitude, these sheets have tilt angles of ~20-30° (vertical wavelengths of 5-6 cm), consistent with the vertical temperature microstructure (Gregg and Sanford, 1987). The nearly-horizontal 1-cm laminae in the shadowgraph images appear to be salt remnants that have continued to be shear-tilted long after instability has disrupted the finger fluxes and molecular processes have smoothed the temperature and velocity microstructure.

The critical Stern or inverse finger Richardson number $R_{if}^{-1}{}_c \sim 3\text{-}8$ is the weakest link in this model. Laboratory measurements and numerical simulations (Schmitt, 1979; McDougall and Taylor, 1984; Shen, 1989; Whitfield et al., 1989; Taylor and Bucens, 1989) contain much scatter at the low density ratios of oceanographic interest. More laboratory and numerical studies are needed in the $R_p=1\text{-}2$ regime.

In light of these results and the prevalence of near-inertial shear in the ocean, it is difficult to explain how vertical banding could be observed anywhere. Internal wave shear was weaker (~0.4N) in, above and below the C-SALT thermohaline staircase than the 0.7-1.0N typically found in the pycnocline (Garrett and Munk, 1979; Evans, 1981). It may be that below the Mediterranean salt tongue and in the Tyrrhenian Sea (Williams, 1975), shear is so weak that vertical fingers can grow unhindered. This would require shears <0.1N.

The model fluxes are sensitive to density ratio R_p and the magnitude of the near-inertial shear. Higher density ratios or shears leads to a smaller finger contribution to the total flux so that the combined finger/molecular flux ratio is greater than one. For a flux ratio greater than one, the buoyancy-flux is downgradient or 'diffusive' and tends to smooth

finestructure, preventing formation and maintenance of a staircase (Kelley, 1988). This sensitivity may explain why well-defined thermohaline staircases are found in only a few locales despite most of the upper Central waters being favorable to fingering.

Finally, gross diffusivities are estimated by normalizing the average fluxes by gradients smoothed over the staircase structure. The diffusivity of heat $\sim 1.5 \times 10^{-5}$ m^2/s is only slightly greater than molecular while that of salt $\sim 3 \times 10^{-5}$ m^2/s is mostly due to fingers. The model salt diffusivity is an order of magnitude larger than the inferred eddy diffusivity due to turbulence in a diffusively-stable (no fingering) regime with a GM level internal wave field (Gregg and Sanford, 1988). This is because fingers are more efficient at transporting heat and salt than turbulence. While for turbulent mixing $K \sim e \cdot \varepsilon/N^2$ where the mixing efficiency $e=0.1-0.2$, for salt-fingering $K \sim [(R_\rho-1)/(1-R_F)] \cdot \varepsilon/N^2$ where the 'efficiency' $[(R_\rho-1)/(1-R_F)] \sim 1-3$ (Hamilton et al., 1989; Schmitt, 1988). Thus, fingers may be the principal agent of water-mass change on timescales of decades.

REFERENCES

Evans, D.L., 1981: Velocity shear in a thermohaline staircase. Deep-Sea Res., 28A, 1409-1415.

Frankignoul, C.J., 1970: The effect of weak shear and rotation on internal waves. Tellus, 22, 194-203.

Garrett, C., and W. Munk, 1979: Internal waves in the ocean. Ann. Rev. Fluid Mech., 11, 339-369.

Gregg, M.C., and T.B. Sanford, 1987: Shear and turbulence in thermohaline staircases. Deep-Sea Res., 34, 1689-1696.

Gregg, M.C., and T.B. Sanford, 1988: The dependence of turbulent dissipation on stratification in a diffusively stable thermocline. J. Geophys. Res., 93, 12,381-12,392.

Hamilton, J.M., M.R. Lewis and B.R. Ruddick, 1989: Vertical fluxes of nitrate associated with salt fingers in the world's oceans. J. Geophys. Res., 94, 2137-2145.

Holyer, J.Y., 1981: On the collective instability of salt fingers. J. Fluid Mech., 110, 195-207.

Holyer, J.Y., 1984: The stability of long, steady, two-dimensional fingers. J. Fluid Mech., 147, 169-185.

Kelley, D.E, 1988: Explaining effective diffusivities within diffusive oceanic staircases. Small-scale Turbulence and Mixing in the Ocean, J.C.J. Nihoul and B.M. Jamart, Eds., Elsevier, The Netherlands, 481-502.

Kunze, E., 1987: Limits on growing, finite-length salt fingers: A Richardson number constraint. J. Mar. Res., 45, 533-556.

Kunze, E., 1989: The evolution of salt fingers in shear. J. Mar. Res., (submitted).

Kunze, E., A.J. Williams III and R.W. Schmitt, 1987: Optical microstructure in the thermohaline staircase east of Barbados. Deep-Sea Res., 34, 1697-1704.

Lighthill, J., 1978: Waves in Fluids. Cambridge University Press. 504pp (317-337).

Linden, P.F., 1974: Salt fingers in a steady shear flow. Geophys. Fluid Dyn., 6, 1-27.

Lueck, R.G., 1987: Microstructure measurements in a thermohaline staircase. Deep-Sea Res., 34, 1677-1688.

Lueck, R.G., 1989: (this proceedings).

Marmorino, G.O., W.K. Brown and W.D. Morris, 1987: Two-dimensional temperature structure in the C-SALT thermohaline staircase. Deep-Sea Res., 34, 1667-1676.

McDougall, T.J., 1989: The need for interface migration in C-SALT to explain the lateral heat-to-salt ratio of 0.85. (this proceedings).

McDougall, T.J., and J.R. Taylor, 1984: Flux measurements across a finger interface at low values of the stability ratio. *J. Mar. Res.*, **42**, 1-14.

Olbers, D.J., 1981: The propagation of internal waves in a geostrophic current. *J. Phys. Oceanogr.*, **11**, 1224-1233.

Phillips, O.M., 1966: *The Dynamics of the Upper Ocean.* Cambridge University Press, 261pp.

Press, W.H., B.P. Flannery, S.A. Teukolsky and W.T. Vetterling, 1986: *Numerical Recipes: the Art of Scientific Computing.* Cambridge University Press, 818 pp. (547-577).

Schmitt, R.W., 1979: Flux measurements at an interface. *J. Mar. Res.*, **37**, 419-436.

Schmitt, R.W, 1988: Mixing in a thermohaline staircase. *Small-scale Turbulence and Mixing in the Ocean*, J.C.J. Nihoul and B.M. Jamart, Eds., Elsevier, The Netherlands, 435-452.

Schmitt, R.W., H. Perkins, J.D. Boyd and M.C. Stalcup, 1987: C-SALT: An investigation of the thermohaline staircase in the western tropical North Atlantic. *Deep-Sea Res.*, **34**, 1655-1666.

Shen, C.Y., 1989: The evolution of the double-diffusive instability: salt fingers. *Phys. Fluids A*, **1**, 829-844.

Stern, M.E., 1960: The "salt-fountain" and thermohaline convection. *Tellus*, **12**, 172-175.

Stern, M.E., 1969: Collective instability of salt fingers. *J. Fluid Mech.*, **35**, 209-218.

Taylor, J., and P. Bucens, 1989: Laboratory experiments on the structure of salt fingers. *Deep-Sea Res.*, (submitted).

Whitfield, D.W.A., G. Holloway and J.Y. Holyer, 1989: Spectral transform simulations of finite amplitude double-diffusive instabilities in two dimensions. *J. Mar. Res.*, **47**, 241-265.

Williams, A.J. 3rd, 1975: Images of ocean microstructure. *Deep-Sea Res.*, **22**, 811-829.

FIGURE CAPTIONS

Figure 1: Normalized vertical temperature- (upper panel) and salinity-gradients (lower panel) vs vertical wavelength for horizontal wavelengths of *2-7 cm.* The vertical wavelength decreases in time, so time increases to the left. As fingers grow, their vertical gradients increase until the wavelength becomes sufficiently small that molecular diffusion eradicates the signature. This occurs at a vertical wavelength of *3 cm* for temperature and *1 cm* for salt.

Figure 2: *Average* approximate Stern number $\beta<F_S>/v\alpha\bar{T}_z$ vs density ratio R_ρ from laboratory measurements and numerical simulations. The solid curves are model (Kunze, 1987) values for various *critical Ri_f^{-1}* (numbers along right axis). For $R_\rho>1.5$, most of the data are consistent with critical $Ri_f^{-1}=4\text{-}16$. Taylor and Bucens (1989) suggest that the very high values at low R_ρ found by McDougall and Taylor (1984) may be due to their unique initial conditions. However, similar values are found in numerical simulations.

Figure 3: The *average* flux ratio R_F, dissipation rate $<\varepsilon>$, buoyancy-flux $<F_b>$, Cox number $<C_T>$ and time $Nt_c/2\pi$ the sheets take to reach critical inverse finger Richardson number of *4* as a function of horizontal wavelength and initial tilt angle. The first sheets to go unstable are marked by the patch of stippling ($Nt_c/2\pi=5.5$). They have wavelengths and initial tilts corresponding to fastest-growing fingers ($\lambda_x=3$ *cm,* $\theta_o=0°$). Their flux ratios are ~0.8-0.85, dissipations ~$13x10^{-11}$ *W/kg,* buoyancy-fluxes ~$5\text{-}6x10^{-11}$ *W/kg* and Cox numbers *2.* The ridge of high dissipation $<\varepsilon>$ and buoyancy-flux $<F_b>$ running from $\lambda_x=3$ *cm,* $\theta_o=0°$ to ~*8 cm,* *60°* corresponds to sheets which initially have *total* wavelengths equal to the fastest-growing wavelength. Thus, for a given tilt, sheets with the fastest-growing wavelength ultimately grow more than sheets of higher or lower wavenumber.

Figure 4: Contours of average flux ratio R_F, dissipation rate $<\varepsilon>$, buoyancy-flux $<F_b>$, Cox number $<C_T>$ and final tilt angle θ_f for the first sheets to go critical ($\lambda_x=3$ *cm,* $\theta_o=0°$) as a function of critical inverse finger Richardson number Ri_f^{-1} and initial conditions. Stippling indicates the range of C-SALT observations. These are consistent with a critical inverse finger Richardson number of *3-8.*

NUMERICAL MODELING OF SALT FINGERS AT A DENSITY INTERFACE

Colin Y. Shen
Ocean Dynamics Branch, Code 5140
Acoustics Division, Naval Research Laboratory
Washington, D. C. 20375

Abstract

This paper summarizes results from numerical modeling of salt fingers at a density interface by means of pseudospectral computation. The evolution of the fingers at the interface is described for a heat-salt fluid system, a sugar-salt fluid system in a Hele Shaw cell and an ad hoc unity-Prandtl-number fluid. Specific results summarized address issues concerning the structure of the interfacial fingering zone and the finger fluxes. These include the verification of the theoretical finger scale predicted previously based on the hypothesis of finger growth rate maximization and its equivalent buoyancy flux maximization. An interpretation is also made of existing theoretical and laboratory flux results that take into account the evolving mean stratifications of the diffusive components in the fingering zone. The importance of the evolving mean stratifications in limiting the finger zone thickness is pointed out. Finally, the possible existence of a saturated equilibrium finger spectrum is described.

1. Introduction

A recent development in the study of salt fingers is the direct numerical computation of the evolution equations for salt fingers. This approach allows more complete modeling of the double-diffusive fingering processes than possible previously. The computation so far has been restricted mainly to a two-dimensional domain in order to achieve maximum resolution of disparate finger scales. The results so obtained nevertheless remain relevant and useful since the double-diffusive fingering processes occur in both two and three dimensions; valuable insight into the processes can still be gained with the two-dimensional modeling.

This paper presents a summary of recent results from numerical modeling of salt fingers at a density interface between two uniform fluids. The interfacial salt-fingering processes have received considerable attention in the literature both theoretically and experimentally. Here the numerical models are useful for testing existing salt-finger hypotheses as well as for interpreting some recent laboratory measurements. The results summarized are drawn from the present author's own work, in which fingers between two convecting mixed layers are modeled as in the laboratory situation. The entire evolution of the fingers from initial growth to fully developed mixed layer convection is obtained in the computation. The initial finite-amplitude growth stage has also been simulated numerically by Piacsek and Toomre (1980) and Whitfield, et al (1989); both simulations obtained finger growth structures consistent with the ones reported here.

This paper is organized as follows: In Sec.2, numerical experiments on salt fingering at a density interface are summarized. In Sec.3, simulation results from numerical experiments are presented to address three main issues presently of interest in the analytical modeling of fingers. These concern the vertical stratification of the diffusing components in the interface, the limiting condition for finger height, and the buoyancy flux and growth rate maximizations. In Sec.4 different flux results obtained from theories and experiments are interpreted. In Sec.5, evidence for the existence of an equilibrium salt-finger spectrum is given. A proposed model for such a spectrum is briefly described.

2. Numerical Experiments

The numerical salt-finger experiments summarized here were carried out on the Cray X/MP at the Naval Research Laboratory. For the simulations three different kinds of fluid systems were

tried: the heat-salt fluid, the sugar-salt fluid, and ad hoc two-component fluids of low viscosity-to-diffusivity ratios in the range of 1 to 10. The heat-salt and sugar-salt fluids are common types of fluids used in the laboratory experiments. The ad hoc fluids with low viscosity-diffusivity ratios are hypothetical. They serve mainly to provide additional parameter values for comparison with the heat-salt and sugar-salt fluids, both of which have a high viscosity-to-diffusivity ratio of about 10^3. The numerical experiments for these three systems are all similar in design, i.e., two uniform density layers are separated by a horizontal interface and contained in a square computation domain. There is a difference, however, with the sugar-salt system which is further assumed to be contained in a Hele Shaw cell (a narrow gap tank). This choice is made so that the resulting finger structure can be compared directly to the laboratory observation of sugar-salt fingers in a Hele Shaw cell (Taylor and Veronis, 1986), which has so far provided the clearest visualization of finger structure. Another reason is that the narrow gap of the cell constrains the finger motion to be two-dimensional. Thus, the condition in the Hele Shaw cell is closest to the two-dimensional computation of salt fingers, which is employed in all the numerical experiments described here.

The governing equations for salt fingers assume (as usual) an incompressible fluid, a linear equation of state for the fluid density, and a Boussinesq approximation of the density. In two-dimensional form, the equations are as follows:

$$\frac{\partial \nabla^2 \psi}{\partial t} = J(\psi, \nabla^2 \psi) - \frac{g}{\rho_o}\frac{\partial \rho'}{\partial x} + \nu \nabla^4 \psi$$

$$\frac{\partial T}{\partial t} = J(\psi, T) + \kappa_T \nabla^2 T$$

$$\frac{\partial S}{\partial t} = J(\psi, S) + \kappa_S \nabla^2 S$$

$$\frac{\rho'}{\rho_o} = \alpha(T - \bar{T}) + \beta(S - \bar{S})$$

where ψ is the streamfunction, $\nabla^2 \psi$ is the vorticity, and $J(\psi,) = \frac{\partial \psi}{\partial x}\frac{\partial}{\partial z} - \frac{\partial \psi}{\partial z}\frac{\partial}{\partial x}$. The diffusive density components are denoted by T and S, with T being the more rapidly diffusing one; $\bar{T}$ and $\bar{S}$ denote the respective horizontal averages. The constants, α and β, are the respective density contraction (or expansion) coefficients; for a heat-salt system, α is negative. The constant ρ_o is a reference density, and g is gravity. Finally, ν, κ_T, and κ_S are the kinematic viscosity and the diffusivities for T and S, respectively. In the Hele Shaw case the appropriate viscous term is $-\mu \nabla^2 \psi$ which replaces the $+\nu \nabla^4 \psi$ term above, and the momentum equation is reduced to a balance between the buoyacny term and the viscous term. Here $\mu = \nu/d^2$ is the Darcy drag coefficient with d denoting the gap width of the Hele Shaw cell.

The boundary conditions for T'($=T-\bar{T}$), S'($=S-\bar{S}$) and ψ in the above set of equations are periodic. Such boundary conditions dictate that the amount of fluxes leaving and entering the computation box always remains equal. In salt-finger convection this has the effect of maintaining, on average, a constant density difference between the two fluid layers, which allows the convection to possibly reach a statistical equilibrium state. This is in distinct contrast to the, "run down", situation in the laboratory salt-finger experiment in which convection evolves in a closed tank with the density difference between the layers *increasing* steadily with time. Physically, the periodic boundary conditions are equivalent to modeling an unbounded fluid composed of infinitely many identical layers in the vertical.

Spectral calculation in Fourier-wavenumber space has been used to obtain solutions to the above governing equations. This method offers the advantage of an accurate evaluation of finger motions down to near the grid scale, as the physical variables can be represented by complete Fourier-basis functions up to the truncation wavenumber, which is set at 120 for all experiments using a 256^2 grid. The same solution procedure as that described in Shen (1989) is used for all experiments, i.e., leapfrog-forward time-stepping, dealiased pseudospectral evaluation of the Jacobian terms, and implicit treatment of the diffusion terms. In the heat-salt case, the diffusion terms are treated exactly using the integration factor for diffusion. For the various numerical techniques mentioned here, the reader is referred to Canuto, et al. (1988).

The time integration was started in each experiment by applying a small white noise perturbation to the fluid interface. Fig.1 shows three snapshots of the evolving salt-finger density field from the simulations of (a) the sugar-salt case in a Hele Shaw cell, (b) the unity-Prandtl-number case, and (c) the heat-salt case. The density field for each case shows that vertical convection has evolved from the initial white noise disturbance, with the characteristic alternately upgoing and downgoing motion of salt fingering. This alternating fingering motion in the unity-Prandtl- number case is not well shown because of the highly irregular finger structure associated with the low viscosity (Shen, 1989), as well as the weak density contrast between fingers.
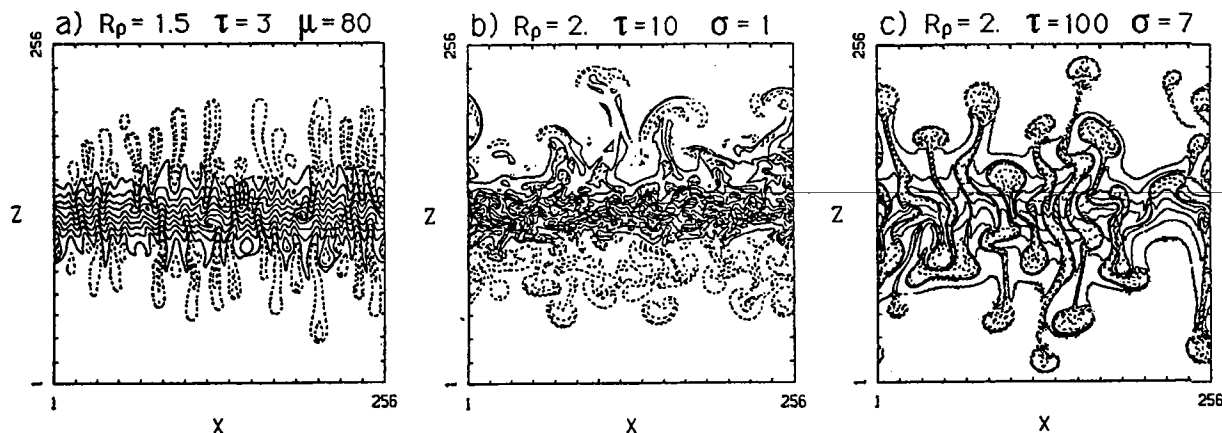
Figure1. Salt-finger density field for (a) the sugar-salt case in a Hele Shaw cell, (b) the ad hoc case with the Prandtl number $\sigma = \nu/\kappa_T = 1$, and (c) the heat-salt case. Contours represent lines of constant density. Dashed conturs mark regions of gravitationally unstable density stratification. $R_\rho = \alpha \Delta T / \beta \Delta S$ is the density ratio based on the T and S differences across the fingering interface. $\tau = \kappa_T/\kappa_S$, and the Darcy drag coefficient μ has been normalized by the Brunt-Vaisala frequency of the interface.

Another feature shown by the density plots is the breakup of the finger convection into plumes. This transition is an important feature previously observed in laboratory salt-finger experiments. In the unity-Prandtl-number case, the plumes show up as large-scale, rapidly expanding mushroom-like thermals. Similar mushroom thermals are also visible in the heat-salt case. The convecting plumes in a Hele Shaw cell do not exhibit the mushroom structure but are elongated like fingers. These elongated plumes are distinguished dynamically from salt fingering by their gravitationally unstable density structure, shown by the dashed density contours in the figure. These dashed contours have density values, respectively, less and greater than that of the uniform layers above and below. Similar gravitationally unstable structure is exhibited by the convecting plumes in the unity-Prandtl-number and heat-salt cases. The plumes for these two latter cases eventually drive the fluid in the layers to convecting turbulence as observed in laboratory experiments. The plumes in the Hele Shaw case, however, do not become turbulent but continue to elongated.

The salt-finger structure from the Hele Shaw case has been compared to the laboratory observation of fingers in a Hele Shaw cell obtained by Taylor and Veronis (1986). This

comparison is directly of interest because, as pointed out earlier, the fingering motion is essentially two-dimensional in a laboratory Hele Shaw cell as in simulation. The narrow, vertically convecting cell structure shown in Fig.1a is consistent with that observed in the laboratory experiment. The simulation also reproduced the finger penetration process observed in the experiment and, additionally, identified two other processes, namely, finger merging and splitting. It has been shown that these processes bring about transition of finger scales in an evolving convection to maintain maximum buoyancy flux (Shen and Veronis, 1989). Fig.2 shows an example of the scale transition produced by these different processes.
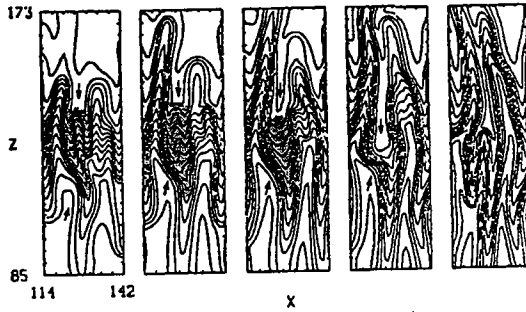
Figure 2. The transition of finger cell width from large to small scale (with time increasing from left to right) through the merging of narrow fingers (shaded regions) and the penetration of wide fingers into the finger zone (arrows). Additional merging and penetration are seen to the right of the shaded regions. The last panel shows the transition to small scale in which the two large penetrating finger cells split to form a pair of narrow fingers. The distance along the x and z axes are given in terms of grid numbers.

3. The Finger Zone

Concerning the interfacial fingering region, there are presently three issues that have received considerable theoretical attention. (a) What is the mean vertical stratification of the S component across this finger zone? (b) What sets the finger height and hence the finger zone thickness? And (c) What sets the finger cell width within this finger zone? Specifically, does the width-selection process promote the maximization of the buoyancy flux or the finger growth rate? Analysis of the simulation results indicates that the S component in the heat-salt system is weakly stratified in the vertical but does not necessarily become uniform as hypothesized in earlier studies. It also indicates that the T stratification plays the important role of limiting finger height and that the hypothesized buoyancy-flux maximization and the finger growth-rate maximization are basically equivalent. More details on these results are given below,

a. The S profile

The amount of S that is lost by fingers to horizontal diffusion depends on the transit time of S through the fingers and the size of the S diffusivity relative to the T diffusivity. For a heat-salt fluid, the low S-to-T diffusivity ratio of 1 to 100 in the presence of a typical convection speed permits little or no diffusion of S in the finger zone. In such a case, upgoing and downgoing fingers retain the S concentration in the respective reservoirs from which they originate, and thus, the horizontally averaged S can be expected to have a uniform value of $\Delta S/2$ over the height of the finger zone, where ΔS is the salt difference between the two reservoirs.

Fig.3 is a plot of four instantaneous vertical S profiles (a-d) from the heat-salt case; the simulation in this case used the value 2 for the system density ratio, $R_\rho = \alpha \Delta T / \beta \Delta S$. These profiles show that S takes on the value of either 0 or 1, i.e., the S value of the lower and upper reservoirs, with negligible loss to diffusion as expected. (The alternating 0 and 1 values occur because of the irregular lateral undulation of the upgoing and downgoing finger cells past the profiling position.) The mean vertical profile $\bar{S}$ (Fig.3, profile e), however, does not exhibit the expected uniform $\Delta S/2$ value, but shows S changing systematically across the finger zone. The cause of this stratification cannot be attributed to the finger undulation, which by itself can at most produce irregular distortion of $\Delta S/2$ values, not the systematic change of $\bar{S}$ with depth. The actual reason has to do with the vertical change of the finger cell width. The cell width tends to decrease in the direction of

the flux as the convection speed accelerates. Given this tendency, it can be readily shown that the $\bar{S}$ is necessarily a function of z and takes on the form, $(\Delta S/2)[b(z)/\delta]$, where b(z) denotes the width of the tapered fingers, assumed here antisymmetrical for the upgoing and downgoing fingers; δ is the vertical average of b(z). Physical presence of the tapered finger width is visible in the density contour plot (Fig.1c). Although the $\bar{S}$ stratification does not vanish, finger convection clearly weakens it, as is evident from the contrast between $\bar{S}$ (profile e) and $\bar{T}$ (profile f); the latter profile is mostly unaffected by convection. The weakening of $\bar{S}$ has implication to the finger flux as will be discussed in Sec.4.
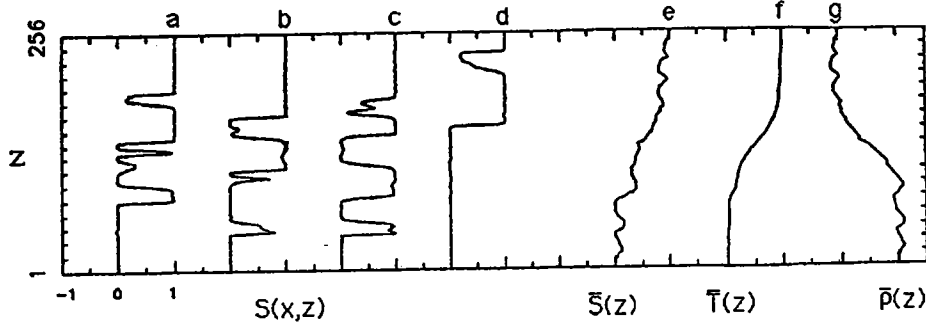
Figure 3. Profiles a, b, c, and d are instantaneous vertical S profiles as a function of the depth z chosen from four different horizontal locations x for the heat-salt case with $R_\rho=2$. The range of S values have been normalized to between 0 and 1. Profile e is the mean S profile computed by horizontally averaging over all x. Profiles f and g are the corresponding horizontal averages of T and ρ, respectively.

b. Finger height

What limits the finger height and hence the fingering-zone thickness has been studied from the view point of the stability of the fingers. Stern (1969) showed that the fingers can become collectively unstable to perturbation when the ratio $A=F_\rho/(v\bar{\rho}_z)$ in the finger zone is greater than a critical value, where F_ρ is the horizontally averaged mean density flux and $\bar{\rho}_z$ is the vertical mean density gradient. For a given density difference $\Delta\rho$ across the finger zone, this critical condition implies that for the existence of fingering the finger height, H $(=\Delta\rho/\bar{\rho}_z)$, can not be greater than $\Delta\rho v A/F_\rho$, where A denotes the critical value of 1/3 (Holyer, 1984). Experimental measurements of A in the finger zone have consistently obtained a value greater than 1/3 required for finger stability. Similarly large A values are also obtained from the simulations (Fig.4). These disagreements with the theoretical critical value have not yet been resolved by recent more thorough analyses of the stability (Howard and Veronis, 1987; Holyer,1984)
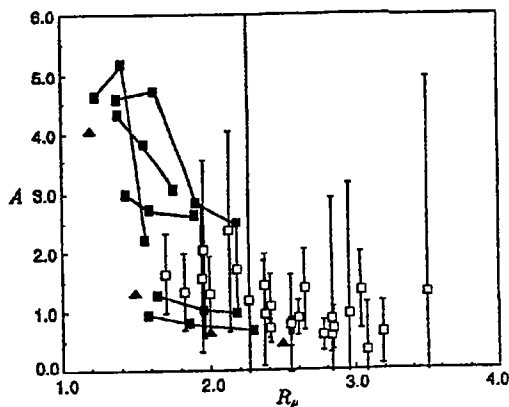
Figure 4. Stern number A versus R_ρ from laboratory measurements (open squares) of Taylor and Bucens (1989), with additional data (solid squares) from McDougall and Taylor (1984) as well as numerical simulation results (solid triangles) from Shen(1990). (Figure adapted from Taylor and Bucens, 1989)

An alternative explanation of the finger height, however, can be provided based on the difference in the evolution of the mean fields, $\bar{T}$ and $\bar{S}$. The evolution of these two mean quantities is governed basically by two processes, the mean vertical flux divergence and the mean vertical diffusion. The $\bar{S}$ evolution tends to be affected mostly by the flux divergence because of the small S diffusivity, while the $\bar{T}$ evolution is affected more strongly by vertical diffusion. The consequence of the convective spreading of $\bar{S}$ by flux divergence is that the $\bar{S}$ interface across the finger zone tends to expand rapidly in the vertical exceeding that of the $\bar{T}$ interface. This creates the situation sketched in Fig.5, where the density-destabilizing $\bar{S}$ stratification near the edges of the interface is not stabilized by the $\bar{T}$ stratification as convection evolves. In these gravitationally unstable regions, the necessary condition for the existence of salt fingering, namely, $|\alpha \bar{T}_z|/|\beta \bar{S}_z| > 1$, is obviously violated. It follows that the fingering is necessarily limited by the thickness of the evolving $\bar{T}$ interface. The presence of unstable (inverted) density regions in the actual mean density profile from the simulation can be seen in Fig.3, profile g.
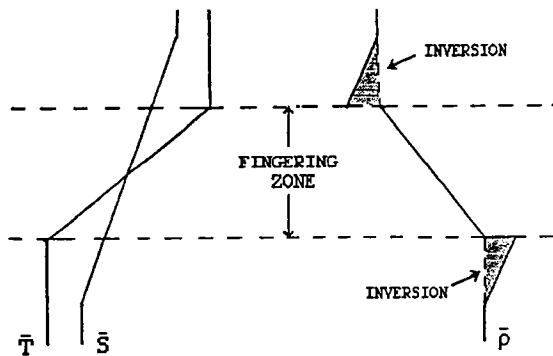
Figure 5. A sketch of $\bar{T}$, $\bar{S}$ and $\bar{\rho}$ across the fingering zone. The shaded regions are the gravitationally unstable density stratifications due to the extension of the S stratification beyond the T -stratified fingering zone.

c. Flux and growth rate maximization

The salt-finger models of Howard and Veronis (1987) and Stern (1976) postulate that physically realizable fingers are those which maximize the vertical buoyancy flux. On the other hand, the models of Schmitt (1979a) and Kunze (1987) assert that the flux and scales are set by those fingers which grow most rapidly from initial perturbation. Prediction based on this latter assumption agrees well with the dominant finger wavenumber that occurred in the simulations; the agreement exists way beyond the initial finger growth stage to which assumptions of fastest growing fingers is expected to be applicable. Fig.6 shows two examples of this persistent agreement after fingers have ceased to grow and the kinetic energy of the convection has reached equilibrium. Analysis indicates that in this later stage the fingers, although not growing temporally, are 'fastest growing' in the spatial sense; that is, their amplitudes increase with distance in the direction of the flux at the maximum possible rate. It is in this sense that the assumption of the fastest growth continues to be applicable.

The above interpretation of fastest growing fingers as spatially growing fingers can be made by noting that in the finger zone interior, the temporal growth of the finger perturbation amplitudes, T' and S', at a given depth will eventually be offset by the advection of smaller T' and S' amplitudes to that depth from reservoirs above and below. Incorporating this vertical advective effect in the fastest growing finger model mentioned above, the vertical convection speed w can be shown to become steady, increasing only with distance, $Z>0$, in the direction of the flux as $|w|=\lambda_m Z$, where λ_m is equivalent to the growth rate of the fastest growing finger. The T' and S' amplitudes are similarly steady and increase with Z as $|T'|=[\lambda_m/(\lambda_m+\kappa_T k_m^2)]|\partial \bar{T}/\partial z|Z$ and $|S'|=[\lambda_m/(\lambda_m+\kappa_S k_m^2)]|\partial \bar{S}/\partial z|Z$, where k_m is equivalent to the wavenumber of the fastest growing finger. This dependence of w, T' and S' on Z is consistent with that found in the simulations

(Shen and Veronis, 1989). Under the foregoing interpretation, maximizing growth rate then becomes the same as maximizing the rate of increase of w with Z. In this case it can be shown with above steady state solutions that the buoyancy flux too is maximized. This consequence is thus in accord with the buoyancy flux maximization assumed in the finger models of Stern (1976) amd Howard and Veronis (1987). The models based on these two different but essentially equivalent assumptions have all obtained nearly the same optimal finger wavenumber in the heat-salt case. The difference in the flux ratios obtained in these models has to do with the magnitude of $\partial S/\partial z$ assumed in each model. This is discussed further in Sec.4.
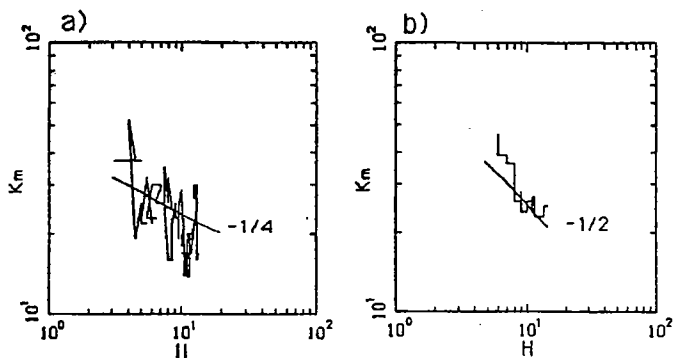
Figure 6. Wavenumber k_m of the fastest growing finger mode versus the finger zone thickness H, for (a) the unity-Prandtl-number case (Shen, 1989) and (b) the Hele Shaw cell case (Shen and Veronis, 1989). The theoretical relationship for each case is indicated by a sloping straight line. Here both k_m and H are given in dimensionless units.

4. Finger Fluxes

Two flux quantities that have been the focus of laboratory measurements are the coefficient c in the 4/3 power law for the salt flux, i.e., $F_S = c(\beta \kappa_T g)^{1/3}(\Delta S)^{4/3}$, and the density flux ratio, $R_f = \alpha F_T/\beta F_S$, of heat to salt. For comparison with laboratory measurements, the values of c determined from the simulations are plotted in Fig.7a which includes laboratory data from Taylor and Bucens (1989) (henceforth referred to as TB) as well as those form McDougall and Taylor (1984) (henceforth referred to as MT) and Schmitt (1979b). The values of density flux ratio from the simulations are plotted in Fig.7b together with the laboratory data from MT. These figures show that in the low R_ρ range, the simulation values of c and R_f are generally close to those of MT. The c values tend to be somewhat higher than those obtained by TB and Schmitt. The R_f values, on the other hand, are about 0.2 lower than those of Schmitt and TB (not shown).

The differences between measurements noted above have been attributed to the different experimental conditions under which measurements were made; specifically, it has been suggested that the salt flux, and hence c and R_f, could be affected by the initial S difference used in the experiment and by the manner in which the fingering interface is initially set up (MT and TB). One possible objection to such an explanation is that the experimental conditions could have similarly affected the heat flux and thus, in the case of R_f, rendered the ratio R_f of the two fluxes unaffected. Analysis of the flux results from the simulations indicates that the differences are likely the consequence of salt fingering itself. In the case of R_f, it can be shown that the weakened mean salt gradient, $\bar{S}_z$, caused by fingering can influence the final R_f values. In the case of the salt flux and c, the dependence of the buoyancy flux on the mean density gradient in the finger zone appears to be the determining factor.

The effect that $\bar{S}_z$ has on R_f has been well illustrated in past salt-finger studies. The finger models of Stern (1976) and Howard and Veronis (1987) show that in the limit of vanishing $\bar{S}_z$, the R_f ratio approaches a low value, ~0.25. At the other limit, i.e., maximum $\bar{S}_z$ for a given ΔS across the finger zone, Schmitt (1979a) and Kunze (1987) show that R_f reaches a value of about 0.6 for density ratio $R_\rho > 2$. (In these theoretical models maximization of buoyancy flux or its equivalent, the growth rate maximization, has been assumed as discussed earlier in Sec.3c.) The actual $\bar{S}_z$

occurring in the finger zone, as shown in Sec.3a, tends to fall somewhere in between the above two $\bar{S}_z$ limits. Fig.7b shows the theoretical estimates of R_f (the x symbols) repeated for the finger models mentioned above using the finger zone $\bar{S}_z$ from the simulations. (Further details are given in Shen, 1990.) The estimates fall between the values of 0.25 and 0.6 obtained by the previous investigators, but are in reasonably good agreement with those determined directly from the simulations as well as with those measured by MT. The agreement with MT's measurements could be fortuitous as the precise $\bar{S}_z$ values are not known in their experiments.; nevertheless, that $\bar{S}_z$ could crucially affect the determination of R_f is strongly suggested by the above estimates.
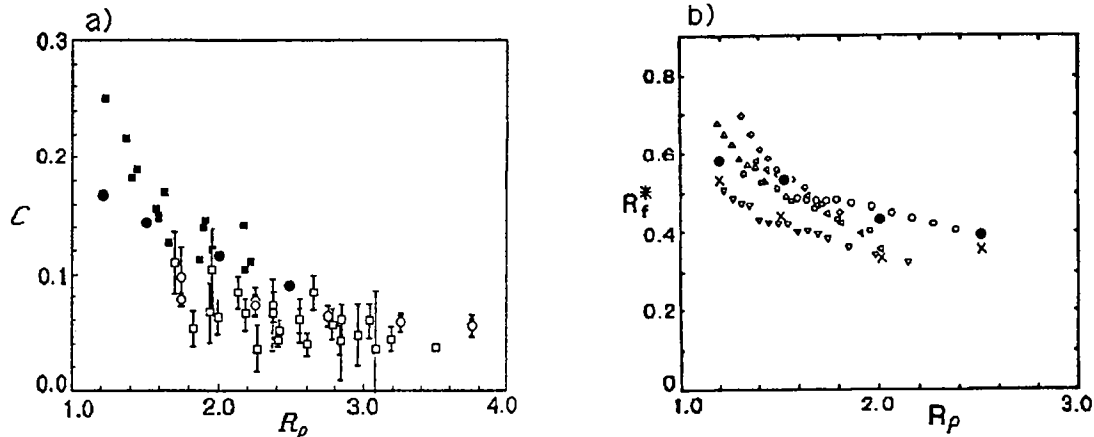
Figure 7. (a) Coefficient c in the 4/3 power law for salt flux versus R_ρ in a heat-salt system from laboratory measurements (open squares) obtained by TB with additional data (solid squares) from MT and (open circles) from Schmitt (1979b). Results from numerical simulations are marked with solid circles (Shen, 1990). (b) The density flux ratio R_f versus R_ρ from laboratory measurements (open circles and triangles) of MT with additional results (solid circles) from numerical simulations and (x) from theoretical estimates (Shen, 1990). The * symbol on R_f is to indicate that the conduction heat flux has been removed from the laboratory data. (Fig.7a adapted form TB; Fig.7b adapted from MT.)

For the coefficient c, the key factor appears to be the dependence of the mean density flux, F_ρ, on the mean density gradient, $\bar{\rho}_z$. The simulation results indicate that these two mean quantities are proportional. This relationship is implied by the constancy of the Stern number ratio, $A=F_\rho/(\nu\bar{\rho}_z)$. Although the relevance of this ratio to the evolution of fingers is presently unclear as discussed in Sec.3b, the simulations show that this ratio approaches approximately a stationary constant with the evolving convection. This tendency has been observed in all cases simulated; some examples are given in Shen (1989). Laboratory determination of A is subject to large measurement uncertainty. Nevertheless, in the heat-salt case, measurements so far appear to indicate the existence of a constant value for the Stern number A, that is of approximately unity magnitude around $R_\rho=2$ (see Fig.4). If A is in fact a constant around $R_\rho=2$ as the evidence suggests, then it is possible for experiments done with different $\bar{\rho}_z$ to have different density fluxes via the Stern number relationship and hence different salt fluxes and c values. In MT's experiments, thinner density interfaces were typically produced, which would tend to yield larger $\bar{\rho}_z$ than experiments that use thicker interfaces as those carried out by TB, which compare closely to MT's experiments in the choice of ΔS and ΔT. This difference could have thus contributed to the larger salt flux and c value obtained in MT's experiments. It may be noted that the Stern number relationship invoked here has also been used by Schmitt (1988) and Kunze (1987) to satisfactorily explain the low salt (buoyancy) flux measured in ocean density interfaces, which are typically an order of magnitude thicker than those produced in laboratory experiments, whence $\bar{\rho}_z$ and finger fluxes for the ocean interfaces can be expected to be correspondingly weaker.

5. Equilibrium Finger Spectrum

With the white noise initial perturbation applied to the interface, multiple finger modes were excited in the simulation. Initially this broad band finger spectrum grows in T and S amplitudes as

envisioned by Schmitt (1979a), i.e., with the spectral amplitude sharply peaked at the wavenumber of the fastest growing finger mode. However, as finger convection evolves, the spectral amplitudes of low wavenumber modes also begin to grow and eventually catch up to that of the fastest growing mode, resulting in a final spectral level that is flat between the lowest wavenumber resolvable and the wavenumber of the fastest growing mode. The spectral level of high wavenumber modes (beyond the fastest growing finger wavenumber), on the other hand, are strongly damped with the amplitude decreasing rapidly toward zero. Thus the shape of the spectrum which the fingers ultimately evolve to in the simulation is as shown in Fig.8. This spectral shape is obtained in all the salt finger cases that have been simulated. Such a spectral shape is consistent with that of ocean temperature finger spectra obtained by Gargett and Schmitt (1982). For a spectrum of this shape, the corresponding horizontal T gradient spectrum necessarily has a +2 spectral slope. This is consistent with the slope of the horizontal temperature gradient spectra measured in the ocean by Marmorino (1987) and Mack (1989) as well as that obtained in the laboratory experiments by Taylor and Bucens (1989). The latter experiments have also obtained horizontal S gradient spectra consistent with those in the simulations.
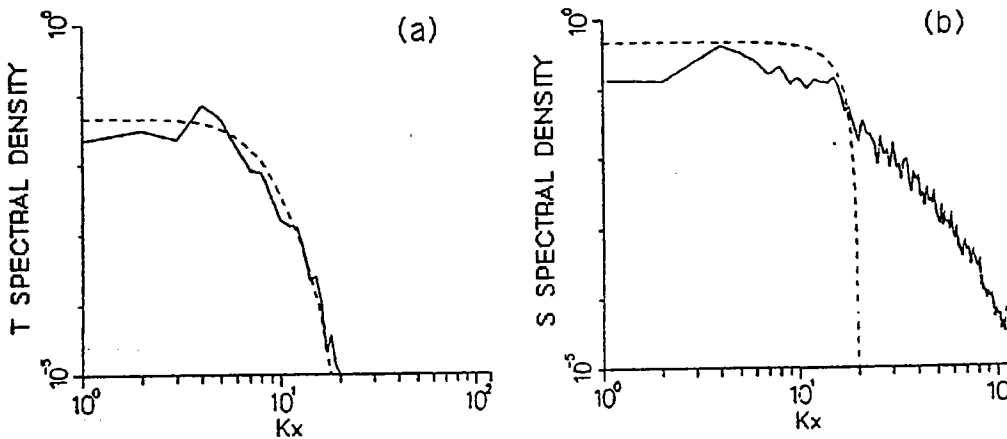
Figure 8. The horizontal wavenumber spectrum for (a) T' variance and (b) S' variance from numerical simulations (solid curves) and the theoretical upper bound calculation (dashed curves). The spectral peaks in the simulation wavenumber spectra have no statistical significance.

The evidence from the simulations, ocean measurements and laboratory experiments all point to the existence of an 'equilibrium' horizontal wavenumber spectrum for fingers. The shape of this spectrum as shown in Fig.8 is characterized by nearly constant spectral density followed by rapid decay beyond the wavenumber of the fastest growing mode. This 'equilibrium' shape can be compared to the 'spectral upper bound' for finger T' and S' amplitudes obtained from the finger model referred to at the end of Sec.3c. That model takes into account the nonlinear vertical advective effect (Shen, 1989), which leads to the solutions of upper bounds for T' and S'. The upper bound amplitudes normalized by ΔT and ΔS are $T'/\Delta T = \lambda/(\lambda + \kappa_T k^2)$ and $S'/\Delta S = \lambda/(\lambda + \kappa_S k^2)$, where k is the wavenumber and λ is the positive root of the finger dispersion relation $\lambda = \lambda(k)$. Fig.8 (dashed curves) shows the spectral densities given by the upper bounds, approximated here as $(T'/\Delta T)^2/2$ and $(S'/\Delta S)^2/2$, and the corresponding T' and S' variance spectra from the simulation for the heat-salt case at $R_\rho = 2$. There is generally a good agreement between the model and the simulation except at the high wavenumber end of the S' spectrum where the simulation spectrum has more variance, perhaps because of the 'square-wave' structure of S' fluctuations not accounted for in the model. This comparison suggests that the double-diffusive process causes T' and S' fluctuations at all scales ultimately to saturate and the T' and S' spectra to equilibrate. It should be pointed out that the fastest growing mode in the sense discussed in Sec.3c remains the dominant mode. Separate analyses of buoyancy flux spectra have shown that the peak of the flux spectrum nearly always occurs around the fastest growing mode wavenumber, even though the spectral

densities for the fastest growing mode in the T' and S' variance spectra are statistically no larger than those at other scales.

6. Conclusions

Results from numerical modeling of salt fingers have made it possible to address a number of important issues that arise from laboratory and theroretical studies of salt fingering. This paper summarized some of the modeling results that address issues related to salt fingering at a density interface. The main conclusions of this paper are: (1) An accurate knowledge of mean vertical S stratifications in the interfacial finger zone is required for the comparison and prediction of the ratio of T to S density fluxes. (2) The finger density flux can be proportional to the mean vertical density gradient in the finger zone via the Stern number relationship. (3) The density-stabilizing T stratification controls the finger height and thus the thickness of the finger zone. (4) The preferred scale for finger width is that which maximizes the finger growth rate or equivalently the rate of buoyancy flux generation, both before and after convection has reached equilibrium. Finally, (5) the finger wavenumber spectrum for T and S evolves toward the equilibrium shape of constant spectral density level with diffusive decay occuring beyond the wavenumber of the fastest growing finger mode.

The study of salt fingers by means of direct numerical simulation is a fairly recent development as mentioned in the introduction. Such simulation yields full solutions of fingering motion, allowing wide aspects of fingering processes to be studied. The results summarized in this paper represent only a fraction of what can be potentially extracted from the solutions. Further future numerical modeling of salt fingers would most likely be fruitful toward a full understanding of their properties. It would also be of interest to extend current two-dimensional simulations to three dimensions as more computing power becomes available. The extension to three dimensions should allow more complete modeling of the mixed-layer dyamics above and below the finger zone. Additional laboratory experiments with heat-salt fluids would also be desirable, particularly, the measurement of the mean T and S stratifications in the finger zone. These two mean field quantities have been generally taken as known variables in laboratory experiments or theoretical studies. But, as has been pointed out in this paper, they in fact evolve with fingers and can significantly affect the finger fluxes in the process (conclusions 1-3 above). In future laboratory studies these mean field quantiites need to be treated as an intrinsic part of the fingering process and measured together with the finger fluxes.

7. Acknowledgement

8. References

Canuto, C., M. Y. Hussaini, A. Quarteroni, and T. A. Zang, 1988. *Spectral methods in fluid dynamics*. Springer-Verlag, New York, pp 557.

Gargett, A. E. and R. W. Schmitt, 1982. Observations of salt fingers in the central waters of eastern North Pacific. J. Geophys. Res., 87(C10), 8017-8029.

Howard, L. N. and G. Veronis. 1987. The salt finger zone. J. Fluid Mech., 189, 1-23.

Hoyler, J. Y., 1984. The stability of long, steady two-dimensional salt fingers. J. Fluid Mech. 147, 169-185.

Kunze E., 1987. Limits on growing, finite length salt fingers: a Richardson number constraint. J. Marine Res., 45, 533-556.

Linden, P.F., 1973. On the structure of salt fingers. Deep-Sea Res., 20, 325-340.

Mack, S. A., 1989. Towed chain measurement of ocean microstructure. J. Phys. Oceanogr., 19, 1108-1129.

Marmorino, G. O., 1987. Observations of small-scale mixing processes in the seasonal thermocline. Part I: Salt fingering. J. Phys. Oceanogr., 17, 1339-1347.

McDougall, T. J. and J. R. Taylor, 1984. Flux measurements across a finger interface at low values of the stability ratio. J. Marine Res., 42, 1-14.

Piacsek, S. A. and J. Toomre. 1980. Nonlinear evolution and structure of salt fingers. in *Marine Turbulence*. edited by.G.J. Nihoul. Elsevier, New York, p193.

Schmitt, R. W. 1979a. The growth rate of super-critical salt fingers. Deep-Sea Res., 26A, 23-40.

Schmitt, R. W., 1979b. Flux measurements on salt fingers at an interface. J. Marine Res., 37, 419-436.

Schmitt, R. W., 1988. Mixing in a thermohaline staircase. In: *Small-Scale Turbulence and Mixing in the Ocean*, J. Nihoul and B. Jamart (Editors), Elsevier Oceanography Series, 46, Elsevier, New York, pp435-452.

Shen, C. Y., 1989. The evolution of the double-diffusive instability: salt fingers. Phys. Fluids A, 1(5), 829-844.

Shen, C. Y., 1990. Numerical experiments on salt fingers in a heat-salt system. Preprint. To be submitted to J. Fluid Mech.

Shen, C. Y. and G. Veronis, 1989. Scale transition of double-diffusive finger cells. Phys. Fluids A. Submitted.

Stern, M. E., 1969. Collective instability of salt fingers. J. Fluid Mech., 35, 209-218.

Stern, M. E., 1976. Maximum buoyancy flux across a salt finger interface. J. Marine Res., 34, 95-110.

Taylor, J. and G. Veronis, 1986. Experiments on salt fingers in a Hele Shaw cell. Science, 231, 39-41.

Taylor, J. and Paul Bucens, 1989. Laboratory experiments on the structure of salt fingers. Deep-Sea Res.

Turner, J. S., 1967. Salt fingers across a density interface. Deep-Sea Res., 14, 599-611.

Turner, J. S., 1985. Multicomponent convection. Annual Reviews of Fluid Mechanics, 17, 11-44.

Whitfield, D. W. A., G. Holloway and J. Y. Holyer, 1989. Spectral transform simulations of finite amplitude double-diffusive instabilities in two dimensions. J. Mar. Res., 47, 241-265.

Inversion of C-SALT data

Jae Hak Lee and George Veronis

Department of Geology and Geophysics

Yale University

P.O.Box 6666, New Haven, CT 06511

Abstract

The inverse procedure based on the advective-diffusive equation and mass continuity is applied to C-SALT data to determine velocity and vertical diffusion coefficients. It is shown that the horizontal velocity is highly variable but very weak and the vertical velocity is downward. The vertical diffusion coefficients of both temperature and salinity show positive values and the former is bigger than the latter. The calculated vertical flux ratio of density by heat and salt is about 0.88 which is somewhat bigger than the values measured by salt finger experiments. The estimations for vertical flux across the interfaces show that the vertical diffusion transports heavier water downward and dominates over the vertical convective flux which transports lighter water downward. This result suggests that the salt fingering activity is an important physical process maintaining the staircases in C-SALT region.

1 Introduction

Knowing the velocity and the diffusion coefficient is essential to understanding the physics of the thermohaline staircase. Only a few direct measurement of velocity have been made. The vertical diffusivity has often been parameterized using the flux law based on laboratory experiments but recently the applicability to salt fingers in the ocean has been questioned by the results from the C-SALT experiment(Schmitt *et al.*,1987).

We have applied the inverse method to the data from C-SALT to determine the velocity and the vertical diffusion coefficients. The model is based on the advective-diffusive equation and mass continuity. Different macroscopic vertical diffusion coefficients are used for different tracers. To check the appropriateness of the model, the diffusion coefficients have not been constrained to be positive. The results reported here are based on the distributions of temperature and salinity.

2 Formulation

The model makes use of the steady state advective-diffusive and mass continuity equations. Assuming that the advective processes are balanced by vertical diffusion, the equations are

$$\vec{V} \cdot \nabla C + w \frac{\partial C}{\partial z} = \frac{\partial}{\partial z} K_v^c \frac{\partial C}{\partial z} \tag{1}$$

$$\nabla \cdot \vec{V} + \frac{\partial w}{\partial z} = 0 \tag{2}$$

where $\vec{V} = (u, v)$ and w are velocities, C is the tracer concentration (temperature, salinity etc.), and K_v^c is the diffusion coefficient of tracer C. It is assumed that the diffusion coefficient is different for each tracer.

Vertically integrating the equations in a layer

$$\nabla \cdot (\overline{\vec{V}C}) + [wC - K_v^c \frac{\partial C}{\partial z}]_b^t = 0 \tag{3}$$

$$\nabla \cdot \overline{\vec{V}} + [w]_b^t = 0 \tag{4}$$

where $\overline{()}$ is the integral, and b and t represent the bottom and the top of the layer respectively. $\overline{\vec{V}}$ is replaced by the product of the layer thickness and the vertically averaged velocity.

Equations (3) and (4) are written in the finite-difference forms based on a seven-point grid network(Figure 1). C_0 corresponds to $C_{i,j,k}$; $u_{i+\frac{1}{2}}$ to $u_{i+\frac{1}{2},j,k}$; h_{k-1} to $h_{i,j,k-1}$ etc..

$$\frac{(C_0 + C_{i+1})(h_0 + h_{i+1})}{2l_x} u_{i+\frac{1}{2}} - \frac{(C_{i-1} + C_0)(h_{i-1} + h_0)}{2l_x} u_{i-\frac{1}{2}} \tag{5}$$

$$+ \frac{(C_0 + C_{j+1})(h_0 + h_{j+1})}{2l_y} v_{j+\frac{1}{2}} - \frac{(C_{j-1} + C_0)(h_{j-1} + h_0)}{2l_y} v_{j-\frac{1}{2}}$$

$$+ \frac{2(h_{k+1}C_0 + h_0 C_{k+1})}{h_0 + h_{k+1}} w_{k+\frac{1}{2}} - \frac{2(h_0 C_{k-1} + h_{k-1} C_0)}{h_{k-1} + h_0} w_{k-\frac{1}{2}}$$

$$+ \frac{4(C_0 - C_{k+1})}{h_0 + h_{k+1}} K_{v\,k+\frac{1}{2}}^c - \frac{4(C_{k-1} - C_0)}{h_{k-1} + h_0} K_{v\,k-\frac{1}{2}}^c = 0$$

$$\frac{h_0 + h_{i+1}}{2l_x} u_{i+\frac{1}{2}} - \frac{h_{i-1} + h_0}{2l_x} u_{i-\frac{1}{2}} + \frac{h_0 + h_{j+1}}{2l_y} v_{j+\frac{1}{2}} \tag{6}$$

$$- \frac{h_{j-1} + h_0}{2l_y} v_{j-\frac{1}{2}} + w_{k+\frac{1}{2}} - w_{k-\frac{1}{2}} = 0$$

where l_x, l_y and h are grid lengths in x, y and z directions respectively. The lengths l_x and l_y are constant but h is variable in this study. Here, u, v, w, K_v^c are unknown variables. The coefficients are given by measured tracer data and grid lengths. There is one equation per grid cell per tracer and a number of tracers is needed to make the system overdetermined. However, there are too few tracers to do so in a real problem, so some simplification is required to overcome the underdeterminancy(as described in Lee and Veronis,1989). For this reason, we have approximated w and K_v^c as

$w = w(z)$ = constant for each layer, and

$K_v^c = K_v^c(z) = \begin{cases} 1. \text{ constant for each layer (model 1), or} \\ 2. \text{ polynomial expansion in } z \text{ direction (model 2).} \end{cases}$
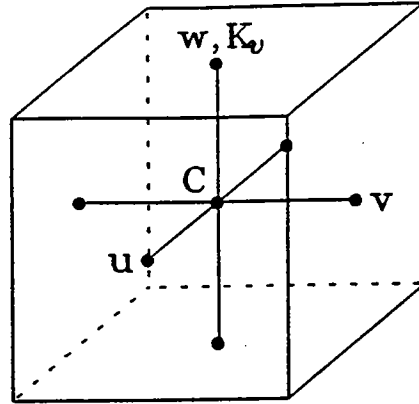
Figure 1: The seven-point grid network for finite differencing.

We have used a low order Legendre polynomial for model 2.

For a given array one can rewrite the system of equations as the linear algebraic equation $Ax = b$, where $A \in \mathcal{R}^{m \times n}$ is the coefficient matrix, $x \in \mathcal{R}^{n \times 1}$ is the vector of unknowns, and $b \in \mathcal{R}^{m \times 1}$ is the data vector. m and n represent the numbers of equations and unknowns respectively. There is no inhomogeneous term in the system described above, so we have changed the system by dividing all elements of x by one of the unknown variables, say x_r. Then, the new algebraic form is written as

$$Gy = d, \tag{7}$$

where $y = x_i/x_r, (i \neq r) \in \mathcal{R}^{(n-1) \times 1}$ is the vector of relative unknowns, $G \in \mathcal{R}^{m \times (n-1)}$ is the coefficient matrix, and $d \in \mathcal{R}^{m \times 1}$ is the data vector made up of the coefficients in the rth column of A. If there is *a priori* information to determine a value of the reference variable, one can finally obtain values of x from solutions of y.

Solutions have been obtained by the total least squares(TLS) procedure (Golub and Van Loan, 1983). TLS solves the problem which contains noisy data both in the coefficient matrix and in the data vector. Unlike the least squares method, the TLS solutions are independent of the choice of the reference unknown variable in Eq.(7).

3 Data

The data used in this study are chosen from data obtained during the spring cruise in the C-SALT experiment. Calculations were made for the 4×4 horizontal array(boxed in Figure 2). The array lies in the region where the strong thermohaline staircase is observed(Figure 3). Though the step structure appears in most of the region, its characteristic features are not unique between stations. That is, the thicknesses are different for different layers and interfaces, the number of layers is not the same between stations, and the depth of the staircase varies horizontally. These make it difficult to define layers
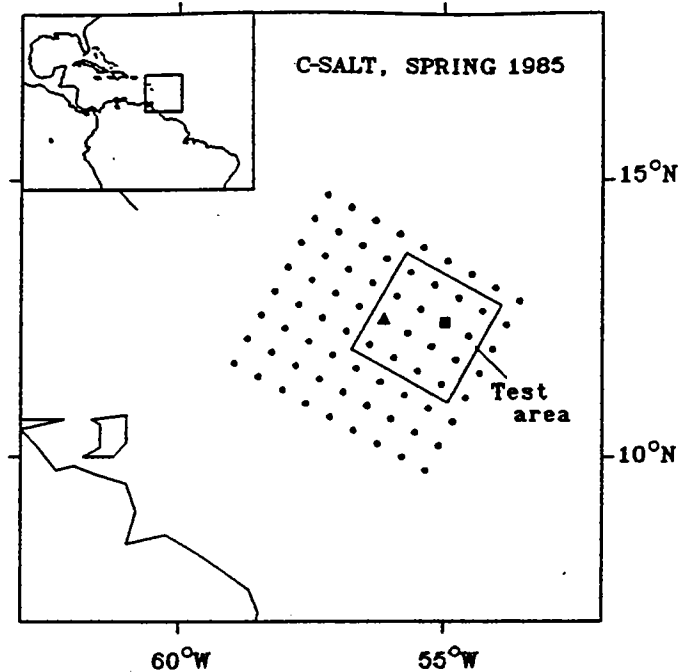
Figure 2: The map of the survey region in C-SALT. The inverse model is applied to the 4×4 array in the boxed area. The mooring station is indicated by ▲.
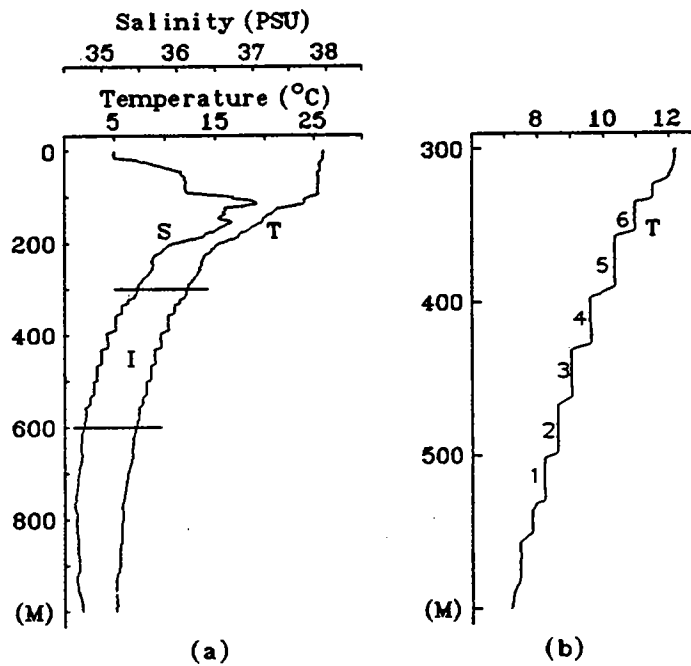
Figure 3: (a) The vertical profile of salinity and temperature at ■ in Figure 2. (b) The detailed temperature profile in region I. Six layers are used for inversion.
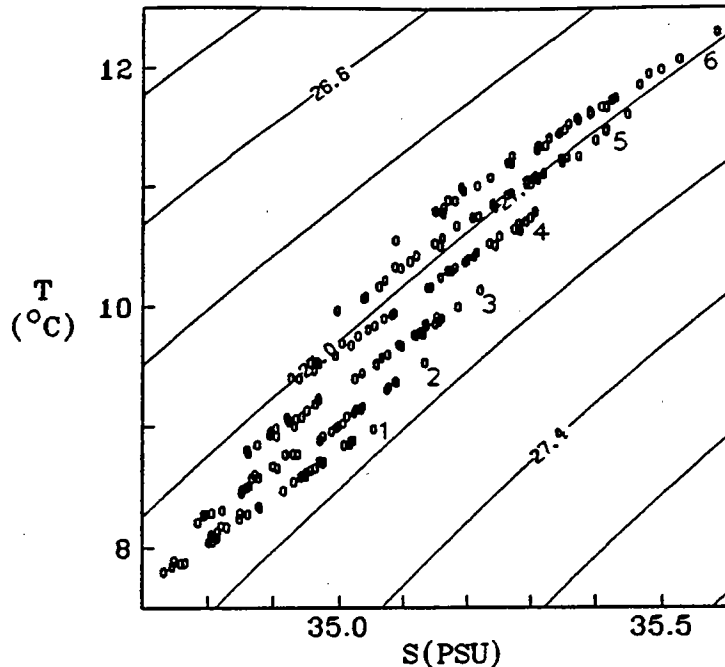
Figure 4: Potential Temperature-Salinity diagram of layers from 4×4 array in Figure 2. The numbers correspond to those in Figure 3(b).

for the inversion by using single properties such as isobaric, isopycnal, or neutral surfaces. To define layers here we have used the layered T-S diagram(Figure 4) which represents the horizontal correlation of layers. Six layers which are shown in Figure 3 are chosen for the inverse model. If the vertical profile does not show the staircase, we have taken means along the depth range so that mean values of temperature and salinity lie on the corresponding line of Figure 4. And also if there is a structure which is not appropriate to the model such as a thick interface and perhaps a smaller mixed layer embedded in a major interface etc., we have changed the shape to fit the layered T-S diagram.

There are 288 equations with two tracers(temperature,salinity) and continuity, and the number of unknowns is 260 in model 1 or 252 in model 2.

4   Results

Figure 5 shows the solutions for horizontal velocity by the two models. The solutions are relative values(the reference variable is a diffusion coefficient of salinity in the top layer in model 1, and is a coefficient of the lowest order in the polynomial expansion of diffusion coefficient of salinity in model 2), and show that the velocity is highly variable but the magnitude generally decreases with depth. There is some disagreement between the velocities calculated from the two models. Though there is a direct measurement of the horizontal velocity at the site marked by a triangle in Figure 2, unfortunately it is
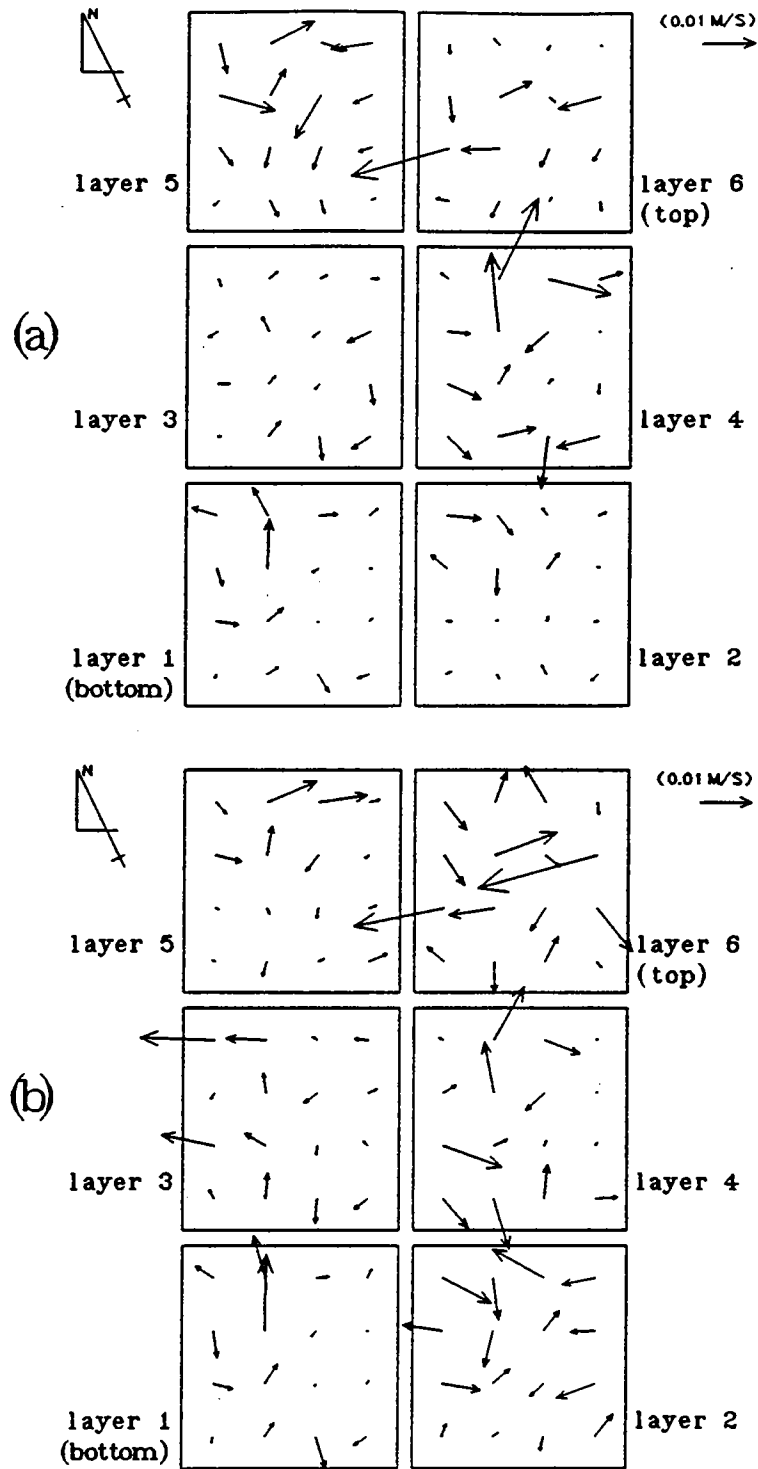
Figure 5: Inverse solutions of the horizontal velocity from (a) model 1 and (b) model 2. The velocity scale at the top right is obtained by assuming that the magnitude of horizontal velocity at the top layer of the mooring site is 0.02 m/s.

Interface	$w(10^{-7}\text{m/s})$	K_v^T $(10^{-4}\text{m}^2/\text{s})$	K_v^S $(10^{-4}\text{m}^2/\text{s})$	R_f
7(top)	-4.0/-5.8	5.9/ 5.6	11.7/11.7	0.83/0.79
6	-4.6/-5.5	5.9/ 7.7	11.7/15.3	0.81/0.84
5	-3.8/-4.5	17.1/ 9.9	32.4/18.0	0.84/0.86
4	-4.4/-4.7	18.9/ 9.9	41.4/18.9	0.80/0.92
3	-2.8/-4.4	9.0/10.8	17.1/16.2	0.90/0.90
2	-2.5/-4.4	4.0/ 5.9	6.3/10.8	1.03/0.89
1(bottom)	-2.4/-3.4	4.8/ 1.4	8.1/ 2.6	0.97/0.96
Mean	-3.5±0.9/ -4.8±0.9	9.4±6.1/ 7.3±3.3	18.3±13.3/ 13.3±5.6	0.88±0.09/ 0.88±0.06

Table 1: Solutions of vertical velocity and vertical diffusion coefficients, and the vertical flux ratio. The two values in each column are the corresponding results of two models(i.e. model 1/model 2). Except for the vertical flux ratio all values are obtained by assuming that the magnitude of horizontal velocity at the top layer in the mooring site is 0.02 m/s.

hard to use it as *a priori* information[1]. But if we estimate the magnitude of horizontal velocity at the mooring site as 0.02 m/s, the velocities in the region are very weak (less than O(0.01 m/s)). The scale shown in Figure 5 is for this case.

All solutions of the vertical velocity are negative(downward) and the magnitude generally decreases with depth(Table 1) in both models. The downward velocity is consistent with Ekman pumping by the mean wind system at the survey region.

For the vertical diffusion coefficient, solutions show all positive values. The diffusivity of salinity is bigger than that of temperature by a factor of about two. These are very important results not only for understanding the physics of C-SALT staircase but also for the inverse model itself. Since different diffusion coefficients emerge for heat and salt, that indicates that something other than turbulent mixing is maintaining the staircases in the C-SALT region. For the inverse calculation itself, it is very meaningful that positive diffusion coefficients can be obtained without requiring that $K_v^c > 0$ in the model. But it may not be true for a general data set. The data used here are taken from the staircase, so the truncation error which is related to the finite-difference approximation is relatively very small when compared with that for general oceanic data.

One interesting result is that the vertical diffusivity of the middle region(interfaces 3,4,5) is bigger than that of layers above or below. Since the mean thicknesses of the mixed layers show the same pattern, it suggests that the thickness of the mixed layer may be related to the size of vertical diffusivity. But this needs further investigation.

The last column in Table 1 shows the vertical flux ratio of density by heat and salt

[1]The mooring data were provided by Dr.H.Perkins. The mooring was deployed the day after the hydrographic measurement. The velocity shows fluctuations which may be dominated by tides and inertial currents and the long term average is near zero. With high fluctuations of the velocity, a one day gap in the data introduces a substantial uncertainty in estimating a velocity magnitude.

Inter-face	$\alpha w \Delta T$ (10^{-11}m/s)	$\beta w \Delta S$ (10^{-11}m/s)	$w \Delta \rho$ (10^{-11}m/s)	αF_T (10^{-9}m/s)	βF_S (10^{-9}m/s)	F_ρ (10^{-10}m/s)
7	-5.4/-7.9	-3.3/-4.8	2.1/3.0	-2.7/-2.6	-3.2/-3.3	-5.5/-6.5
6	-4.7/-5.7	-2.9/-3.5	1.8/2.2	-2.0/-2.8	-2.5/-3.3	-4.7/-5.1
5	-4.8/-5.8	-2.9/-3.5	1.9/2.3	-7.1/-4.3	-8.4/-5.0	-13.4/-6.5
4	-5.1/-5.6	-2.9/-3.3	2.1/2.4	-7.3/-4.0	-9.1/-4.3	-17.8/-3.2
3	-2.8/-4.4	-1.7/-2.6	1.1/1.7	-3.1/-3.0	-3.4/-3.4	-3.6/-3.4
2	-1.8/-3.2	-1.1/-1.9	0.7/1.2	-0.9/-1.3	-0.9/-1.5	0.3/-1.6
1	-1.6/-2.3	-1.0/-1.4	0.6/0.9	-1.1/-0.4	-1.1/-0.4	-0.3/-0.6
Mean	-3.7±1.6/ -5.0±1.9	-2.3±1.0/ -3.0±1.1	1.5±0.7/ 2.0±0.7	-3.5±2.7/ -2.6±1.4	-4.0±3.3 / -3.0±1.6	-6.4±6.7/ -3.8±2.3

Table 2: The vertical flux estimates across the interfaces. The two values in each column are the corresponding results of two models(i.e. model 1/model 2). All values are obtained by assuming that the magnitude of horizontal velocity at the top layer in the mooring site is 0.02 m/s.

which is defined as $R_f = \alpha F_T / \beta F_S$ where $\alpha = -\frac{1}{\rho}\frac{\partial \rho}{\partial T}$, $\beta = \frac{1}{\rho}\frac{\partial \rho}{\partial S}$, $F_T = -K_v^T \frac{\partial T}{\partial z}$ and $F_S = -K_v^S \frac{\partial S}{\partial z}$. Although there is a small difference between the results of the two models, the mean value of R_f is 0.88 which is somewhat bigger than values measured in salt-finger experiments(Schmitt,1979, Mcdougall and Taylor,1984). It is also interesting that the flux ratio increases with depth. The same trend is shown in the slope of the layered T-S diagram.

Table 2 shows the vertical flux estimates across the interfaces. The vertical velocity convects positive anomalies in temperature and salinity downward. For the density anomaly, $\Delta \rho = \beta \Delta S - \alpha \Delta T$, it convects lighter water downward. The vertical diffusive density fluxes due to temperature and salinity, αF_T and βF_S respectively, are downward and are bigger than the vertical convective flux by nearly two orders of magnitude. Since the vertical diffusive density flux due to heat is less than that due to salt, the total vertical density flux which is given by $F_\rho = \beta F_S - \alpha F_T$ is negative, i.e. heavier water downward, and dominates over the positive vertical convective flux of density anomaly. This also suggests that salt fingering activity maintains the staircases in the C-SALT region.

5   Conclusions

The principal findings from inversion of C-SALT data are:
1. It is shown that horizontal velocities are highly variable but very weak (less than O(0.01 m/s)). Since the horizontal velocity is weak, the role of the horizontal diffusive process must be explored.
2. Vertical velocities are downward(probably due to the Ekman pumping) and they

convect lighter water downward across the interfaces.

3. It is shown that all vertical diffusion coefficients are positive and the vertical diffusivity of salt is bigger than that of heat.

4. The calculated vertical flux ratio is about 0.88 which is somewhat bigger than the value measured in laboratory salt finger experiments.

5. Vertical diffusion transports heavier water downward across the interfaces and dominates over the vertical convective flux of density anomaly. It therefore tends to reenforce the stratification. Such a redistribution of density can only be due to double diffusive processes.

References

Lee, J.H. and G. Veronis,1989: Determining velocities and mixing coefficients from tracers. *J. Phys. Oceanogr.*, 19, 487-500.

Golub, G.H. and C.F. Van Loan, 1983: *Matrix computations.* Baltimore, Johns Hopkins Univ. Press, 476 pp.

McDougall, T.J. and J.R. Taylor, 1984: Flux measurements across a finger interface at low values of the stability ratio. *J. Mar. Res.*, 42, 1-14.

Schmitt, R.W., 1979: Flux measurements on salt finger at an interface. *Deep-Sea Res.*, 37, 419-436.

Schmitt, R.W., H. Perkins, J.D. Boyd and M.C. Stalcup, 1987: C-SALT: an investigation of the thermohaline staircase in the western tropical North Atlantic. *Deep-Sea Res.*, 34, 1697-1704.

THE NEED FOR INTERFACE MIGRATION IN CSALT TO EXPLAIN THE LATERAL HEAT-TO-SALT RATIO OF 0.85

Trevor J. McDougall

CSIRO, Division of Oceanography, GPO Box 1538,
Hobart, TAS 7001, Australia.

ABSTRACT

The strikingly constant value of the slopes of the layer properties on the S-θ diagram, at a value of 0.85 calls for an explanation. The observed properties along layers such as this are the result of the divergences of property fluxes and it is shown that a simple explanation of the 0.85 ratio in terms of the vertical divergence of only double-diffusive fluxes would require the flux ratio of salt fingers to be greater than one. This implies that in addition to salt-fingering, there must be some other process or processes at work in CSALT in order to explain the ostensibly simple 0.85 ratio of the gradients of potential temperature and salinity along the layers. It is shown that the interfacial mass flux through the CSALT interfaces is very likely the extra physical process. This small interfacial velocity may only account for a few percent of the salt flux, but is responsible for roughly half of the change in salinity along the layers. We have tended in the past to dismiss this interfacial advection as only being important at very low temperatures across interfaces that have an R_ρ approaching unity (such as in the Weddell Sea), but because of the nature of the "layered coordinate system" that seems a natural one with the CSALT data, the small interfacial advection turns out to be surprisingly important. The required interfacial velocity is only a factor of two larger than that found by extrapolating the results of laboratory experiments to small values of the interfacial salinity difference.

THE NEED FOR SOMETHING BESIDES PURE SALT FINGERS

We begin by assuming that the lateral changes of potential temperature and salinity along the layers are caused by only double diffusion. The salt-fingering buoyancy flux ratio and the vertical density ratio are defined as

$$R_f \equiv \frac{\alpha F^\theta}{\beta F^S} \quad \text{and} \quad R_\rho \equiv \frac{\alpha \theta_z}{\beta S_z}, \tag{1}$$

where the thermal expansion and haline contraction coefficients are defined by

$$\alpha = -\frac{1}{\rho}\frac{\partial \rho}{\partial \theta}\bigg|_{S,p} = \left[-\frac{1}{\rho}\frac{\partial \rho}{\partial T}\bigg|_{S,p}\right]\left[\frac{\partial \theta}{\partial T}\bigg|_{S,p}\right]^{-1} \tag{2}$$

and

$$\beta = \frac{1}{\rho}\frac{\partial \rho}{\partial S}\bigg|_{\theta,p} = \frac{1}{\rho}\frac{\partial \rho}{\partial S}\bigg|_{T,p} + \alpha\frac{\partial \theta}{\partial S}\bigg|_{T,p}, \tag{3}$$

where T is the in-situ temperature and θ is the potential temperature. Assuming a steady state, the lateral advection of properties along the layers, $\mathbf{V} \cdot \nabla_\ell S$ and $\mathbf{V} \cdot \nabla_\ell \theta$ are due to minus the vertical divergence of the double-diffusive fluxes, $-F_z^S$ and $-F_z^\theta$, so that

$$R_\ell \equiv \frac{\alpha \, \mathbf{V} \cdot \nabla_\ell \theta}{\beta \, \mathbf{V} \cdot \nabla_\ell S} = \frac{-\alpha F_z^\theta}{-\beta F_z^S}, \tag{4}$$

and R_ℓ is observed to be 0.85. Our tendency is to assume that the ratio of the double-diffusive flux divergences in (4) is equal to the buoyancy flux ratio, R_f, but there are two reasons why this may not be the case; firstly, the flux ratio may vary with depth, and the second reason is due to the nonlinear nature of the equation of state. This can be seen by deriving an expression for $\alpha F_z^\theta / \beta F_z^S$ by vertically differentiating the definition of the buoyancy flux ratio, (1) to obtain

$$r \equiv \frac{\alpha F_z^\theta}{\beta F_z^S} = R_f \left[1 - \frac{\beta}{\alpha}\left(\frac{\alpha}{\beta}\right)_z \frac{F^S}{F_z^S} \right] + \frac{dR_f}{dz}\frac{F^S}{F_z^S}. \tag{5}$$

The variation of the buoyancy flux ratio will be addressed below so for now, let us take R_f to be constant. The ratio α/β varies by 25% over the vertical extent of the CSALT staircase

(200 m), so that $\frac{\beta}{\alpha}\left(\frac{\alpha}{\beta}\right)_z$ is 0.25/200 m^{-1}. The mean flow in the staircase region is thought to be to the north-west so that the fluid in the layers gets warmer, more saline and denser as it advances through the staircase region. This implies that F_z^S is negative (the same sign as F^S) and that F^S/F_z^S is greater than 200 m: I shall take this vertical length scale over which the double-diffusive salt flux varies to be 300 m. Equation (5) then implies that

$$r = R_f \left[1 - \frac{0.25 \times 300}{200} \right] = 0.625 \, R_f. \tag{6}$$

Under the assumption of this section that the only mixing process is salt-fingering, (4) and (6) imply that the buoyancy flux ratio of the salt-fingering must be $R_f = 0.85/0.625 = 1.36$. This is quite obviously unacceptable as it is energetically inconsistent for the buoyancy flux ratio of double-diffusion to exceed 1. An alternative way of expressing this finding is to say that salt-fingering (with a constant buoyancy flux ratio) would be expected to yield an observed value of $R_\ell \equiv \alpha \, \mathbf{V} \cdot \nabla_\ell \theta / \beta \, \mathbf{V} \cdot \nabla_\ell S$ of $r = 0.625 \, R_f$, which would be between 0.44 and 0.50 for R_f between 0.7 and 0.8.

In this section it has been shown that the most obvious cause of CSALT's lateral heat-to-salt ratio of 0.85, namely the vertical variation of the double-diffusive heat and salt fluxes, is consistent with the data only if the buoyancy flux ratio of the salt fingers is significantly greater than 1. Since this is energetically impossible, it is the aim of this work to deduce what other physical mechanism is acting in conjunction with the salt-finger convection so as to achieve the observed tight correlation of 0.85 on the scaled S-θ diagram, rather than the value

less than or equal to 0.5 that would have been found in this thermohaline staircase if the salt-fingering had been acting alone. It is concluded that the migration (or entrainment) of fluid across the double-diffusive steps is most likely to be the extra process that is required to explain the 0.85 ratio. It will be shown that the required entrainment is quite small in terms of the flux of salt or heat across the steps, and that the buoyancy flux ratio of the combination of salt-fingering and entrainment is very little different to that of salt-fingering alone. This small amount of entrainment has a relatively large influence on the evolution of the layer properties because the vertical advection of fluid through the interfaces inherently acts as a *flux divergence* rather than as a *flux*, and so is much more effective at water-mass conversion than the small change in the buoyancy flux ratio would imply. This is another example in oceanography where vertical advection cannot be overlooked, and yet it is often our habit to do so. It is also very common to confuse fluxes and flux divergences in our thinking. Observed changes in fluid properties in the ocean are always due to flux divergences, and when deducing a flux divergence from known relationships that hold between the fluxes, the nonlinear nature of the equation of state often raises its ugly head as it has in this work.

In addition to the discussion below of the interfacial advection through the CSALT steps, various other processes have been considered. While these processes will not be discussed here, they include (i) the variation of the buoyancy flux ratio with height, (ii) vertical turbulent mixing by isotropic turbulence, (iii) double-diffusive interleaving occurring in the steps, (iv) the possibility that the CSALT steps and layers are actually caused by lateral double-diffusive interleaving rather than as mainly the result of vertical processes, (v) the possibility that the buoyancy flux ratio of salt-fingering is actually greater than 1 in CSALT and the required energy for stirring the stable density flux through the layers comes from breaking internal waves in the layers, (vi) the presence of lateral mixing along the layers, (vii) the presence of lateral mixing along neutral surfaces, and (viii), the possibility that the fluid in the CSALT layers actually gets cooler, less saline and less dense as it moves to the south east rather than to the north west. Most of these processes can be dismissed on the basis of the CSALT data.

HOW MUCH INTERFACIAL ADVECTION IS REQUIRED?

Letting the velocity of fluid through the interface be w^i, the steady-state conservation equations for salt and potential temperature are

$$\mathbf{V} \cdot \nabla_\ell \theta + w^i \theta_z = -F_z^\theta , \tag{7}$$

and

$$\mathbf{V} \cdot \nabla_\ell S + w^i S_z = -F_z^S . \tag{8}$$

Linear combinations of these equations can be taken to eliminate either the lateral or the vertical advection terms, obtaining

$$\mathbf{V} \cdot \nabla_\ell S = -F_z^S \frac{\left[R_\rho - r \right]}{\left[R_\rho - R_\ell \right]} , \tag{9}$$

and

$$\frac{w^i S_z}{-F_z^S} = -\frac{\left[R_\ell - r \right]}{\left[R_\rho - R_\ell \right]} , \tag{10}$$

where R_ℓ and r are defined in the first parts of equations (4) and (5). Continuing to assume that the buoyancy flux ratio is depth-independent, r is close to 0.5 (see the discussion below

(6)) so that $[R_\ell - r]/[R_\rho - R_\ell]$ is about 0.47 in the CSALT staircase. This means that in order for the combined processes of salt-fingering and interfacial advection to explain the 0.85 ratio, interfacial migration must account for 32% (= 100% x 0.47/1.47) of the salinity change that occurs along the layers, with the vertical divergence of the double-diffusive salt flux accounting for the remainder (68%). Is it reasonable to ask this of interfacial entrainment?

Double-diffusive interfaces between two well-mixed layers have been observed to migrate vertically in laboratory experiments (SCHMITT, 1979 and MCDOUGALL (1981b)). This interfacial migration has been ascribed to the asymmetric entrainment of fluid across the interface. The asymmetry is partly due to the larger buoyancy flux in the lower layer of such experiments and partly due to the decreased static stability at the lower edge of the interface. Both of these effects are in turn caused by the nonlinear nature of the equation of state as a function of potential temperature. MCDOUGALL (1981c) proposed that this interfacial advection would be important in the "diffusive" interfaces in the Weddell Sea where large steps in potential temperature occur at low values of the stability ratio. The laboratory experiments of MCDOUGALL (1981b) were specifically designed to measure the rate of interfacial migration, and by extrapolating these results to the conditions appropriate to the Weddell Sea, the interfacial salt and heat fluxes were found to be significant fractions of the double-diffusive fluxes. In more normal situations in the ocean we have tended to ignore the interfacial mass flux because it generally represents a small fraction of the total property fluxes across the double-diffusive interfaces (see, for example, KELLEY, 1987).

The results of the two-layer salt finger laboratory experiments of MCDOUGALL (1981b) were expressed as half the apparent salt flux contributed by the asymmetric entrainment, divided by the double-diffusive salt flux, namely

$$\tilde{E} \equiv \frac{\frac{1}{2}w^i \Delta S}{-F^S},$$ (11)

and was plotted as a function of R_ρ for various values of a parameter, $\tilde{\delta}$, that represented the extent of the nonlinearity of the equation of state, namely

$$\tilde{\delta} = \frac{1}{2\alpha}\frac{\partial\alpha}{\partial\theta}\Delta\theta\frac{R_\rho}{[R_\rho - 1]},$$ (12)

where ΔS and $\Delta\theta$ are the steps of salinity and potential temperature across the interface. The expression "apparent flux of salt " is used because there are subtle issues associated with the actual salt flux across an interface when the corresponding mass flux is non zero (see MCDOUGALL, 1981a). The apparent salt flux is that derived from the temporal change of the layer salinities in a two-layer laboratory experiment. At $R_\rho = 1.6$, the laboratory results can be approximated by the linear relation $\tilde{E} = 0.2\,\tilde{\delta}$. For the CSALT interfaces, $\tilde{\delta} \approx 0.045$, so that by extrapolating the laboratory results to the less nonlinear interfaces of

CSALT, one finds a predicted value of $\tilde{E}$ of only 0.009 so that the interfacial advection contributes only 1.8% of the total apparent salt flux across the CSALT interfaces.

The relevant question then is this:- "Is it consistent to have $w^i \Delta S / -F^S$ as little as 0.018 while (from 10) $w^i S_z / -F_z^S$ is as large as 0.47?" In two-layer laboratory experiments these two ratios are equal because with only a single interface, the apparent salt fluxes from both processes are simply related to the corresponding vertical divergences of the salt fluxes by the mean layer height. In the CSALT situation, the salinity step across an interface is simply the layer height times the mean (large-scale) salinity gradient, but the vertical divergence of the double-diffusive salt flux can be quite a small fraction of the salt-flux.

Using a mean layer height of 21 m (BOYD and PERKINS, 1987) and F^S / F_z^S equal to 300 m as before, the required interfacial velocity can be expressed as

$$\frac{w^i \Delta S}{-F^S} = \frac{21m}{300m} \frac{\left[R_\ell - r\right]}{\left[R_\rho - R_\ell\right]} = 0.033 , \tag{13}$$

which is less than a factor of two larger than the value deduced from the laboratory experiments, namely, 0.018. We must conclude that these previously neglected interfacial mass fluxes caused by the asymmetric entrainment of fluid across the double-diffusive interfaces can be surprisingly efficient at causing water-mass conversion, even though they may account for a much smaller fraction of the apparent property fluxes themselves. The difference between fluxes and flux divergences lies at the root of this issue and we oceanographers are often guilty of ignoring the distinction between them. The interfacial mass flux given by (13) would have the effect of increasing the buoyancy flux ratio (defined in terms of the total apparent fluxes of potential temperature and salinity) from say 0.7 to

0.73 (equal to $\left[R_f + 0.033 R_\rho\right]/1.033$); a very small change in the buoyancy flux ratio. However, because vertical advection is so efficient in causing water-mass conversion, it has saved us invoking a totally unrealistic buoyancy flux ratio of 1.36 to explain the CSALT observations.

REFERENCES

BOYD, J. D. and H. PERKINS (1987) Characteristics of thermohaline steps off the northeast coast of South America, July 1983. *Deep-Sea Research,* **34,** 337-364.

KELLEY, D. E., (1987) Interface migration in thermohaline staircases. *Journal of Physical Oceanography,* **17,** 1633-1639.

MCDOUGALL, T.J. (1981a) Double-diffusive convection with a non-linear equation of state. I. The accurate conservation of properties in a two-layer system. *Progress in Oceanography,* **10,** 71-89.

MCDOUGALL, T.J. (1981b) Double-diffusive convection with a non-linear equation of state. II. Laboratory experiments and their interpretation. *Progress in Oceanography,* **10,** 91-121.

MCDOUGALL, T.J. (1981c) Fluxes of properties through a series of double-diffusive interfaces with a non-linear equation of state. *Journal of Physical Oceanography,* **11,** 1294-1299.

SCHMITT, R. W. (1979) Flux measurements on salt fingers at an interface. *Journal of Marine Research,* **37,** 419-436.

Discriminating Salt-Fingering from Turbulent Induced Microstructure in Towed Conductivity Array Data

Stephen A. Mack and Howard C. Schoeberlein

The Johns Hopkins University
Applied Physics Laboratory
Johns Hopkins Rd
Laurel, Maryland 20707

Abstract

Measurements made with a towed array of co-located temperature and conductivity sensors are used to evaluate techniques for discriminating between microstructure patches caused by turbulence and those caused by double-diffusion. Horizontal tows in the Sargasso Sea reveal numerous patches that are identified as due to salt-fingering and others as due to turbulence. Density ratio, conductivity gradient spectral slope, and conductivity gradient kurtosis are evaluated as potential discriminators. The density ratio computed from single sensor pairs gives unreliable values when the sensors fail to cut through isopycnal surfaces. Spectral slopes have been computed using both a direct spectral technique, which is computationally inefficient, and a technique using ratio of variance in two wavenumber bands. The power ratio slope technique shows good separation between the distributions for salt-fingering and turbulence with salt-fingering slopes > 1.2 and turbulence slopes < 1.2. Kurtosis ($K = <c'^4>/<c'^2>^2$) also shows good separation with $K < 4$ for salt-fingering and $K > 4$ for turbulence. These discriminators improve upon the use of R_ρ alone since they reveal the detailed characteristics of the patch and are robust for various tow angles with respect to isopycnal surfaces. The distribution for $\log(K)$ is more nearly gaussian than that for kurtosis and shows less overlap between salt-fingering and turbulence. A discrimination technique using a log-likelihood approach for the joint probability density functions of slope and $\log(K)$ is suggested.

Introduction

Studies to investigate the relationship between internal waves and turbulence and to understand the importance of double-diffusion and turbulence to ocean mixing require a knowledge of the cause of the observed microstructure as well as the volume fraction of each contribution. To separate turbulence from double-diffusion, field measurements can be conducted in a diffusively stable environment, which excludes the possibility of double-diffusion. However, continuous measurements of vertical temperature and salinity are required to ensure that fine-scale (of order few meters) temperature or salinity inversions are not present (Gargett and Schmitt, 1982). Alternatively, studies of salt-fingering or diffusive convection can be conducted in the environments favoring these instabilities. While this can enhance the likelihood of observing these instabilities, it does not exclude the possibility of turbulence. Simultaneous measurements of the small-scale signature of mixing and measurements of the finestructure environment are really required to discriminate between double-diffusive and turbulent induced microstructure. In this way, ocean measurements that cover both the diffusively stable and diffusively unstable regimes can be used to investigate the importance of turbulence, salt-fingering, and diffusive convection.

In this paper we explore various techniques applied to a towed array of co-located temperature and conductivity sensors to discriminate between salt-fingering and turbulence. We have evaluated the density ratio ($R_\rho = \alpha T_z/\beta S_z$), conductivity gradient spectral slope, and conductivity gradient kurtosis ($K = <c'^4>/<c'^2>^2$). Several studies have shown that salt-fingering is more likely in the supercritical regime of the density ratio between 1 and 2 (Schmitt 1979, Schmitt and Georgi 1982, Mack 1985, 1989). Other studies (Gargett and

Schmitt 1982, Marmorino 1987, Marmorino and Greenewalt 1988, Mack 1989, Shen 1989) indicate that spectral slopes for temperature or conductivity gradient should be ≈ 2 for salt-fingering and less than or equal to 1 for turbulence. Holloway and Gargett (1987) suggested kurtosis as a potential discriminator. Marmorino and Greenewalt (1988) applied this to a towed conductivity sensor.

A useful discriminator should be both accurate and computationally efficient. Density ratio requires vertical gradients of temperature and salinity and is ideally suited to vertical profilers. However, vertical profilers do not measure the mostly horizontal signature of salt-fingers and are unable to cover large areas. Towed array conductivity sensors usually lack the necessary intersensor calibration accuracy to provide the meaningful vertical salinity gradients between vertical sensors to measure R_ρ. Mack (1989, "M89") described the use of a single sensor pair (temperature and conductivity) to compute density ratio from towed sensors. As long as the sensors cut through isopycnal surfaces and a component of the vertical is measured, useful R_ρ values can be obtained. Towed arrays cover large distances, measure vertical swaths, and detect the horizontal signature of salt-fingers. However, unreliable R_ρ values are obtained when the tow path is parallel to isopycnals. Furthermore, R_ρ is computed from smoothed temperature and salinity gradients, but smoothing causes a lack of correlation at the edges of patches where the microstructure abruptly starts or ends. It is important to supplement R_ρ information with measurements that exploit the character of the mixing to obtain the best estimate of the frequency of occurrence of the different mixing events. Spectral slope or kurtosis could be quite useful discriminators if they provide characteristics sufficiently different in salt-fingering and turbulence and if they are computationally efficient.

Experimental and Analysis Description

The towed array consists of 30 pairs of nearly co-located planar four-electrode conductivity cells (Farruggia and Fraser, 1984) and Thermometrics P20 thermistors spaced 50 cm apart. The instrument system and data set (Sargasso Sea, Fall 1984, tows near 30°N, 70°W) are described in M89. Only the characteristics relevant to this paper are discussed here. The conductivity output has been pre-emphasized with an analog filter that has no gain at low frequencies and rises at 6 dB per octave from approximately 0.7 Hz to 100 Hz. A 5-pole Bessel anti-alias filter with 3-dB frequency at 160 Hz has been applied. Conductivity was sampled at 320 samples per second. The measured spatial response of the conductivity sensor (3 dB down at 8 cpm) has been used to correct for the conductivity spectra out to 30 cpm.

We consider three tow segments of approximately 2.2 km each (as shown in Figures 5, 7 and 8 of M89) that include patches identified as likely salt-fingering or turbulence based on R_ρ and spectral slope. Localized portions of these tow segments have been used to generate the spectral slope and kurtosis distributions for salt-fingering and turbulence. These are labelled "Case 1 SF Local" (M89 Figure 5 sensors 5-17 from 08:00 - 08:03:30), "Case 2 SF Local" (M89 Figure 7 sensors 6-14, 16 from 19:00 - 19:05) and "Case 3 Turb Local" (M89 Figure 8 sensors 22-25, 28-30 from 08:51:30 - 09:00). Spectral slope has been computed every 1 sec (~3 m of tow) by direct spectral method incorporating least-squares fit to the conductivity gradient spectra (corrected for electronics and sensor spatial response) over the wavenumber range of 0.7 to 12 cpm in order to avoid the peak in the salt-finger spectra typically seen between 10 and 20 cpm.

A more computationally efficient technique for estimating slopes makes use of the variance in two wavenumber bands computed by bandpass filtering, squaring, and averaging after editing, applying de-emphasis filter, and differentiating the raw pre-emphasized conductivity data. This technique assumes a spectral slope model such that

$G(k) = k^p$, where $G(k)$ is the gradient spectrum, k is the wavenumber, and p is the slope; it uses a sensor response of the form $|H(k)|^2 = 1+ak+bk^2+ck^4$; and then integrates $G(k)|H(k)|^2$ over two bands (low band = 0.3 to 1 cpm and high band = 3 to 20 cpm). This process is repeated for p = -0.5 to 3.5, and a table of expected log power ratio (ELPR) vs. slope is constructed where:

$$ELPR = \log_{10}\left\{\frac{\int\limits_{high-band} G(k)|H(k)|^2\,dk}{\int\limits_{low-band} G(k)|H(k)|^2\,dk}\right\} \qquad (1)$$

Conductivity gradient variance in the two bands is computed for the data (30 m smoothing of the low band is applied to include an equal number of cycles in both the low and high band) and the 'observed' log of the ratio of the variance is computed (Observed Log Power Ratio). If a microstructure patch is encountered (zero-crossings greater than 2, see M89), the slope is determined by means of a table lookup and interpolation of the model ELPR.

Results

One of the tow regions used for generating the statistics appropriate to salt-fingering is shown in Figure 1. The first 6 minutes were shown as Figure 5 in M89. The salt-finger patch is seen by sensors 3 through 17 during the first 3.5 minutes. Note the excellent correlation between the microstructure and low R_ρ values as depicted by the gray scale superimposed on the pre-emphasized conductivity (plotted in min-max format every 0.25 sec.) Although there is a good correlation between low R_ρ and microstructure, note that some sensors such as 17 have R_ρ values that are outside the gray scale range but appear to be part of the same patch. This occurs when the chain does not cut through isopycnals.

Conductivity gradient spectra have been computed every 1 sec for the 'Case 1 SF Local' sensors as well as the 'Case 2 SF Local' and 'Case 3 Turb Local' regions. Some representative spectra are shown in Figure 2. The spectra were computed using geometric band averaging over 16 bands. The distribution of spectral slopes over several hundred 1-sec intervals are shown in Figure 3a. The nearly gaussian distributions (shown by the dashed lines) have means of 1.91 and 0.79 respectively for salt-fingering and turbulence. The histograms show a reasonable separation at 1.4 with about 15% of each distribution overlapping the other. Slightly lower slopes were obtained by least-squares fit to the raw spectra without geometric band averaging.

The distributions of spectral slopes obtained by the power ratio technique are shown in Figure 3b. The mean slope is 1.50 for salt-fingering and 0.71 for turbulence. The means are less than those for the direct spectral technique, particularly for the salt-fingering case (the high wavenumber band includes part of the roll off region of the spectra), but the standard deviation has decreased. The two distributions now cross at about a slope of 1.2 with only about 10% overlap. Hence a better separation between the salt-finger and turbulent distributions is obtained by the power ratio technique.

Holloway and Gargett (1987) noted that the salt-finger observations of Gargett and Schmitt (1982) showed a limited amplitude temperature signature compared with turbulence and suggested the kurtosis as a potential discriminator. They found a mean kurtosis of 3.04 for data identified as salt-fingering and a value of 6.75 for turbulence. They suggested kurtosis in part because of the possibility of computation in near real time and thus a near real-time survey of the extent of salt-fingering. Kurtosis of the pre-emphasized conductivity has been computed on 1 sec intervals after the conductivity has been wild-

CASE 1 SALT FINGER
(304) 8:0:0 - (304) 8:3:30

CASE 2 SALT FINGER
(303) 19:0:0 - (303) 19:5:0

CASE 3 TURBULENCE
(306) 8:51:30 - (306) 9:0:0

(a)

CASE 1
(304) 8:0:0 - (304) 8:12:0

CASE 2
(303) 19:0:0 - (303) 19:12:0

CASE 3
(306) 8:50:0 - (306) 9:2:0

(b)
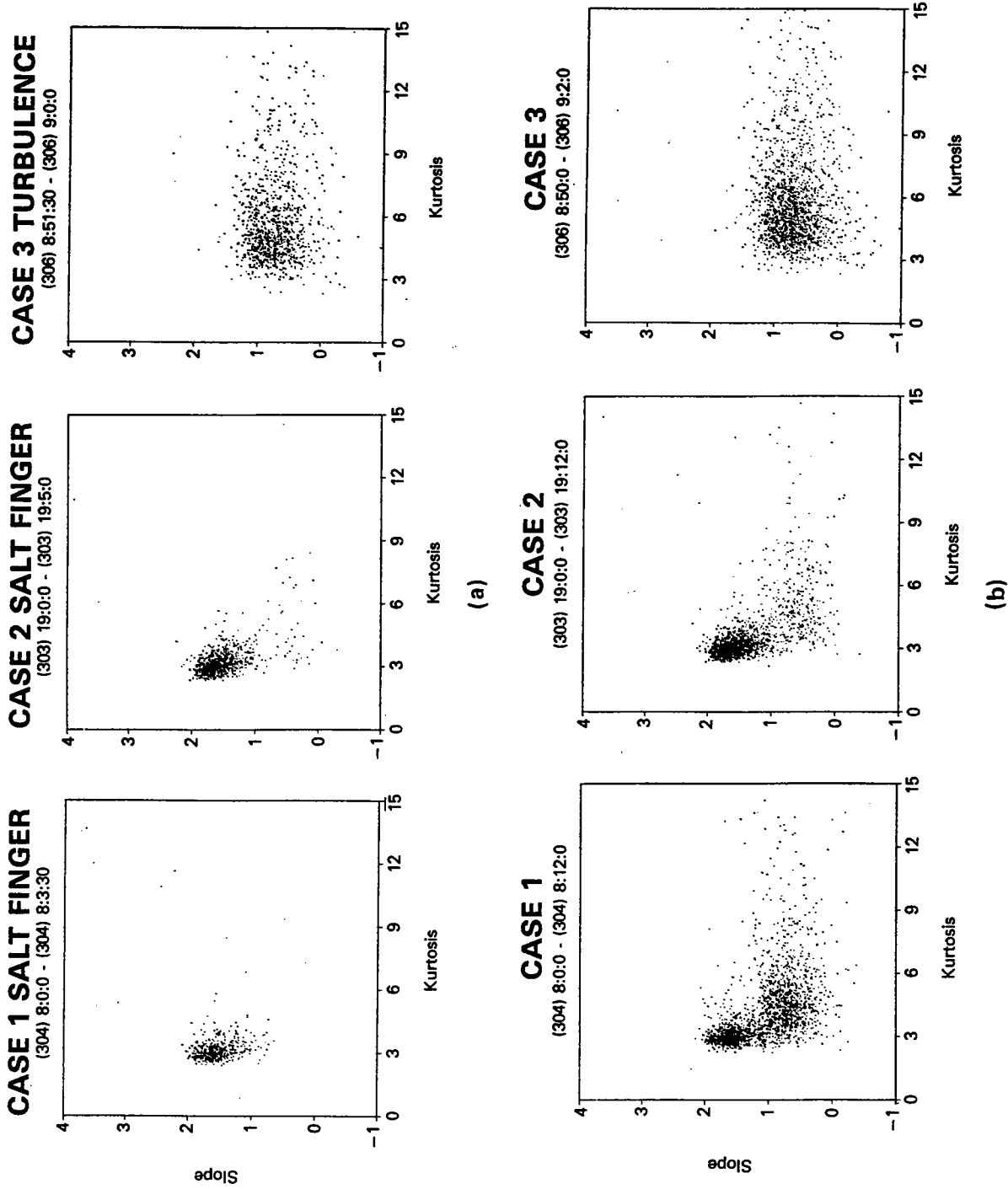
Fig. 7 Scatter plots of slope versus kurtosis. (a) "Local" region (b) full array over 12 min of tow.
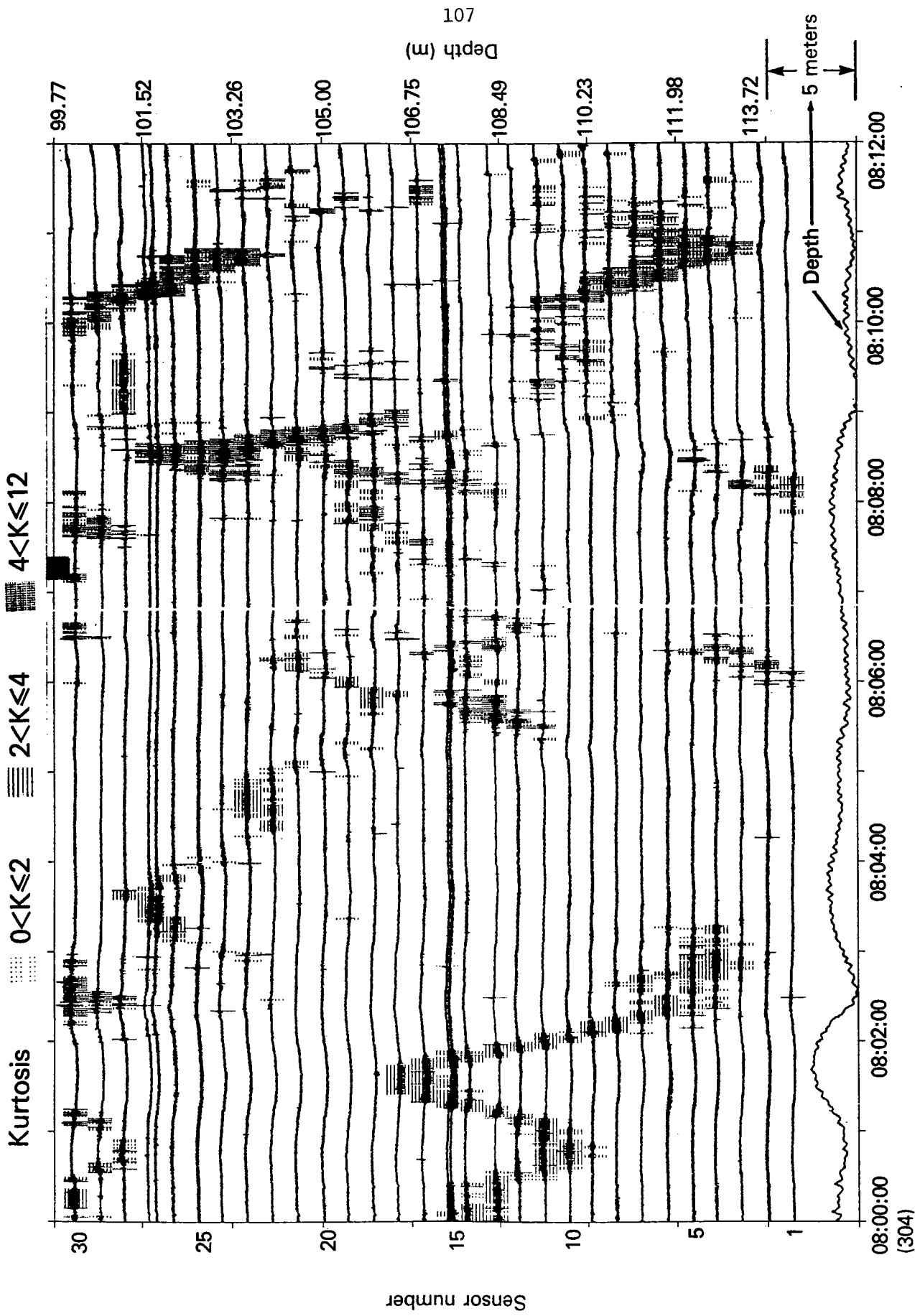
Fig. 6 Pre-emphasized conductivity showing kurtosis gray scale.

Spectral slope ▓ −1<S≤1.2   ▓ 1.2<S≤10
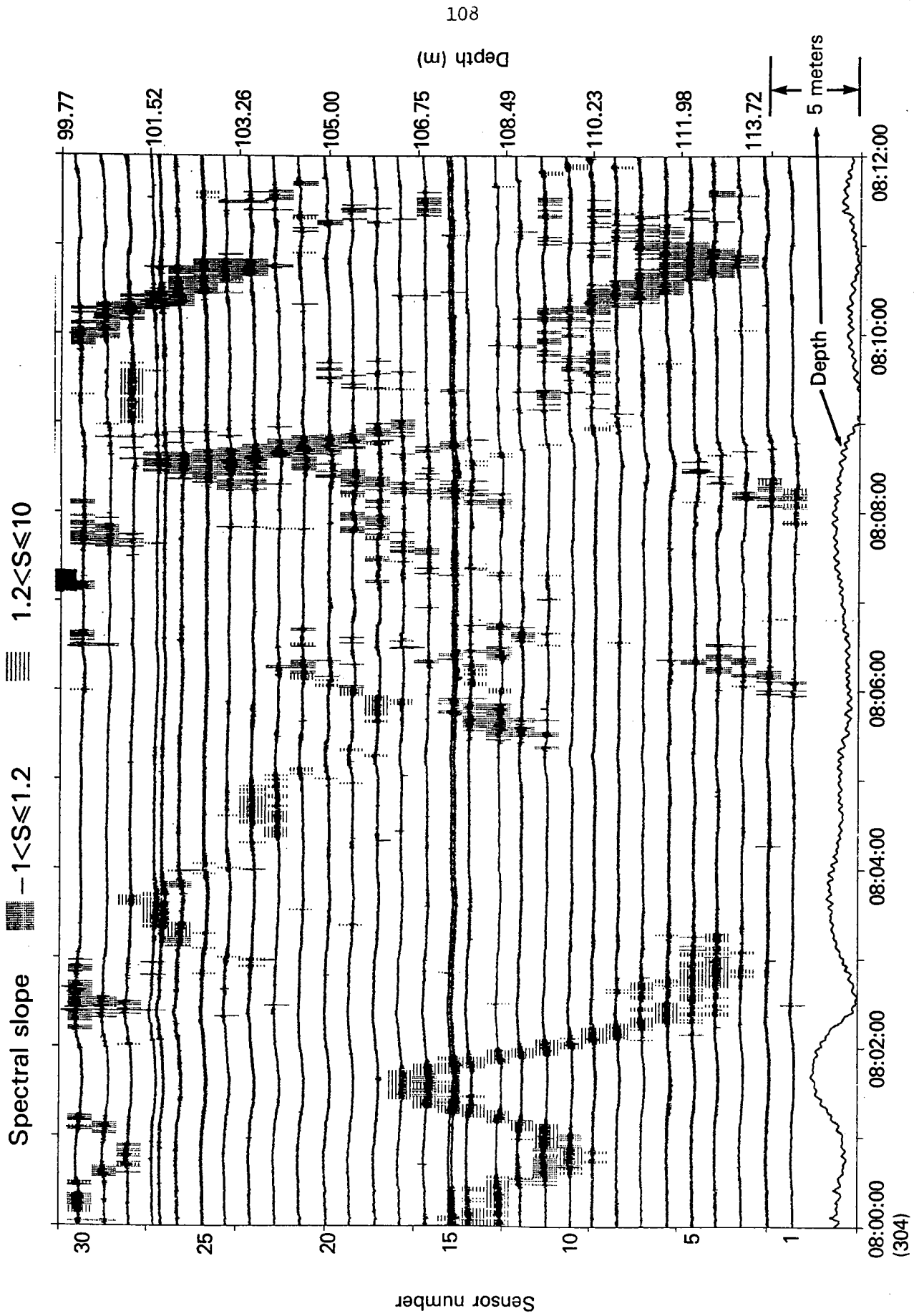
Fig. 5 Pre-emphasized conductivity showing spectral slope gray scale.

109

Fig. 4 Histograms of (a) kurtosis and (b) spectral slopes (power ratio slope technique).
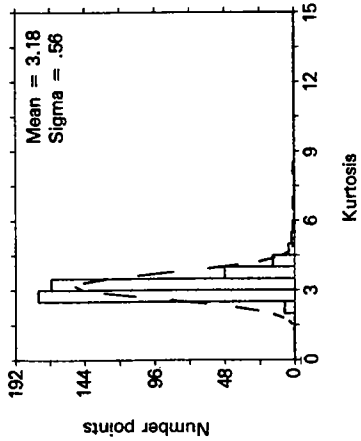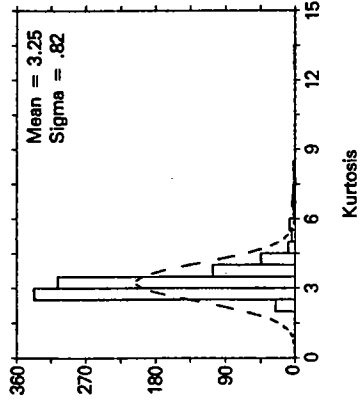
CASE 1 SALT FINGER   **CASE 3 TURBULENCE**

(a)

CASE 1 SALT FINGER   **CASE 3 TURBULENCE**

(b)

Fig. 3 Histograms of spectral slope (a) using direct spectral computation with geometric band averaging, and (b) using power ratio technique.
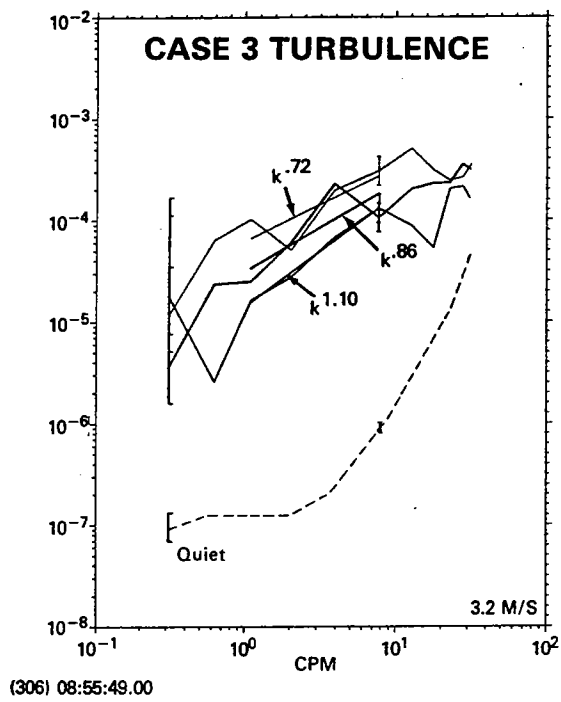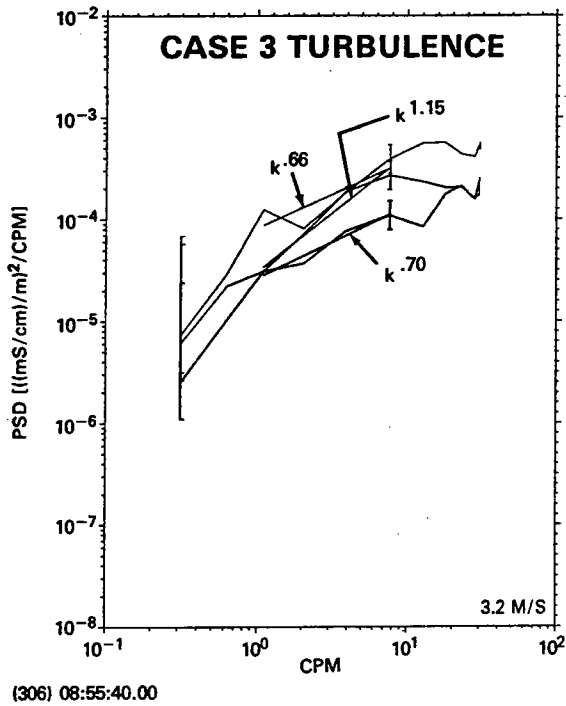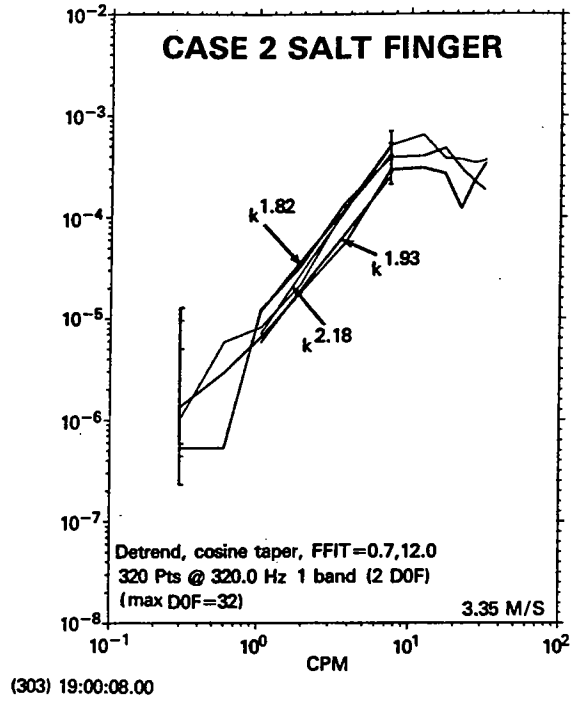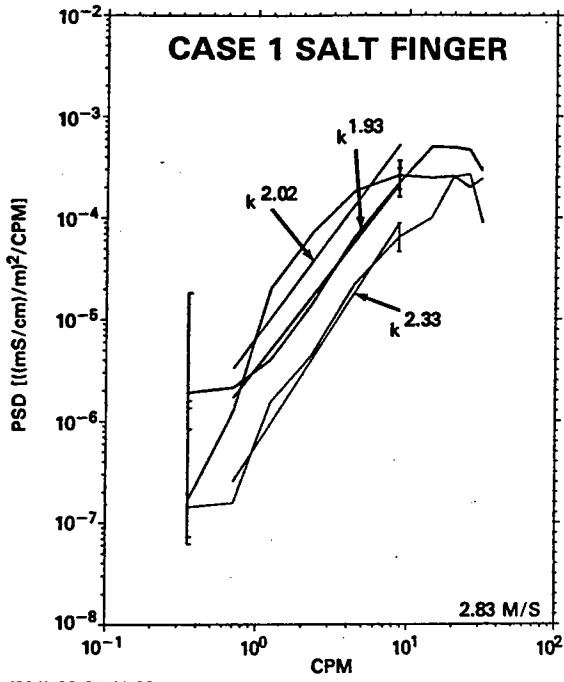
Fig. 2 Conductivity gradient spectra for salt-fingering and turbulence.
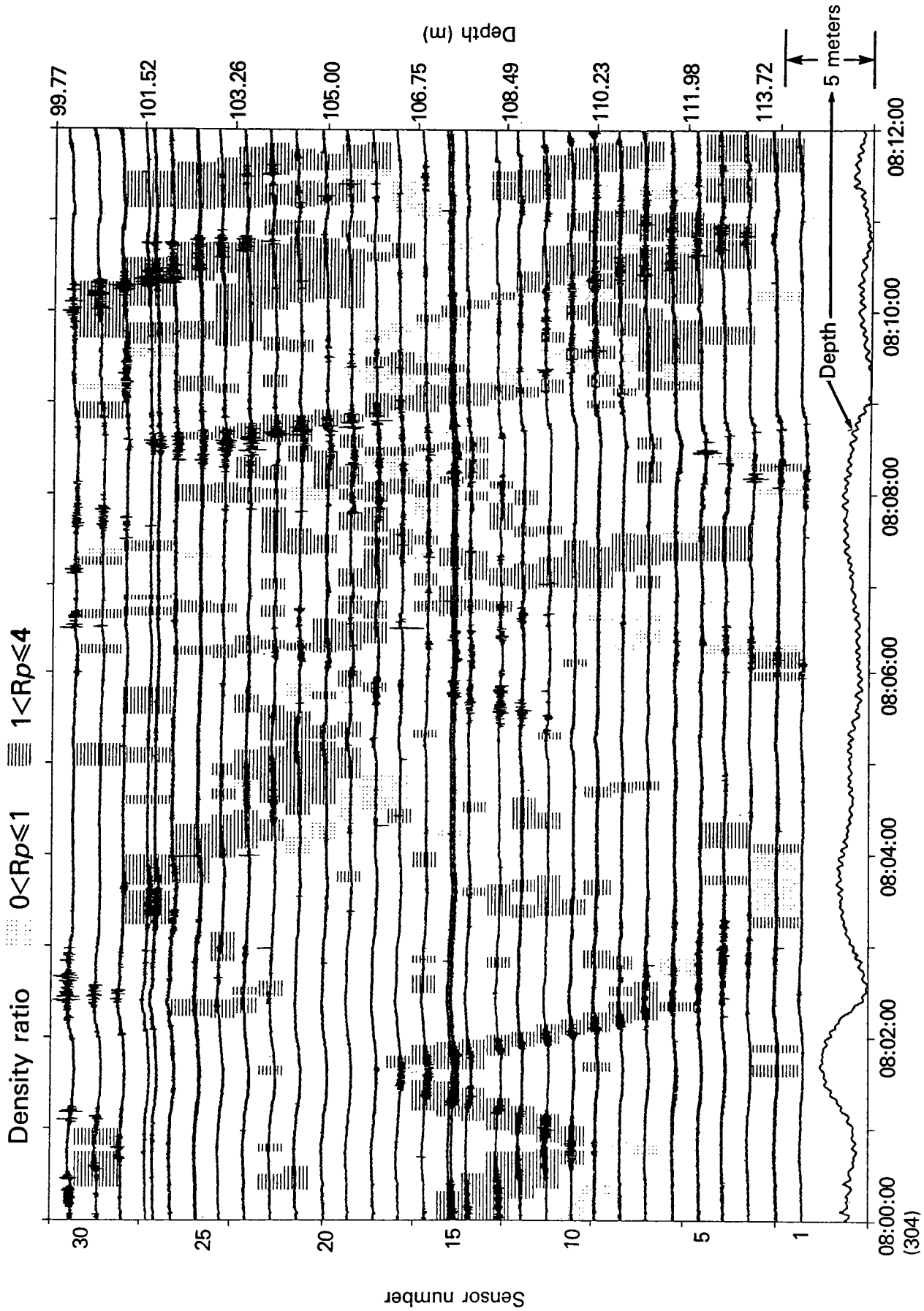
Fig. 1 Pre-emphasized conductivity with density ratio gray scale. The patch used to generate statistics for salt-fingering ('Case 1 SF Local') is shown in the first 3.5 minutes.

point edited and de-meaned. The kurtosis histograms for the three 'Local' tow segments are shown in Figure 4a. These are compared with the spectral slope histograms computed by the power ratio technique in Figure 4b. The salt-fingering regions have a mean kurtosis of about 3.2 and standard deviation of 0.56 to 0.82, whereas the turbulent regions have a mean of 6.11 with a much larger standard deviation of 3.4. The distributions have minimum overlap at K≈4. Note that the kurtosis histograms have long tails at high K values, suggesting that y=log K would give a better fit to a gaussian model. Table 1 summarizes the statistics for the spectral slopes and kurtosis.

We have used the criteria suggested by the slope and kurtosis histograms and applied this to the 2.2 km tow segments that include the regions from which our histograms were computed and other microstructure patches of unknown origin. Figure 5 shows the 'Case 1' tow segment with a gray scale based on slope using the criteria that slopes >1.2 imply salt-fingering and slopes ≤ 1.2 imply turbulence. This technique clearly improves upon the R_ρ gray scale plot of Figure 1. In particular the microstructure observed by sensor 17 at ~08:01:30 is identified along with the rest of the contiguous patch as due to salt-fingering. Several of the other patches later in the tow are identified as mostly due to turbulence even though some have R_ρ values less than 2.

The results from discriminating on the basis of kurtosis, where K ≤ 4 implies salt-fingering and K > 4 implies turbulence, are shown in Figure 6. The patch from 08:00 to 08:03 is identified as due to salt-fingering. The patches later in the tow are identified as mostly turbulence but with a small percent indicated as potentially salt-fingering.

These results suggest the joint use of slope and kurtosis to identify the percent of salt-fingering and turbulence. An indication of the joint distributions is given by the scatter diagrams shown in Figure 7. The upper plots (7a) represent only the data points generated from the population of just salt-fingering or turbulence ('Local'). The lower plots (7b) include all 12 minutes (2.2 km) of tow and all working sensors surrounding the 'Local' regions. 'Case 1 Salt-finger' and 'Case 2' both show a tight distribution of nearly all salt-fingering. With the inclusion of the full array, the distribution grows to include the lower slopes and higher kurtosis values of turbulence. Only 'Case 3' includes just turbulence for both the local and full 12-min regions. These distributions are similar to the results of Marmorino and Greenewalt (1988).

We are currently exploring optimal discrimination techniques under the assumptions that spectral slope (S) and log(K) are distributed as a stationary, bivariate normal distribution in both salt-finger and turbulent regions. We estimate the parameters of the joint density function (mean, variance, and co-variance of S and log(K)) in salt-finger and turbulent regions and form the log-likelihood ratio given by:

$$\lambda(S,\log(K)) = \ln\left[\frac{P(S,\log K|SF)}{P(S,\log K|Turb)}\right] \qquad (2)$$

Such a technique provides a statistically rigorous way of deciding what should be called salt-fingering (λ > 0) and turbulence (λ < 0) and further offers a measure of the relative error in such estimates. This work is currently in progress.

Summary

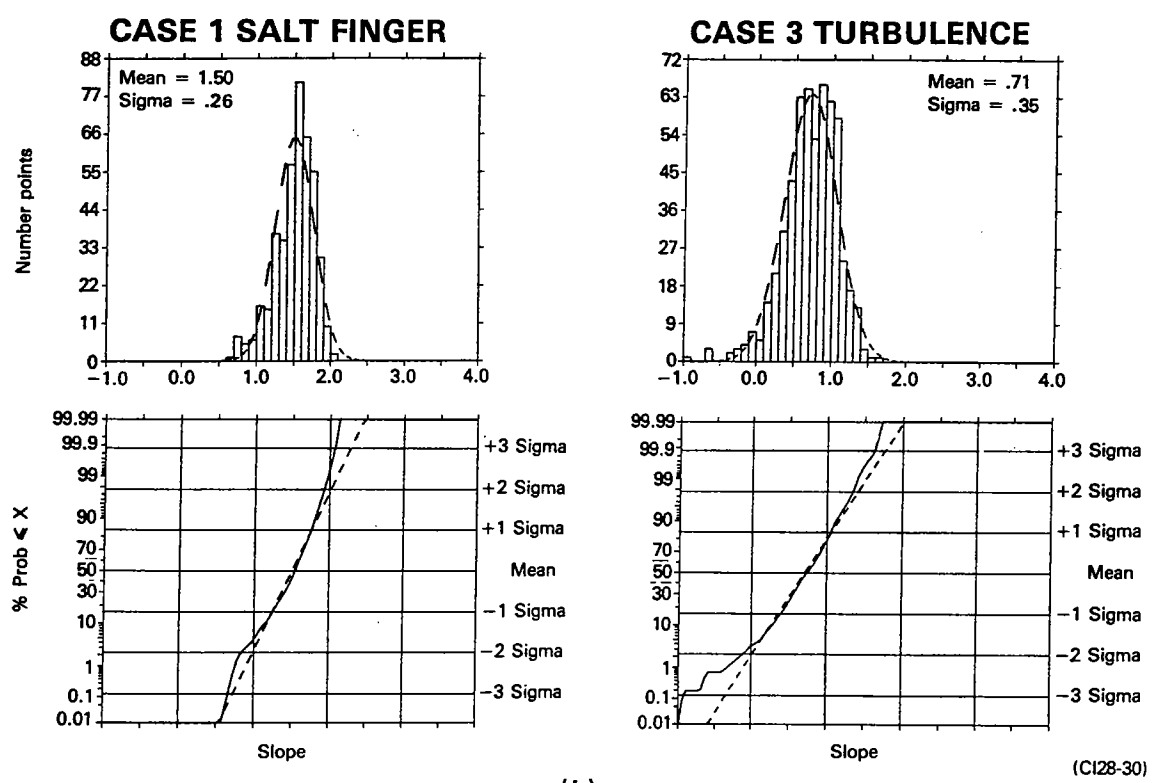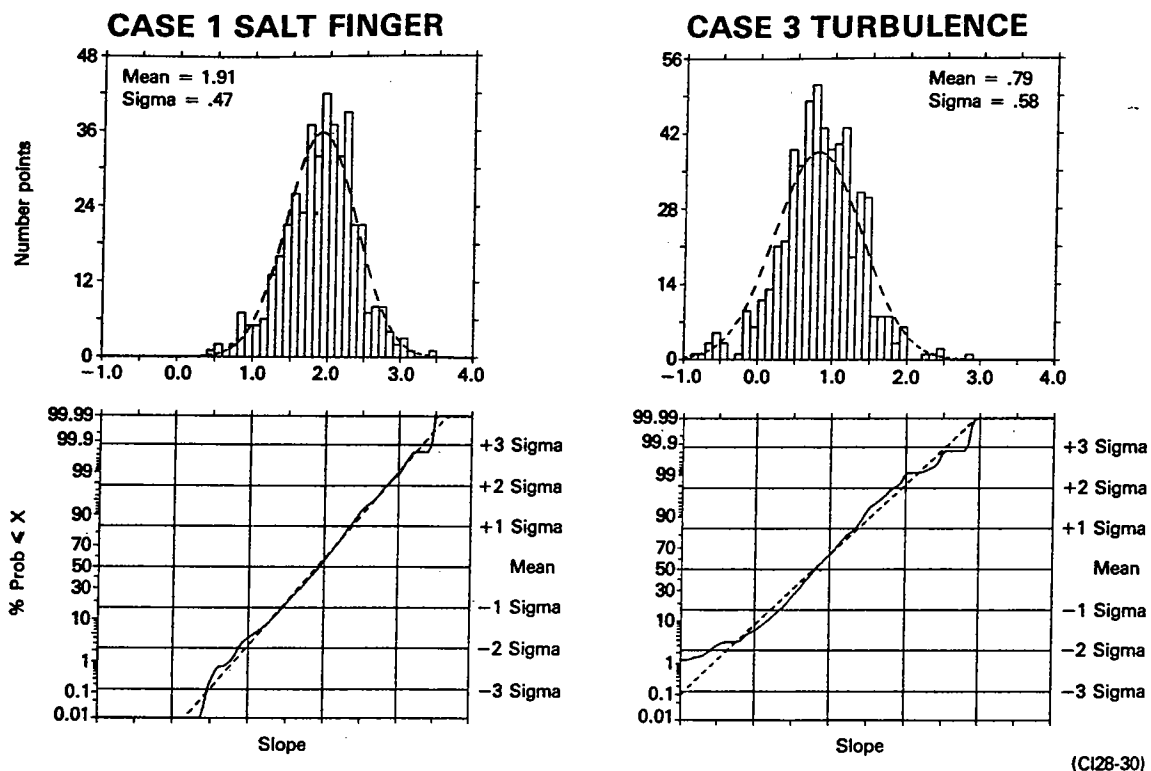Conductivity gradient spectral slope and kurtosis are applied to towed array data to distinguish salt-fingering from turbulence. For our towed data in the Sargasso Sea, these discriminators are more effective than R_ρ, particularly where tows are parallel to isopycnals. The power ratio technique of computing slopes is computationally efficient and shows good discrimination between salt-fingering and turbulence. These discriminators should improve upon the use of R_ρ alone since they can identify the portion of turbulence

at R_ρ values that could also support salt fingering and can help remove any ambiguity of interpretation. Optimal use of the joint statistics of slope and kurtosis is suggested.

Acknowledgements:

References

Farruggia, G.J., and A.B. Fraser, 1984: Miniature towed oceanographic conductivity apparatus. *Proc. IEEE Conf. Ocean '84*, 1010-1014.

Gargett, A.E., and R.W. Schmitt, 1982: Observations of salt fingers in the central waters of the Eastern North Pacific. *J. Geophys. Res.*, **87**, 8017-8092.

Holloway, G., and A.E. Gargett, 1987: The inference of salt fingering from towed microstructure observations. *J. Geophys. Res.*, **92**, 1963-1965.

Mack, S. A., 1985: Two-dimensional measurements of ocean microstructure: the role of double diffusion. *J. Phys. Oceanogr.*, **15**, 1581-1604.

Mack, S.A., 1989: Towed-chain measurements of ocean microstructure. *J. Phys. Oceanogr.*, **19**, 1108-1129.

Marmorino, G.O., 1987: Observations of small-scale mixing processes in the seasonal thermocline. Part 1: Salt fingering. *J. Phys. Oceanogr.*, **17**, 1339-1347.

Marmorino, G.O., and D. Greenewalt, 1988: Inferring the nature of microstructure signals. *J. Geophys. Res.*, **93**, 1219-1225.

Schmitt, R.W., 1979: The growth rate of super-critical salt fingers. *Deep-Sea Res.*, **26**A, 23-40.

Schmitt, R.W., and D.T. Georgi, 1982: Finestructure and microstructure in the North Atlantic Current. *Deep-Sea Res.*, **40** (Suppl.), 659-705.

Shen, C.Y., 1989: The evolution of the double-diffusive instability: Salt fingers. *Phys. Fluids A*, **1**, 829-844.

Table 1. Statistics for spectral slope (by different slope techniques), kurtosis and log-kurtosis.

	Case 1 Salt-Finger		Case 2 Salt-Finger		Case 3 Turbulence	
	Mean	Sigma	Mean	Sigma	Mean	Sigma
Slope (Raw Spectra)	1.64	.47	1.45	.64	.57*	.51
Slope (Geo Band Ave Spectra)	1.91	.47	1.73	.66	.79*	.58
Slope Power Ratio (smoothing)	1.50	.26	1.49	.33	.71*	.35
Kurtosis	3.18	.56	3.25	.82	6.11	3.40
Log Kurtosis	0.50	.064	0.50	.081	0.75	0.16

* sensors 22-25 not included.

THE SCALED DISSIPATION RATIO AS AN INDICATOR OF SALT FINGER MIXING

James M. Hamilton and Neil S. Oakey
Physical and Chemical Sciences Branch, Department of Fisheries and Oceans,
Bedford Institute of Oceanography, Dartmouth, Nova Scotia, Canada, B2Y 4A2

ABSTRACT
     The ratio of thermal to turbulent kinetic energy dissipation, Γ, as determined from microstructure measurements, was shown by Oakey (1988) to be larger in regions where double diffusion was favored. Hamilton, Lewis and Ruddick (1989) developed a model using this "scaled dissipation ratio", Γ, to distinguish between turbulent mixing and salt finger mixing. This is necessary because of the discrepancy between the calculated vertical mixing rates for each of the two processes. To explore this model a preliminary analysis of microstructure measurements from the top 500 m. of the Canary basin is discussed here. Although there may be a suggestion of some salt finger activity from the calculated values of Γ, problems with the merging of EPSONDE and CTD data, and the selection of appropriate averaging intervals, means that further work is required.

1.0 INTRODUCTION

Oakey(1988) showed that regions near a MEDDY where salt fingering was favored had an excess of large values of Γ. Γ, the "scaled dissipation ratio" is the ratio of thermal to turbulent kinetic energy dissipation calculated from microstructure quantites. Hamilton, Lewis and Ruddick (1989) considered two different vertical mixing models and demonstrated that it was necessary to be able to distinguish between them before accurate vertical mixing rates could be calculated from observations of microstructure data. The two models, a turbulent mixing model and a salt finger model, describe two rather different physical processes. The major difference between them is that turbulence, which uses shear in the flow to produce mixing, acts to raise the potential energy of the water column. Salt fingering on the other hand extracts energy from the salinity field to produce the mixing, resulting in a lowering of the center of mass of the water column. This basic difference in the energetics of the two processes leads to different mixing rates as calculated from the relevant observable quantities. Even if all of the mean and microstructure quantities are properly measured, an incorrect assumption about which of the two mixing processes dominates can result in errors in mixing rates of a factor of 2 or 3 (Hamilton et. al., 1989).

It was proposed by Hamilton et. al. that observations of the scaled dissipation ratio, Γ, could be used to distinguish between the two mixing

processes. If it is assumed that $\bar{T} = \bar{T}(z)$ only, then Γ is defined in terms of measurable quantities as

$$\Gamma = \frac{N^2 \chi_T}{2 \, \epsilon \, \bar{T}_z^2} \, . \tag{1}$$

Here, N is the buoyancy frequency, χ_T ($= 6 \, D \, \overline{T_z'^2}$) is the rate of dissipation of thermal variance where D is the molecular diffusivity of heat, and ϵ ($= 7.5 \, \nu \, \overline{u_z'^2}$) is the turbulent kinetic energy dissipation where ν is the kinematic viscosity of water. Fluctuating quantities are denoted by primes while mean quantities are denoted by over-bars.

The microstructure quantities, χ_T and ϵ, can be estimated using EPSONDE. We will examine the value of Γ as an indicator of salt fingering activity using a CTD and EPSONDE data set from the Canary Basin of the North-Eastern Atlantic. Here low values of the density ratio, R_ρ ($= \alpha \, T_z / \beta \, S_z$) and some steppiness in the T-S profiles, suggest the presence of salt fingers (Schmitt, 1979; Mack, 1985).

2.0 THE MIXING MODELS

2.1 The Turbulent Mixing Model

In a turbulent non-double-diffusive system, the vertical diffusivity of any scalar variable is given by

$$K_{scalar,t} = \Gamma_t \, \epsilon / \, N^2 \tag{2}$$

(Osborn, 1980; Oakey, 1982), where Γ_t is a constant of proportionality in a turbulent system. Osborn (1980) proposed a value for Γ_t of 0.2 based on energy arguments. Lilly et. al. (1974) found $\Gamma_t = 0.33$ from atmospheric measurements, while oceanic values of 0.26 have been measured (Oakey, 1982 ; $\Gamma = 0.26 \pm 0.21$, and similar values from Oakey, 1985).

2.2 The Salt Finger Model

In a salt finger system, Hamilton et. al.(1989) have shown that the vertical diffusivity for salt is given by

$$K_{s,f} = [R_\rho(\Gamma_f + 1) - 1] \, \epsilon / \, N^2 \tag{3}$$

where Γ_f is the value of Γ characteristic of a salt finger system. They also derived an expression for Γ_f in terms of the salt finger flux ratio, r_f

$$(= F_{T,f} / F_{S,f})\ as$$

$$\Gamma_f = \frac{r_f (R_\rho - 1)}{R_\rho (1 - r_f)} \qquad (4)$$

By assuming that Stern's [1975] equation for the salt finger flux ratio which is given as

$$r_f = R_\rho^{1/2} [\ R_\rho^{1/2} - (R_\rho - 1)^{1/2}] \qquad (5)$$

is appropriate in oceanic salt finger systems, they found that the values of Γ_f as computed from (4) are significantly different than those expected in a turbulent system for all but very low values of R_ρ.

3.0 THE DATA

The data set used in this analysis consists of a merged set of EPSONDE and CTD data. Values of χ_T, ϵ, and T_z averaged over 15 m. have been calculated from EPSONDE microstructure measurements for 92 drops, over a depth range of 150 to 450 m. Values of N and R_ρ averaged over 40 m. have been obtained from CTD casts. These casts were not done simultaneously with EPSONDE drops, but were typically within two kilometers and two hours of the corresponding EPSONDE station. Upon merging of the corresponding profiles from each of the two instruments, R_ρ was recomputed to make use of the 15 m. temperature gradient data available from the EPSONDE data set using

$$R_\rho = \frac{g\,\alpha\,T_z}{g\,\alpha\,T_z - N^2} \qquad (6)$$

Over 1000 values of Γ and R_ρ computed on a 15 m. scale were derived from this data set for statistical interpretation and comparison to the mixing models.

4.0 DATA ANALYSIS AND DISCUSSION

In an attempt to better understand the nature of the mixing between 150 and 450 m. in the Canary Basin, the dependence of Γ on R_ρ was examined. A functional dependence in the case of salt fingers is expected, but not for shear-driven turbulence.

Shown in Figure 1 are the measured Γ values plotted as a function of R_ρ. A program (Dan Kelley, Personal Communication) which uses Tukey's (1977)

box-and-whisker method, is used to display the data. The bar through each
box designates the median for the prescribed R_ρ range, with upper and lower
quartiles defined by the horizontal borders of the box (50 % of the data is
within the box). The "whiskers" extend to the most extreme data point that
is within 1.5 interquartile ranges of the upper and lower quartiles. Minor
outliers, shown as open circles, represent data points that fall between 1.5
and 3 interquartile ranges beyond the upper and lower quartiles, while
extreme outliers, which fall outside 3 interquartile ranges, are shown as
filled circles.
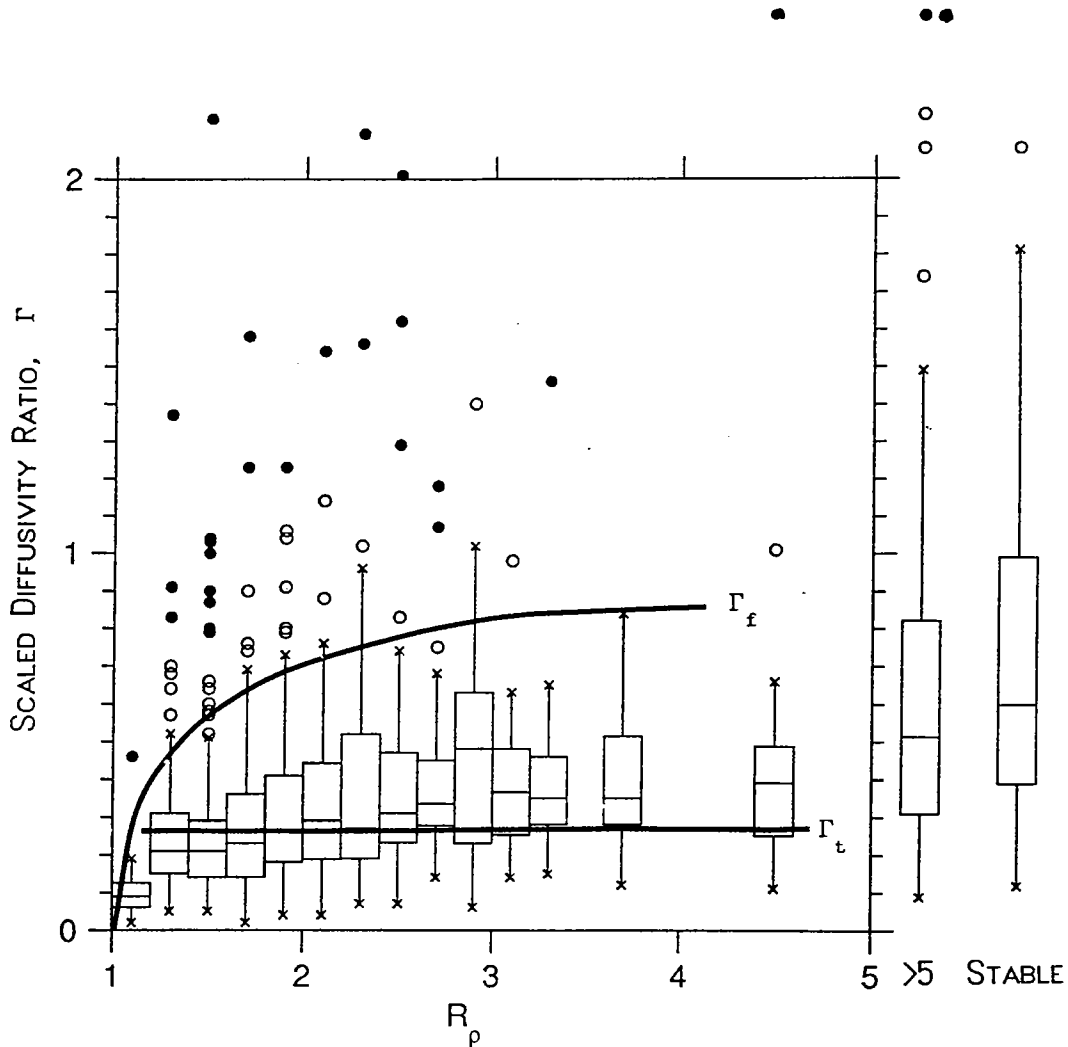
Figure 1 - *Computed 15 m. averaged* Γ *values from 92 EPSONDE stations over the depth interval, 150 - 450 m. Also shown are expected values for turbulence* $(\Gamma_t=0.26)$, *and for salt fingers* (Γ_f) *where (Eqn 5) is considered appropriate for the salt finger flux ratio.*

Also shown in Figure 1 are the curves which describe the values expected
for Γ for each of the two models. A value of 0.26 is used for Γ_t, while Γ_f
is described by (4) where Stern's expression for the salt finger flux ratio

is considered appropriate. The measured Γ values, which have been calculated according to the description in Section 3.0, show a functional dependence on R_ρ, which is not expected if turbulence dominates in the mixing. However, at values of $R_\rho > 2$ it is unlikely that salt fingering can be occurring to any great extent, yet the measured Γ values continue to increase. The Γ_{obs} in the range stable to salt finger formation is much larger than the turbulent value we would expect. The data as processed here must be considered suspect.

To resolve the apparent problem with the computation of Γ, several areas need to be addressed. It has been assumed that merging of 40 m. averaged CTD data with the EPSONDE data is reasonable, considering the closeness of the stations in space in time. It might be instructive to compare the temperature gradients as computed from each of the instruments to see at what scale the two correlate well. This might be the most sensible scale on which to compute Γ. The data available to us here was processed for a different purpose, so may not be ideal for this type of analysis in its present form.

Another area of concern is the way in which R_ρ has been computed. The N computed from the CTD on a 40 m. scale, and temperature gradient from EPSONDE on a 15 m. scale was used in equation (6) to calculate a local EPSONDE value of R_ρ. R_ρ was then correlated with Γ_{obs} which was determined from values of ϵ, χ_T, and T_z measured with EPSONDE. Where the salinity gradient contributes significantly to the density gradient, as is the case here, this approach may not be appropriate.

Further work with the data set is required before it can be clearly determined whether microstructure measurements from this region lend support to the salt fingering mixing model of Hamilton et. al. (1989). It is interesting that there are many large outliers in the Γ data at low R_ρ. This may be a suggestion that salt finger activity is producing large values of Γ consistent with their model. There are, however, large values of Γ at larger R_ρ where only turbulent mixing is expected. These values are thought to be a result of merging and scaling of available data from instruments measuring on different space and time scales. Particularly, the calculation of N and the application of equation (6) at large R_ρ may be suspect. Further work is required before a conclusive answer to these questions can be obtained. Therefore, the result shown in Figure 1 must be accepted only with reservations.

5.0 ACKNOWLEDGEMENTS

6.0 REFERENCES

Hamilton, J.M., M.R. Lewis and B.R. Ruddick, Vertical fluxes of nitrate associated with salt fingers in the World's oceans, J. Geophys. Res., 94, C2, 2137-2145, 1989.

Lilly, D.K., D.E. Waco and S.I. Adelfang, Stratospheric mixing estimated from high-altitude turbulence measurements, J. Appl. Meteor., 13, 488-493, 1974.

Mack, S.A., Two-dimensional measurements of ocean microstructure: The role of double diffusion, J. Phys. Oceanogr., 15, 1581-1604, 1985.

Oakey, N.S., Determination of the rate of dissipation of turbulent energy from simultaneous temperature and velocity shear microstructure measurements, J. Phys. Oceanogr., 12, 256-271, 1982.

Oakey, N.S., Statistics of mixing parameters in the upper ocean during JASIN phase 2, J. Phys. Oceanogr., 15, 1662-1675, 1985.

Oakey, N.S., Estimates of mixing inferred from temperature and velocity microstructure, in Small-scale Turbulence and Mixing in the Ocean; Proceedings of the 19th International Liege Colloquium on Ocean Hydrodynamics, edited by J.C.J. Nihoul and B.M. Jamart, Elsevier, New York, 1988.

Osborn, T.R., Estimates of the local rate of vertical diffusion from dissipation measurements, J. Phys. Oceanogr., 10, 83-89, 1980.

Schmitt, R.W., The growth of super critical salt-fingers, Deep Sea Res., Part A, 26, 23-40, 1979.

Stern, M.E., Ocean Circulation Physics, Academic, San Diego, Calif., 1975.

Tukey, J.W., Exploratory Data Analysis. Addison-Wesley, Reading, Mass., 1977.

Salt–Finger Fluxes in a Meddy

Dave Hebert
College of Oceanography
Oregon State University
Corvallis, OR 97331–5503

ABSTRACT

Salt–finger fluxes based on changes in salinity and temperature profiles through the centre of a Mediterranean salt lens over a year are compared to estimates of salt–finger fluxes using laboratory flux laws, a model of Kunze(1987) and a criterion of Stern(1976) applied to some of the steps observed in the profiles. The fluxes using laboratory flux laws are an order of magnitude larger than the observed fluxes while fluxes using Kunze's model for thick interfaces and Stern's criterion are consistent with the observed fluxes.

The rate at which the Meddy lost salt is compared to an estimate based on the flux estimate through the bottom of the Meddy by salt–fingers. This salt–finger rate is approximately two orders of magnitude too small. Simple salt–finger fluxes through the base of the Meddy cannot be responsible for the observed lost of the salt content of the Meddy.

1. INTRODUCTION

Past salt–finger flux estimates in the ocean have been made by applying laboratory flux laws to observed steps in the salinity and temperature profiles (*e.g.* Lambert and Sturges, 1977; Schmitt and Evans, 1978). The applicability of these laboratory flux laws, also known as the $4/3$ laws since the fluxes depend on $\Delta S^{4/3}$ where ΔS is the change in salinity across the salt–fingering interface between two homogeneous layers, has been questioned recently (Gregg and Sanford, 1987; Kunze, 1987; Lueck, 1987; Schmitt, 1988). Assuming that the buoyancy flux provided by salt–fingers F_b balanced the dissipation ϵ observed in the salt–fingering interfaces, dissipation measurements in C–SALT staircases (Gregg and Sanford, 1987; Lueck, 1987) gave a F_b approximately 30 times smaller than the buoyancy flux calculated using the laboratory flux laws on the observed steps.

There are several problems in comparing ocean dissipation rates in salt–fingering interfaces with buoyancy fluxes using laboratory flux laws (Hebert, 1988c). One major problem is that the buoyancy flux due to salinity $(g\beta F_S)$ is partially compensated by the buoyancy flux due to temperature $(g\alpha F_T)$. Thus, the total buoyancy flux $(F_b = g\beta F_S(1 - \gamma))$ depends on the flux ratio $\gamma = \alpha F_T/\beta F_S$. Laboratory flux measurements (Schmitt, 1979; McDougall and Taylor, 1984) find that γ ranges from 0.6 to 0.7 when the density ratio $R_\rho = \alpha \partial T/\partial z/(\beta \partial S/\partial z)$ is approximately 2 and that $\gamma \to 1$ as $R_\rho \to 1$ (Stern, 1975). A 10% error in the estimates of $g\beta F_S$ and $g\alpha F_T$ in the laboratory experiments gives an uncertainty in γ and F_b of 35% if $\gamma = 0.7$ and 60% if $\gamma = 0.8$. As $\gamma \to 1$, the uncertainty in F_b increases dramatically. Also, laboratory flux experiments have not been performed for R_ρ less than 1.2.

Rather than attempt to examine the applicability of the laboratory flux laws in the ocean by comparing the difference between the salinity and temperature fluxes, it would be more desirable to compare the salinity and temperature flux estimates using these

laboratory formulae directly with the observed fluxes or flux divergences in the ocean. In this note, the fluxes estimated from the large—scale vertical changes in a Mediterranean salt lens will be compared with estimates based on the observed steps in the profiles (Section 2). In Section 3, the salt–flux estimates by salt–finger at the bottom of the Meddy will be compared to the salt lost rate of the Meddy over one year.

2. SALT FINGER FLUXES

The study of a Mediterranean salt lens (Meddy) over a two year period (Hebert, 1988a,b; Armi et al., 1989) allows us to estimate the vertical flux due to salt–fingers. Mediterranean salt lenses are coherent anticyclonic eddies of Mediterranean water found in the North Atlantic which are several tens of kilometers in radius and hundreds of metres in thickness. The salt lens discussed in this paper was tracked in the eastern North Atlantic using SOFAR floats which allowed the Meddy to be found and surveyed four times (Figure 1) with CTD and velocity profilers. Armi et al.(1989) have summarized the observations

Figure 1. The trajectory of the Meddy over a two year period as shown by a SOFAR float. The float track is marked every 10 days by a solid dot. Location and size of the Meddy at each survey are shown to scale (solid circle: core, open circle: total size, dashed circle: salinity front).
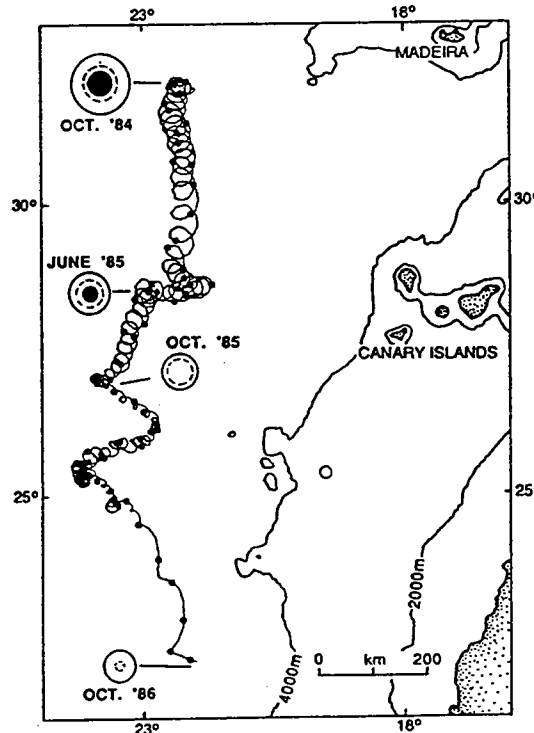
made during the study of this Meddy. The Mediterranean salt lens, located at a depth of 1000 db, was much warmer (2.5°C) and saltier (0.6 PSU) than the Atlantic water at the same depth. With this salinity and temperature anomaly we would expect double–diffusive processes to be active at the top (diffusive convection) and bottom (salt–fingers) of the Meddy. In fact, steps in the salinity and temperature profiles at the top and bottom of the central region of the Meddy were present; a positive sign that double–diffusion processes were likely an important mixing mechanism in these regions. For the first two survey periods, the Meddy had a central core region which has very small or non–existent

horizontal gradients. Any change at the centre of the Meddy was most likely due to vertical mixing. By the third survey period, intrusions had reached the centre of the Meddy (Figure 1). Hebert(1988a) showed that the total horizontal flux of salt and heat due to intrusions was more than two orders of magnitude larger than the total vertical flux due to salt–fingers as estimated below. Therefore, we cannot assume that changes at the centre of the Meddy after the third survey were due to salt–fingers. Also, flux estimates based on changes between the June 1985 and October 1985 survey periods are likely to be overestimates but we can't determine their effect on the observed fluxes since we don't know when the intrusions reached the centre of the Meddy. The changes in the centre of the Meddy over the first three surveys will be assumed to result from mixing in the vertical (i.e., a one–dimensional model).

As the Meddy aged, it moved in an erratic but generally southward direction (Figure 1) into cooler, fresher background water (Hebert, 1988b). The separation between isopycnals at the centre of the Meddy decreased with time as the total angular momentum of the Meddy decreased. As the Meddy moved southward, the depth of the isopycnals in the background water also changed. These effects will change the vertical structure of the Meddy without producing a vertical (diapycnal) flux by salt–fingers. To eliminate these non–mixing effects, the vertical profiles were stretched to have the same vertical density structure as the June 1985 survey (Figure 2). Details of this pressure stretching are given in Hebert(1988c).
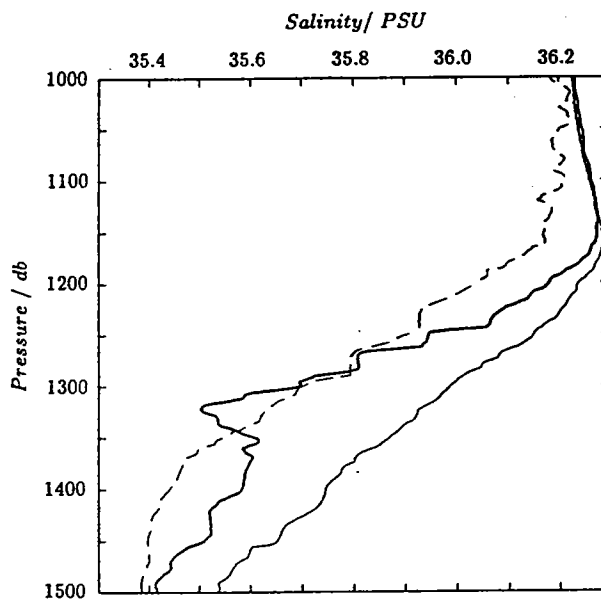
Figure 2. Profiles of salinity through the centre of the Meddy for the three survey periods: October 1984 (thin line), June 1985 (thick line) and October 1985 (dashed line). The salinity profiles for the October 1984 and October 1985 survey periods have been stretched (see text).

Any change in the vertical salinity structure of the Meddy in this stretched pressure system is assumed due to a vertical flux divergence. In other words,

$$\frac{\partial}{\partial t} \int_{p_1}^{p_2} S\ dp = F_S(p_2) - F_S(p_1) \tag{1}$$

where $F_S(p)$ is the salinity flux at pressure p. To estimate the average salt–finger flux, it is necessary to determine the pressure interval over which to determine the total salinity change. The upper pressure limit is obvious; it can be anywhere in the stably stratified region but a pressure of 1150 db was chosen to reduce the influence of the intrusions for the third survey. Thus $F_S(p_1) = 0$. The location of the lower pressure is more subjective. It is necessary to choose a pressure when salt–fingers were active for the three surveys, say when $R_\rho < 1.5$. It should also be where steps were observed for the June 1985 survey period since we want to compare the flux determined in this section with estimates based on the observed steps. Finally, it was decided to use the pressure where the flux would be a maximum between the second and third surveys, that is, the pressure where the salinity profiles from the two surveys intersect (Figure 2). The pressure chosen was 1286 db.

From the changes in the salinity structure of the Meddy centre, we find both $g\alpha F_T$ and $g\beta F_S$ are $5 \times 10^{-9} W\ kg^{-1}$ (October 1984 — June 1985) and $9 \times 10^{-9} W\ kg^{-1}$ (June 1985 — October 1985). The net buoyancy flux is zero since we forced the vertical density structure in all profiles to be the same (*i.e.* $\gamma = 1$). Of course, this is incorrect since we know that the density flux ratio is less than 1 for salt–fingers (*e.g.* Schmitt, 1979); it is necessary to account for $\gamma \neq 1$ in determining the stretched pressure.

A flux ratio less than 1 implies that as a parcel of water loses salt (assuming there is no flux into it), it also loses mass thus becoming lighter. With a flux of salt and heat into a parcel as well as out of the parcel, the change in density of the parcel is $\rho_0(1 - r)\Delta S$ where ΔS is the change in salinity of the parcel and $r = (\alpha \partial F_T/\partial z)/(\beta \partial F_S/\partial z)$, the ratio of flux divergences. Since γ is a function of R_ρ and R_ρ varies over the salt–fingering region, both γ and r will vary over this region. Assuming that γ does not change significantly between the salt–finger flux into and out of the parcel, then $r = \gamma$. Table 1 of Hebert(1988c) showed that γ, based on a fit to laboratory flux measurements and a theoretical model of fastest growing fingers, ranged from 0.63 to 0.94 for the observed steps. Rather than choosing a functional dependence for γ (and r) on R_ρ such as Kunze's(1987) relationship, I decided to use a constant value of 0.7 for r. To determine the new stretched pressure for the October 1984 and October 1985 survey profiles, it is necessary to find the pressure of the water parcel $(p_{\Delta T})$ that had a pressure p_0, density ρ_0, and salinity S_0 for June 1985 survey and had a density $\rho_{\Delta t}$ and salinity $S_{\Delta t}$ for the October survey and satisfies the relationship

$$\rho_{\Delta t}(p_{\Delta t}) - \rho_0(p_0) = \rho_0(1 - r)\beta[S_{\Delta t}(p_{\Delta t}) - S_0(p_0)] \tag{2}$$

We see that when $r = 1$ that the density flux due to salinity is completely compensated by the density flux due to temperature. The density of a water parcel remains the same as it loses salt; this is the pressure stretching used for Figure 2.

The difference between the three salinity profiles, with the profiles for the October 1984 and October 1985 survey periods stretched using (2), is reduced (Figure 3). (The large increase in salinity in the June 1985 profile at approximately 1320 db forces the pressure coordinate for the October 1984 and October 1985 profiles to be greatly stretched producing the almost homogeneous layers in the October 1984 and October 1985 profiles below 1320 db.) The salt–finger fluxes using the change in the salinity and temperature profiles in the pressure range 1150–1286 db are:

|	$g\alpha F_T/(10^{-9}W\ kg^{-1})$	$g\beta F_S/(10^{-9}W\ kg^{-1})$	$F_b/(10^{-9}W\ kg^{-1})$
October 1984—June 1985	2.2	2.9	0.7
June 1985—October 1985	3.3	4.5	1.2

Figure 3. Profiles of salinity through the centre of the Meddy for the three survey periods: October 1984 (thin line), June 1985 (thick line) and October 1985 (dashed line). The salinity profiles for the October 1984 and October 1985 survey periods have been stretched using $r = 0.7$(see text).
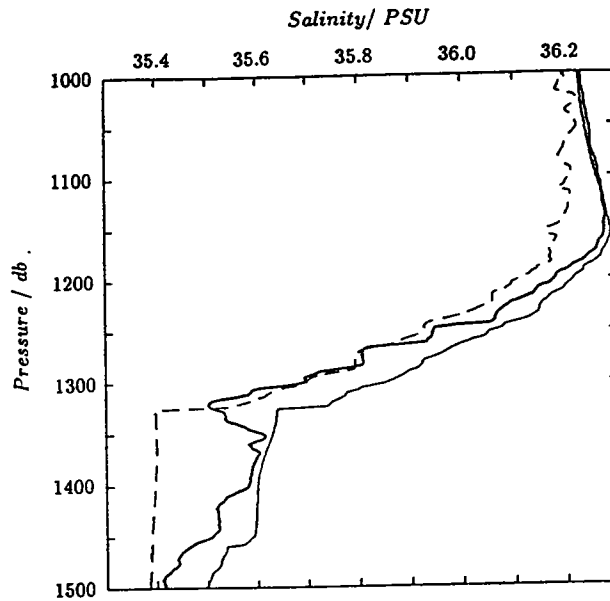
In the above discussion, the point of view for determining the change in the salinity profiles was a Lagrangian one. That is, the position of an individual parcel of water was tracked between the three surveys (using the assumption that the flux divergence ratio was 0.7). It is also possible to examine the $\gamma \neq 1$ effect from an Eulerian point of view (McDougall, 1987). The change in salinity on an isopycnal is

$$\frac{\partial S}{\partial t} = -\frac{\partial F_S}{\partial z}\left[\frac{R_\rho - r}{R_\rho - 1}\right] \quad \text{where} \quad \frac{\alpha \partial F_T/\partial z}{\beta \partial F_S/\partial z} \tag{3}$$

The salinity profiles in Figure 2 have been stretched in such a way that changes in salinity at a constant pressure represents changes in salinity on an isopycnal. To correct the flux estimates using these profiles for $\gamma \neq 1$, it is necessary to determine the factor $(R_\rho - r)/(R_\rho - 1)$. Using a R_ρ of 1.3 and assuming $r \approx \gamma \approx 0.7$ as before, the flux estimates found for $\gamma = 1$ should reduce by a factor of 2 to give the true salt–finger fluxes — approximately what is found when the profiles were stretched using $r = 0.7$.

Hebert(1988c) examined several of the steps during the June 1985 survey (see Table 1 in Hebert, 1988c). Fluxes of salinity, temperature and buoyancy for these steps were determined using the laboratory flux law formulae of Kelley(1986), Kunze's(1987) model and Stern's(1976) criterion. The average fluxes from these different formulae are shown in Figure 4. (Note: For the fluxes based on Stern's(1976) criterion, A=4 was used instead of A=1 as used in Hebert, 1988c.) We see that both the laboratory flux laws as presented by Kelley(1986) and the *maximum* fluxes using Kunze's(1987) model for *thin* interfaces are more than an order of magnitude larger than *maximum* fluxes predicted by Kunze's(1987)

model for *thick* interfaces. Using Stern's criterion (with $A = 4$), we find the fluxes are approximately the same as found for Kunze's(1987) model for *thick* interfaces.

The average fluxes based on laboratory measurements (either Kelley's(1986) formulae or Kunze's(1987) *thin* interface formulae) are an order of magnitude larger than the fluxes determined from the change in the structure of the Meddy (Figure 4). The *maximum* flux estimates using Kunze's(1987) model for *thick* interfaces or Stern's(1976) criterion (with A=4) are in good agreement with the estimates using the change in salinity at the base of the Meddy.
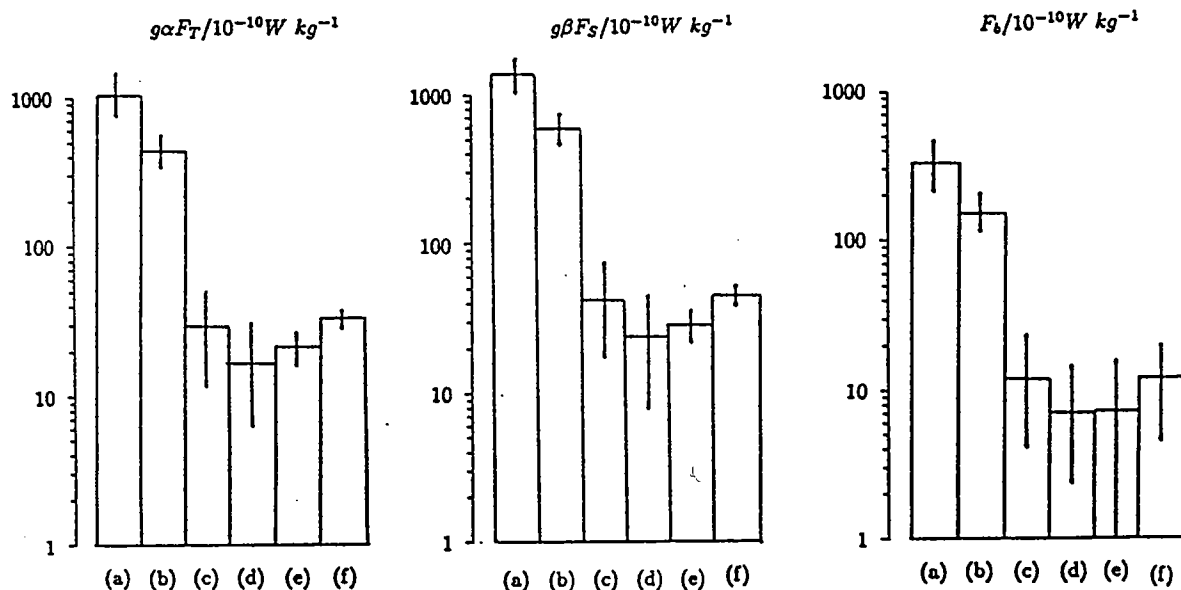
Figure 4 Average salt finger fluxes using (a) laboratory flux laws á la Kelley(1986), (b) Kunze's(1987) *thin* interface formulae, (c) Kunze's(1987) *thick* interface formulae and (d) Stern's(1976) criterion (A=4) applied to steps observed during June 1985. Salt finger flux estimates from changes in the salinity and temperature structure of the Meddy using $r = 0.7$ for (e) October 1984–June 1985 and (f) June 1985–October 1985.

3. DECAY OF THE MEDDY

To determine the decay of the Meddy by salt–finger fluxes at the base of the Meddy, it is necessary to determine both the salt flux by salt–fingers and the area over which the salt–finger flux is occurring. In the previous section, we found the vertical flux of salt to be approximately $5 \times 10^{-7} PSU\ m\ s^{-1}$ at the centre of the Meddy. The region where salt–fingering may be present can be determined by Turner angle (Figure 5). It is generally believed salt–fingers are very active when then Turner angle is greater than $78.7°$ $(R_\rho < 1.5)$. We see that the base of the Meddy is one area where salt–fingering should be occurring (Figure 5). Assuming the above salinity flux occurred over this region, which extended to a radius of approximately 17 km, the Meddy would be losing salt at a rate of 900 $kg\ s^{-1}$. The observed rate of salt lost ranged from $2.5 \times 10^4 kg\ s^{-1}$ to $6.6 \times 10^4 kg\ s^{-1}$ over the October 1984 — October 1985 period (Hebert, 1988a; Armi *et*

Radius / km
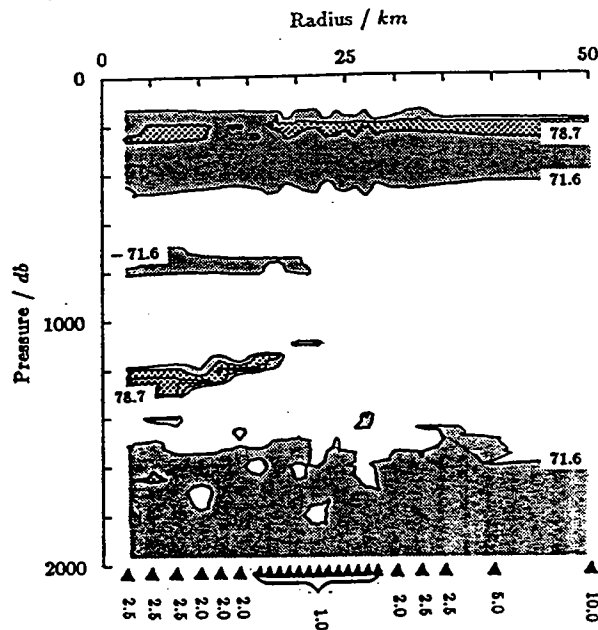
Figure 5. Turner angle for the June 1985 survey period. Shaded regions show where $|Tu| > 71.6°$. Salt fingering regions are those areas where the Turner angle is greater than $45°$; diffusion convection regions are where $Tu < -45°$. The heavily shaded regions delineate areas where $Tu > 78.7$ ($R_\rho < 1.5$).

al., 1989). Definitely, the fluxes due to salt–fingers at the base of the Meddy were not responsible for the large observed changes in the salt content of the Meddy.

Intrusions were present at the outer edge of the Meddy for all surveys (Armi et al., 1989). Estimates of fluxes by these intrusions using different models and representations (Hebert, 1988a; Ruddick and Hebert, 1988; Hebert et al., 1989) were found to agree with horizontal flux estimates based on the observed salt lost rate and horizontal extent of the Meddy (Hebert et al., 1989). Intrusions transport salt to the outer edge of the Meddy where the salt is removed from the vicinity of the Meddy by some unknown process.

4. SUMMARY

Fluxes determined from laboratory flux laws and a model by Kunze(1987) applied to some observed steps during the second survey, June 1985, of the Meddy were compared to fluxes estimated from changes in the salinity and temperature structure of the centre of the Meddy. The maximum fluxes through thick interfaces (Kunze, 1987) or fluxes using Stern's(1976) criterion with A=4 agreed with the observed fluxes (using a flux divergence ratio of 0.7). The maximum fluxes predicted for thin interfaces (Kunze, 1987) or fluxes determined from empirical fits of laboratory measurements (Kelley, 1986) are an order of magnitude larger than the observed fluxes.

Evidence that the high fluxes predicted by laboratory flux laws are incorrect came from dissipation measurements made through salt–fingering regions. As stated in the introduction, there could be several problems in comparing observed dissipation measurements and estimated buoyancy fluxes (Hebert, 1988c). The average dissipation measured by Oakey(1988) in the salt–fingering region was $\sim 20 \times 10^{-10}W\ kg^{-1}$. This dissipation rate agrees with the buoyancy flux found for the $r = 0.7$ case. The buoyancy flux from Kunze's(1987) model for the maximum flux through thick interfaces also agrees with the observed dissipation rate. The laboratory flux laws overestimate the buoyancy flux

128

by an order of magnitude. It appears that dissipation measurements from microstructure profilers can be used to determine buoyancy fluxes in salt–fingering regions.

A major difficulty with both the Kunze(1987) and Stern number methods for determining salt–fingering fluxes is that the vertical gradient of salinity and temperature through the interface must be known. It is desirable to determine the fluxes by salt–fingers in terms of larger scale properties such as the size of the homogeneous layers between the interfaces as found for the diffusive regime by Kelley(1984) or R_ρ (Schmitt, 1981). Schmitt(1981) attempted to parameterize the salt–finger fluxes, using laboratory flux laws, as an eddy diffusivity that depended on R_ρ. For the Meddy, the diffusivity for salt would be $O(10^{-4}m^2s^{-1})$ using the proper flux. Assuming that the fluxes used by Schmitt(1981) overestimated the true flux by an order of magnitude as found for the Meddy, the eddy diffusivity determined for the Meddy would agree with revised estimates of Schmitt's(1981) diffusivities. Until the physics which determines the size of the convection region and/or a parameterization for the thickness of this layer or the salt–finger flux on larger scale gradients is found, it will be necessary to determine the thickness of salt–fingering interfaces to calculate fluxes of salinity, temperature and/or buoyancy.

ACKNOWLEDGMENTS

I thank Ray Schmitt for the invitation and financial support to attend this interesting meeting. This work was completed while I was at Dalhousie University and supported by grants (to B. Ruddick) and a graduate scholarship from the Natural Sciences and Engineering Research Council (Canada). The cooperation of the other investigators (L. Armi, N. Oakey, J.F. Price, P.L. Richardson, H.T. Rossby and B. Ruddick) in the Meddy experiment made this project an enjoyable and fruitful one.

REFERENCES

Armi, L., D. Hebert, N. Oakey, J. Price, P. Richardson, T. Rossby and B. Ruddick. 1989. Two years in the life of a Mediterranean salt lens, *J. Phys. Oceanogr.*, 19:354-370.

Gregg, M.C. and T.B. Sanford. 1987. Shear and turbulence in thermohaline staircases, *Deep Sea Res.*, 34:1689-1696.

Hebert, D. 1988a. *A Mediterranean Salt Lens*, Ph.D. Thesis, Dalhousie University, Halifax, NS.

Hebert, D. 1988b. Mediterranean Salt Lenses, In *Small-Scale Mixing in the Ocean*, Elsevier Oceanography Series, vol. 46, edited by J.C.J. Nihoul and B.M. Jamart, Elsevier, N.Y., USA.

Hebert, D. 1988c. Estimates of salt–finger fluxes, *Deep Sea Res.*, 35, 1887-1901.

Hebert, D., N. Oakey and B. Ruddick. 1989. Evolution of a Mediterranean salt lens: Scalar properties, *J. Phys. Oceanogr.*, (submitted)

Kelley, D. 1984. Effective diffusivities within oceanic thermohaline staircases, *J. Geophys. Res.*, 89:10484-10488.

Kelley, D. 1986. *Oceanic Thermohaline Staircases*, Ph.D. Thesis, Dalhousie University, Halifax, NS.

Kunze, E. 1987. Limits on growing, finite–length salt fingers: A Richardson number constraint, *J. Mar. Res.*, 45:533-556.

Lambert, R.B. and W. Sturges. 1977. A thermohaline staircase and vertical mixing in the thermocline, *Deep Sea Res.*, 24:211-222.

Lueck, R.G. 1987. Microstructure measurements in a thermohaline staircase, *Deep Sea Res.*, 34:1677-1688.

McDougall, T. 1987. Thermobaricity, cabbeling and water–mass conversion, *J. Geophys. Res.*, 92:5448-5464.

McDougall, T.J. and J.R. Taylor. 1984. Flux measurements across a finger interface at low values of the stability ratio, *J. Mar. Res.*, 42:1-14.

Oakey, N.S. 1988. Estimates of mixing inferred from temperature and velocity microstructure In *Small-Scale Mixing in the Ocean*, Elsevier Oceanography Series, vol. 46, edited by J.C.J. Nihoul and B.M. Jamart, Elsevier, N.Y., USA.

Ruddick, B.R. and D. Hebert. 1988. The mixing of Meddy "Sharon" *Small–Scale Mixing in the Ocean*, Elsevier Oceanography Series, vol. 46, edited by J.C.J. Nihoul and B.M. Jamart, Elsevier, N.Y., USA.

Schmitt, R.W. 1979. Flux measurements at an interface, *J. Mar. Res.*, 37:419-436.

Schmitt, R.W. 1981. Form of the temperature–salinity relationship in the Central Water: Evidence for double–diffusive mixing, *J. Phys. Oceanogr.*, 11:1015-1026.

Schmitt, R.W. 1988. Mixing in a thermohaline staircase In *Small–Scale Mixing in the Ocean*, Elsevier Oceanography Series, vol. 46, edited by J.C.J. Nihoul and B.M. Jamart, Elsevier, N.Y., USA.

Schmitt, R.W. and D.L. Evans. 1978. An estimate of the vertical mixing due to salt–fingers based on observations in the North Atlantic Central Water, *J. Geophys. Res.*, 83:2913-2919.

Stern, M.E. 1975. *Ocean Circulation Physics*, Academic Press, N.Y.

Stern, M.E. 1976. Maximum buoyancy flux across a salt finger interface, *J. Mar. Res.*, 34:95-110.

The Growth of Salt Fingers After Disruption by Turbulence †

J. Taylor
Centre for Water Research, University of Western Australia
Nedlands, WA 6009

ABSTRACT

We studied the re-establishment of salt fingers after disruption by turbulence in a laboratory experiment in which the effects of background oceanic turbulence were simulated by dropping a square-bar grid through a gradient zone containing well developed salt fingers. As the turbulence generated by the grid decays the high wavenumber cut-off of the velocity shear spectrum will fall below the fastest growing finger wavenumber when $\epsilon \sim Pr \nu N^2$ and the salt fingers should begin to reform. Flow visualisation and calculations of the buoyancy flux ratio derived from horizontal temperature and conductivity profiles showed that the fingers did re-form in a timescale consistent with this argument. Maximum finger Cox numbers were reached after a period of 5 to 7 times the e-folding time of the fastest growing salt fingers. While this period is of the same order as the predicted timescale for fingers to reach their limiting amplitude, there was also significant modification of the background T and S gradients in this time in the laboratory experiments and this may also have been important in limiting the finger amplitude.

INTRODUCTION

It is probable that salt fingers in the ocean will often be disrupted by intermittent turbulence driven by processes quite independent of the fingers. So to understand the contribution of salt fingering to vertical mixing in the ocean we need to find out how salt fingers respond to imposed turbulence. Here we describe laboratory experiments in which we investigated the re-establishment of salt fingers following the decay of energetic turbulence.

Briefly, the experiments entailed setting up salt fingers in the gradient region between two uniform layers. Turbulence was then generated by a grid falling through the salt fingers. The subsequent decay of the turbulence and growth of the fingers was followed by recording repeated horizontal and vertical temperature and conductivity profiles through the gradient region. The fingers were also visualised by adding fluorescent dye to the upper layer and illuminating from the side with a laser generated light sheet.

In previous laboratory experiments *Linden* [1971] found that steady mechanical mixing generated by oscillating a grid in the layers above and below a finger region completely dominated salt fingering when the rms turbulent velocity near the interface, u', was 4.5 times the finger velocity, w. In the ocean we would expect most turbulent events to be similarly energetic and illustrate this with the following argument based on laboratory measurements of decaying grid turbulence [*Itsweire et al.*, 1986] and typical conditions in the C-SALT staircase [*Kunze*, 1987]. A weak turbulent event in the gradient zone in the staircase would be one which had a dissipation of turbulent kinetic energy just sufficient to support a positive buoyancy flux. In their laboratory experiments *Itsweire et al.* [1986] found that $\overline{\rho' w'} = 0$ if $\epsilon = \epsilon_{tr}$ where

$$\epsilon_{tr} = 15(\pm 1)\nu N^2 \tag{1}$$

where N is the buoyancy frequency; ν is the kinematic viscosity (the constant in Eq. 1 was dependent on the grid parameters, 15 was the minimum value found). For a typical C-SALT interface this gives ϵ_{tr} of $3.3 \times 10^{-9} \mathrm{W\,kg^{-1}}$ and the corresponding vertical scale for an overturn, given by the Ozmidov scale ($l_o = 2\pi(\epsilon/N^3)^{1/2}$), is 0.2 m. The rms turbulent velocity, $u' \sim (\epsilon l_o)^{1/3} = 8.7 \times 10^{-4} \mathrm{ms^{-1}}$, compared to a typical C-SALT finger velocity, estimated by *Kunze* [1987], of $1 \times 10^{-4} \mathrm{ms^{-1}}$, giving $u'/w = 8.7$. Comparing this scaling result with *Linden's* [1971] experimental results suggests that even when conditions

---

† Environmental Dynamics Report ED-329-JT

are apparently favourable to salt fingers, such as in the C-SALT gradient zones, they could be disrupted by weak turbulence. Clearly then it is important to understand the transient response of salt fingers to turbulence.

In the following, we consider the conditions under which fingers reform after disruption and review theoretical predictions of their growth rate and time to reach maximum amplitude. We then describe the experiments and show the evolution of the horizontal temperature gradient spectrum in the growing fingers as well as the evolution of the buoyancy flux ratio, Cox number and stability ratio. Finally, we review the comparison between the model and experimental results and discuss possible implications for oceanic salt fingering.

PRELIMINARIES

In a decaying turbulent velocity field salt fingers should first begin to form when the organised boundary layers which drive the salt fingers are not disrupted by the turbulent strain field. This should occur when the appropriate turbulence spatial scale, the wavenumber at which the rate of strain due to turbulent fluctuations is balanced by viscous diffusion, the Kolmogorov wavenumber

$$k_K = (\epsilon/\nu^3)^{1/4} \tag{2}$$

is of the same order as the most favoured scale for the evolving salt fingers. The appropriate salt finger scale is the wavenumber which gives the maximum growth rate [Kunze, 1987]

$$k_{fg} = \left[(\frac{g\alpha\overline{T}_z}{\nu\kappa_T})(1 - R_\rho^{-1})\right]^{1/4}, \tag{3}$$

where we define: $R_\rho = \alpha\overline{T}_z/\beta\overline{S}_z$, the salt finger stability ratio; $\overline{T}_z$ and $\overline{S}_z$, the mean vertical T and S gradients; α and β, the "expansion" coefficients for T and S and κ_T the thermal diffusivity. Rewriting k_{fg} in terms of the buoyancy frequency, N, given by $N^2 = g\alpha\overline{T}_z(1 - R_\rho^{-1})$ and equating k_K and k_{fg} we estimate that the dissipation rate when fingers may be formed is

$$\epsilon_f \sim Pr\nu N^2 \tag{4}$$

where Pr is the Prandtl number ν/κ_T. The ratio of ϵ_f to ϵ_{tr} (Eq. 1) is $Pr/15 \approx 1/2$ for heat and salt (although it is likely that there is a further O(1) constant on the right hand side of Eq. 4). The magnitude of ϵ_f/ϵ_{tr} is also consistent with the argument advanced in the introduction that when $\epsilon > \epsilon_{tr}$ salt fingers will be disrupted by turbulence.

Eq. 4 gives an estimate for conditions under which salt fingers can begin to form as turbulence decays. To estimate the timescale for the fingers to become established we used the salt finger growth rate in a region of constant T and S gradients and zero mean shear by Schmitt [1979] and Kunze [1987]. The maximum growth rate (normalised by N) is

$$\frac{\sigma_{max}}{N} \approx \frac{1}{Pr^{1/2}}\left[(\frac{R_\rho}{R_\rho - 1})^{1/2} - 1\right] \tag{5}$$

where we have assumed that $\tau \ll R_\rho$ (where $\tau = \kappa_S/\kappa_T$). As discussed by Schmitt and Evans [1978] the e-folding timescale (defined as σ_{max}^{-1}) for the fingers varies approximately linearly from one buoyancy period $(2\pi/N)$ at $R_\rho = 2$ to 3.6 buoyancy periods at $R_\rho = 5$. In Kunze's [1987] model of finite length fingers these e-folding times are doubled. Kunze also predicts times for the fingers to reach a limiting amplitude, determined by the horizontal shear between the fingers reaching a critical value,

$$\sigma_{max}t_{max} = ln\left[(\frac{8Pr}{C_wRi_f})^{1/2}(R_\rho - 1)^{1/4}(\sqrt{R_\rho} + \sqrt{R_\rho - 1})^{3/2}\right] \tag{6}$$

	U ms^{-1}	Re_g	C_d	ϵ_0 m^{2}s^{-3}	Experiment
1	0.112	6.0×10^3	0.924	1.30×10^{-2}	1,2,3
2	0.057	3.0×10^3	0.924	1.68×10^{-3}	9,10
3	0.044	2.3×10^3	–	7.82×10^{-4}	6,7,8

Table 1. Grid parameters. The grid Reynolds number is defined as $Re_g = UM/\nu$ where $M = 0.05$ m is the grid mesh size and U is the grid fall speed.

where Ri_f is the critical finger Richardson number and C_w is a constant equal to $\frac{1}{4}$ if the fingers have a square planform. Typical values of t_{max} are from $4.7\sigma_{max}^{-1}$ at $R_\rho = 2$ to $5.9\sigma_{max}^{-1}$ at $R_\rho = 5$, assuming Ri_f is 0.25.

The long finger models may have limitations when applied to laboratory salt fingers. For instance, the models assume that the fingers are growing in a region with uniform background gradients and that, since there is no flux divergence in z, that these gradients are independent of time. This may not be true in a laboratory experiment where, as we shall see, the timescale for the mean gradients to evolve can be of the same order as the predicted times for the fingers to reach their limiting amplitude.

EXPERIMENTS

The experiments were performed in a tank 1200 mm long, 400 mm wide and 500 mm high constructed of 10 mm thick clear acrylic sheet. To minimise heat transfer between the fluid and the environment the tank sat on a base of expanded polystyrene foam 90 mm thick and all sides were insulated with 50 mm sheets of the same material. A 10 mm thick sheet of foam was also floated on the free surface. A section of the insulation on the front of the tank could be removed to enable flow visualisation.

At the start of a run the tank was filled to a depth of 200 mm with filtered tap water which was then heated to the desired upper layer temperature by circulating it through an external thermostat. When the set temperature was reached a measured quantity of salt and rhodamine WT dye was mixed into the upper layer. At this stage the temperature and conductivity probes and floating lid were positioned. The lower layer of fresh tap water was then introduced through three diffusers mounted on the bottom of the tank and the tank filled to a depth of around 400 mm. When filling was complete a square bar grid of 50 mm mesh size with 10 mm bars was allowed to fall through the water column. Subsequently both horizontal and vertical temperature and conductivity profiles were recorded. The conductivity and temperature instrumentation and the processing of the profiles was as described by *Taylor and Bucens* [1989] with the exceptions that both direct and differentiated temperature and conductivity signals were recorded and the horizontal probes were traversed at 0.05 ms^{-1}. Salinity was derived from the measured conductivity and temperature (low mean salinities were used in these experiments to minimise the influence of temperature on the salinity calculation).

To visualise the evolution of the fingers the fluorescence of the rhodamine dye was recorded with a video camera. The dye fluorescence was excited by illuminating the tank from the side with a thin (< 1 mm) vertical light sheet generated by a 1.5 w argon-ion laser. The thickness of the sheet was minimised by expanding the laser beam and positioning the waist of the Gaussian laser beam in the region of interest in the tank.

The fall speed of the grid, U, was determined by recording its position in a sequence of frames digitised from videotape. Over the depth range visualised (approximately half the depth) the grid velocity was constant and was used to infer the drag coefficient for the grid,

$$C_d = 2gm/\rho_0 U^2 A \qquad (7)$$

where gm is the immersed weight of the grid, ρ_0 a reference density and A the area of the tank [*Linden*, 1980]. The buoyancy of the grid was adjusted to achieve the different drop speeds shown in table 1.
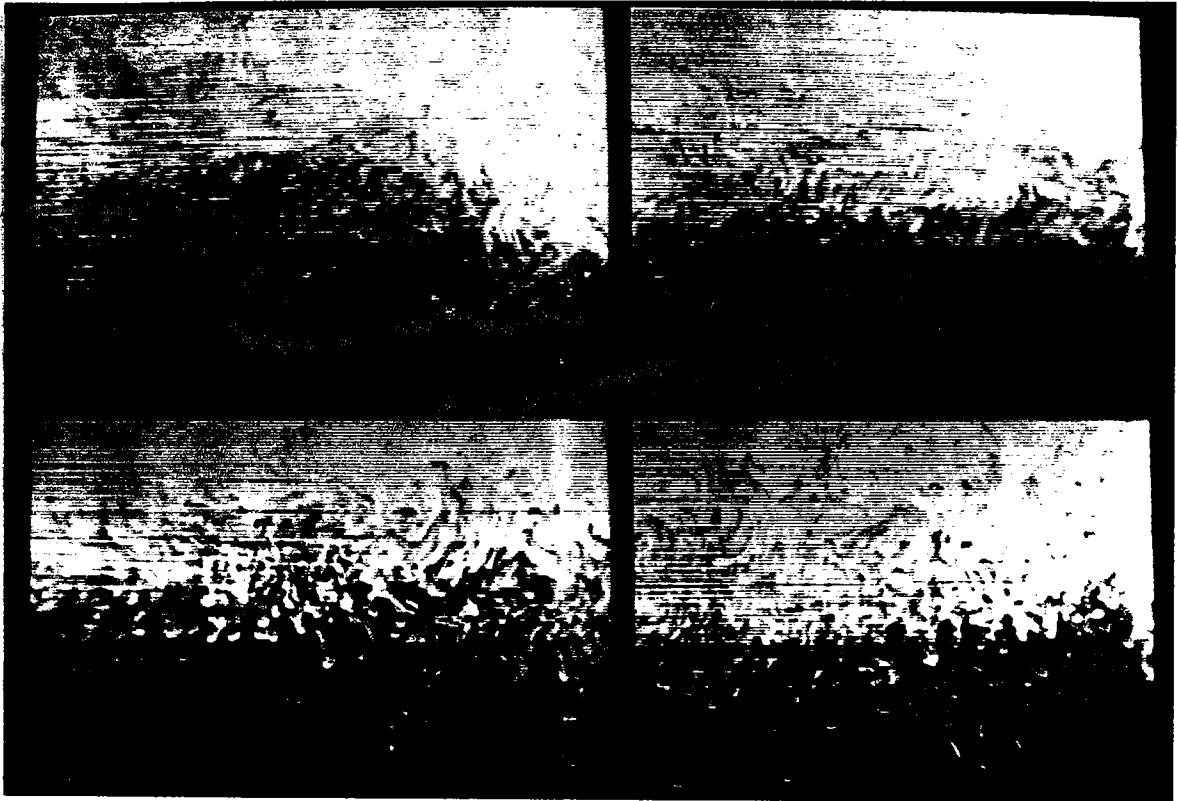
Fig. 1. Dye fluorescence images of the establishing salt fingers in experiment 6. The field of view is 240 × 190 mm. Images were taken at: $Nt = 6.4$ (29 s) top left; 12.3 (56 s) top right; 19.8 (89 s) bottom left; 25.8 (116 s) bottom right with $t = 0$ at the time the grid fell. The turbulence decay timescale, Nt_{tr}, was 3.8 for this experiment and the predicted finger e-folding time, $N(\sigma_{max})^{-1}$, was 22.2.

RESULTS

The dye fluorescence field after the decay of the grid turbulence and the establishment of the salt fingers is shown in Fig. 1. The rapidity of the growth of the fingers is shown by the fact that fingers are clearly established in the second image, which was captured less than half a finger e-folding period after the grid was droppped.

Decay of the Grid Turbulence

Itsweire et al. [1986] have made comprehensive measurements of the decay of grid turbulence behind a stationary grid in a stratified water tunnel. In particular, their experimental results show that the dissipation decays with increasing distance from the grid according to a power law

$$\epsilon = \epsilon_0(Ut/M)^{-2.6} \tag{8}$$

which is independent of the stratification (at least while $\epsilon > \epsilon_{tr}$). In our experiments the development of the turbulence in the gradient region as a function of time should parallel the downstream development of the turbulence in the water channel as it is advected through the test section, provided that the influence of the grid stopping at the bottom of the tank is small. The power per unit mass input by the grid in falling through one mesh spacing ($t = M/U$) is $\frac{1}{2}C_dU^3/M$ and assuming that this power input is balanced by turbulent dissipation gives an estimate for ϵ_0 (Table 1). Using ϵ_0 and Eq. 8 and Eq. 1 we could estimate the decay time for the grid turbulence. To determine N^2 the vertical temperature gradient profile was filtered with a low-pass filter (3 db point at 10 cpm) then the first point where the filtered temperature gradient

exceeded 0.5 of the mean (and where a depth threshold was exceeded) was taken as the upper edge of the gradient zone. A similar procedure was used to find the lower edge of the gradient. The mean density gradient was then calculated from the average temperature and conductivity gradients between these two depths. To average some of the distortion of the mean profile caused by the falling grid the mean of N^2 from the first two profiles was used in calculating turbulence and finger times scales.

Table 2 shows the estimated time for $\overline{\rho'w'}$ to fall to zero in each experiment. Clearly, without direct measurements of the dissipation, these values are only approximate, however, they show that the rapid reformation of the fingers we observed in these experiments (illustrated by Fig. 1 and the time that fingering was first observed in the videotape, table 2) are consistent with the decay timescale for the turbulence and the transition criterion given by Eq. 4. Also shown in this table is the value of the Cox number [*Osborn and Cox*, 1972] for the first horizontal profile. *Itsweire et al.* [1986] found that when $\epsilon = \epsilon_{tr}$ the Cox number was $5.4(\pm2)Pr$ or approximately 40 for heat. All Cox numbers for the first horizontal profiles were greater than 40, indicating that the turbulence was still active at the time of the first horizontal profile, consistent with the calculated decay times.

The large values of $\epsilon_0/\nu N^2$ (table 2) show that the initial turbulence generated by the grid was more active than is typical for turbulence in the ocean thermocline; at least that is when the turbulent dissipation is averaged in vertical intervals greater than several meters (for example *Gregg* [1989] found a maximum 10 m average $\epsilon/\nu N^2$ of 2.2×10^3 over a range of oceanic conditions). Of course, the peak dissipation values within these vertical averages could be much higher. However, *Linden's* [1971] laboratory results show that weak turbulence levels could disrupt the fingers and we suggest that the comparative intensity of the initial turbulence level in these experiments is relatively unimportant. We would expect the fingers to be completely destroyed by any turbulent event in which $\epsilon > \epsilon_{tr}$.

Experiment	$\epsilon_0/\nu N^2$	C	Nt_1	Nt_{tr}	Nt_f	$N\sigma_{max}^{-1}$	$R_{\rho 0}$
1	1.9×10^4	77	–	4.4	–	50.1	5.5
2	8.2×10^4	456	1.4	3.7	–	13.2	2.0
3	3.4×10^4	256	1.6	4.1	12	14.6	2.2
6	1.1×10^3	192	3.6	3.8	10	22.2	2.9
7	2.2×10^3	337	1.8	3.5	–	–	–
8	1.9×10^3	221	2.4	3.5	5	16.7	2.4
9	2.6×10^3	106	2.2	3.9	14	33.7	4.0

Table 2. Turbulence and salt finger time scales. C is the Cox number for the first horizontal profile and Nt_1 is the dimensionless time of that profile. Ut_{tr}/M and Nt_{tr} are the dimensionless times for $\epsilon = \epsilon_{tr}$ from Eq. 8 and Nt_f is the time fingers were first observed in the video. $N\sigma_{max}^{-1}$ is the e-folding time for finite length fingers [*Kunze*, 1987] (twice the value from Eq. 5) and $R_{\rho 0}$ an estimate of the stability ratio just after the grid fell. In experiments 1 and 2 video records of finger formation were not recorded. Experiment 7 was stratified with heat only.

Establishment of salt fingers

Evolution of the Temperature Gradient Spectrum.

A band averaged spectrum of the horizontal temperature gradient, ϕ_T, was calculated from FFTs of 1024 point segments of each horizontal profile. Prior to calculating the FFT the linear trend was removed from each segment and a Hanning window applied. As well, the average temperature for each horizontal profile was computed and compared with the nearest, in time, vertical profile. If the average temperature of the horizontal profile did not fall within the gradient region in the vertical profile the horizontal profile was disgarded. However, even with this precaution it is possible that, because of the large amplitude internal waves generated by the grid, sections of the profile may have fallen outside the finger zone. Since the characteristics of the temperature gradient spectrum within the fingers and in the convecting layers above

and below the fingers are quite different [*Taylor and Bucens*, 1989] the spectra may be biased by passing through the convecting or decaying turbulence regions above and below the fingers. In further analysis some spectra will be tested for stationarity using techniques described by *Imberger* [1989].
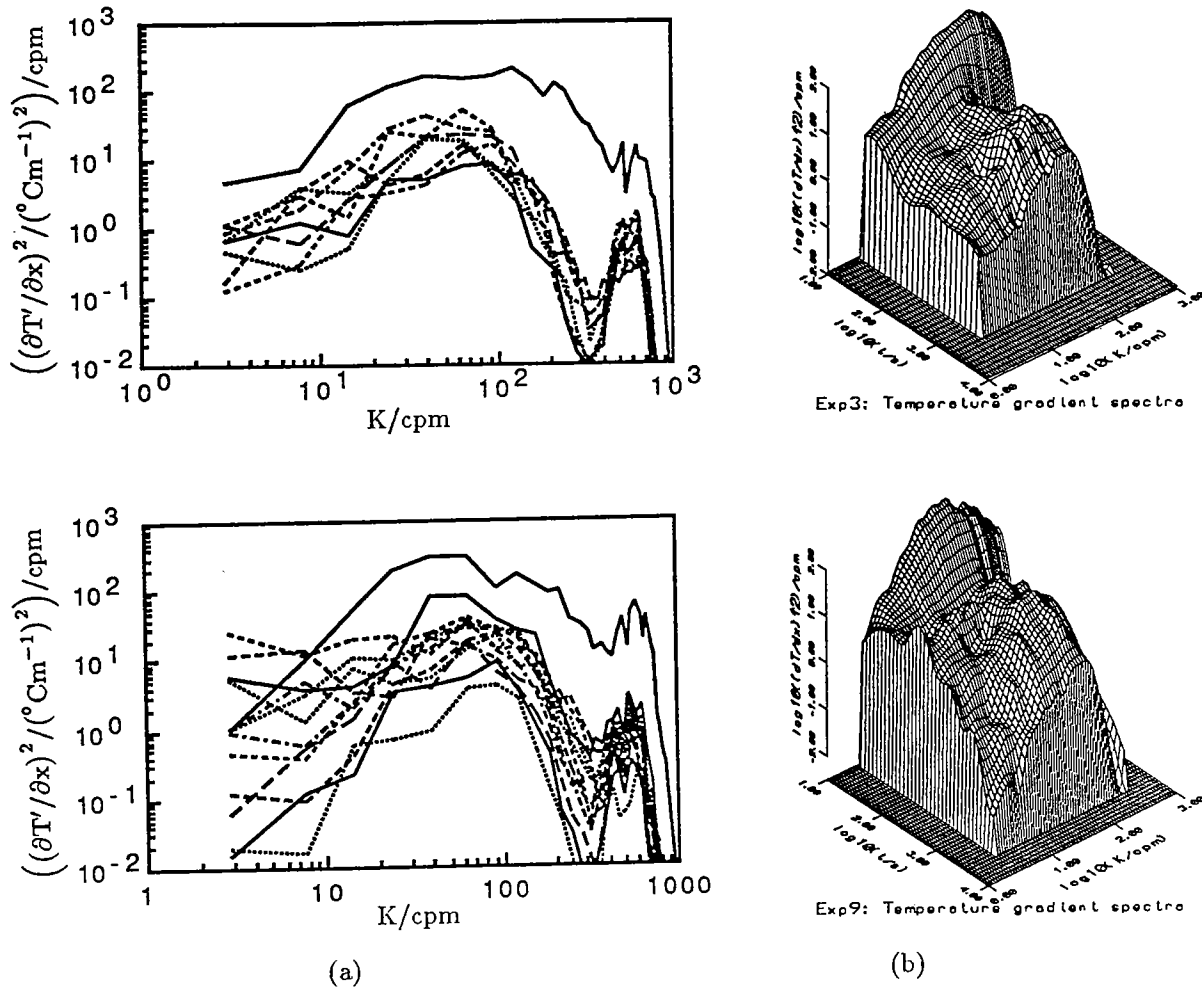
Fig. 2. Horizontal temperature gradient spectra from experiments 3 (upper) and 9 (lower). (a) raw spectra (b) interpolated spectra.

Fig. 2 shows the evolution of ϕ_T in experiments 9 and 3. In (a) the raw spectra are shown while in (b) the time evolution of the same spectra have been emphasised by interpolating the spectra on to a regular grid and using a logarithmic time axis. The interpolated spectra were cut-off at a wavenumber of 400 cpm to remove the contribution from high frequency noise which lies beyond the limits of resolution of the thermistor.

The dominant features of the spectra are the initial rapid drop in power with the decay of the grid turbulence and the emergence of a peak due to salt fingers at a wavenumber of around 100 cpm. In most experiments there was no well defined minimum in the peak amplitude of ϕ_T between the decay of the turbulence and growth of the fingers. Comparison with two runs with similar density gradients but no salinity gradients suggests that the lack of a clear minimum is due both to the rapid growth of the fingers and slow decay of the temperature gradients left by the turbulence or generated by internal waves. The only experiment which had a very well defined minimum amplitude had the strongest density stratification and the highest initial R_ρ.

At the low wavenumber end of the spectrum there was often an increase in power at first (as in exp 9, fig.2b), presumably as energy was transferred from turbulence to internal waves, then a decrease as the

internal wave field decayed. The peak in the spectrum due to salt fingers becomes more prominent as a result of a decrease in the level of the spectrum at low wavenumbers and corresponding increase in the slope of the spectrum for $K < K_{peak}$. As the fingers evolved the high wavenumber cut-off in the temperature gradient spectrum moved to lower wavenumbers, this is best illustrated by the raw spectra from experiment 9 which was allowed to run down for longer than the other experiments. The shift in cut-off wavenumbers is consistent with the behaviour of the equilibrium finger wavenumber [Stern, 1975] which Taylor and Bucens [1989] found marked the high wavenumber limit of the finger spectrum. Overall the bandwidth of the finger spectrum decreases as the fingers run down the salinity gradient, although the peak remains close to the fastest growing wavenumber given by Eq. 3, even for $R_\rho \approx 20$.

Evolution of overall parameters.

We can derive several quantities from the horizontal profiles of temperature and conductivity and their respective gradients which give a more quantitative picture of the development of the fingers. These include the x-component of the Cox number [Osborn and Cox, 1972]

$$C_x = \overline{\left(\frac{\partial T'}{\partial x}\right)^2} / (\overline{T_z})^2.$$

(9)

C_x is of interest since, by comparing measurements of the fluxes through a salt finger interface derived from the rate of change of the properties of the convecting layers above and below the fingers, Taylor and Bucens [1989] have shown much of the thermal buoyancy flux through salt fingers can be accounted for by the simple steady balance between vertical advection of heat and horizontal diffusion implied in deriving the Cox number [Gargett and Schmitt, 1982].

We also compared the wavenumber of the peak in the temperature gradient (K_{peak}) spectrum with the theoretical finger wavenumber, $(2\sqrt{2}\pi)^{-1}k_{fg}$ (Eq. 3), and derived an estimate for the buoyancy flux ratio, R_f^*, defined as

$$R_f^* = (\alpha/\beta)(c_T \sigma_w \sigma_T / c_S \sigma_w \sigma_S)$$

(10)

where σ_w is the rms vertical velocity and σ_T and σ_S are the rms temperature and salinity respectively. c_T and c_S are correlation coefficients. If we take $c_T = c_S$ [Taylor and Bucens, 1989] then R_f^* can be derived from integrating the T and S spectra. We computed two estimates for R_f^*; one based on the variance found by integrating over all wavenumbers up to a 400 cpm (the 3db point for the conductivity sensor response) and the other by integrating only from K_{peak} to 400 cpm. The two estimates of R_f^* were calculated to show the contribution of the low wavenumber portion of the spectra to R_f^*.

To emphasise the transient aspects of these experiments the results to be presented in the remaining figures have been plotted against $\sigma_{max}t$ where σ_{max} is the maximum growthrate (Eq. 5) based on the average of R_ρ and N from the first two vertical profiles. The time origin was set where $\epsilon = \epsilon_{tr}$ (Table 2).

Buoyancy flux ratio: For turbulent mixing the flux ratio defined by Eq. 10 should ideally be equal to R_ρ and hence be greater than one. As salt fingers begin to dominate R_f^* falls below one and on the basis of previous laboratory experiments should approach a relatively constant value lying between 0.5 and 1.0. The data follow this trend although the estimates (solid lines in Fig. 3), calculated by integrating over the full wavenumber range, are greater than one for a longer time consistent with the slower decay of the low wavenumber fluctuations in the gradient spectra. At high wavenumbers the rapid establishment of the fingers is shown by the fact that most R_f^* estimates are less than one at the time of the second profile. By 4 e-folding periods the two estimates of R_f^* have converged.

In experiment 1, which had the highest initial R_ρ, R_f^* was greater than one for a longer time than in the other runs. This difference in behaviour is due in part to two factors. Firstly, because there was no peak in the temperature gradient spectrum in the second horizontal profile the two estimates of the flux ratio calculated from this profile were equal and greater than one. Secondly, there was then a break in the data collection due to an equipment malfunction which limited the time resolution of the flux ratio estimates. However, it may also be possible that the growth rate scaling breaks down at high initial stability ratios and this should be investigated further.
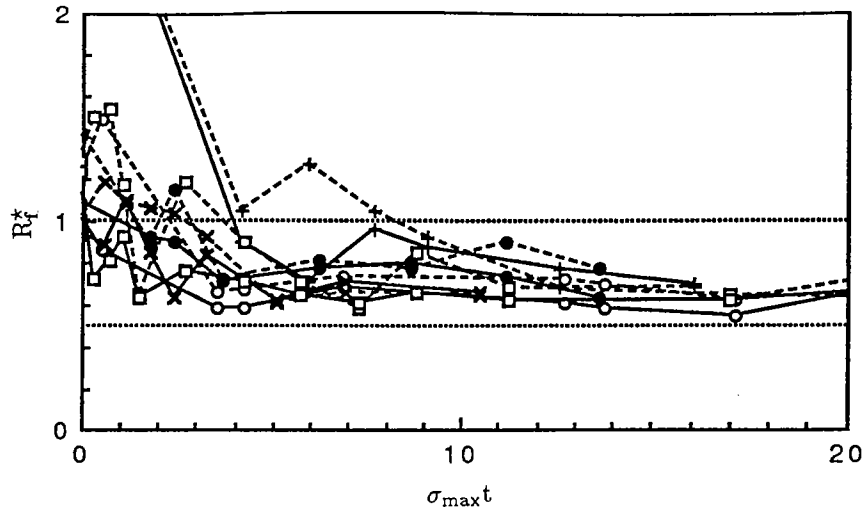
Fig. 3. Estimates of the flux ratio plotted against $\sigma_{max}t$. Estimates connected by dotted lines were calculated by integrating the T and S spectra from the minimum wavenumber to 400 cpm. Solid line is calculated by integrating from K_{peak} to 400 cpm. Symbols are; $+$ exp 1, o exp 3. $\times$ exp 6, $\bullet$ exp 8, exp 9.
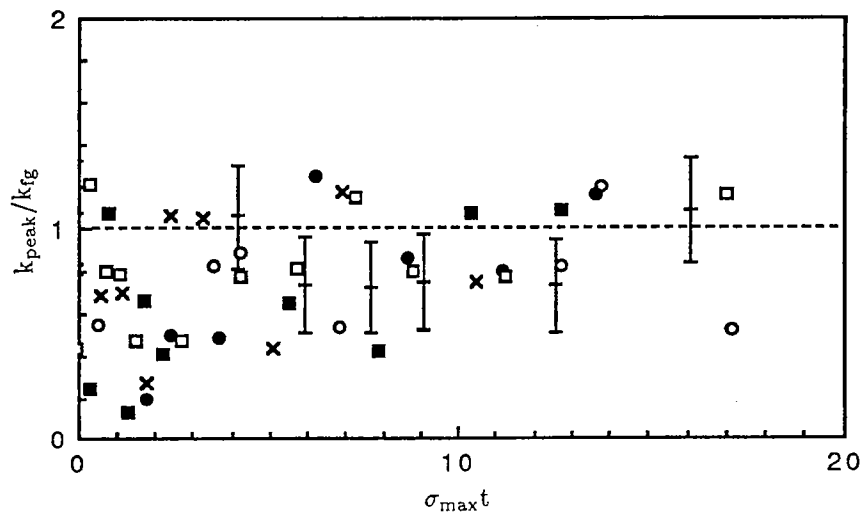
Fig. 4. k_{peak}/k_{fg} plotted against $\sigma_{max}t$. Symbol: exp 2, others as for Fig. 10. Error bars show the typical uncertainty in K_{peak} caused by the spacing of the frequency estimates in the band averaged spectra.

Peak wavenumber: We have already commented that the peak in the temperature gradient spectrum correlates quite well with $(2\sqrt{2}\pi)^{-1}k_{fg}$ given by Eq. 3. Fig. 4 shows that this is particularly true in a well developed finger field. For $\sigma_{max}t > 5$ almost all the spectral peaks fell within one error bar of $k_{peak}/k_{fg} = 1$, noting that the size of the error bars simply indicates the relatively coarse frequency resolution of the band averaged spectra. At earlier times the peak wavenumbers were more scattered with their values depending on exactly what stage of the evolution of the decayed turbulence/growing fingers the profile captured.

The Cox number: The x-component of the Cox number (Fig. 5) decreased rapidly as the grid turbulence decayed, passed through a minimum then grew again as the salt fingers became established and their amplitude increased. The time to reach maximum Cox numbers was in the region of 5 to 7 e-folding periods, times reasonably consistent with those to reach the limiting finger amplitude from Eq. 6. The Cox number then decreased gradually as the fingers ran down, a trend consistent with the decrease in Cox number with
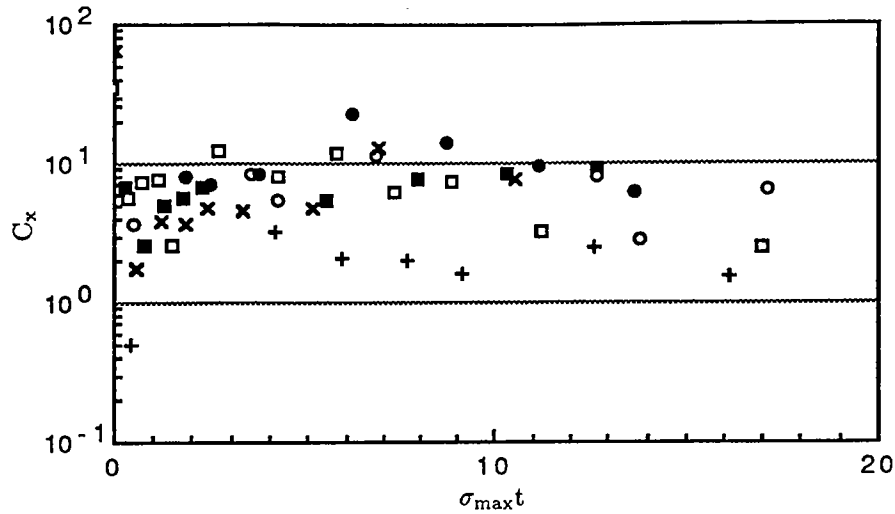
Fig. 5. The x component of the Cox number, C_x plotted against $\sigma_{max}t$. Symbols as for Fig. 4.
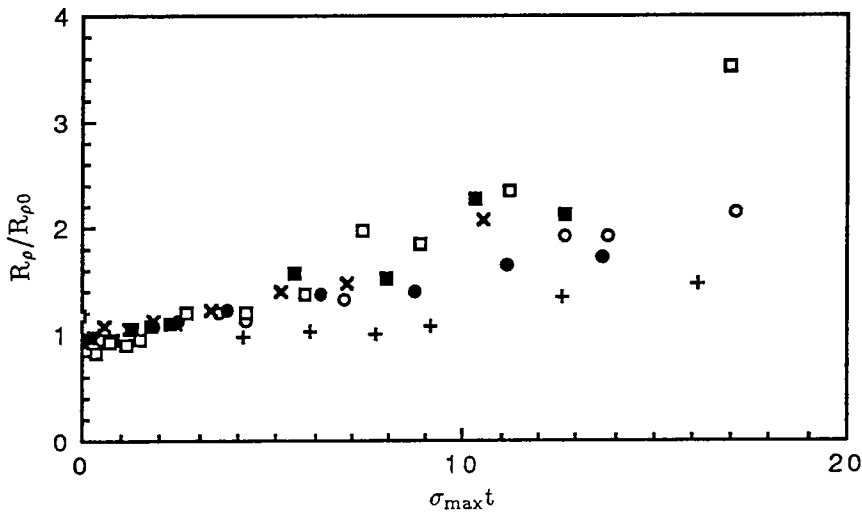
Fig. 6. R_ρ/R_{ρ_0} plotted against $\sigma_{max}t$. Symbols as for Fig. 4.

increasing R_ρ observed by *Taylor and Bucens* [1989]. The higher values of the Cox number shown on Fig. 5 relative to the earlier work (note to make a direct comparison the present results need to be doubled to account for isotropy in the horizontal) are probably due to the different methods used to estimate $\overline{T_z}$ in the two sets of experiments. In the present experiments the edge of the finger zone was not as clearly defined as it was in the earlier laboratory work due to the thickening of the gradient by the grid turbulence and the method of calculating $\overline{T_z}$ was probably influenced by the weaker temperature gradients at the edges of the finger zone.

The stability ratio: In any salt fingering run-down experiment R_ρ increases as the S gradient in the fingers decreases and R_ρ changes in this way in the present experiments (Fig. 6). However, the fact that the fingers are growing in the initial stages is shown by the way in which the rate of change of R_ρ with time is, on average, greater at later times than it is in the first 3 to 4 e-folding periods. The scaling of the time axis by the maximum finger growth rate (table 2) also collapses the data from all but experiment 1 well at earlier times. After the initial growth period we would expect other factors, such as the thickness of the gradient region as compared to depth of the reservoir layers, to affect the rate at which the system runs down and would not expect the growth rate scaling of time to collapse the data.

In the 5 to 7 finger e-folding periods over which it takes the Cox number to reach its maximum value Fig. 6 shows that R_ρ increased by an average of 50%. Such a change in R_ρ suggests that in a moderately scaled laboratory experiment, like the present one, the rundown timescale of the property differences across the finger zone is too close to the timescale for the finger's evolution for an accurate determination of the limiting conditions across the finger zone.

DISCUSSION

Our experiments have shown that, at moderate stability ratios in the laboratory, salt fingers will become established rapidly after turbulence has decayed to the state where a positive buoyancy flux can no longer be supported. This was most clearly shown by the behaviour of the flux ratio, which at wavenumbers greater than the fastest growing finger wavenumber, was generally dominated by salt fingering ($R_f^* < 1$) between the times when the first and second horizontal profiles were taken (and corresponding to one finger e-folding period). Maximum finger Cox numbers were reached within 5 to 7 $(\sigma_{max})^{-1}$, of the order of the time for the fingers to reach a limiting amplitude predicted by $Kunze$ [1987]. However, it is not clear that this can be interpreted as the fingers reaching a self-limiting amplitude as the variation of R_ρ with time shows that, because the experiments were carried out in a relatively shallow tank, the mean T and S gradients in the fingers were changing in a similar time to the theoretical estimates for the time for the fingers to reach a limiting amplitude.

The results of these experiments suggest that against a background of intermittent oceanic turbulence salt fingers should be become established rapidly in the quiet periods between events. However, even when the mean T and S gradients are favourable to salt fingering, much of the ocean appears to be quiet without the microstructure signatures of turbulence or salt fingering [Mack, 1989]. Recent work by Kunze [this volume] shows that, even in the absence of turbulence, the unsteady background shear in the ocean places severe constraints on the finger growth rate and, like turbulence, could be important in restricting the range of R_ρ in which fingers can grow in the ocean.

REFERENCES

Gargett, A. E. and R. W. Schmitt (1982) Observations of salt fingers in the central waters of the Eastern North Pacific. *J. Geophys. Res.*, *87*, 8017–8029.

Gregg, M. C. (1989) Scaling turbulent dissipation in the thermocline. *J. Geophys. Res.*, *94*, 9686–9698.

Linden, P. F. (1971) Salt fingers in the presence of grid-generated turbulence. *J. Fluid Mech.*, *49*, 611–624.

Linden, P. F. (1980) Mixing across a density interface produced by grid turbulence. *J. Fluid Mech.*, *100*, 691–703.

Imberger, J. I. (1989) On the nature of turbulence in a stratified water body. Part II: Application to lakes. submitted to *J. Phys. Oceanogr.*.

Itsweire, E. C., K. N. Helland and C. W. Van Atta (1986) The evolution of grid generated turbulence in a stably stratified fluid. *J. Fluid Mech.*, *162*, 229–338.

Kunze, E. (1987) Limits on growing, finite-length salt fingers: a Richardson number constraint. *J. Mar. Res.*, *45*, 533–556.

Mack, S. A. Towed-chain measurements of ocean microstructure. *J. Phys. Oceanogr.*, *19*, 1108–1129.

Osborn, T.R. and C.S. Cox (1972) Oceanic fine structure. *Geophys. Fluid Dyn.*, *3*, 321–345.

Schmitt, R. W. (1979) The growth rate of supercritical-salt fingers. *Deep-Sea Res.*, *26*, 23–40.

Stern, M. E. (1975) *Ocean Circulation Physics*. Academic Press, New York, 246pp.

Taylor, J. and P. Bucens (1989) Laboratory experiments on the structure of salt fingers. *Deep-Sea Res.*, (in press).

AN EXPERIMENTAL STUDY ON THERMOHALINE STAIRCASES

by

H.J.S. Fernando and C.Y. Ching

Department of Mechanical & Aerospace Engineering
Arizona State University
Tempe, AZ 85287-6106, USA

1. Introduction:

Interest in the genesis and dynamics of thermohaline staircase structures - a series of turbulently convecting layers separated by thin, stable, diffusive density interfaces - has been revived recently because of the increasing number of oceanic observations that report their existence (Padman & Dillon 1987, Muench et al. 1990). The upward transport of heat and salt through the oceanic double-diffusive layers is said to play a prominent role in the regional heat and salt budgets. A large number of laboratory experiments on various aspects of this problem, e.g., layer-formation mechanism, height of the layers, convection within the layers, heat and salt fluxes across the interfaces, and interfacial migration, have been reported. The main purpose of this paper is to summarize some results of a set of laboratory studies pertinent to: i) the thicknesses of the convecting layers; and ii) interfacial migrations. The details of the experimental procedure, results and relevant theoretical considerations will be given in a future publication.

2. Thickness of the Convecting Layers

Two opinions on the formation mechanism of thermohaline staircase structures exist. Turner (1968) considered the case of heating of a stable salinity gradient from below and proposed that the second convecting layer, which is above the first one, is formed when the thermal boundary layer, which "rides" on the growing first layer, becomes unstable at a critical Rayleigh number. The thickness of the first convecting layer at the onset of the instability was considered to be the thickness h_1 of the bottom layer of the staircase. Based on this assumption a model, which was tested using laboratory experiments, was developed to predict h_1. This model has been extended to the prediction of the thicknesses of the remaining layers of the staircase by Huppert & Linden (1979). A different view was taken by Fernando (1987), who proposed that the layer thicknesses are determined by a balance of the vertical kinetic and potential energies of the turbulent eddies within the layers. The accompanying analysis yielded an expression for h_1, which was tested using a laboratory experiment. A generalization of this work to oceanic and laboratory layers, that are located far from solid boundaries, has been reported by Fernando (1989). Accordingly, the height of the layers h, stemming from the transformation of an initially-smooth

salinity gradient of stability frequency N_s to a staircase of interfacial density-stability ratio R_ρ, is given by

$$h = c_1 \left(\frac{q_h}{N_s^3}\right)^{1/2} \frac{(1 - c_2 R_\rho)}{\left(1 - R_\rho^{-1}\right)^{3/4}}$$

(1)

where q_h is the heat flux transmitted through the layers, and c_2 depends on the nature of the diffusive interface ($c_2 = 0.15$ for the low-stability regime and $\tau^{1/2}$ for the diffusive regime, where τ is the Lewis number, the ratio of the molecular diffusivities of salt and heat). Based on the results of previous studies, c_1 was estimated as 12.5. A comparison of (1) with available oceanic data indicated a satisfactory agreement with $c_1 = 14$, but laboratory tests of (1) are yet to be reported. To this end, a thermohaline staircase was generated in the laboratory by heating a linearly (salinity) stratified fluid from below, as in Turner (1968). While the staircase is evolving, vertical salinity S and temperature T profiles through the layers were taken; h for different layers, R_ρ and the conductive heat flux through the interfaces were extracted from this information. A comparison of the measurements with (1) is shown in Figure 1, for the experiments carried out at different N_s and bottom buoyancy (heat) fluxes q_o. The regime of the interface and hence c_2, was determined by calculating the Rayleigh number and R_ρ of the layers and by using Figure 6 of Fernando (1989); all of the interfaces were found to be in the diffusive regime. Note that the data include h for the second to fifth layers of the staircases. The best-fit line to the data shows a gradient of 1.002 and $c_1 = 11$, indicating support for (1). It is also noted that Kelley (1984) has proposed an alternative formulation for h.

3. Interfacial Migration

The mechanisms responsible for interfacial migration and the effects of interfacial migration on heat and salt fluxes and layer thickness have been discussed, in detail, by Kelley (1987). When differential turbulence levels exist across an interface due to convergence of the buoyancy flux, the interface tends to migrate towards the side with the lower turbulence level. The unsteady nature of the buoyancy transport process, nonlinearity of the equation of state (McDougall 1981), or a combination thereof may contribute to the non-uniform spatial distribution of the buoyancy flux. As was first pointed out by Kelley (1987), and experimentally verified by Muench et al. (1990), sometimes the interfaces can split and then migrate to form additional layers.

$$\left(\frac{q_h}{N_s^3}\right)^{1/2} \frac{(1-\tau^{1/2}R_\rho)}{(1-R_\rho^{-1})^{3/4}} \quad (cm)$$
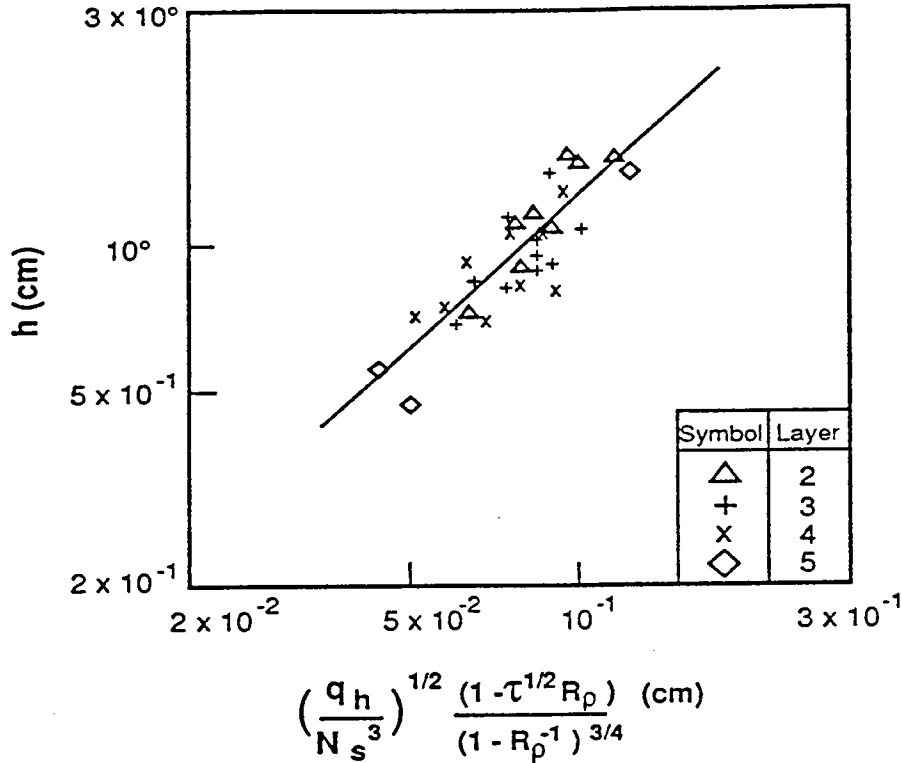
Figure 1: A plot of h versus $(q_h/N_s^3)^{1/2}(1-\tau^{1/2}R_\rho)(1-R_\rho^{-1})^{-3/4}$. The layer number (the bottom layer was assigned number one) corresponding to each data point is also indicated. The parameters ranges were $3.75 \times 10^{-6} > q_h > 7.88 \times 10^{-7}$ (m²s⁻³) and $1.3 > N_s > 1.0$ (rad s⁻¹).

The interfacial migration model of Kelley (1987) assumes that the interfacial-migration velocity u_e is determined by the resultant of two velocities, evaluated by assuming that either one or the other layer is not convecting. Based on previous laboratory experimental results, the (uni-directional) entrainment law for a single-layer convecting case was taken as $E = c_3 Ri_h^{-1}$, where $E = u_e/w_*$ is the entrainment coefficient, u_e is the entrainment velocity, w_* is the convective velocity, $Ri_h = \Delta bh/w_*^2$ is the Richardson number based on the buoyancy jump Δb across the interface and $c_3 = 0.25$. It should, however, be kept in mind that this entrainment law is valid only in a limited parameter range. At very high Ri_h, the entrainment process is dominated by molecular diffusive effects and the entrainment rates are small (Phillips 1977); at low Ri_h the interfacial stratification becomes unimportant and high entrainment rates, as in non-stratified fluids, can be seen. It is the latter mechanism which is of interest here because of its possible role in the evolution of oceanic staircases with relatively low R_ρ and large q_h.

A set of salinity profiles obtained during the experiments is shown in Figure 2. During the experiments, at first, the bottom mixed layer is developed; it grows until its growth is inhibited by buoyancy effects, whence a second layer is formed above the first. This sequence of events continues, forming multiple layers. Figure 3 shows the time evolution of h_1, from which the initial rapid growth and the transition to a slowly growing regime, when $h_1/(q_o/N_S^3)^{1/2} = 42.7$, is evident. Note that this value of h_1 is close to the quasi-steady height h_e of the bottom layer above which, according to Fernando (1987), the thermohaline staircase can be sustained. The shadowgraph observations also confirmed the evolution of the second convecting layer after growth levels off at h_e. When $h_1 > h_e$, the movement of the interface is sluggish, but after some time, indications of a sudden migration of the interface to a new h_1, from which the interface resumes its sluggish growth can be seen. This rapid growth was recurrent, followed by a period of sluggish growth.

A possible cause for this sudden "jump" of the interfacial position is the drop of the interfacial stability below a critical value, thereby making the interface susceptible to engulfment by turbulent eddies, as if no buoyancy forces were present. If the thickness of the interface is δ, the stability of the interface is signified by the interfacial Richardson number $Ri_\delta = \Delta b \delta /w_*^2$; when Ri_δ decreases below a critical value, say Ri_c, the "jump" phenomenon can be expected. During the experiments, T and S profiles were taken at specific time intervals and Ri_δ was calculated from the profiles taken before and after well-identifiable interfacial "jump" events. The results are shown in Figure 4 and indicate a drop of Ri_δ below a critical value before a rapid migration event. Because the data were taken at discrete intervals, this critical value is hard to estimate, but analysis of a large number of profiles suggest that $Ri_c \simeq 2$.
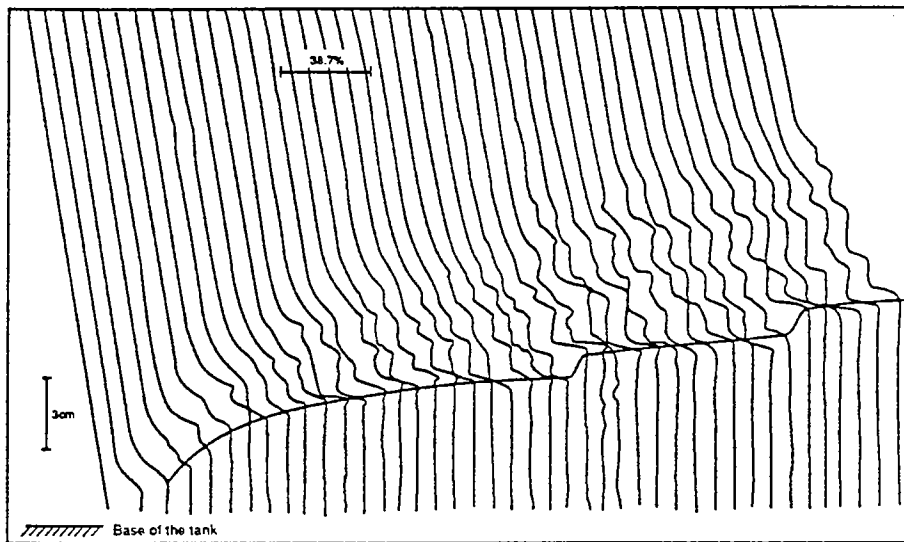
Figure 2:   A set of temperature profiles taken at 2 min. intervals. The scales of the plot are indicated and the estimated upper boundary of the first layer is shown by the solid line. The experimental parameters are $N_s = 1.04$ (rad s^{-1}) and $q_o = 2.04 \times 10^{-6}$ $m^2 s^{-3}$.
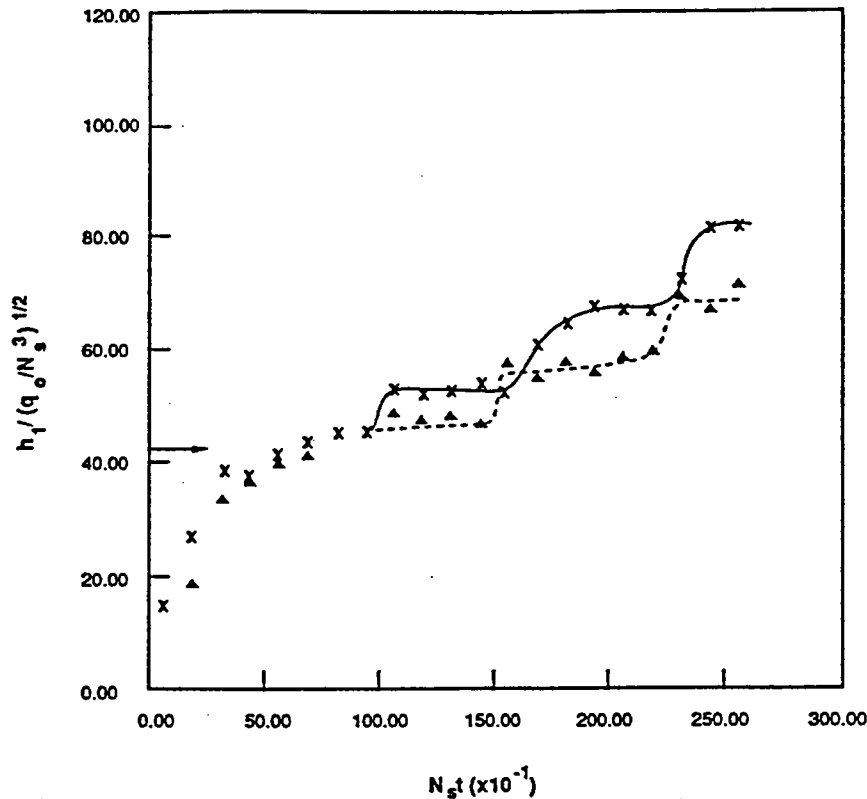
Figure 3: The growth of the non-dimensional thickness of the first convecting layer with non-dimensional time. The data for two experiments with $N_s = 1.04$ rad s^{-1}, and $q_o = 2.0 \times 10^{-6} m^2 s^{-3}$ (x) and $2.9 \times 10^{-6} m^2 s^{-3}$ (▲) are shown. Also indicated by an arrow is the minimum h_1 that is required for the development of a staircase structure (Fernando 1987).

4. Mixed-Layer Growth Without Multiple Layering

It is instructive to note that heating of a stable salinity gradient from below does not always lead to staircase structures. Under certain conditions (which involve high salinity stratifications and low heat-fluxes), the mixed layer continues to grow, beyond h_o, without any evidence of multiple layering. This situation is depicted in Figure 6 (a,b). Apparently, under these conditions, the mixed-layer growth is diffusion dominated and u_e is determined by the competing effects of the weakening of the interfacial buoyancy gradient by diffusion and entrainment of the weakened layer by the turbulent eddies. It can be shown theoretically that the nature of the interfacial events in such situations is determined by the relative magnitudes of R_ρ and $\tau^{1/2}$ (Fernando & Zangrando 1990); here R_ρ is the ratio of buoyancy gradients, above the mixed layer, due to salinity $g\beta \overline{S}_z$ and temperature $g\alpha \overline{T}_z$. Diffusion-controlled entrainment takes place when $R_\rho < \tau^{1/2}$, and contraction of the mixed layer (detrainment) occurs when $R_\rho > \tau^{1/2}$. No interfacial movement is possible when $R_\rho = \tau^{1/2}$. Figure 7 shows the results of Hull et al. (1989) concerning the growth of convective mixed layers in ammonium chloride solar ponds. The solid line represents the theoretical demarcation line $R_\rho = \tau^{1/2}$ between entraining (E) and non-entraining (N) cases. Note the good agreement between the theoretical prediction and experimental observations.

5
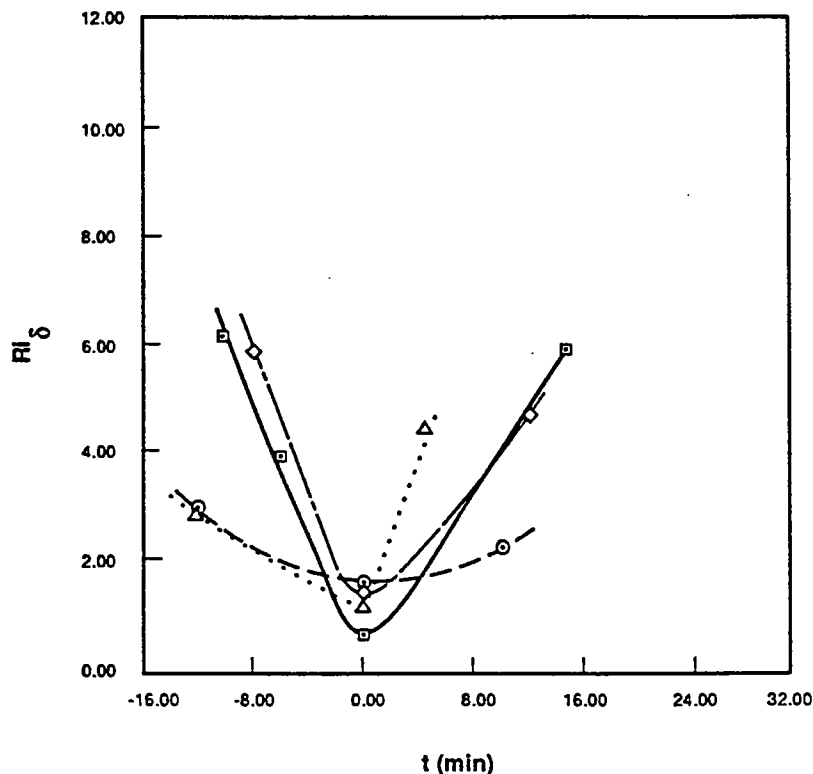
Figure 4:   The variation of the interfacial Richardson number during an interfacial "jump" event. The ranges of parameters are $3.77 \times 10^{-6} > q_o > 7.5 \times 10^{-7}$ ($m^2 s^{-3}$) and $1.4 > N_s > 1.0$ (rad s^{-1}). The profile taken just before the appearance of a rapid entrainment event was arbitrarily assigned t=0.

Figure 5 shows a photograph taken during a rapid-growth event.
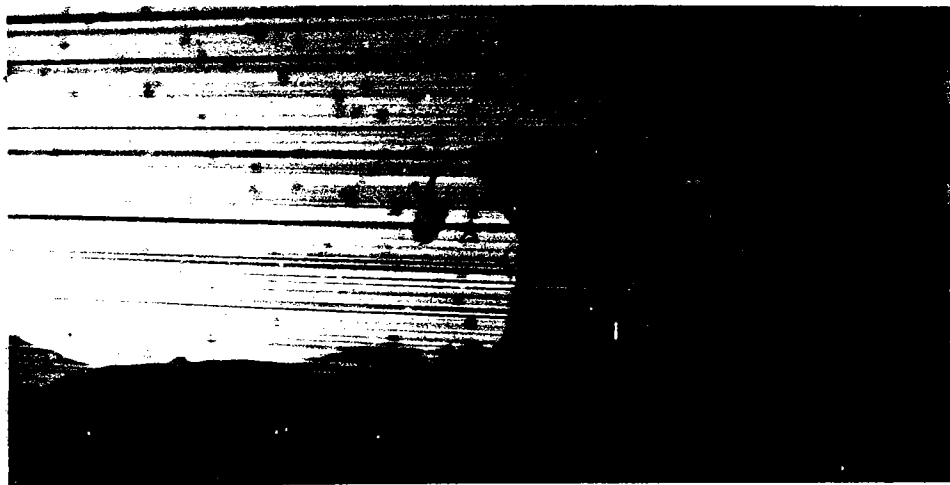
Figure 5:   A photograph taken at the onset of a "rapid" entrainment event. The bottom layer was dyed with fluorescein and the illumination was provided by an Argon-ion laser sheet. The photograph was taken through an optical filter that can only transmit fluoresced light so that only the bottom layer is visible. The figure shows the englufment of the fluid of the second layer by the overturning fluid motions (eddies) of the bottom layer (Feature A).
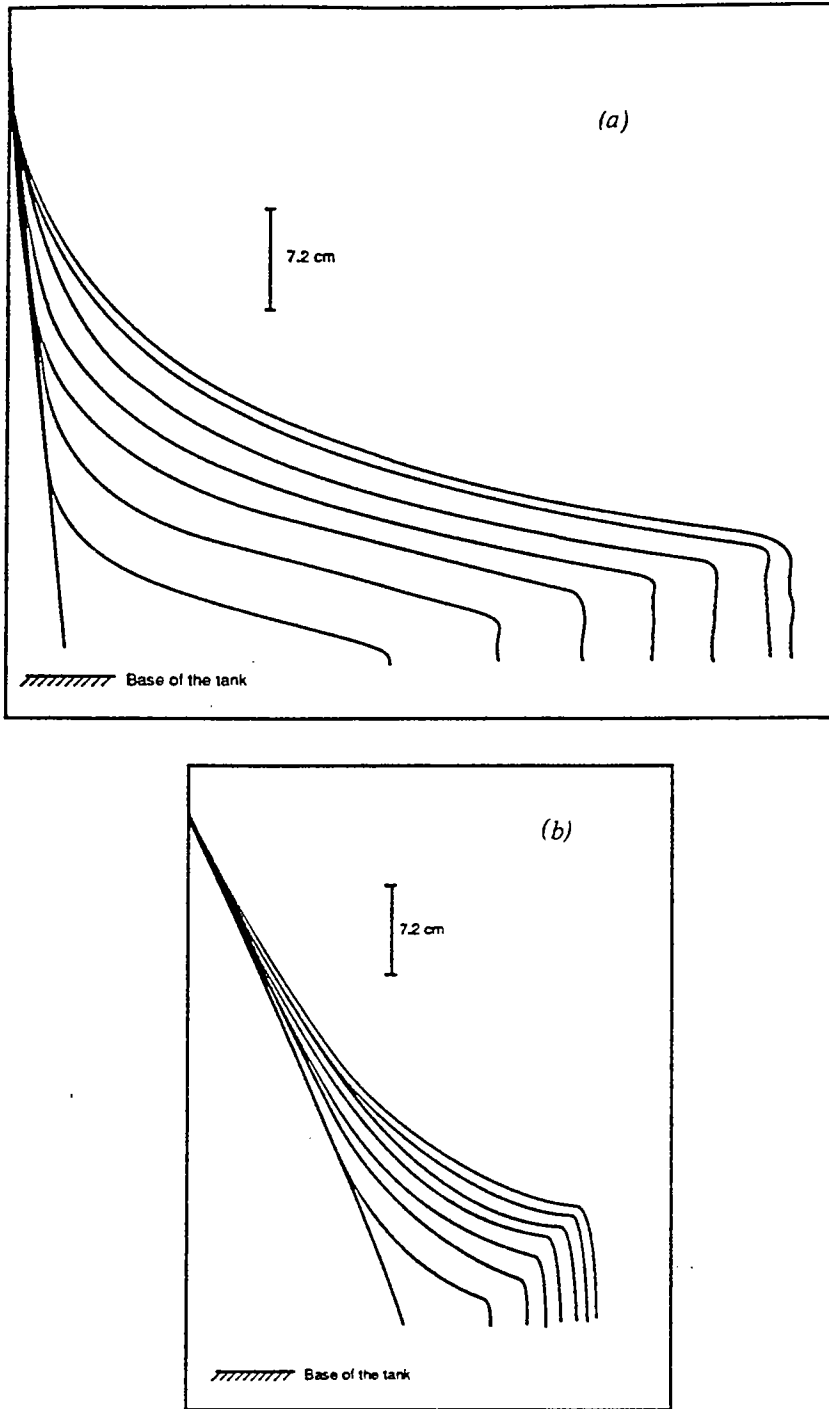
Figure 6: Time evolution of (a) temperature (b) salinity profiles when multiple layers are absent: $q_o = 3.78 \times 10^{-7}$ m²s⁻³ and $N_* = 1.98$ rad s⁻¹. According to Fernando (1987), the multiple layers should be expected when $h_1 \simeq 1$ cm.
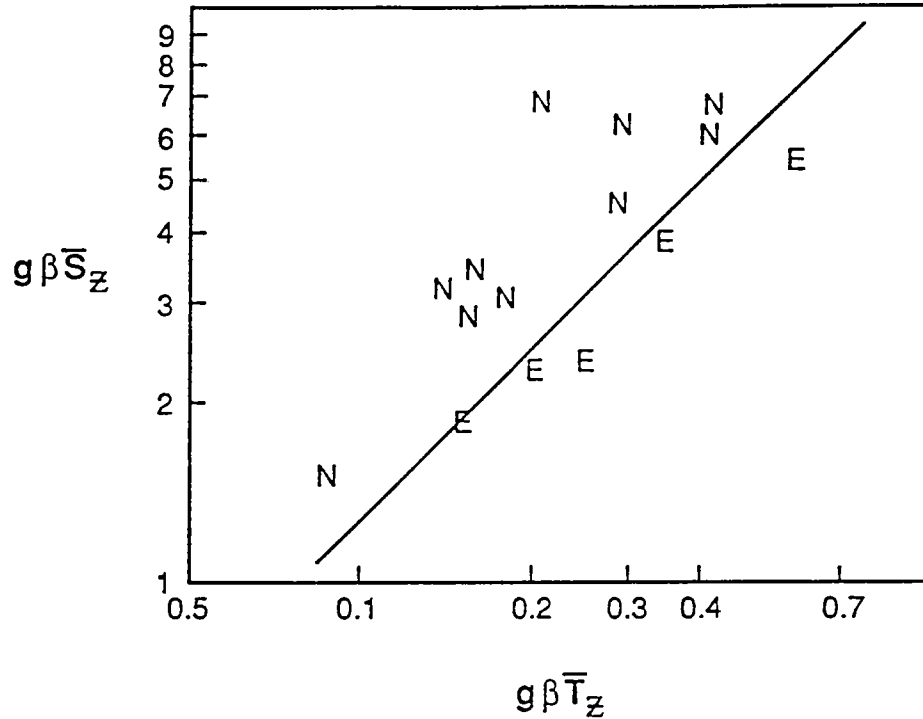
Figure 7: The results of the experiments of Hull et al. (1989). The units are in ms^{-2}.

5. Summary and Conclusions

Some results of an experimental study that was carried out to investigate properties of thermohaline staircase structures were summarized in the foregoing sections. Evidence was presented in support of the theoretical layer-thickness formula (1), which can be used to predict the layer thicknesses of oceanic staircases. It was pointed out that the entrainment law for uni-directional entrainment is determined by the operating regime within the parameter space so that the application of laboratory-based entrainment laws to oceanic interfacial-migration prediction models should be done with caution. When $Ri_\delta < 2$, anomalously high entrainment rates could be observed. The heating of a salinity gradient from below does not always lead to multiple layering. In such cases, the mixed-layer growth is diffusion controlled and the evolutionary characteristics are determined by the relative magnitudes of R_p and $\tau^{1/2}$.

References:

Fernando, H.J.S., 1987: The formation of a layered structure when a stable salinity gradient is heated from below. *J. Fluid Mech.*, 182, 425-442.

Fernando, H.J.S., 1989: Oceanographic implications of laboratory experiments on diffusive interfaces. *J. Phys. Oceanogr.*, 19(11), 1707-1715.

Fernando H.J.S. and F. Zangrando, 1990: in preparation.

Huppert, H.E. and P.F. Linden, 1979: On heating a stable salinity gradient from below. *J. Fluid Mech.*, 95, 431-464.

Hull, J., D.L. Bushnell, D.G. Sempstrote, and A. Pena, 1989: Ammonium sulfate solar pond: observations from small-scale experiments. *Solar Energy*, 43, in press.

Kelley, D., 1984: Effective diffusivities within thermohaline staircases. *J. Geophys. Res.*, 89(C6), 10,484-10,488.

Kelley, D., 1987: Interface migration in thermohaline staircases. *J. Phys. Oceanogr.*, 17(10), 1633-1639.

McDougall, T.J., 1981: Double-diffusive convection with a non-linear equation of state. Part II. *Prog. in Oceanogr.*, 10, 91-121.

Muench, R., H.J.S. Fernando and G.R. Stegan, 1990: Temperature and salinity staircases in the Northwestern Weddell sea. *J. Phys. Oceanogr.*, in press.

Padman, L. and T.M. Dillon 1987: Vertical heat fluxes through the Beaufort sea thermohaline staircase. *J. Geophys. Res.*, 92(C10), 10,799-10,806.

Phillips, O.M., 1977: Dynamics of the upper ocean. Cambridge University Press.

Turner, J.S., 1968: The behaviour of a salinity gradient heated from below. *J. Fluid Mech.*, 33, 183-200.

LABORATORY EXPERIMENTS IN DOUBLE-DIFFUSIVE CONVECTION

R. Krishnamurti

Dept. of Oceanography

Florida State University

ABSTRACT

In the first of two sets of experiments, (work done with L.N. Howard) a horizontal layer of fluid is subjected to a destabilizing temperature gradient and a stabilizing salinity gradient such that the layer is statically stably stratified. This is achieved by using porous boundaries between the working fluid layer and reservoirs of controlled temperature and salinity. The overall heat flux is fixed by the power input to an electrical heater. Thermal and saline Nusselt numbers are measured for fixed heating rates. A marked hysteresis is observed in the Nusselt number-power input curves obtained by increasing, then decreasing the heating rate. The minimum Rayleigh number at which convection occurs is measured and found to vary with the salt Rayleigh number and with the diffusivities ratio. For certain values of these parameters, this minimum Rayleigh number was found to be an order of magnitude below the linear theory prediction. This parameter-dependence is discussed in relation to some mathematical models of double-diffusive convection.

In the second set of experiments (work done with Y. Zhu) the set-up was as in the first set but now a uniform vertical mass flux was imposed through the layer. For sufficiently large imposed flux, the stabilizing salt gradient is swept away from most of the interior. However the destabilizing thermal temperature gradient is little affected because of the larger thermal diffusivity. Linear stability analysis and laboratory experimental results are presented.

INTRODUCTION

This is a report on some laboratory experiments designed to test certain linear stability theories and other mathematical theories on double-diffusive convection. These theories treat a layer of fluid whose density is determined by temperature and salinity, and whose lower boundary is maintained at temperature $T_0 + \Delta T$, salinity $S_0 + \Delta S$, while the upper boundary is maintained at temperature T_0, salinity S_0. The slower diffusing salt is stabilizing and the faster diffusing heat is destabilizing, but the boundary values are arranged so that the density decreases monotonically upwards. Linear stability theory (1,2) indicates that such a layer would be unstable to an oscillatory disturbance when the Rayleigh number R_T, defined below, exceeds a certain critical value R_{os} given by:

$$R_{os} = \frac{27}{4} \pi^4(1+\tau)(1+\frac{\tau}{\sigma}) + \frac{(\sigma+\tau)}{(\sigma+2)}R_s$$

Here, $R_s = g\beta\Delta S \, d^3/\kappa\nu$ is the salt Rayleigh number, $R_T = g\alpha\Delta T \, d^3/\kappa\nu$ is the thermal Rayleigh number, d is the layer depth, g the gravitational acceleration, α the thermal expansion coefficient, β the salt contraction coefficient, ΔS the salinity difference across the layer, ΔT the temperature difference across the layer, κ_s the salt diffusivity, κ the thermal diffusivity, ν the kinematic viscosity, $\sigma = \nu/\kappa$ the Prandtl number, and $\tau = \kappa_s/\kappa$ the diffusivity ratio. This linear stability result is indicated in figure 2. Veronis (1965) analysed the finite amplitude problem using a truncated five-component model with stress-free boundaries, and found steady subcritical flows at Rayleigh numbers as low as R_{min} given by $R_{min} = \tau R_s$. This is plotted in figure 2 and labelled "Veronis." For heat and salt diffusing in water $\tau \simeq 10^{-2}$ so that R_{min} would be smaller than R_{os} by a factor of 10^{-2}. However, with more modes included in the analysis, R_{min} was found to increase (Veronis, 1968), thus leaving in doubt the actual magnitude of R_{min} for the Boussinesq equations. (This latter study by Veronis was restricted to $\tau \geq 0.1$ and no subcritical flow was found.) However, Veronis gave the following convincing physical argument for the possibility of occurrence of subcritical instability. If some finite amplitude disturbance initially stirs the fluid layer, the internal distribution of temperature and salinity would be nearly isothermal and isohaline, with boundary layers to match the internal fields to the imposed boundary values. After the initial disturbance the temperature field would diffuse back towards its destabilizing linear profile, but the slower diffusing salt field would be still nearly isohaline in the interior. Thus most of the fluid layer experiences a destabilizing temperature field but no stabilizing salt field so it may be possible for such an initial finite amplitude disturbance to survive, even at Rayleigh numbers such that an infinitesimal amplitude disturbance could not grow on the linear profiles. But the magnitude of the minimum Rayleigh number and its parameter dependence could not be accurately determined by the low order model.

In their numerical studies Huppert and Moore (1978) found steady finite amplitude flows below the oscillatory critical Rayleigh number. The minimum Rayleigh number of occurrence of these steady flows for $\tau = 0.1$, $\sigma = 10$ was given by $R_{min} = 1033 + 0.844\, R_s$. For $R_s \gg 10^3$, $R_{min} \simeq 0.844\, R_s$. We note that for the same parameters $R_{os} \simeq 0.92\, R_s$.

Proctor (1981) showed, using boundary layer arguments with finite amplitude ε, that for $\tau \ll \varepsilon \ll 1$ and for rigid boundaries, steady finite amplitude convection could occur above a minimum Rayleigh number given by $R_{min} = R^{(o)} + C\tau^{4/11} R_s^{6/11}$ where $R^{(o)}$ is the critical Rayleigh number for $R_s = 0$. This result is valid for $R_s\tau^{2/3} \ll 1$ and is labelled "Proctor" in figure 2.

Finally, Joseph (1970) in a generalized energy analysis of global stability showed that, for stress free boundaries and the case of $R_s > \tau^3 R_T$, the necessary and sufficient condition for stability is that the Rayleigh number be less than the following:

$$R_T < \iota \, R_s + 2\left[\frac{27}{4}\pi^4(2-\iota^2) \, \iota \, R_s\right] + \frac{27}{4}\pi^4(1-\iota)^2$$

The results for rigid and for free boundaries are shown and labelled "Joseph" in figure 2.

Thus we have R_{min} given by the linear instability criterion, by steady subcritical flows with various degrees of applicability to experiments, and by a lower bound from the energy method. The divergence of these predictions is clear from figure 2.

For the second set of experiments the boundaries are once again maintained at fixed temperature and salinity, but a uniform vertical velocity w_0 is imposed. In the absence of convection, the heat and salt equations are, in steady state,

$$w_0 \frac{dT}{dz} = K\frac{d^2T}{dz^2} \; , \qquad w_0 \frac{dS}{dz} = K\frac{d^2S}{dz^2}$$

The dimensionless numbers controlling the shapes of the profiles of T and S are the Peclet numbers $\gamma_T = w_0 d/K$ and $\gamma_s = w_0 d/K_s$. Profiles of T and S are shown in figure 3. A linear stability analysis for small γ_s and γ_T is shown in figure 4. The oscillatory instability curve is modified slightly, but the monotonic instability curve is markedly decreased for increasing γ_s. Physically this seems reasonable since the sweeping of the salt field by the imposed w_0 removes the stabilizing salt gradient in most of the fluid layer.

THE LABORATORY EXPERIMENTS

The purpose of these experiments with controlled temperature and salinity boundary conditions, was to measure heat and salt fluxes, and hence heat and salt Nusselt numbers. From these results we can determine the parameter range in which convection occurred, thereby testing the existing theories regarding minimum Rayleigh number for convection to occur, as well as parameter dependence of fluxes.

Four different tanks were used in these experiments. The largest was 45 cm in diameter, the remaining three were 20 cm in diameter. The working fluid layer was set at various depths from 0.5 to 2.54 cm. The top and the bottom boundaries of this layer are formed by tightly stretched porous membranes (Versapor 800) of thickness .008 in. This membrane allows heat and salt to diffuse through it but fluid is not allowed to flow through. By measuring salt diffusion across the membrane it was determined that its diffusivity was very nearly the same as that of water. In view of its thinness then, the boundary condition on the working fluid is one of constant temperature and constant salinity. Both above and below this working fluid layer are reservoirs of water of controlled salinity and temperature. The fluid is subjected to a destabilizing

temperature gradient and a stabilizing salinity gradient by heating and salting the lower reservoir, and cooling and freshening the upper reservoir. The overall heat flux is fixed by the power input to an electrical heater in the lower reservoir, and the temperature of the boundary is maintained uniform by stirring the fluid in the reservoir. Constant stirring was accomplished with teflon-coated magnetic stirring bars mounted in each reservoir and driven from outside the reservoirs by electro-magnet coils. A guard bath surrounding each tank is maintained at a temperature equal to that in the lower reservoir. Thus all of the heat input is carried upward through the working fluid layer. In the upper reservoir, a coil of tubing with circulating cold water from a constant temperature circulator kept the upper reservoir temperature fixed. This upper reservoir was also stirred constantly in the same manner as the lower reservoir. For each setting of the heater, the cooling circulator temperature was set so that the mean temperature of the working fluid remained approximately constant throughout all the experimental runs. The boundary salinities are held fixed by flushing the reservoirs with water of fixed salinities. Because the boundaries are porous, care was taken to prevent forced flow through the working layer. Thus when the top reservoir was being flushed with fresh water, the pipes to the bottom reservoir were closed. Then the top reservoir would be closed, the pipes to the bottom reservoir opened, which was then flushed with saline water. This process was controlled by an oscillator circuit operating a set of solenoid values. While the solenoid valves were open, the flow rate was controlled by the dripping of the flushing fluid from a capillary tube fed from a constant-head reservoir. The outflow from each reservoir was collected in bottles. A rotating table holding 48 bottles was arranged to collect the outflow for one hour for each pair of bottles. At the end of 24 hours, the volume flow per hour and the specific gravity of each sample were measured. Salinities were deduced from the specific gravity.

Our procedure for the conduct of an experiment was as follows. A stabilizing salinity gradient was established by maintaining the flushing of both reservoirs while there was no heating or cooling and the temperatures of the two reservoirs were equal. (This takes from 1 to 15 days depending upon the layer depth and upon the diffusivities of the solutes used.) Then, a small rate of heating of the bottom and cooling of the top reservoir was started and maintained until a steady state became established. The power input, the temperatures of each reservoir (T_b in the bottom, T_t in the top), the salinity in each reservoir (S_b in the bottom, S_t in the top), the volume flow rates (q_b through the bottom, q_t through the top reservoir), and the two salinities $S^{(in)}$ of the inflow and the two salinities $S^{(out)}$ of the outflow were measured. Then this procedure was repeated after a small increment in the heating and cooling rates. If at some stage convection set in, the salinity difference across the layer would drop. We compensated for this approximately, by increasing q, but as a result R_s was only approximately constant during the course of one series of experiments. After convecton had set in, we decreased the heating

rate and corresponding cooling rate by small decrements, waiting for steady measurements after each step, then repeating the above measurements. This procedure was followed until convection had ceased and the measured quantities gave a Nusselt number of unity. Because of hysteresis, it was important to run each series of experiments continuously. Thus one series would run continuously for many weeks. Power failures or breakdowns midway in a series required restarting the series.

The above data allows us to compute Nusselt numbers. In the steady state, the total heat flux F_T is given by the total power input V^2/R divided by the area A of the working layer, where V is the rms voltage drop across the heating element of resistance R. The thermal Nusselt number N_T is the ratio of the total to the conductive heat fluxes:

$$N^T = \frac{V^2 d}{J A R k \Delta T}$$

where $\Delta T = T_b - T_t$, k is the thermal conductivity of the working fluid and J is the mechanical equivalent of heat.

Similarly the total salt flux F_s, in the steady state is, (using top reservoir data, for example) $F_s = q_t(S_t^{out} - S_t^{in})/A$. The salt Nusselt number N_s is the ratio of the total to the diffusive salt fluxes:

$$N_s = \frac{q_t(S_t^{out} - S_t^{in})}{k_s \Delta S A} d$$

where $\Delta S = S_b - S_t$.

The second set of experiments was performed at lower values of R_s since we knew from the results of the first set that hysteresis would then be minimum and linear stability theories could be tested.

DISCUSSION OF THE RESULT

Figures 1a, b, c show that the Nusselt number remains one as the power is increased and the Rayleigh number is approximately 80% of the linear oscillatory value R_{os}. However, once convection sets in and the Nusselt number is 3 or 4, decreasing the power input does not result in a cessation of convection, until R has been decreased in some cases to approximately 1/20 of R_{os}. This value of Rayleigh number below which the Nusselt number drops to unity is labelled R_{min}. A series of experiments with differing values of R_s and τ each gives an R_{min} which is shown in figure 3. It appears to be as far away as possible from the five diverging theoretical curves. There is agreement of all of these only at very small R_s.

In an effort to understand the observed R_{min} we propose the following simplified model. As the power input is lowered and the convection weakens, the salt boundary layers thicken so that the convecting layer, now of thickness $d_I < d$ is sandwiched between these two diffusive layers. We suppose that convection ceases when the conditions of this d_I layer satisfies the linear oscillatory instability criterion:

$$R_T z x^3 = R_c + \frac{\tau}{1+\sigma} R_s y x^3$$

where $x = d_I/d$, $y = S_I/\Delta S$, $z = T_I/\Delta T$ and where S_I and T_I are the salinity and temperature at the interface between the convecting and diffusing layers. In addition to this cut-off condition, we must match the fluxes at the interface. Here we assume that the diffusive flux in one oscillation period (given by linear theory) is carried away by the convective flux. This gives us the following two relations:

$$\left(\frac{1}{y}-1\right) = \frac{1}{2\sqrt{\tau}}\left(\frac{1}{x}-1\right)\left(\frac{\sigma R_s}{1+\sigma}\right)^{1/4} y^{1/4} x^{3/4}$$

$$\left(\frac{1}{z}-1\right) = \frac{1}{2}\left(\frac{1}{x}-1\right)\left(\frac{\sigma R_s}{1+\sigma}\right)^{1/4} y^{1/4} x^{3/4}$$

We find the minimum R_T consistent with these flux conditions. This is labelled R_A in figure 2.

In the second set of experiments the Rayleigh number and flux curves are shown in figures 5a, b, c. Figure 6 shows that the amplitude of oscillations goes to zero at R_T greater than the R_c indicated by arrows, at which the Nusselt number drops to unity, indicating that steady convection does occur below the R for oscillatory convection when γ_s is sufficiently large.

REFERENCES
(1) Walin, G. "Note on the stability of water stratified by both salt and heat." *Tellus*, Vol. 16, 1964, pp. 389-393.
(2) Veronis, G. "On finite amplitude instability in thermohaline convection." *J. Mar. Res.*, Vol. 23, 1965, pp. 1-17.
(3) Veronis, G. "Effect of a stabilising gradient of solute in thermal convection." *J. Fluid Mech.*, Vol. 34, 1968, pp. 315-336.
(4) Huppert, H.E. and Moore, D.R. "Non-linear double diffusive convection." *J. Fluid Mech.*, Vol. 78, 1976, pp. 821-854.
(5) Proctor, M.R.E. "Steady subcritical thermohaline convection." *J. Fluid Mech.*, Vol. 105, 1981, pp. 507-521.
(6) Joseph, D.D. *Archive for Rational Mechanics and Analysis.* Vol. 36, pp. 285-292.

FIGURE 1

THERMAL NUSSELT NUMBER N_T vs POWER INPUT P_*

SALINE NUSSELT NUMBER N_s vs POWER INPUT P_*

RAYLEIGH No. R_T vs POWER INPUT P_*

$$R_s = \frac{g\beta\Delta S\,d^3}{\kappa\nu}$$

$$R_T = \frac{g\beta\Delta T\,d^3}{\kappa\nu}$$

$$P = \frac{g\alpha d^4}{\rho\,c_n^2\,\nu A}\left(\frac{V^2}{R}\right)$$

$$P_* = P/R_s$$

FIGURE 2

158
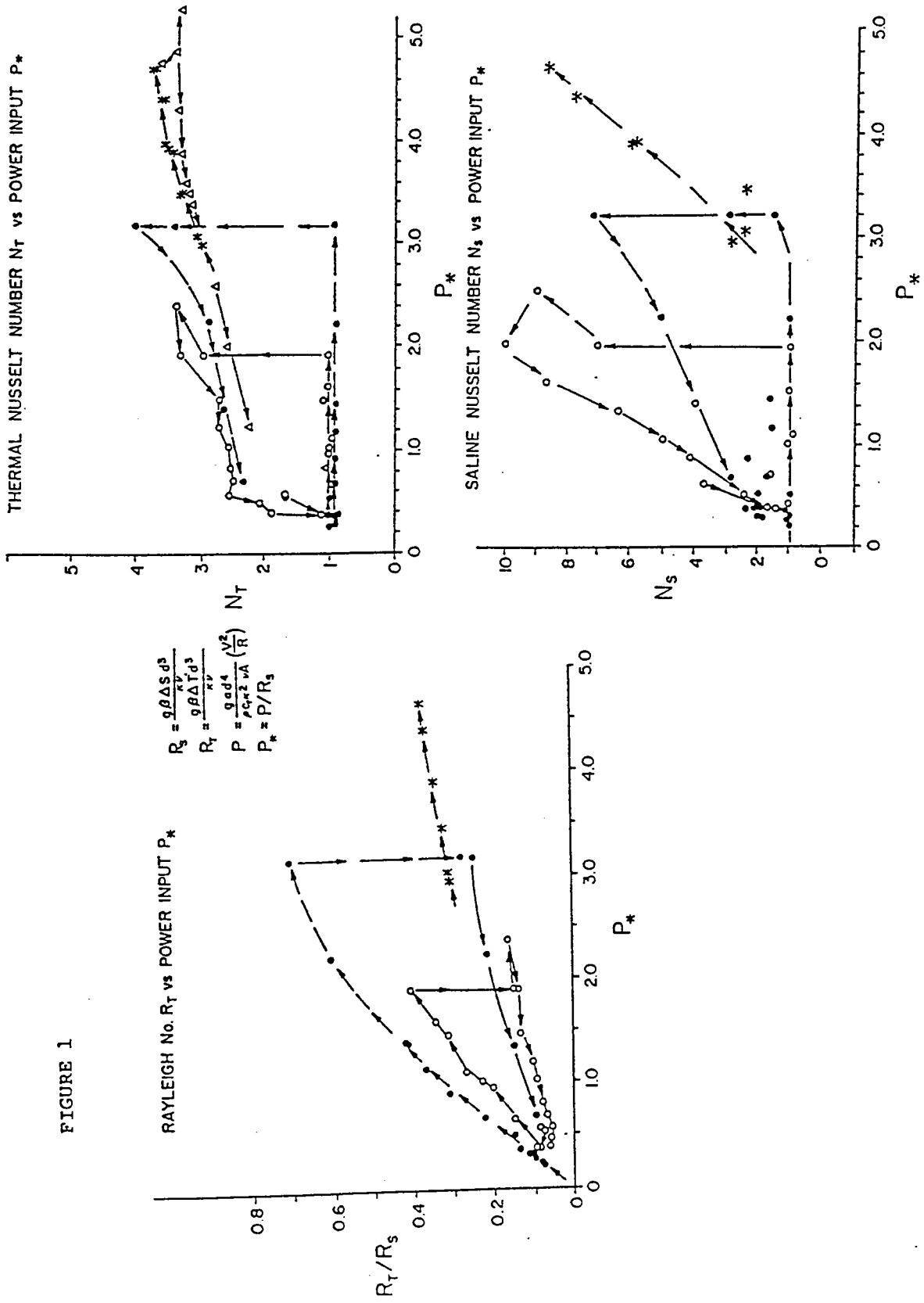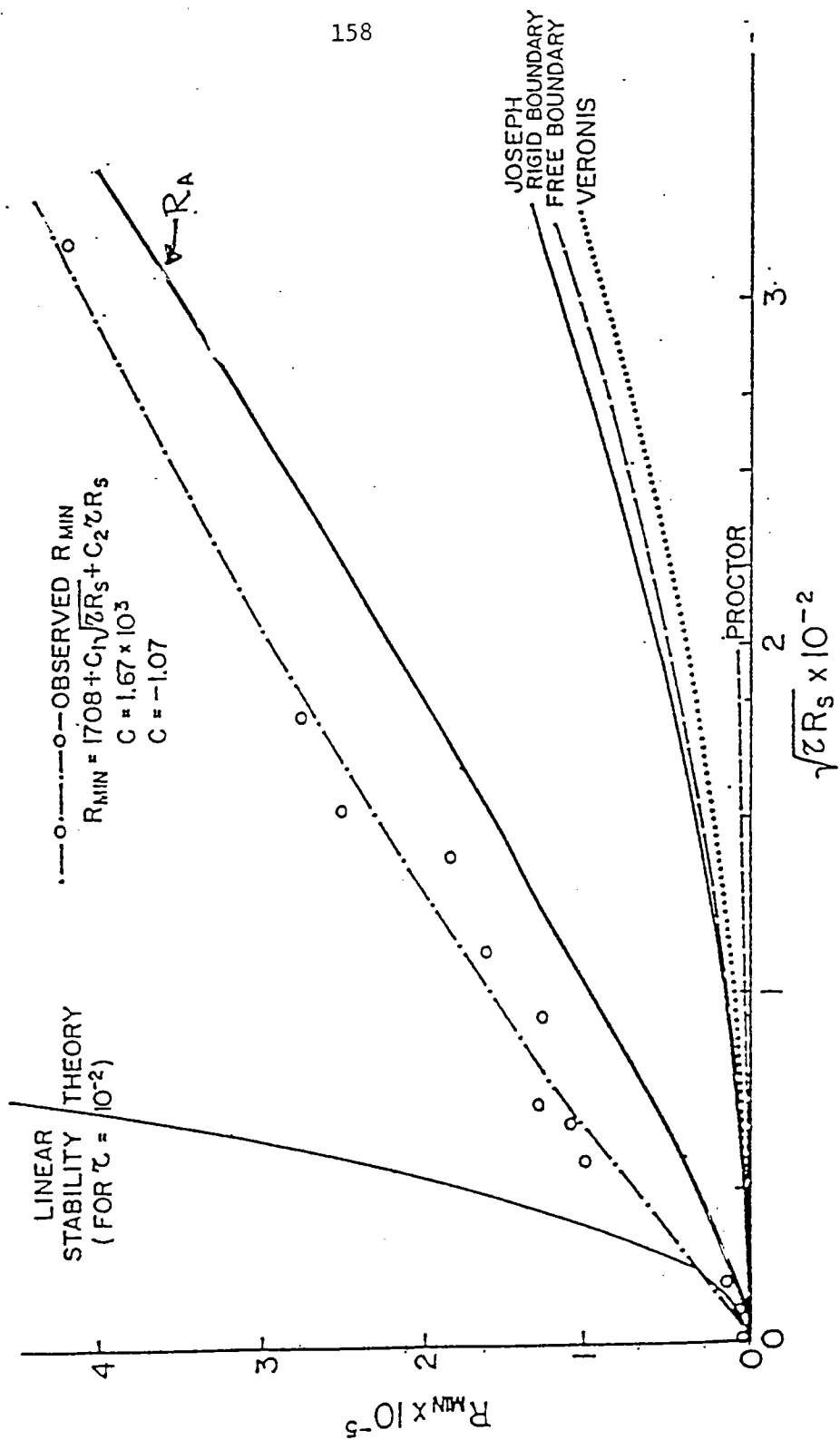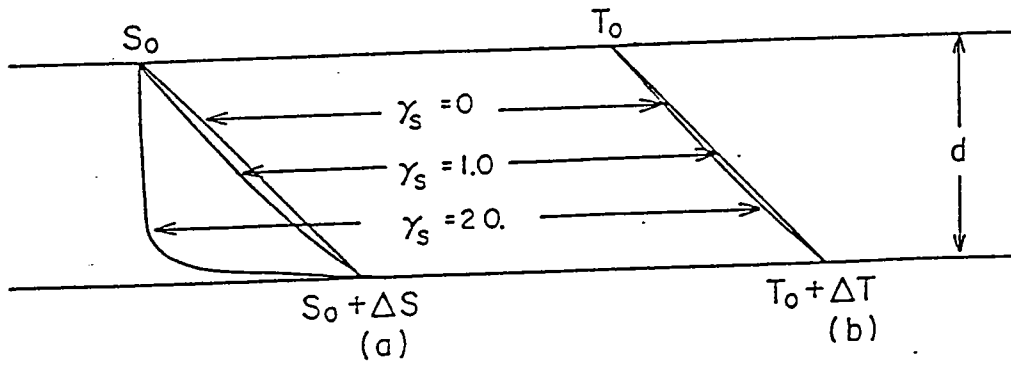
Figure 3a Salinity (a), and temperature (b) profiles of the basic state for three values of the Peclet number $\gamma_s = w_s d/\kappa_s$.
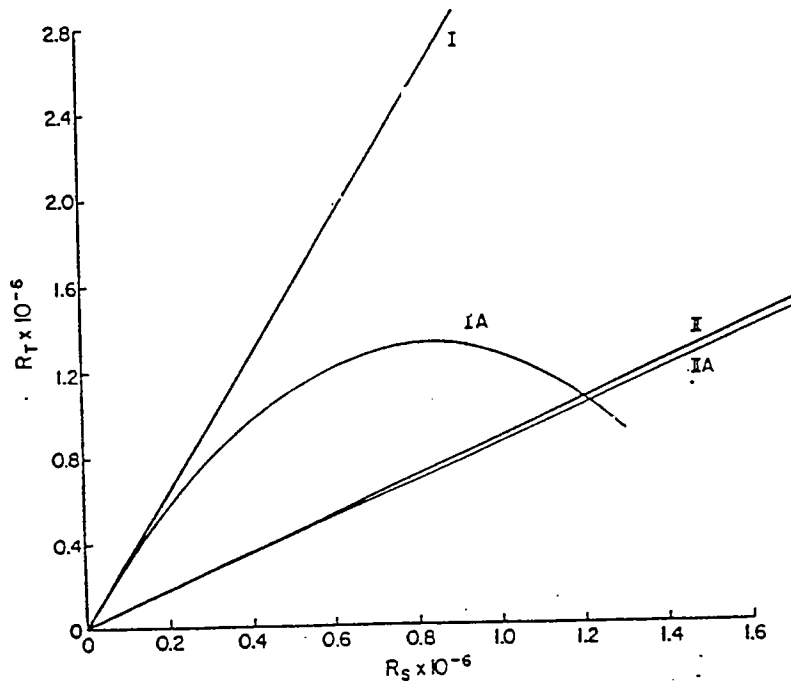
Figure 3b Stability diagram. I. marginal curve for overturning (monotonic) instability ($\gamma_s = 0$, $\tau = 10^{-1/2}$), IA. marginal curve for monotonic instability, ($\gamma_s^2 = 10^{-1}$, $\tau = 10^{-1/2}$, $a^2 = \pi^2/2$), II. marginal curve for oscillatory instability ($\gamma_s = 0$, $\sigma = 7$), IIA. marginal curve for oscillatory instability for $\gamma_s = 1$, $\sigma = 7$.

THERMAL RAYLEIGH NUMBER R_T vs POWER INPUT P

FIGURE 4

THERMAL NUSSELT NUMBER N_T vs THERMAL RAYLEIGH NUMBER R_T

SALT NUSSELT NUMBER N_S vs THERMAL RAYLEIGH NUMBER R_T
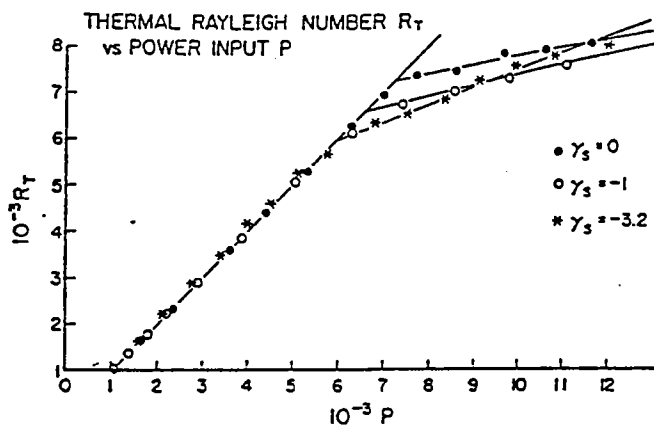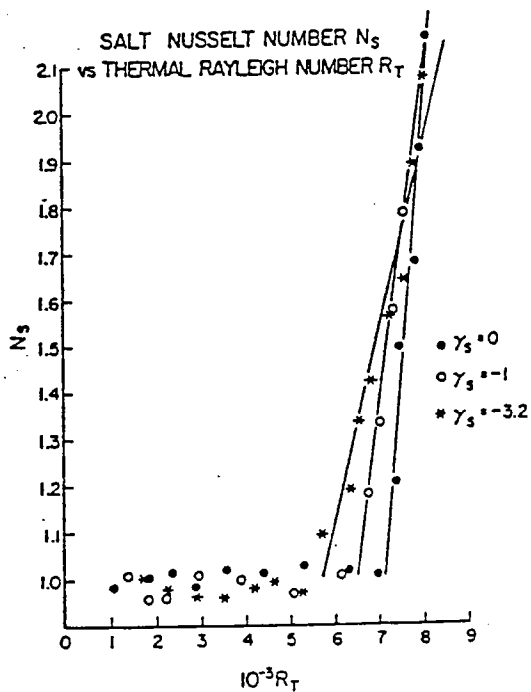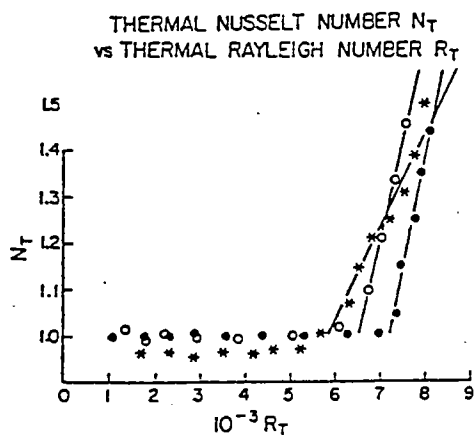
FIGURE 5
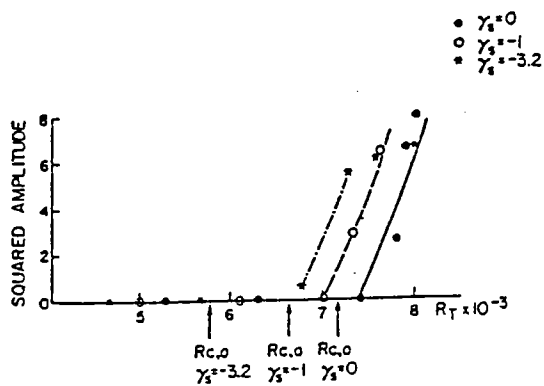
Diffusive-Convective Staircases in the Arctic Ocean

Laurie Padman

College of Oceanography
Oregon State University
Corvallis, OR 97331

Abstract

This paper is a summary of the results obtained from an analysis of microstructure data from the Arctic Internal Wave Experiment, followed by a review of work still in progress and a discussion of possible future programs. Diffusive-convective (d-c) staircases are a common feature in Arctic Ocean (T, S, σ_t) profiles, and their existence appears to be an indicator of where no other energetic processes are present, based on a comparison of where steps are, and are not, found. Horizontal variability of individual layers suggest than processes on scales of $O(1)$ km are important: intermittent internal wave breaking and non-turbulent straining are obvious possibilities. The diffusively driven convection in the layers appears from simple energy/dissipation arguments to be important to the decay of the internal wave field, and a parameterization of the d-c instability for large-scale models may need to take this interactive relationship between double-diffusion and internal waves into account. Similar measurements from the Yermak Plateau, near where the Atlantic Water first enters the Arctic, suggest that steps cannot be found where turbulent mixing is large: in this case it may be necessary to estimate the role of the differing molecular diffusivities of heat and salt in setting the effective vertical diffusivities of both parameters in mixing patches.

1. Introduction

Diffusive-convective (d-c) staircases have been found in many regions of the Arctic Ocean, in particular the Canada Basin and Beaufort Sea (Fig. 1), and on the upper edges of intrusions of Atlantic water into the ambient Arctic water north of the Yermak Plateau (the bibliography to this paper contains several references to these observations which are not explicitly referred to in the text). The most recent observations from the Arctic Internal

Wave Experiment (AIWEX) have been discussed by Padman and Dillon (1987, 1988, 1989; hereafter PD87, PD88, and PD89), and the first section of this paper will summarize the findings of those papers. More recent data collected during the Coordinated Eastern Arctic Research Experiment (CEAREX) in March-May 1989 will also be discussed as a contrast to the low energy environment of the Canada Basin. The final section suggests ways in which further studies may be able to improve our understanding of the principal dynamic and thermodynamic processes in geophysical d-c staircases.

Figure 1. Location of AIWEX (A), CEAREX (C), and Ice Island T-3 measurements by Neshyba, Neal and Denner (1971) (N). Arrows indicate circulation of Atlantic Water.

1.1 Setting

The Arctic Ocean is a semi-enclosed basin which is predominantly ice-covered for most of the year. Relatively warm, salty, Atlantic Water (AW) enters the Arctic as the West Spitzbergen Current, flowing northward through Fram Strait, around the islands of Svalbard, then generally anti-clockwise around the Arctic. The inferred flow of AW is shown in Fig. 1. The location of AIWEX, CEAREX, and the measurements reported in Neshyba, Neal and Denner (1971) from the ice island T-3, are also indicated. AIWEX was located on the southern side of the clockwise Beaufort Gyre, a flow which is the reverse of the general Arctic circulation and driven by both mean atmospheric conditions and the perturbations due to the Chukchi Cap. CEAREX involved an ice camp drift from deep water north of the Yermak Plateau, partially up the slope, then westward across northern Fram Strait.

Typical profiles of temperature, T, salinity, S, and density, σ_t, at both the CEAREX and AIWEX sites are shown in Fig. 2. The surface mixing layer in each case is very close to the freezing point for the observed salinity, because of contact with the ice. The Atlantic layer is seen as a temperature maximum of about $2.5°C$ at 250 m at CEAREX, and $0.5°C$ at > 450 m in AIWEX. In the former case, the mixed layer is contiguous with the AW: in the latter case the shallow mixed layer is buffered from the AW by the Bering Strait Summer and Winter layers. In both cases, however, the result is a layer of fluid above the AW core which is unstable in the d-c sense to double-diffusive mixing. Below the AW core at CEAREX, the necessary conditions for the salt-fingering instability are also found, although this region will not be addressed in the present paper.
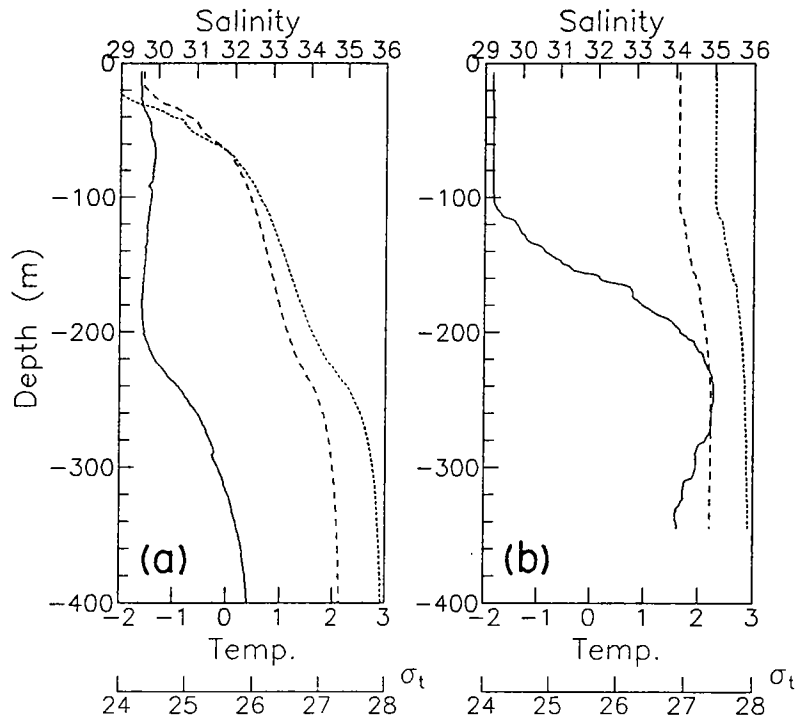
Figure 2. Typical profiles of T (solid), S (dashed) and σ_t (dotted) for (a) AIWEX and (b) CEAREX.

Why study the d-c staircase in the Arctic? PD87 and PD89 showed that the heat flux through the staircase, even including the observed probability of shear instabilities in the internal wave field, is orders of magnitude too small to explain the loss of AW heat as a vertical diffusive process, so that previous suggestions of the major heat loss occurring through interactions with lateral boundaries remain the most plausible. However, the staircase is of interest for several reasons, some of which have already been published:

- Measurements of the thermal microstructure provides valuable support for conceptual models derived from instability theories and laboratory observations.
- The semi-regular sequence of well-mixed layers and sharp interfaces is a unique acoustic medium.

- Existing heat flux "laws" can be validated by comparison to the thermal microstructure in both the interfaces and the layers.
- The ice pack provides a stable platform for internal wave vertical and horizontal coherence measurements, which are necessary to interpret the effect of internal wave shear on the staircase.
- There exists the possibility, not yet fully explored, that the mixing of internal wave momentum by the layer convection may be a significant sink of internal wave energy. If this is the case, the principal role of the staircase may be to modify the internal wave climate throughout the water column.

There is, therefore, a need to understand the interaction of the d-c staircase with the velocity field, and to be able to determine the necessary conditions for the existence of a staircase. We are presently treating the d-c steps as simply one component of the Arctic system, whose ability to modify the internal wave spectrum may be relevant to turbulent mixing elsewhere in the water column, and also to the availability of internal wave momentum for critical layer absorption in submesoscale eddies (Manley and Hunkins, 1985; Padman *et al.*, 1990).

2. Previous Results

2.1 Distribution of staircase parameters

PD87 measured not only the mean characteristics of the AIWEX staircase, ΔT, ΔS, and density ratio R_ρ for each interface (or 'sheet'), and the height H of the layers, but also the probability distributions for each parameter as a function of depth. These distributions do not support the view of a uniform series of stacked, regular sheets and layers, but rather show that these parameters vary in depth, horizontal position, and presumably time. The staircase can be thought of then as a set of interleaving laminae of finite extent, and with a time-dependence set by such processes as intermittent large-scale mixing events, non-turbulent internal wave straining, and local vertical flux divergences due to the differing properties of adjacent interfaces.

2.2 Heat and salt flux estimates

PD87 found by application of the Marmorino and Caldwell (1976) flux laws that the heat flux through the staircase, using the mean temperature step and density ratio in 10 m vertical bins, was about 0.05 W m^{-2} in the upper staircase, decreasing to about 0.01 W m^{-2} in the deep staircase, suggesting a vertical divergence of heat flux. However, by considering instead the *distribution* of heat fluxes resulting from the joint distributions of ΔT and R_ρ, a less divergent profile emerged, with a mean heat flux of about 0.08 W m^{-2}. Fluxes of salt were obtained from the Huppert (1971) equation for the buoyancy flux ratio as a function of R_ρ. Both heat and salt fluxes are smaller than needed to explain the decay of the AW as it circulates around the Canada Basin.

2.3 Horizontal coherence of layers

PD88 found d-c steps in almost all profiles which reached below 300 m throughout the AIWEX drift of 200 km. When this observation is added to those from T-3, and the extensive set of hydrocasts in the western Canadian Arctic by Melling *et al.* (1984), it appears that the d-c staircase is ubiquitous above the AW core in the Canada Basin/Beaufort Sea, except close to boundaries. The horizontal continuity of individual features is, however, less simple to determine. Analysis of a 20 h series of closely spaced microstructure profiles showed that many layers could be tracked continuously over the approximately 600 m of drift: since the deep circulation velocities are low, this is also the expected track length at the depth of the steps. However, some layers thinned until they disappeared into a sheet, others were destroyed by localized turbulent mixing on vertical scales of several layer heights, and the temperature in many layers varied significantly from one profile to the next. Tracking layers by temperature becomes unreliable when the temperature change from one profile to the next exceeds a significant fraction of a typical ΔT across a step: this often occurs in the AIWEX data for stations more than 50 m apart.

2.4 Comparison with conceptual/laboratory models

PD89 investigated the thermal microstructure through the AIWEX staircase in terms of conceptual models based on linear instability theory (Veronis, 1965), the mechanistic ideas of boundary layer separation suggested by Linden and Shirtcliffe (1978), and flow visualization experiments. Many thermal anomalies were found in the otherwise homogeneous layers, with temperature and length scales consistent with those expected from the separation of the buoyant, predominantly thermal, boundary layer of the diffusive interface, when the boundary layer Rayleigh number approaches $O(1000)$. These buoyant anomalies are found only within 0.5 m of their source interface: a vertical velocity scale for them based on a simple balance between Stokes drag and buoyancy is about 2 mm s^{-1}, giving a decay time scale of $O(200)$s. The implied diffusivity is then $O(10^{-5})$m^2 s^{-1} ($\gg \kappa_T$, the molecular diffusivity), consistent with the interpretation of the layer as being actively turbulent, based on the large layer Rayleigh number of $O(10^8)$.

Heat flux estimates based on the Marmorino and Caldwell (1976) flux laws can be approximately validated from the measurement of temperature gradients within the interfaces. The typical observed gradients of 0.1°C m^{-1} imply heat fluxes of 0.06 W m^{-2}, very close to the MC76 values.

2.5 The addition of internal waves to staircase thermodynamics

Perhaps the most interesting aspect of the AIWEX analysis is the staircase response to the internal wave field. As discussed above, the ice pack provided the opportunity to make detailed measurements of the horizontal and vertical coherence scales, spectra, and total energy of the internal wave field, which was found to be fundamentally different from the mid-latitude canonical internal wave field as represented by the Garrett-Munk "universal" spectrum. Levine *et al.* (1987) found that the mean energy density was only 0.05 of the canonical value, while the frequency spectrum was proportional to ω^{-1}, rather than ω^{-2}. Levine (1989) has shown from coherence measurements that fitting the observations to a

G-M form requires a much richer vertical modal structure than canonical, represented by an increase in the 'equivalent' number of vertical modes, $j*$, from 3 to 30. Interestingly, the result of these modifications is to maintain the shear variance at almost the canonical level, with a 'variance' Richardson number of $O(2)$, as found by Desaubies and Smith (1982) for mid-latitude internal waves. This observation lends credence to Munk's (1981) suggestion that the internal wave field saturates when the probability of mixing is some constant value.

PD89 averaged the dissipation rates for the two turbulent patches found in the rapidly sampled sequence, estimated the heat and salt fluxes within them by a constant flux Richardson number, then scaled the values by the observed probability of mixing, about 1.5%. The result was an increase through shear instability of about 20% in the total heat flux, and a factor a 10 in salt flux, the difference in the two being that diffusive convection transports heat much more effectively than salt, while shear instabilities mix properties according to their stratification on the scale of the mixing event, where salt stratification is the dominant term in the density equation. Even so, neither flux appears to be important in the large scale heat and salt budgets of the region.

3. Research in Progress

The results of the previous section indicate that our present mode of operation, making vertical profiles of T, C, and velocity shear microstructure, is a viable way of verifying the analytical and laboratory visions of the thermodynamics of d-c staircases. In addition, we have been able to assess the importance of the addition of internal waves to the staircase evolution. The principal result from the Arctic studies, that even with internal waves the d-c fluxes are negligible, is not necessarily true elsewhere: in regions where ΔT is large or R_ρ small, d-c fluxes may be significant, and the AIWEX data provides support for the application of existing flux laws to these other regions. However, perhaps by looking at the Arctic environment as a system where the steps are passively responsive to larger scale processes, we are missing other processes of importance.

3.1 The Role of Diffusive Convection on Internal Wave Energy Dissipation

Consider the system depicted in Fig. 3. Internal waves with vertical scales much larger than an individual layer height impinge upon an existing staircase structure. Each internal wave component is a wave propagating at some angle to the vertical from a source, for example from the surface where the waves are forced by the relative motion of the under-ice topography through the mixed layer. Although the applied wave velocity profile through a particular layer varies with time, the double-diffusively driven convection can partially homogenize the momentum within the layer. Fig. 3 shows a velocity profile which might result for a steady applied shear: in this case the final velocity gradient in the layer is given by stress continuity, so by estimating the eddy viscosity K_m in the layer and assuming viscosity in the interface to be purely molecular, we can relate the velocity shears in both layers and sheets. The kinetic energy released by this process is lost either as dissipation to heat, or through buoyancy fluxes, essentially entrainment of gravitationally stable sections of the adjacent interfaces into the turbulent layers.

We can estimate the rate of loss of kinetic energy, ε, from the turbulent properties of the layer, i.e. integral length and velocity scales, calculate the maximum dissipation rate, and compare it to the divergence of internal wave energy flux. By making the assumption that the velocity shear is linear, ε reduces to a simple function of shear, layer height H, and a constant which relates the turbulent length scale to the layer height. Present rough estimates of the downward energy flux, based on a G-M type model spectrum with the AIWEX parameters invoked, suggest that provided the turbulent length scale exceeds $0.1H$, the staircase can dissipate most of the incident wave energy for the observed mean energy levels.
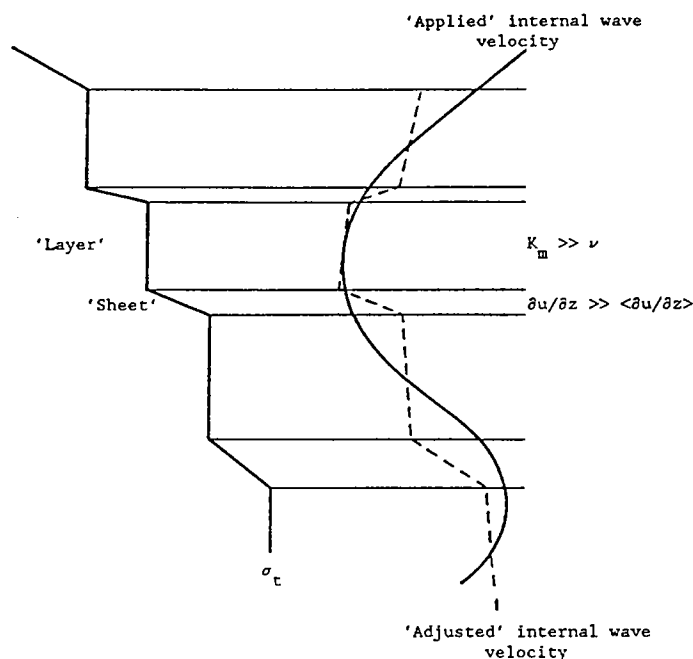
Figure 3. Schematic of internal wave/diffusion convection interaction model. Mixing in layers is driven by double-diffusive convection originating at the interfaces, and results in an effective viscosity $K_m \gg \nu$, the kinematic viscosity. Internal wave kinetic energy is dissipated as the time-dependent 'applied' internal wave velocity profile is continuously adjusted by mixing towards the 'adjusted' profile. Intensification of shear $\partial u/\partial z$ relative to the local mean gradient $\langle \partial u/\partial z \rangle$ at interfaces may lead to shear instabilities such as Kelvin-Helmholtz billowing. Large-scale mixing by shear instabilities independent of the diffusive convection (Gregg, 1989) is not shown but may also be important.

This is a significant result, because much of the energy input at the surface by wind stress comes in storm events. Open ocean measurements find that even so, the internal wave energy level remains roughly constant, to within a factor of 2 or so, while in the Arctic, the energy level decays rapidly following a storm (pers. comm. M. Levine). A possible interpretation is that there is a dissipation process unique to the Arctic which rapidly attenuates vertically propagating energy, so that the energy density is closer to being in equilibrium with the wave generation processes than in the open ocean. While there are

many plausible candidates in the Arctic, such as the unique surface boundary condition and the generation spectrum being tied to the 2-dimensional horizontal wavenumber spectrum of the under-ice topography, it is also possible that absorption in the staircase is a significant sink.

Testing this hypothesis may be difficult: the process is likely to be continuous at a low level which tracks the slowly varying wave shear, rather than consisting of intermittent, large, easily observable events as in shear instability. It is also not clear how a staircase might first evolve from an initially smooth density profile if the ambient internal wave field in the absence of steps were to be comparable to G-M canonical levels. However, we can imagine a plausible scenario where the layers are actually initiated by breaking events in the internal wave field, resulting immediately in d-c absorption of further incident wave energy, which acts to sharpen the initial interfaces by entrainment as part of the total energy balance.

While all this is speculative, it does suggest a real possibility for diffusive convection to be important to the overall energetics of the Canada Basin. A further topic being pursued by Murray Levine and myself is the role of critical layer absorption of internal wave energy by submesoscale coherent vortices in the Canada Basin, and part of this project is an understanding of the reasons for the anomalous internal wave spectrum. There is thus a potential for feedback from the steps into the energetics of SCVs, which are known to be a major component of the momentum, heat and salt fields in the upper 300 m.

3.2 Double-Diffusion in CEAREX

Typical profiles of Turner angle, Tu, for both AIWEX and CEAREX (Fig. 4) show that while in AIWEX only the d-c instability is possible in the sampled depth range, in CEAREX both the d-c and salt-fingering instabilities are possible. Furthermore, Tu in sections of CEAREX approaches more closely to $-90°$ than anywhere during AIWEX. Since $-90°$ corresponds to $R_\rho=1$, i.e. the most energetic regime for the d-c instability, we would expect that d-c layering might be even more well-developed in CEAREX than in AIWEX. However, this is not the case. Very few steppy features are actually found in over 1400 microstructure profiles, either above (d-c) or below (salt-fingering) the AW temperature and salinity maximum near 250 m. Presently we attribute this observation to two factors, (a) the early age of the AW inflow (see Fig. 1), and (b) the high values of turbulent kinetic energy dissipation rate, which appear to be correlated with the diurnal topographically trapped vorticity wave associated with the Yermak Plateau (Hunkins, 1986; Chapman, 1989). Unless aided by the creation of finestructure by some other process, d-c steps take several months to form themselves out of an initially small perturbation to otherwise uniform temperature and salt gradients. Conventional wisdom is that steps therefore need several months in a peaceful environment to grow a well-developed staircase structure. The diurnal cycle of energetic mixing events (in some cases turbulence extends from the surface to over 250 m), would be sufficient to erase any steps which may drift into the region affected by the vorticity wave. Any step-like structures, which are found at most depths randomly located in time, are presumably simply finestructure associated with active or decayed mixing events, independent of the double-diffusive nature of the density stratification.

There is still a need, however, to determine whether our previous assumption of equal diffusivities for salt and heat in turbulent patches is really valid in a d-c regime, even when layering is not present. Since the salt and thermal microstructure exist at different scales because of their differing molecular diffusivities, there is some potential for their enhanced eddy diffusivities also to differ. While this may be an important research area to understanding the turbulent limit of a d-c environment, it is not addressable with the CEAREX data set because of our inability to resolve the salinity microstructure. With our present sensor, a Neil-Brown conductivity cell, our best resolution of salinity is about 10-20 cm, about 100 times that of the Batchelor wavelength for salt at the observed dissipation rates.
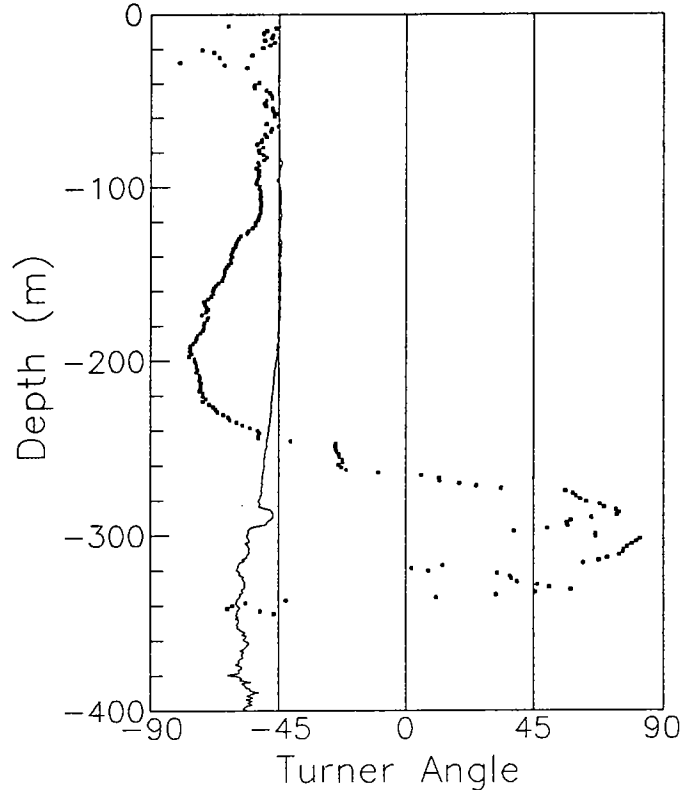
Figure 4. Typical profiles of Turner angle, Tu, for AIWEX (solid) and CEAREX (symbols). $Tu<-45°$ is d-c unstable: $Tu>+45°$ is salt-fingering unstable.

4. Suggested Further Research

The following research topics are suggested in no particular order, however the combination of these efforts could substantially clarify our understanding of diffusive convection in geophysical environments.

4.1 Revisit Lake Vanda (Antarctica)

Lake Vanda is a saline, ice-covered lake in Antarctica which is well-known for its d-c staircase (Shirtcliffe and Calhaem, 1968; Huppert and Turner, 1972), resulting in a net flux

of heat from the surface to the bottom (about 65 m), and bottom temperatures of near 25°C. Although R_ρ is high, about 7.5, the temperature steps are very large compared with the Canada Basin data, leading to large heat fluxes, determined both from laboratory flux laws and by the large scale heat budget for the lake. In addition, the land-fast ice cover implies no energetic source for internal waves, so the site should be a good candidate for a study of pure d-c layering. Microstructure profiling equipment such as our RSVP is now sufficiently developed to be able to measure thermal and velocity microstructure reliably in this environment. The high heat, and hence buoyancy, fluxes through the interfaces are presumably reflected in high layer dissipation rates. An investigation of the length, velocity, and dissipation scales of the pure d-c driven layer turbulence is therefore well suited to this site. Lake Vanda would be used as a large laboratory tank, without the concomitant problem of secondary circulations induced by lateral boundaries.

4.2 Numerical simulation

Simulation can be used to verify with non-linear equations, the conditions for interface breakdown which have previously been derived analytically with a linear stability analysis (Veronis, 1965). One of the perplexing features of laboratory work is the apparent dependence of flux ratio on the magnitude of the heat flux: there is at least a factor of two difference in salt flux over the common geophysical density ratio range of $2 < R_\rho < 8$, for flux laws from different experimenters. The present limit to 2-D simulation (pers. comm. C. Shen) may pose a problem in interpretation, but as at least a qualitative guide to the salt flux dependence on changing heat flux, it could be valuable.

4.3 Understand Kelley's (1984) layer height model

Despite the poor coverage in R_ρ in Kelley's original data set, basically just a low and a high R_ρ point, the addition of the AIWEX data set shows that this empirical law is capable of predicting layer height to about a factor of two. The AIWEX data falls below the proposed curve, although when all layer heights are plotted against it, the curve is seen to describe an upper limit to AIWEX step heights. The proposed form is intriguing because it essentially reduces to a constant layer Rayleigh number which is much larger than the assumed value for transition to 3-dimensional turbulence. The best existing explanation is Fernando's recent work relating the layer scale turbulence properties to the entrainment rate of the bounding interfaces. It is believed that Lake Vanda measurements (see 4.1) would be a useful tool in verifying this model and therefore explaining the Kelley curve.

4.4 Laboratory measurements of wave attenuation due to diffusive convection

Our results from interpreting AIWEX data suggest that at least in the Canada Basin, the interaction of internal waves with the staircase is probably the most important role of the staircase, since the d-c fluxes are too low to be important of themselves. There are a number of useful studies which I would hope could be addressed in laboratory tanks.

- The effect on the decay rate of interfacial waves for a constant density step as the two-component stratification is varied from diffusively stable through a range of R_ρ. This would be combined with flux estimates and flow visualization in order to determine if

interfacial instabilities might be an important source of flux enhancement, as expected at low R_ρ where the flux ratio is known to approach unity.

- The effect on the decay rate of large scale waves through a series of multiple steps as the two-component stratification is varied as above.
- The effect of the d-c instability on turbulent diffusivities of heat and salt in an actively turbulent regime. An experiment such as reported by Taylor for the salt-fingering instability may allow a better interpretation of our CEAREX data, as well as providing clues to how the steps initially develop in a geophysical context.

4.5 Revisit the Canada Basin

In view of the discussions based largely on C-SALT analyses, there is evidence that further microstructure data from the Arctic Ocean, with supporting data (moorings) designed specifically for a staircase study, may be of value in understanding other processes in the staircase, such as the isopycnal fluxes of heat and salt required to balance vertical divergences. This suggestion is based largely on the possibility of the present Canadian Ice Island (see EOS, September 12, 1989) leaving its present location in shallow water and entering the Beaufort Gyre circulation over the deep water of the Canada Basin. This would provide an inexpensive platform for collection of a longer time series for step tracing, as well as a vertically dense mooring measuring T and S, covering several steps. Our AIWEX experience indicates that isopycnal displacements are not larger than a few meters, so that it should be possible to retain a few steps in the aperture of a mooring spanning perhaps 30 m only. The microstructure system used in AIWEX could not be run continuously for more than 30 h based on manpower constraints: the revised system used in CEAREX and available for future studies can be run continuously for several days (in CEAREX we obtained 20 days with a maximum data gap of 1 h).

5. Acknowledgements

6. References

(Some of these references are not referred to explicitly in the text)

Chapman, D.C., Enhanced subinertial diurnal tides over isolated topographic features, *Deep-Sea Res.*, **36**, 815–824, 1989.

Coachman, L.K. and K. Aagaard, Physical oceanography of Arctic and Subarctic seas, in: *Marine Geology and Oceanography of the Arctic Seas*, pp. 1–72, Springer, New York, 1974.

Desaubies, Y.J.F. and W.K. Smith, Statistics of Richardson number and instability in oceanic internal waves, *J. Phys. Oceanogr.*, **12**, 1245, 1259, 1982.

Gregg, M.C., Scaling turbulent dissipation in the thermocline, *J. Geophys. Res.*, **94**, 9686–9698, 1989.

Hunkins, K., Anomalous diurnal tidal currents on the Yermak Plateau, *J. Marine. Res.*, **44**, 51–69, 1986.

Huppert, H.E., On the stability of a series of double-diffusive layers, *Deep-Sea Res.*, **18**, 1005–1021, 1971.

Huppert, H.E. and J.S. Turner, Double-diffusive convection and its implications for the temperature and salinity structure of the ocean and Lake Vanda, *J. Phys. Oceanogr.*, **2**, 456–461, 1972.

Kelley, D.E., Effective diffusivities within oceanic thermohaline staircases, *J. Geophys. Res.*, **89**, 10484–10488, 1984.

Levine, M.D., C.A. Paulson and J.H. Morison, Observations of internal gravity waves under the Arctic pack ice, *J. Geophys. Res.*, **92**, 779–782, 1987.

Levine, M.D., Internal waves under the Arctic ice pack during AIWEX: the coherence structure, *J. Geophys. Res.*, (in press), 1989.

Linden, P.F. and T.G.L. Shirtcliffe, The diffusive interface in double-diffusive convection, *J. Fluid. Mech.*, **87**, 417–432, 1978.

Manley, T.O. and K.L. Hunkins, Mesoscale eddies of the Arctic Ocean, *J. Geophys. Res.*, **90**, 4911–4930, 1985.

Marmorino, G.O. and D.R. Caldwell, Heat and salt transport through a diffusive thermohaline interface, *Deep-Sea Res.*, **23**, 59–67, 1976.

Melling, H., R.A. Lake, D.R. Topham and D.B. Fissel, Oceanic thermal structure in the western Canadian Arctic, *Continental Shelf Research*, **3**, 233–258, 1984.

Munk, W.H., Internal waves and small-scale processes, in: *Evolution of Physical Oceanography*, B.A. Warren and C. Wunsch, editors, MIT Press, Cambridge, 264–291, 1981.

Neal, V.T., S. Neshyba and W. Denner, Thermal stratification in the Arctic Ocean, *Science*, **166**, 373–374, 1969.

Neshyba, S., V.T. Neal and W. Denner, Temperature and conductivity measurements under ice-island T-3, *J. Geophys. Res.*, **76**, 8107–8120, 1971.

Neshyba, S., V.T. Neal and W. Denner, Spectra of internal waves: *in situ* measurements in a multiple-layered structure, *J. Phys. Oceanogr.*, **2**, 91–95, 1972.

Padman, L. and T.M. Dillon, Vertical heat fluxes through the Beaufort Sea thermohaline staircase, *J. Geophys. Res.*, **92**, 10799–10806, 1987.

Padman, L. and T.M. Dillon, On the horizontal extent of the thermohaline steps in the Canada Basin, *J. Phys. Oceanogr.*, **18**, 1458–1462, 1988.

Padman, L. and T.M. Dillon, Thermal microstructure and internal waves in an oceanic diffusive staircase, *Deep-Sea Res.*, **36**, 531–542, 1989.

Padman, L., M.D. Levine, T.M. Dillon, J.H. Morison and R. Pinkel, Hydrography and microstructure of a cyclonic Arctic eddy, *J. Geophys. Res.*, (submitted), 1990.

Perkin, R.G. and E.L. Lewis, Mixing in the West Spitzbergen Current, *J. Phys. Oceanogr.*, **14**, 1315–1325, 1984.

Shirtcliffe, T.G.L. and I.M. Calhaem, Measurements of temperature and electrical conductivity in Lake Vanda, Victoria Land, Antarctica, *N.Z.J. Geol. and Geophys.*, **11**, 976–981, 1968.

Veronis, G., On finite amplitude instability in thermohaline convection, *J. Marine Res.*, **23**, 1–17, 1965.

What Drove the Intrusions that mixed Meddy "Sharon"?

Barry Ruddick
Department of Oceanography
Dalhousie University
Halifax, N.S., B3H 4J1, Canada

Abstract

The intrusions from Meddy "Sharon" were found to be laterally coherent in a sequence of stations extending radially outward. The migration of these intrusions across density surfaces had a distinct pattern, sloping in opposite senses in the upper and lower part of the Meddy. This pattern was found to be consistent with that expected for the McIntyre (1970) instability for Prandtl number less than one, in which case mass flux (equal in heat and salt) dominates over viscosity. The slopes were also consistent with thermohaline intrusions, in which diffusive fluxes dominate in the upper, diffusively stratified portion of the Meddy, and finger fluxes dominate in the lower, finger-stratified part. In either case, the intrusions are driven by mass fluxes, not by momentum fluxes.

1. Introduction

From October 1984 to October 1986, an anticyclonic eddy of Mediterranean overflow water was tracked in the Northeast Atlantic and its movements, evolution, turbulent mixing, and decay were monitored. This is the longest an identifiable oceanic water parcel has ever been tracked (Armi et al, 1988,1989). The originators of the experiment, Larry Armi and Tom Rossby, wanted to understand the role played by these "Meddies" in the dispersion of salt and heat throughout the Atlantic. For instance, Armi and Stommel (1983) calculated that if three Meddies per year were to enter the β-triangle region and disperse their salt anomaly, the resulting salt flux divergence could equal the advective flux divergence in that area. The mechanisms of movement and the processes that govern the evolution and salt loss of the Meddy will obviously influence the role played by Meddies in lateral dispersion in the deep ocean.

Another reason for interest in the experiment was that it provided a unique opportunity to observe the changes over time of an identified water parcel, and to therefore infer the rates and mechanisms of mixing. By comparing these inferred mixing rates with the directly observed microstructure and finestructure signatures, we can learn which mixing mechanisms dominate and how rapidly they work. The observations of the Meddy at four stages of its life (Armi et al, 1989) clearly show lateral mixing of the core by intrusions (these can be seen in fig. 1 below), and that the inward erosion of the salinity and velocity structure is associated with the intrusions. The turbulent microstructure in the intrusive region, and in the salt fingering region below the core (Oakey, 1988), was found to be greatly intensified with a ratio of thermal to velocity variance dissipation inconsistent with purely mechanical turbulence. Hebert (1988,1989) interprets the partial erosion from below of the Meddy core and the formation of a series of steps and mixed layers, as being due to salt finger mixing, and finds that the salt finger fluxes must be an order of magnitude weaker than predicted by laboratory-based flux laws, but are consistent with Kunze's (1987) Stern Number criterion. He estimates that the salt loss by vertical salt fingering leads to a salinity decay timescale of 20 years, a factor of 20 slower than observed. Hebert et al (1989) find that the loss of salt and heat content, kinetic and potential energy, and the aspect ratio changes of the Meddy are consistent with the dominance of lateral processes, with a radial salt diffusivity of $K_H \approx 2 \text{ m}^2\text{s}^{-1}$.

It appears from the above as though lateral intrusions succeeded in mixing salt, heat, and angular momentum radially outward, to be dispersed in the surrounding ocean as the Meddy
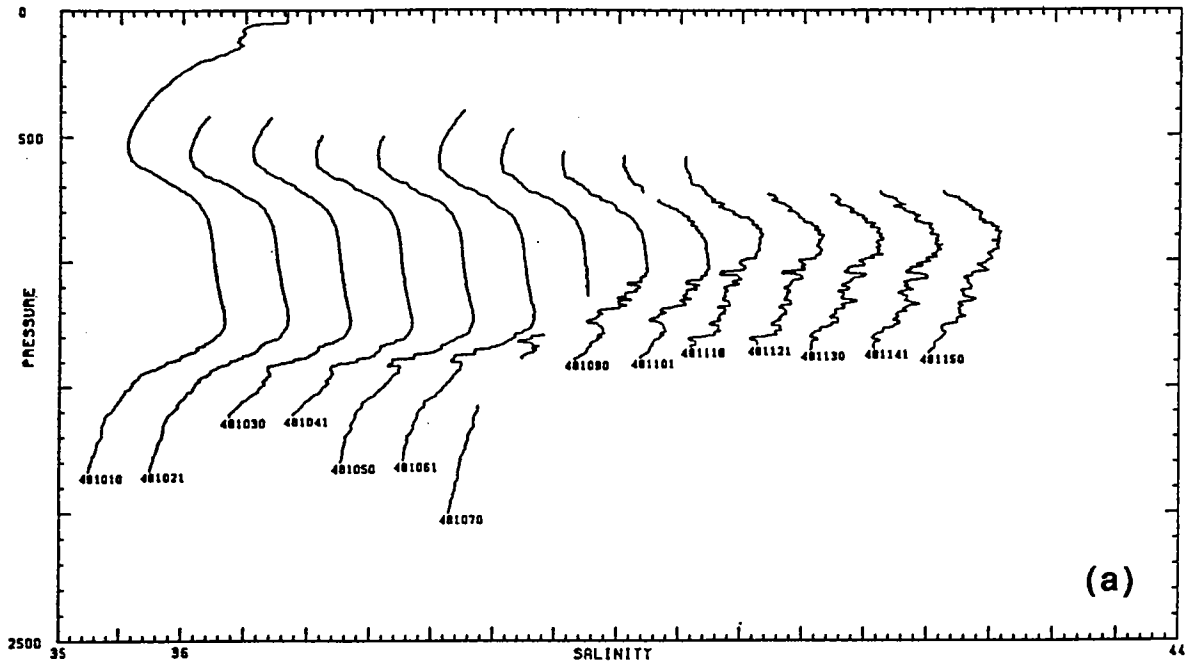
Survey I : October 1984

Figure 1a. Sequence of salinity (PSU) vs pressure (decibars) stations from the outer core and intrusive regions of the Meddy. The salinity scale is correct for the leftmost station, closest to the core; successive stations have been offset by 0.5 PSU.

Figure 1b. positions of the stations shown in (a). The radius of the intrusion-free core is shown as the innermost circle. The outer circle shows the extent of the intrusive region.

drifted. Figure 1a, taken from Hebert et al (1988), shows a sequence of salinity vs depth traces from the first survey of the Meddy. The positions of these stations with respect to the Meddy is shown in figure 1b. Figure 1b also shows schematically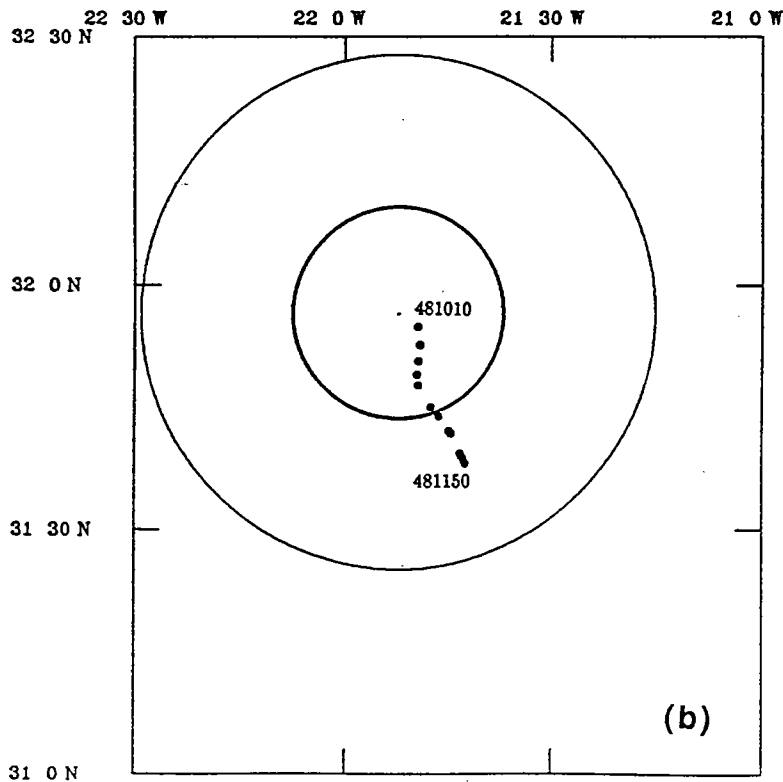 the (assumed circular) intrusive region, with salinity inversions larger than 0.01 PSU, and the intrusion-free core region. The final six profiles are from a closely-spaced "tow-yo", in which the CTD was raised and lowered as rapidly as possible over a limited depth range while the ship was steaming radially, resulting in a station spacing of less than 1 km. Several of the inversions in this sequence appear to be laterally coherent, and are more so when plotted against density rather than pressure. In this note we examine the slope of these intrusions with respect to isopycnals in order to determine whether they are driven by angular momentum diffusion (McIntyre, 1970), or by unequal mixing of heat and salt as in the thermohaline intrusion models exemplified by Stern (1967). In the next two sections, we review these instabilities, focussing on the relationships between instability dynamics and intrusion slope, and then we compare the observed slope with the model predictions.

2. The McIntyre (1970) Instability

While investigating the flow at large Prandtl number in a differentially heated rotating annulus, McIntyre (1968) discovered that viscosity can destabilize the flow. He investigated the linear instability of a baroclinic vortex (McIntyre, 1970) and found that unequal diffusivities of momentum v and mass κ allow small-amplitude axisymmetric layering motions to grow exponentially even when the flow is stable according to classical inviscid criteria. The instability is thus analogous to salt fingering with the two diffusing components being mass and angular momentum. There is also an overstable oscillatory instability analogous to thermohaline double-diffusion, but McIntyre (1970) showed that the direct instability always occurs before the oscillatory one, and since the direct instability has greater advective effects and produces larger T-S anomalies, we will not consider the oscillatory mode further. Calman (1977) demonstrated in the laboratory that layering can occur at large Richardson number, and verified that the dependence of critical Richardson number and fastest-growing wavelength on Prandtl number $\sigma = v/\kappa$ were in accord with predictions for $\sigma > 1$.

McIntyre described the physical mechanism for frictional destabilization in the following way. Consider a basic state consisting of a circular baroclinic vortex in thermal wind balance:

$$f\overline{v}_z = g\alpha\overline{T}_r. \tag{1.}$$

where $\overline{v}(r,z)$ is the azimuthal velocity, $\alpha\overline{T}(r,z)$ is the density field, and overbars denote the basic state. As shown in figure 2, the vertical gradient in the (radial) Coriolis force is balanced by the vertical gradient in the pressure gradient force (PGF), and this is supported by the isopycnal tilt. We now consider the perturbations to be influenced by friction but not diffusion of mass. Consider moving a parcel of fluid from point A to point B in the (r,z) plane. This motion corresponds to motion in the "wedge of instability" in baroclinically unstable flows. The motion of mass downward across geopotentials, but downgradient from dense fluid to light, tends to reduce the slope of isopycnals and constitutes a release of potential energy. If the fluid parcel can remain at position B, this potential energy release will be the source of energy for the perturbations. Will the fluid parcel remain at B, continue onward, or return to A? If friction is absent, the Coriolis force acting on the radial velocity of the parcel during its travels from A to B act in the azimuthal direction to decelerate the parcel (this can also be seen to be a consequence of angular momentum conservation). Thus, when the parcel reaches point B, the Coriolis force is reduced, and the pressure gradient force acts to restore the parcel to point A. With neither friction nor diffusion acting on the parcel, it will undergo an inertial oscillation about point A if perturbed. However, if friction prevents the parcel from decelerating as it moves to point B, then the Coriolis force on the parcel will not be reduced, and the parcel can "slide down" the gravitational potential. The

instability takes the form of sloping layers with dynamics similar to salt fingers, in which the unstable (in the radial direction) density field is convected by the perturbation, which can grow because of the more rapidly diffusing angular momentum field.
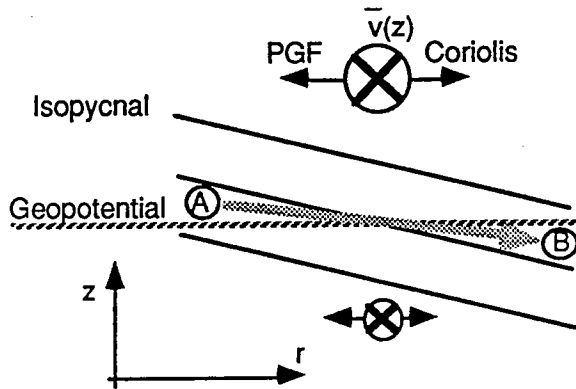
Figure 2. Sketch of the basic state baroclinic shear flow showing the direction of fluid parcel displacements for $\sigma>1$. A geopotential (level) surface is shown as a dashed line. Isopycnals are shown as solid lines.
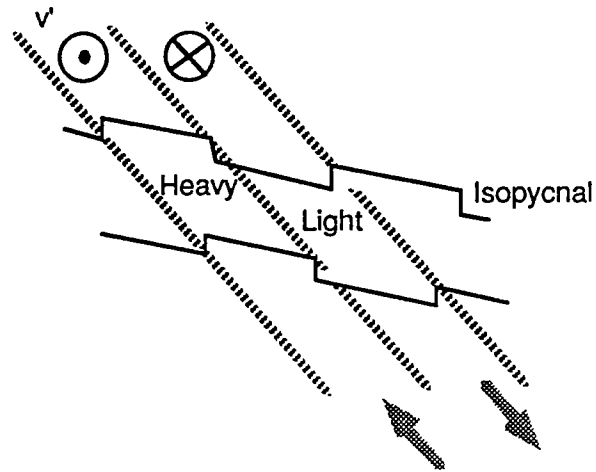
Figure 3. Sketch of the isopycnal displacements and velocity perturbations for $\sigma<1$. The orientation of the disturbance is shown by the dashed lines. Isopycnals are shown as solid lines.

A similar argument can be made for the case $\sigma<<1$, in which mass diffusion dominates over friction. The perturbations sketched in figure 3 tilt in the same sense as the mean isopycnals, but much more steeply. Consider the effect of advection in the mean gradients on an upgoing parcel of fluid. Advection of density (predominantly the term $w(\partial \rho/\partial z)$) causes the density perturbation to become positive, and gravity acting on this perturbation density gives rise to a restoring force. Advection of momentum in the vertical shear (the term $w(\partial \bar{v}/\partial z)$ in the azimuthal momentum equation) produces a negative v-perturbation (out of the page) and a perturbation Coriolis force which reinforces the original upward motion. If neither friction nor diffusion are important, the perturbation acts like an internal wave, bobbing up and down as buoyancy and inertia forces alternately dominate. However, if diffusion can act to reduce the restoring density perturbations, the perturbation Coriolis forces reinforce the original motion and cause the perturbation to grow.

The simple physical arguments above suggest that the instability has two distinct mechanisms. For $\sigma>1$, the perturbations have a shallow slope, and friction erases the velocity perturbations, allowing the density perturbations to release the gravitational potential energy of the basic state. For $\sigma<1$, the perturbations have a steep slope, and diffusion erases the restoring density perturbations. The perturbations transfer y-momentum downgradient, releasing the kinetic energy of the mean shear flow.

McIntyre (1970) gives bounds enclosing all unstable disturbance slopes:

$$\tan\phi_{1,2} = \frac{(\sigma+1)}{2}\left[1\pm\left\{1-\frac{Ri}{Ri_c}\right\}^{\frac{1}{2}}\right]\tan\Gamma \qquad (2.)$$

where: ϕ is the angle *to the vertical* made by the disturbance orientation

$\Gamma = \tan^{-1}\{\bar{v}_z/(f + \bar{v}_r)\}$ is the angle made by the lines of constant circulation $C=fr+\bar{v}$

$\Theta = \tan^{-1}\{\bar{T}_z/\bar{T}_r\}$ is the angle to the vertical made by the mean isopycnals

$Ri = \tan\Theta/\tan\Gamma$ is the modified Richardson number

$Ri_c = (\sigma+1)^2/4\sigma$ is the critical Richardson number, with growth when $Ri<Ri_c$.

If $Ri<1$, the system is unstable to direct overturning (McIntyre calls this the "classical" instability), so $1<Ri<Ri_c$. It can then be shown that:

$$\tan\Theta < \tan\phi < \sigma\tan\Gamma \quad \text{for } \sigma>1, \text{ and} \tag{3.}$$
$$\sigma\tan\Theta < \tan\phi < \tan\Gamma \quad \text{for } \sigma<1. \tag{4.}$$

These limits are shown in figure 4. For $\sigma>1$, the disturbance slopes lie between those of the geopotentials and isopycnals. For $\sigma<1$, the disturbance slopes lie between the vertical and the lines of constant circulation, which are closer to vertical than the isopycnals.
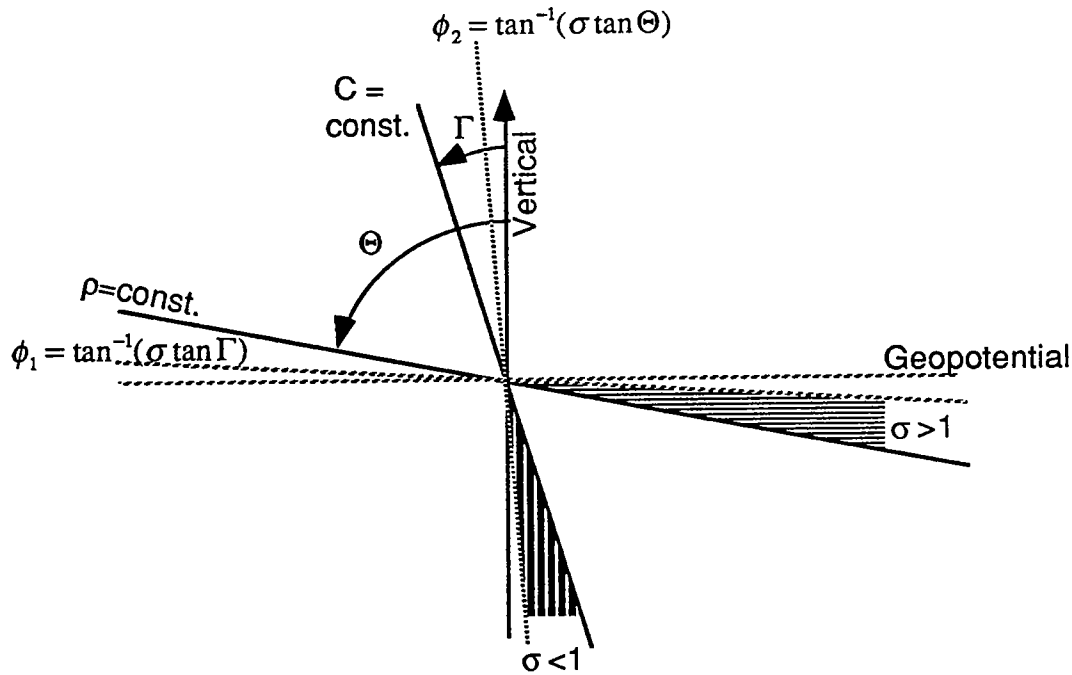
Figure 4. Range of allowed orientations of McIntyre's (1970) instability, corresponding to equations 3 and 4.

3. Thermohaline Intrusions

Stern (1967) discovered that lateral T-S gradients were unstable to quasi-horizontal intrusive layering driven by double-diffusive vertical mixing. A warm salty intrusive layer can have salt fingers below it and diffusive thermohaline convection above it. Turner (1978) found in a series of laboratory experiments that warm salty intrusions can slope either upwards or downwards as they extend laterally according to whether the finger or diffusive buoyancy fluxes dominate. If the finger fluxes dominate, the ratio of heat to salt change along the layer is

$$\frac{d(\alpha T)}{d(\beta S)} = \gamma_F \tag{5.}$$

where α and β are the thermal and haline expansion coefficients, and γ_F the salt finger flux ratio. Eq. 5 is equivalent to

$$\frac{1}{\rho}\frac{d\rho}{d(\beta S)} = 1 - \gamma_F, \tag{6.}$$

which states that intrusions will become less dense as they become less saline (and vice-versa) if salt fingers dominate. Similarly, if diffusive fluxes act alone with salt/heat flux ratio γ_D, the ratio of heat to salt change along the layers is

$$\frac{d(\alpha T)}{d(\beta S)} = \frac{1}{\gamma_D}, \tag{7.}$$

which is equivalent to

$$\frac{1}{\rho}\frac{d\rho}{d(\beta S)} = 1 - \gamma_D^{-1}, \tag{8.}$$

and in this case intrusions will become less dense as they become more saline and vice-versa.

Most models of the intrusion process (Stern, 1967, Toole and Georgi, 1981, Ruddick and Turner, 1979) assume for simplicity that the finger fluxes dominate. In-situ observations have often noted intrusive layers migrating across isopycnals in a manner consistent with this assumption (Joyce, Zenk, and Toole, 1978, Gregg, 1980). However, some intrusion models (Ruddick, 1984, McDougall, 1985a,b) have argued that the density changes induced in the layers by salt finger fluxes must eventually lead to the diffusive fluxes becoming important, and vice-versa, so that both finger and diffusive fluxes may be important in intrusions.

4. Intrusion Slopes in Meddy "Sharon"

The Meddy core rotated anticyclonically about once each six days, and the isopycnal tilts necessary to maintain the high pressure in the core must be in the sense shown in figure 5a. Intrusive motions associated with the McIntyre (1970) instability for $\sigma > 1$ have slope more horizontal than the isopycnals as in the left of figure 5a, and since the Meddy core is salty, the density versus salinity graph for intrusions will be as shown in figure 5b. Similarly, for $\sigma > 1$, intrusions slope more steeply than isopycnals, leading to the pattern in figure 5c.

(a) Meddy structure

(b) McIntyre: σ>1

(c) McIntyre: σ<1

(d) thermohaline,
finger fluxes only

(e) thermohaline,
diffusive fluxes only

(f) thermohaline,
both fluxes
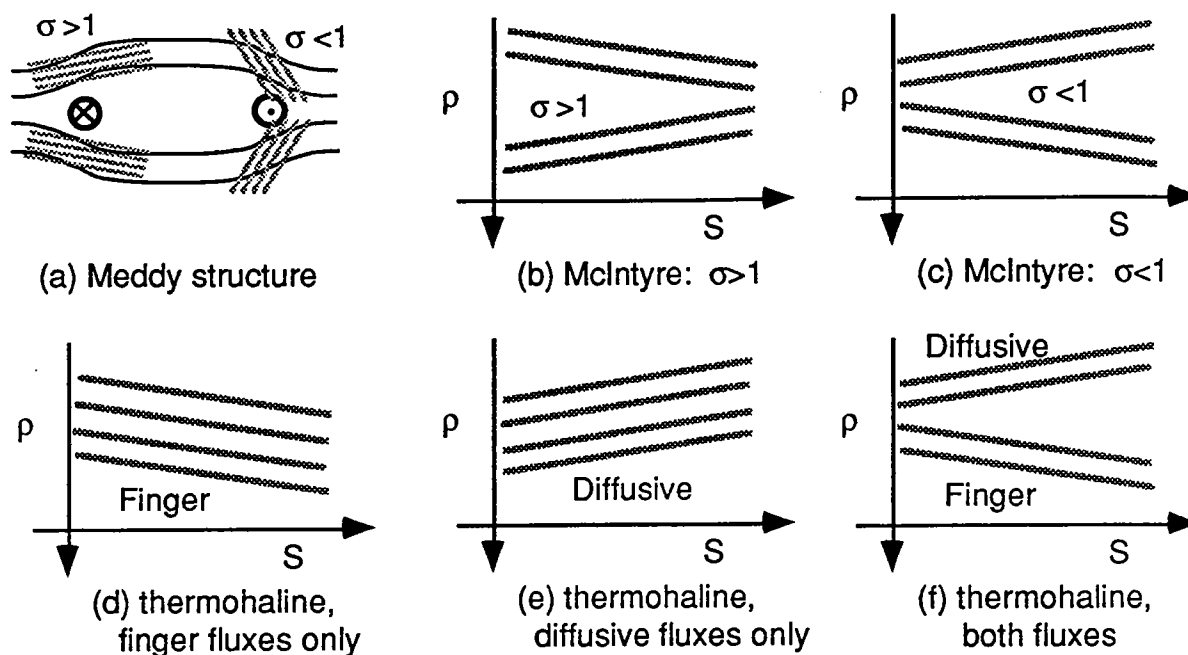
Figure 5. (a) Velocity structure (arrows pointing into and out of the page) and associated isopycnal (solid lines) slopes of the Meddy. The grey lines in groups of four represent the slopes expected for McIntyre (1970) intrusions according to eqs. 3 and 4. (b,c) Expected pattern of salinity vs density of McIntyre intrusions for Prandtl number greater and less than one, respectively. (d) Expected pattern for thermohaline intrusions in which finger fluxes dominate. (e) Expected pattern for thermohaline intrusions in which diffusive fluxes dominate. (f) Expected pattern for thermohaline intrusions in which finger fluxes dominate in the lower half, but diffusive fluxes dominate in the upper half.

As we saw in Figure 1, the overall stratification of the Meddy (averaging over several intrusions) was diffusive sense above 900 m depth, and finger sense below about 1000 m. If the intrusions are thermohaline, we expect one of three things: (1.) they can be influenced primarily by salt finger fluxes over the whole depth range (as argued by Ruddick and Turner 1979, and assumed by Stern, 1967), with slope as in figure 5d, (2.) they can be influenced primarily by diffusive fluxes with slope as in figure 5e, or (3.) they can be influenced by diffusive fluxes in the upper part (eq. 8) and finger fluxes in the lower part (eq. 6), with slopes as in figure 5f.

In figure 6 we show a sequence of S vs σ_1 ($\sigma_1 = \rho_1$-1000, where ρ_1 is the density referenced to 1000 db pressure) curves from downtraces 481101-481150, the closely spaced intrusive stations in fig.1. The positive extrema in S have been marked by circles, the negative extrema by squares. Several intrusions can be tracked from one station to the next, consistently crossing isopycnals, although the traces tend to obscure the picture somewhat. It is possible to link the obvious intrusion extrema together, ensuring that no two extrema from the same station are linked, and then to use the pattern thus developed to help deduce further links between the extrema.
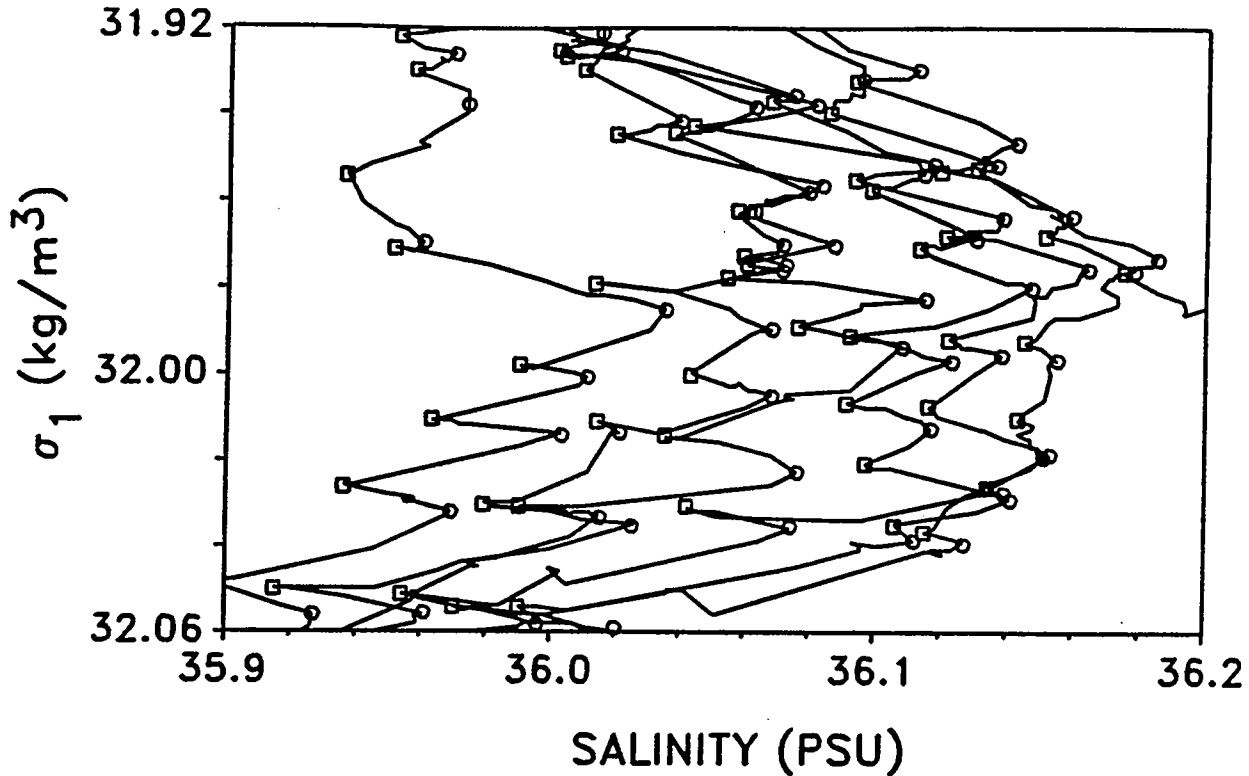
Figure 6. Potential density (σ_1) versus salinity for the closely-spaced stations 481101-481150. Positive S-extrema are marked by circles, negative extrema by squares.

The results of this linking of intrusive S-extrema are shown in figure 7a for the positive extrema, 7b for the negative extrema. The filled circles (or squares, in the case of fig. 7b) denote intrusions of greater than 0.01 PSU salinity excursion. These were used in regressions of S on σ_1, resulting in the solid lines shown. The slopes show a clear pattern of intrusions crossing isopycnals, consistent only with figure 5c or 5f. The uncertainties on the regression slopes are small enough that this pattern could not have occured by chance. The slopes are inconsistent with any of the other hypotheses summarized in figures 5b, d, and e.

5. Discussion

The McIntyre (1970) instability discussed in section 2 assumes $\kappa_S = \kappa_T \neq \nu$ in its parameterization of small-scale vertical fluxes (equal heat and salt diffusivities, unequal to viscosity. The parameterizations for thermohaline intrusions assume $\kappa_S \neq \kappa_T$ (for salt fingers, $\kappa_T = \gamma_F R_\rho^{-1} \kappa_S$), so that heat and salt diffusivities are unequal. If the intrusions are caused by the McIntyre instability, then mass diffusion must dominate over viscosity. Since there is no known oceanic mixing mechanism giving Prandtl number less than one, this seems to be an unlikely possibility. If the intrusions are thermohaline in nature, then the diffusive regions must dominate the buoyancy fluxes in the upper part of the Meddy and finger fluxes the lower part. This seems plausible, since the upper part of the Meddy is stratified in the diffusive sense overall, and the lower part is stratified in the finger sense. In any case, the intrusions must be driven by mass fluxes, not by viscous effects.
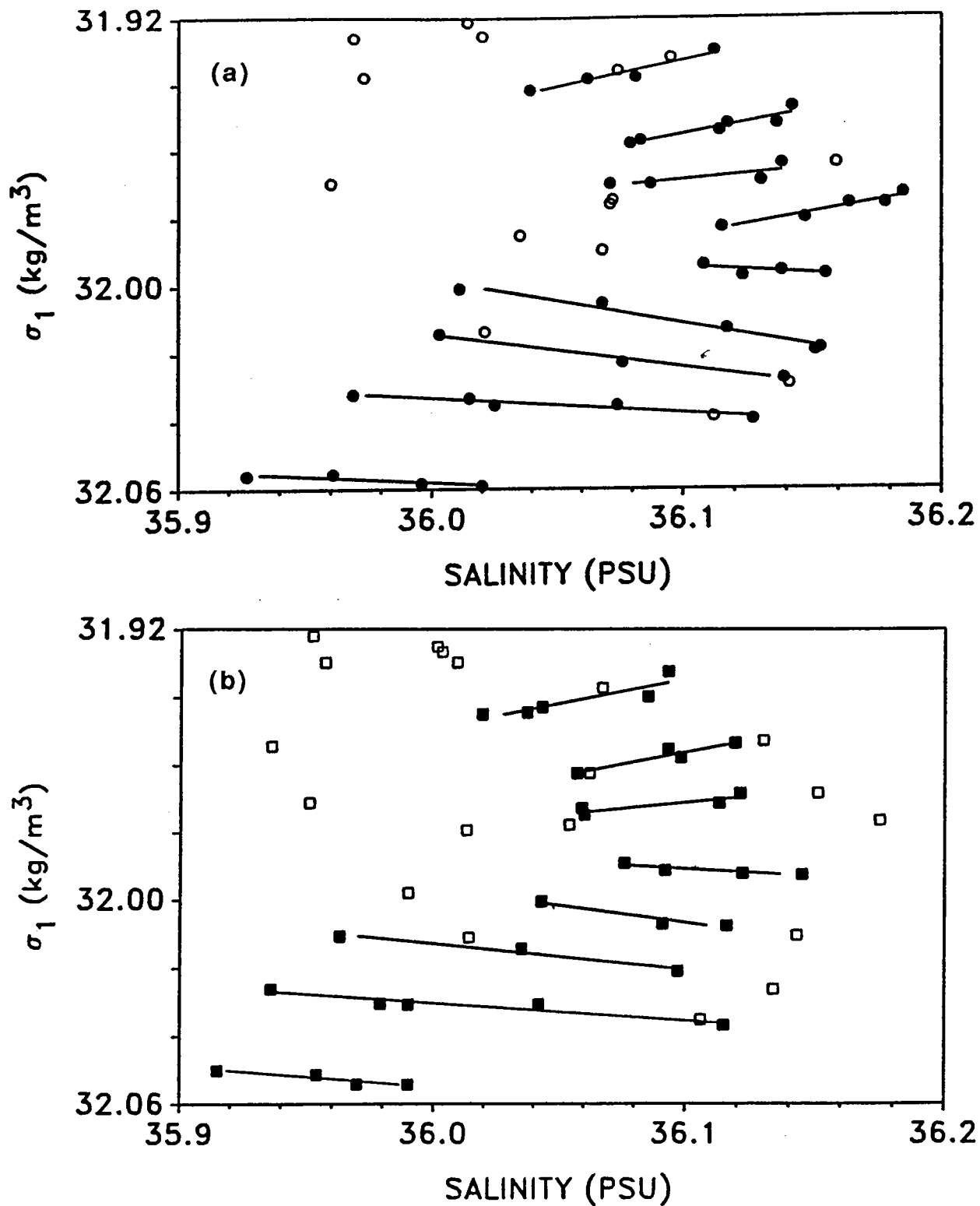
Figure 7. (a) S vs potential density (σ_1) locations of positive extrema from fig. 6. Extrema associated with intrusions of salinity peak-to-peak amplitudes greater than 0.01 PSU are shown as filled circles, and these are used in regressions of S on σ_1, shown as solid lines.

(b) As in (a), but for negative extrema, shown as solid or open squares.

6. Acknowledgements

7. References

Armi, L., D. Hebert, N. Oakey, J. Price, P. Richardson, T. Rossby, B. Ruddick (1988). The movements and decay of a Mediterranean Salt Lens. *Nature*, 333, 649-651.

Armi, L., D. Hebert, N. Oakey, J. Price, P. Richardson, T. Rossby, B. Ruddick (1989). Two years in the life of a Mediterranean Salt Lens. *J. Phys. Oceanogr.* 19, 354-370.

Armi, L., H. Stommel (1983). Four views of a portion of the North Atlantic Subtropical Gyre, *J. Phys. Oceanogr.*, 13, 828-857.

Calman, Jack, 1977. Experiments on high Richardson number instability of a rotating stratified shear flow, *Dyn. Atmos. Oceans*, 1, 277-297.

Gregg, M.C., 1980. Three-dimensional mapping of a small thermohaline intrusion. *J. Phys. Oceanogr.*, 10, 1468-1492.

Hebert, D., 1988. A Mediterranean salt lens, Ph. D. thesis, Dalhousie University, Halifax, N.S.

Hebert, D., 1989. Estimates of Salt finger fluxes. *Deep-Sea Res.*, 35(12), 1887-1901.

Hebert, D., N. Oakey, B. Ruddick, L. Armi, J. Price, P. L. Richardson, and T. Rossby, 1988. C.T.D. Data collected during the survey of a Mediterranean salt lens. Canadian Data report of Hydrography and Ocean Sciences No. 61, Fisheries and Oceans Canada, 379 pp.

Hebert, D., N. Oakey, B. Ruddick, 1989. Evolution of a Mediterranean salt lens, Submitted, *J. Phys. Oceanogr.*

Joyce,T.M., W. Zenk, and J.M. Toole, 1978. An anatomy of the Antarctic polar front in the Drake Passage. *J. Geophys. Res.*, 83, 6093-6113.

McDougall, T. J., 1985a. Double-diffusive interleaving. Part I: Linear stability analysis. *J. Phys. Oceanogr.*, 15, 1532-1541.

McDougall, T. J., 1985b. Double-diffusive interleaving. Part II: Finite-amplitude, steady-state interleaving. *J. Phys. Oceanogr.*, 15, 1542-1556.

McIntyre, M.E., 1970. Diffusive destabilization of the baroclinic circular vortex. *Geophys. Fluid Dyn.*, 3, 321-345.

McIntyre, M.E., 1968. The axisymmetric convective regime for a rigidly bounded rotating annulus. *J. Fluid Mech.* 32, 625-655.

Oakey, N., 1988. Estimates of mixing inferred from temperature and velocity microstructure.*Small-scale Mixing in the Ocean*, Elsevier Oceanography Series, Vol. 46, J.C.J. Nihoul and B. M. Jamart, Eds.

Ruddick, B., 1984. The life of a thermohaline intrusion. *J. Mar. Res.*, 42, 831-852.

Ruddick, B., D. Hebert, 1988. The mixing of Meddy "Sharon". *Small-scale Mixing in the Ocean*, Elsevier Oceanography Series, Vol. 46, pp. 249-262, J.C.J. Nihoul and B. M. Jamart, Eds.

Ruddick, B., Turner, J.S., 1979. The vertical length scale of double-diffusive intrusions. *Deep-Sea Res.*, 26A, 903-913.

Stern, M.E., 1967. Lateral mixing of water masses. *Deep-Sea Res.*, 14, 747-753.

Toole, J.M., and D.T. Georgi, 1981. On the dynamics and effects of double-diffusively driven intrusions. *Prog. Oceanogr.*, 10, 121-145.

Turner, J.S., 1978. Double-diffusive intrusions into a density gradient. *J. Geophys. Res.*, 83, 2887-2901.

THE BEHAVIOR OF DOUBLE DIFFUSIVE INTRUSION IN A ROTATING SYSTEM
APPLICATION TO LABORATORY AND FIELD EXPERIMENTS

J. YOSHIDA
Tokyo University of Fisheries
4-5-7 Konan, Minato-ku, Tokyo 108, Japan

H. NAGASHIMA
Institute of Physical and Chemical Research(RIKEN)
2-1 Hirosawa, Wako-shi, Saitama 351-01, Japan

H. NIINO
Meteorological Research Institute
1-1, Nagamine, Yatabe, Tsukuba, Ibaraki 305, Japan

ABSTRACT

The linear theory of double diffusive intrusion in a rotating system is applied to several laboratory and field data on thermohaline intrusions. The results show that the intrusions are strongly affected by the effect of rotation, and the observed thickness of intrusions agree fairly well with those predicted by the theory.

1 INTRODUCTION

Yoshida, Nagashima and Niino(1989)(hereafter referred as YNN) investigated the effects of earth's rotation on the stability of a thermohaline front of finite width by means of a linear theory. They found that when the rotation is present two different types of unstable modes are possible. When the front is narrow and a Rossby radius of deformation based on Ruddick and Turner's vertical scale(1979) is large compared with the width of the front, the fastest growing intrusion is nearly two-dimensional (non-rotational mode) and it's vertical scale is given by Ruddick and Turner's scale. When the Rossby radius becomes small, in addition to the non-rotational mode, there appears another unstable mode(rotational mode) which has smaller vertical wavenumber than the non-rotational mode. By the introduction of rotation, the fastest growing mode has non-zero along-frontal wavenumber, namely, the intrusion becomes tilted in the along-frontal direction. When the Rossby radius of deformation is sufficiently small

compared with the width of front, transition from the non-rotational mode to the rotational one occurs. The transition from non-rotational to rotational mode becomes less pronounced when the width of front is increased for a fixed horizontal density compensating gradients of temperature and salinity. For a wide front the growth rate and vertical wave number for both modes becomes similar, which agrees with the results of previous studies for infinite front that rotation does not modify the behavior of the intrusion except for the occurrence of along-frontal tilt.

In the present study, we applied our theory to the results of laboratory experiments (Chereskin and Linden(1986)) and field observations (Voorhis, Webb and Millard(1976), Horne(1978), Posmentier and Houghton(1978) and Meddy(Ruddick and Hebert(1988)) data on thermohaline intrusions. We are particularly interested in evaluating the effect of rotation on the intrusions and comparing the observed thicknesses of intrusions with the predicted ones.

2 GOVERNING PARAMETERS

In their linear theory, YNN found that stability of the front is described by the four parameters, Frontal stability parameter $Ra = N^2 d^6 / \kappa_e^2 a^2$, Nondimensional Coriolis parameter $\tilde{f} = f d^2 / \kappa_e$, the Schmidt number $\epsilon = \nu_e / \kappa_e$ and Turner number $\xi = \beta S_z / \alpha T_z$. Where N is the Brunt-Väisälä frequency, κ_e is the vertical eddy diffusion coefficient of salt, a is half width of the front, f is the Coriolis parameter, ν_e is the eddy kinematic viscosity, α and β are the temperature expansion and saline contraction coefficients, respectively and T_z and S_z are vertical temperature and salinity gradient, respectively. In their theory ξ is between 0 and 1, so that the basic stratification supports the salt finger convection. d is proportional to Ruddick and Turner's characteristic vertical length scale

$$d = \frac{g \Delta \rho (1 - \gamma)}{\rho_0 N^2},$$

where, g is the gravitational acceleration, $2\Delta\rho$ is density difference due to horizontal temperature or salinity gradient across the front, γ is the density flux ratio, ρ_0 is a reference density.

The frontal stability parameter Ra gives a criterion on the width of the front. If Ra is decomposed into

$$Ra = \frac{a^4 (d/a)^6 N^2}{\kappa_e^2},$$

one notices that, for a given horizontal gradients of salinity and temperature (i.e., d/a - const), large(small) Ra corresponds to a wide(narrow) front. YNN found that $Ra/\tilde{f}^2 = N^2 d^2 / f^2 a^2$ rather than $\tilde{f}$ itself is useful for describing the effect of rotation

on the intrusions. Note that this parameter corresponds to the stratification parameter(Pedlosky, 1987, p.356) or reciprocal of the internal rotation Froude number. That is, the large(small) value of this parameter corresponds to that the Rossby radius of deformation $\lambda_d = Nd/f$ is large(small) compared with the width of the front, and thus the thermohaline intrusion is in non-rotational(rotational) mode.

Most of the values of these parameters can be estimated from the observed values such as the width of the front, vertical temperature and salinity gradients and so on. However, there are severe difficulties in determining the Schmidt number ϵ. κ_e could be determined from 4/3 power law for vertical salt flux (Stern and Turner(1969)) and horizontal salinity difference across the front (see Niino(1986)). The value of κ_e thus determined ranges from $10^{-3}cm^2/sec$ to $10^{-1}cm^2/sec$. Much less is known about the magnitude of ν_e. If we use molecular value($10^{-2}cm^2/sec$) instead, ϵ may be of $O(10) - O(10^{-1})$. For simplicity, ϵ is taken to be unity in the following analysis. The density flux ratio γ is known to be a function of Turner number ξ (e.g. Schmitt(1979)), and is constant value 0.56 for $\xi < 0.5$(Turner(1967)). From typical POLYGON area data(Fedorov(1978)), ξ is calculated to be 0.15, then γ is taken to be 0.56 in the following analysis.

3 RESULTS AND DISCUSSION

Thermohaline intrusion has been observed both in laboratory and field. For laboratory experiments, double diffusive thermohaline intrusions in a rotating system was investigated by Chereskin and Linden(1986). They produced intrusions by sidewall heating a salinity gradient in a rotating tank, and obtained thicknesses of intrusions. Field observations on thermohaline fronts sometimes reveal the existence of intrusion layers. In some cases, double diffusion is considered to be the driving mechanism. Voorhis, Webb and Millard(1976), Horne(1978) and Posmentier and Houghton(1978) conducted precise CTD observations near Shelf/Slope Water or Slope Water Front regions in the North Atlantic. They discovered frontal intrusion layers and pointed out the possible role of double diffusive mixing on thermohaline intrusions. Recently, small subsurface eddies having large anomaly in properties have found in the Atlantic(McDowell and Rossby 1978). These eddies are considered to be Mediterranean origin, and called as Meddy. The importance of the Meddy for transporting anomalous temperature, salinity and nutrients are discussed by many investigators(e.g. Armi et al. 1989). Ruddick and Hebert(1988) pointed out that thermohaline intrusion are the dominant mechanism for mixing of the Meddy, and discussed the intrusion processes occurred in Meddy in precise detail.

Having estimated the parameters described in section 2 based on above mentioned data, we have used YNN's theory and calculated the growth rate σ_{max}, the vertical wavenumber m_{max} and the along-frontal wavenumber l_{max} of the fastest growing mode for each case. The results are listed in Table.1a(laboratory experiments) and Table.1b(field observations) together with the values of parameters. These results are also plotted on Fig.1(laboratory experiments) and Fig.2(field observations), in which m_{max} are plotted against $Ra/\tilde{f}^2$ for various combination of $\tilde{f}$ and Ra.

For laboratory experiments data(see Fig.1), in all experimental runs, intrusions should be categorized as rotational mode($Ra/\tilde{f}^2 < 1$) and the fronts are relatively narrow($Ra \sim O(10) - O(10^3)$). The predicted vertical wavelength show fairly good agreement with the observed ones, except for two cases where the fronts are extremely narrow.

For field observation data(see Fig.2), intrusions are categorized as rotational mode, but fronts are relatively wide ($Ra \sim O(10^1) - O(10^9)$). We can also see the fairly good agreements between them. But for the Meddy data, there exists a large discrepancy between them. One reason for the occurrence of such discrepancy considered is the difficulties of determining the Schmidt number ϵ. Ruddick and Hebert (1988) pointed out that if the Schmidt number is 40, the vertical scale of the intrusions in the Meddy is well coincided with that predicted by Toole and Georgi's(1981) theory. If we use this value instead, the predicted vertical wavelength becomes 38.7, and is also well coincided with the observed value of 27.3.

4 CONCLUDING REMARKS

The linear theory of double diffusive intrusion in a rotating system is applied to some laboratory and field experiments data on thermohaline intrusion. The results show that such intrusions are strongly affected by the rotation, and the observed thickness of intrusions agree fairly well with the predicted ones. But the estimation of κ_e and ν_e is rather critical in predicting the behavior of double diffusive thermohaline intrusions. As for the Turner number ξ and the density flux ratio γ, recent works(somewhere in this issue) report that these values should be close to unity and hence 0.85 in the North Atlantic frontal region. Further improvement in evaluation of such parameters is needed in future.
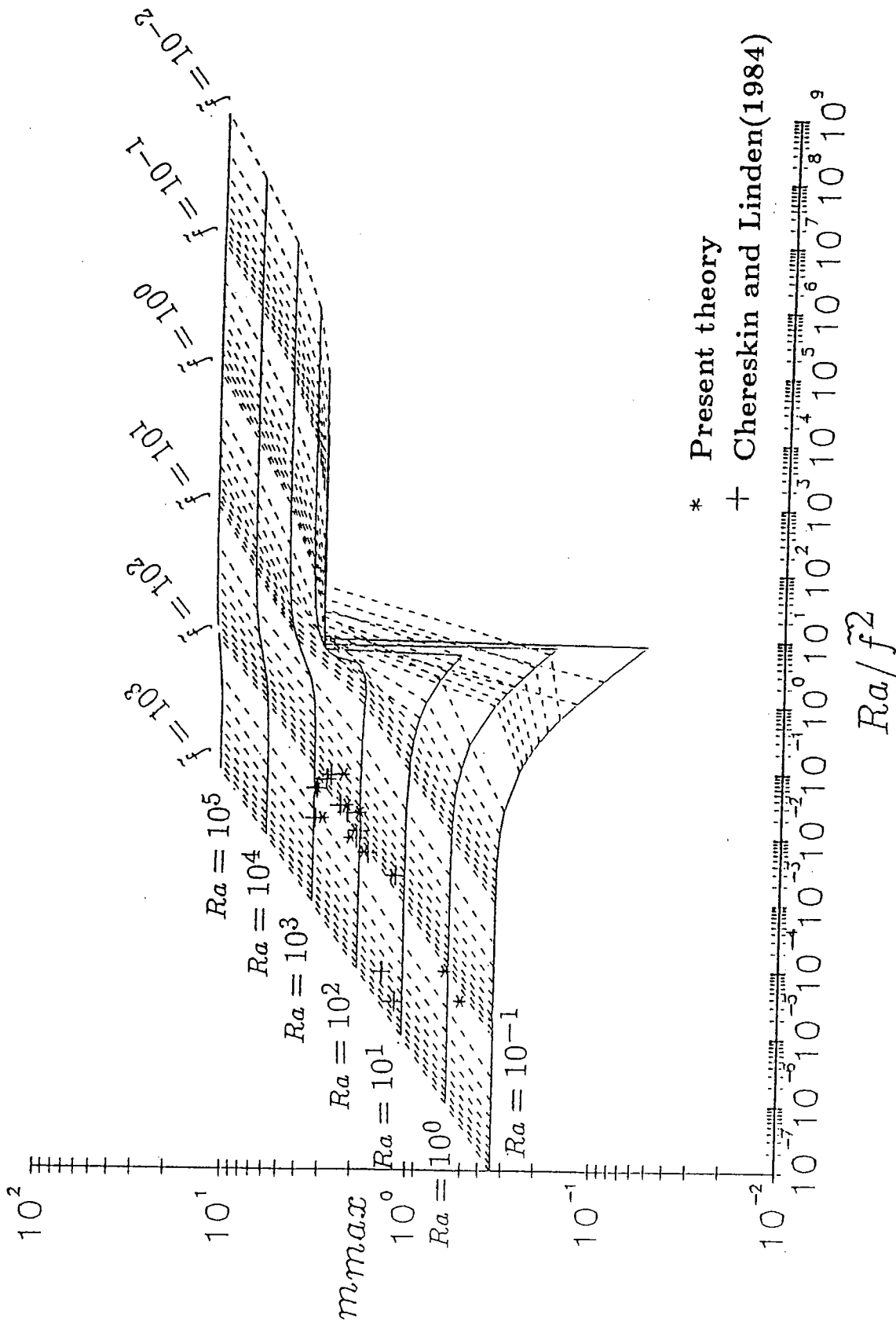
4 ACKNOWLEDGMENT

Table 1a. Comparison with Chereskin and Linden's(1986) experiment. Schmidt number $\epsilon = \nu/\kappa_e = 1$, Turner number $\xi = 0.15$. γ(density flux ratio)=0.56. Half width of the front $a = 10cm$.

$f(s^{-1})$	$N(s^{-1})$	$2\Delta\rho/\rho$	$\kappa_e(cm^2/sec)$	$d(cm)$	$\tilde{f}$	Ra	$\lambda_d(cm)$	$Ra/\tilde{f}^2$	m^*	m	$H^*(cm)$	$H(cm)$	l
0.32	1.31	4.96×10^{-3}	2.73×10^{-3}	0.623	4.55×10^1	1.35×10^2	2.551	6.51×10^{-2}	2.10	2.45	1.86	1.6	4.72
0.41	1.23	5.49×10^{-3}	3.35×10^{-3}	0.782	7.48×10^1	3.08×10^2	2.347	5.51×10^{-2}	2.50	2.59	1.96	1.9	6.20
0.50	1.20	5.61×10^{-3}	3.19×10^{-3}	0.840	1.10×10^2	4.94×10^2	2.016	4.06×10^{-2}	2.90	2.93	1.81	1.8	8.16
0.51	1.16	5.47×10^{-3}	3.34×10^{-3}	0.876	1.17×10^2	5.44×10^2	1.993	3.97×10^{-2}	2.90	2.89	1.90	1.9	8.38
0.51	1.11	3.43×10^{-3}	2.86×10^{-3}	0.600	6.41×10^1	7.02×10^1	1.306	1.71×10^{-2}	1.70	1.98	2.22	1.9	7.62
0.59	1.33	5.39×10^{-3}	3.33×10^{-3}	0.657	7.64×10^1	1.28×10^2	1.481	2.19×10^{-2}	2.00	2.17	2.06	1.9	7.84
0.80	1.18	5.15×10^{-3}	2.93×10^{-3}	0.797	1.73×10^2	4.15×10^2	1.176	1.38×10^{-2}	2.70	2.94	1.85	1.7	13.20
0.90	1.29	5.13×10^{-3}	4.31×10^{-3}	0.665	9.22×10^1	7.72×10^1	0.952	9.07×10^{-3}	1.80	1.67	2.32	2.5	10.76
1.11	1.37	5.87×10^{-3}	4.33×10^{-3}	0.674	1.16×10^2	9.40×10^1	0.832	6.92×10^{-3}	1.90	1.76	2.23	2.4	12.90
1.30	1.39	5.42×10^{-3}	4.39×10^{-3}	0.605	1.08×10^2	4.90×10^1	0.647	4.18×10^{-3}	1.60	1.52	2.38	2.5	14.10
1.61	1.41	4.56×10^{-3}	4.81×10^{-3}	0.494	8.18×10^1	1.26×10^1	0.433	1.87×10^{-3}	1.10	1.07	2.83	2.9	14.80
3.00	1.26	1.46×10^{-3}	1.13×10^{-3}	0.198	1.04×10^2	7.49×10^{-1}	0.083	6.90×10^{-5}	0.56	1.13	2.20	1.1	38.30
4.50	1.31	1.34×10^{-3}	1.10×10^{-3}	0.168	1.15×10^2	3.21×10^{-1}	0.049	2.40×10^{-5}	0.46	1.05	2.29	1.0	53.00

Table 1b. Comparison with field observations. Schmidt number $\epsilon = \nu/\kappa_e = 1$, Turner number $\xi = 0.15$ and γ(density flux ratio) =0.56

	$f(s^{-1})$	$N(s^{-1})$	$2\Delta\rho/\rho$	$\kappa_e(m^2/s)$	$d(m)$	$\tilde{f}$	Ra	$\lambda_d(m)$	$Ra/\tilde{f}^2$	m^*	m	$H^*(m)$	$H(m)$	l	$a(km)$
1	5.68×10^{-5}	3.00×10^{-4}	2.72×10^{-4}	3.0×10^{-5}	1.31×10^2	3.22×10^4	1.37×10^9	6.89×10^3	1.32×10^0	116.4	27.3	7.04	30.0	57.6	6
2	9.35×10^{-5}	1.25×10^{-2}	6.80×10^{-4}	3.1×10^{-4}	1.88×10^1	1.06×10^2	8.84×10^2	2.51×10^3	7.87×10^{-2}	3.4	4.2	34.7	28.0	6.8	9
3	4.00×10^{-3}	1.29×10^{-2}	1.52×10^{-4}	4.2×10^{-5}	3.89×10^0	1.45×10^1	2.09×10^1	1.26×10^3	9.94×10^{-2}	1.2	2.5	19.4	10.0	2.5	4
4	9.35×10^{-3}	1.25×10^{-2}	7.00×10^{-4}	1.2×10^{-4}	1.92×10^1	2.80×10^2	2.08×10^4	2.56×10^3	2.65×10^{-1}	7.2	10.9	16.7	11.0	8.0	5

l :Nondimensional horizontal wavelength(along front)

1. Meddy(1984)
2. Posmentier and Houghton(1978)
3. Horne(1978)
4. Voorhis et al.(1976)

f :Coriolis parameter
N :Brunt-Väisälä frequency
$2\Delta\rho/\rho$:Density difference across front
κ_e :Vertical eddy diffusivity of salt
$d = g\Delta\rho/\rho(1-\gamma)/N^2$:Characteristic vertical length scale
$\tilde{f} = fd^2/\kappa_e$:Non-dimensional Coriolis parameter
$Ra = N^2d^6/\kappa_e^2a^2$:Frontal stability parameter
$\lambda_d = Nd/f$:Rossby radius of deformation
$Ra/\tilde{f}^2 = (\lambda_d/a)^2$
m^* :Non-dimensional vertical wavelength(Theory)
m :Non-dimensional vertical wavelength(Field)
$H^* = 2\pi d/m^*$:Height scale of intrusion(Theory)
$H = 2\pi d/m$:Height scale of intrusion(Field)

Fig.1 Comparison with Chereskin and Linden's(1986) experiment for the predicted and observed vertical wave number m_{max} for the fastest growing mode. m_{max} are plotted as a function of $Ra/\tilde{f}^2$ for $\epsilon = \nu/\kappa_e = 1$ and $\xi = \beta S_z/\alpha T_z = 0.15$. Solid lines show the functional dependence for a fixed value of Ra and dashed lines show that for a fixed value of $\tilde{f}$.

Fig.2 Comparison with field experiments for the predicted and observed vertical wave number m_{max} for the fastest growing mode. m_{max} are plotted as a function of $Ra/\tilde{f}^2$ for the fastest growing mode. m_{max} are plotted as a function of $Ra/\tilde{f}^2 = (\lambda_d/a)^2$ for $\epsilon = \nu/\kappa_e = 1$ and $\xi = \beta S_z/\alpha T_z = 0.15$. Solid lines show the functional dependence for a fixed value of Ra and dashed lines show that for a fixed value of $\tilde{f}$.

4 REFERENCES

Armi, L., D. Hebert, N. Oakey, J. Price, P. Richrdson, T. Rossby and B. Ruddick 1989: Two years in the life of a Mediterranean salt lens. J. Phys. Oceanogr., 19, 354-370.

Chereskin, T.K. and P.F. Linden 1986: The effect of rotation on intrusions produced by heating a salinity gradient. Deep-Sea Res., 33, 305-322.

Fedorov, K.N. 1978: *The Thermohaline finestructure of the ocean.* Oxford, Pergamon Press, 170pp.

Horne, E.P.W. 1978: Interleaving at the subsurface front in the Slope Water off Nova Scotia. J. Geophys. Res., 83, 3659-3671.

McDowell, S.E. and H.T. Rossby 1978: Mediterranean Water. An intense mesoscale eddy off the Bahamas. Science, 202, 1085-1087.

Niino, H. 1986: A linear stability theory of double-diffusive horizontal intrusions in a temperature-salinity front. J. Fluid Mech., 171, 71-100.

Pedlosky, J. 1987: *Geophysical Fluid Dynamics, Second Edition.* Springer-Verlag, 710pp.

Posmentier, E.S. and R.W. Houghton 1978: Fine structure instabilities induced by double diffusion in the Shelf/Slope Water front. J. Geophys. Res., 83, 5135-5138.

Ruddick, B.R. and J.S. Turner 1979: The vertical length scale of double-diffusive intrusions. Deep-Sea Res., 26A, 903-913.

Ruddick, B.R. and D. Hebert 1988: The mixing of Meddy "Sharon". In *Small scale turbulence and mixing in the ocean(eds. C.J. Nihoul and B.M. Jamart).* 249-262 Elsevier.

Schmitt, R.W. 1979: Flux measurements on salt fingers at an interface. J. Mar. Res., 37, 419-436.

Stern, M.E. and J.S. Turner 1969: Salt fingers and convecting layers. Deep-Sea Res., 34, 95-110.

Toole, J.M. and D.T. Georgi 1981: On the dynamics and effects of double-diffusively driven intrusions. Progress in Oceanogr., 10, 123-145.

Turner, J.S. 1967: Salt fingers across a density interface. Deep-Sea Res., 14, 599-611.

Voorhis, A.D., D.C. Webb and R.C. Millard 1976: Current structure and mixing in the shelf/slope water front south of New England. J. Geophys. Res., 81, 3695-3708.

Yoshida, J., H. Nagashima and H. Niino 1989: The behavior of double-diffusive intrusion in a rotating system. J. Geophys., Res., 94, 4923-4938.

THE BEHAVIOR OF DOUBLE DIFFUSIVE GRAVITY CURRENT LABORATORY AND NUMERICAL EXPERIMENTS

H. NAGASHIMA

Institute of Physical and Chemical Research(RIKEN)

2-1 Hirosawa, Wako-shi, Saitama 351-01, Japan

J. YOSHIDA AND M. NAGASAKA

Tokyo University of Fisheries

4-5-7 Konan, Minato-ku, Tokyo 108, Japan

ABSTRACT

The behavior of double diffusive gravity current are investigated both by laboratory and numerical experiments. For laboratory experiment, the behavior of double diffusively induced secondary currents are investigated. We obtained a simple power law for the velocity maximum of the current vs. density ratio. For numerical experiment, double diffusive lock-exchange flow were produced with extremely small density differences. The results shows that initial density anomaly due to salt between the lock-gate have a strong influence on the behavior of current.

1 INTRODUCTION

The behavior of gravity current has been investigated extensively relating to the problem of the waste water discharge near the coast and the meteorological problem, such as the Dust Devil and so on(e.g. Benjamin(1968)). But if the density of the current system is determined by two properties, such as temperature and salt, large differences of the molecular diffusivities between them might cause the vigorous convection under certain circumstances. That is, double diffusive convection. There are very few studies about the behavior of double diffusive gravity current(Thangam and Chen(1981), Maxworthy(1983), McDougall(1984) and Yoshida, Nagashima and Ma(1987)).

The dynamic behavior of double diffusive current has investigated intensively by Maxworthy(1983). By considering force balances, he obtained various relationships between the length of current and time. The interesting point he noticed is that when the surface current was produced by releasing the constant volume of solution on the solution which has different properties, the surface current eventually stops. And also he noticed that when the density difference of two solution is very small, secondary current was induced by the vigorous double diffusive convection, and this secondary current might have influence upon the behavior of

surface main current. Yoshida et al.(1987) conducted double diffusive lock–exchange flow experiment with extremely small density difference, and pointed out the possibility of the existence of the current by the double diffusive convection, even if the density difference is exactly the same.

In the present study, we examine the behavior of double diffusive current both by laboratory and numerical experiments. First, we noticed the double diffusively induced secondary currents which was first noticed by Maxworthy(1983), and conducted the same type of experiments as Maxworthy have done, but with rather smaller density differences. The results are shown in section 2. Second, focused upon the results of Yoshida et al., the behavior of double-diffusive lock exchange flow are examined numerically in section 3.

2 LABORATORY EXPERIMENT

We show the schematic definition of the flow field in Fig.1. In the present study we only consider the case when salt finger convection is occurred at the interface. Then we discharge
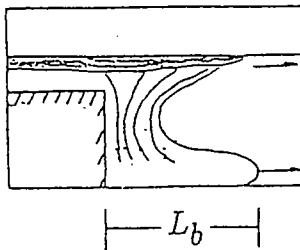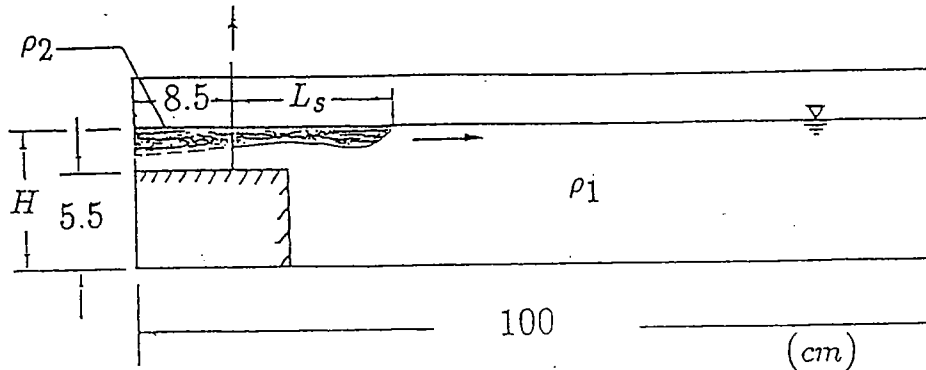
Fig.1 Schematic definition of the flow field. $\rho_1(\text{salt}) = \rho_0(1 + \alpha\Delta T)$. $\rho_2(\text{sugar})=\rho_0(1 + \beta\Delta S)$ (ρ_0 : Reference density, $\alpha\Delta T, \beta\Delta S$: Density anomaly due to salt and sugar), H=Total depth. L_s=:Length of surface current. L_b=:Length of bottom secondary current.

the light sugar water of density $\rho_2 = \rho_0(1 + \beta\Delta S)$ on the slightly heavier salt solution of density $\rho_1 = \rho_0(1 + \alpha\Delta T)$. Here, ρ_0 is reference density, $\beta\Delta S$ and $\alpha\Delta T$ are density anomaly due to sugar and salt, respectively. We changed these density anomalies and total depth H variously and to measure the length of surface and bottom current (L_s and L_b) respectively against time.

In Fig.2, we show the typical example of the flow field. Initially, sugar water is stored in the left reservoir and salt water is stored in the right tank, and barrier is insulted in between. Immediately after the withdrawal of the barrier, ordinary gravity current develops on the surface(Fig.2a). But soon after, salt finger convection develops at the interface(Fig.2b). This
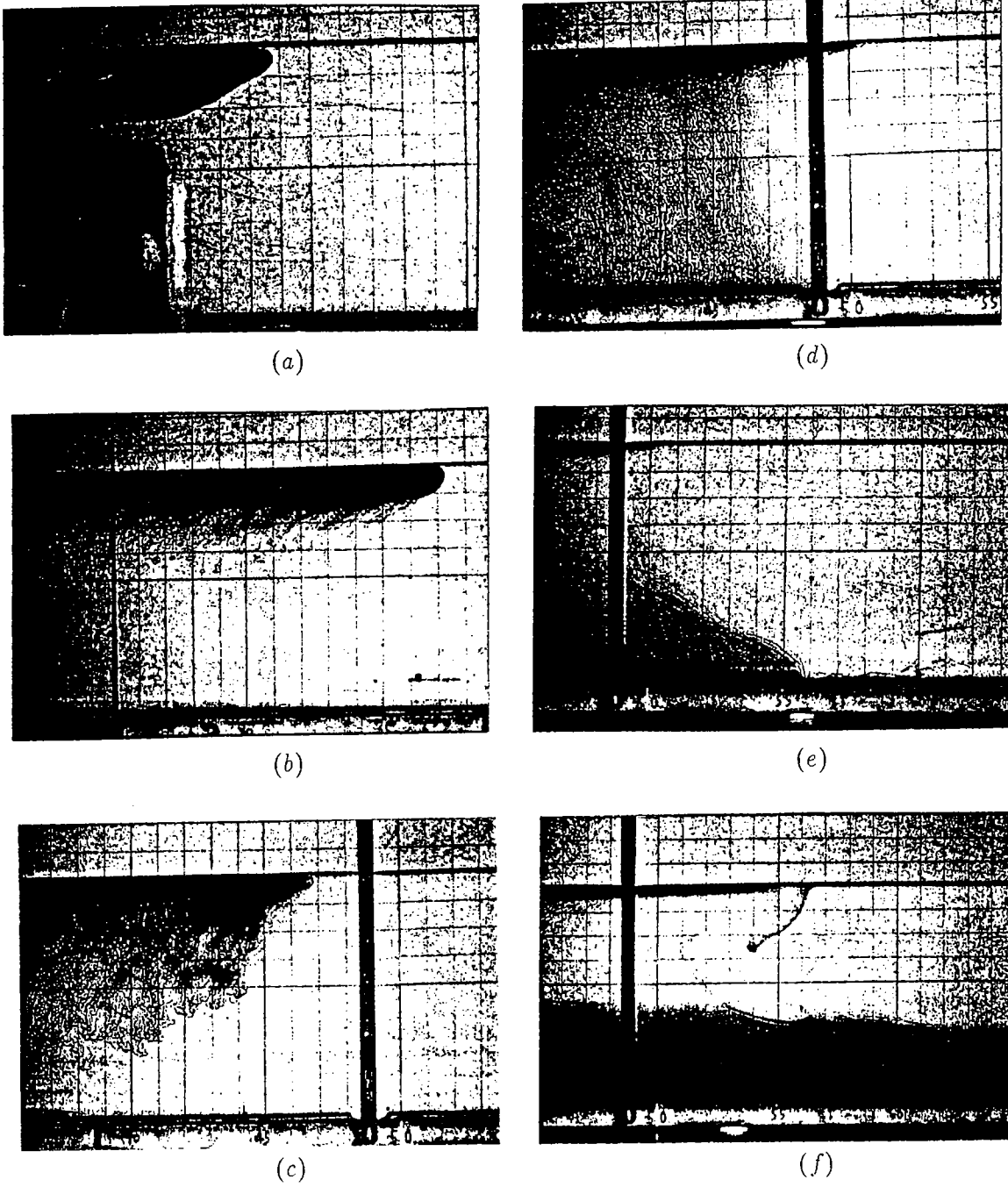
Fig. 2 Sequential flow fields(a-f) of a typical example of double diffusive density current.

salt finger convection develops while surface current keeps advancing, and active convective plume fall down to the bottom of the tank(Fig.2c). As convective motion becomes active, the thickness off the surface current becomes thinner, and some dense fluid are piled on the bottom by falling down plume(Fig.2d). At last, secondary gravity current is formed on the bottom and start to advance. At this time, surface current almost stops(Fig.2e). At later stage the thickness of the bottom current increases and the surface current stays behind, but does not stop any more. Finally, bottom current reaches the end wall and diffusive type interface is formed. Notice that surface current keep on advancing at this stage(fig.2f).

Typical example of the development of surface and bottom current with time are shown in Fig.3a and Fig.3b, respectively. Initially, surface current spreads linearly with time, but gradually decreases its speed and stops. At that time, the formation of the bottom secondary current is completed and current starts to advance. The velocity of this current seems to increase rapidly first and to decrease gradually. It is noted that the surface current does not keep stopping but begins to start again. This is the different phenomena that Maxworthy observed in his experiment.

To focus upon the behavior of secondary current, we plot the velocity of current against time for some cases(Fig.4). We can clearly see that there exists a maximum in the velocity variation with time for each cases. And this velocity maximum(U_{bmax}) becomes large as density difference $\Delta\rho$ becomes small. $\Delta\rho$ is expressed as

$$\Delta\rho = \rho_1 - \rho_2 = \rho_0(\alpha\Delta T - \beta\Delta S) = \rho_0\beta\Delta S(R_\rho - 1) \tag{1}$$

Here, R_ρ is density ratio. It is known that when R_ρ becomes unity, the salt finger convection becomes active and hence vertical transport of T and S becomes large. To notice this, the velocity maximum of the secondary current(U_{bmax}) are plotted against $R_\rho - 1$ in Fig.5. U_{bmax} is normalized by $\sqrt{g^*H}$, where, g^* is reduced gravity defined as $g\Delta\rho/\rho$. It can be seen that normalized maximum velocity becomes large as R_ρ becomes unity, namely as salt finger convection becomes so active. And there exists a simple power law between them, that is, normalized maximum velocity varies as the power of $(-4/5)$ of $R_\rho - 1$.

3 NUMERICAL EXPERIMENT OF DOUBLE DIFFUSIVE LOCK-EXCHANGE FLOW

The results of laboratory experiments in section 2 indicate that the gravity current in double diffusive system are somewhat different from those of a single component case especially when the density difference is very small. Yoshida et al(1987) found that the current velocity for the center lock exchange flow in the double diffusive system is much larger than those in single component case. Moreover, the occurrence of the double diffusively induced currents are suggested even if the density difference approaches zero. In this section, we try to elucidate these findings in the laboratory experiments by using two-dimensional numerical model of the heat(T) and salt(S) system.

(a)

$T(sec)$

$L_s(cm)$

(b)

$T(sec)$

$L_b(cm)$
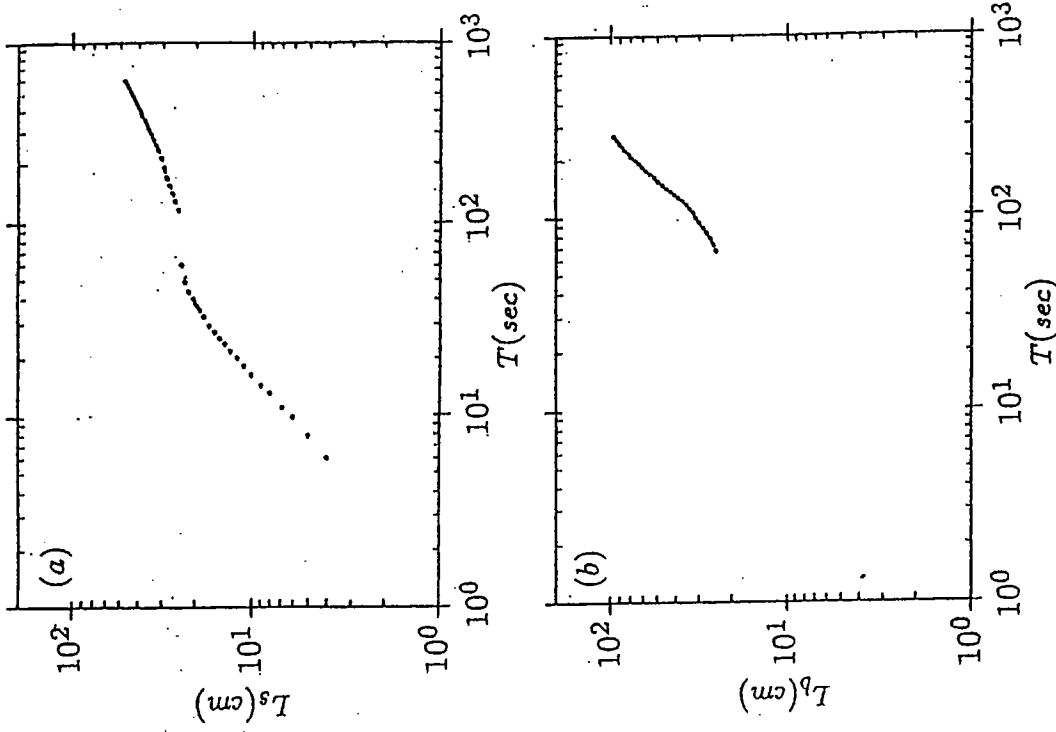
Fig.3 Typical example of time variation of $L_s(a)$ and $L_b(b)$.
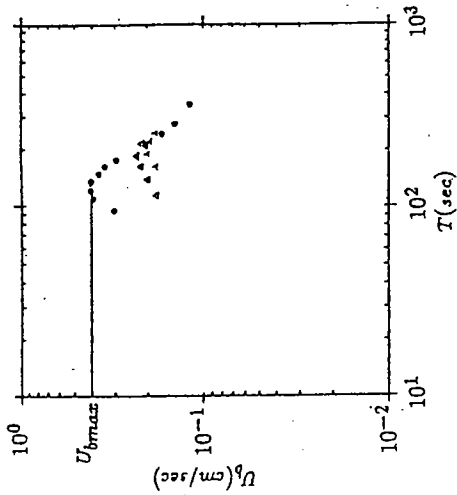
Fig.4 Time variation of secondary current velocity for $\rho_2=1.04253(g/cm^3)$. $\Delta\rho=\rho_1-\rho_2=0.0008(\bullet)$, $0.0024(\triangle)$, $0.0041(\blacktriangle)$. Notice the maximum in the velocity variation.

$U_b(cm/sec)$

U_{bmax}

$T(sec)$

$-4/5$

$R_\rho-1$

$U_{bmax}/\sqrt{(g_*H)}$
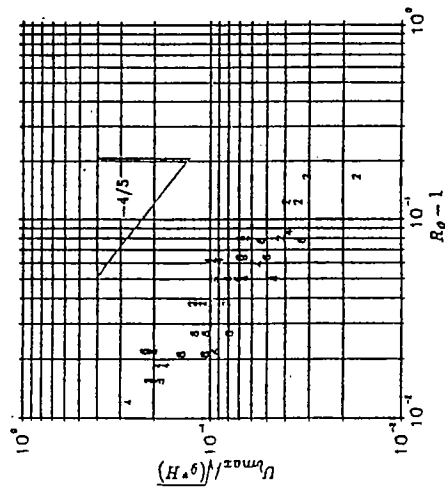
Fig.5 Normalized velocity maximum of secondary current against $R_\rho-1$. Here, $R_\rho=\alpha\Delta T/\beta\Delta S$. $2:\rho_2=1.02008(g/cm^3)$, $4:\rho_2=1.04253(g/cm^3)$, $6:\rho_2=1.06228(g/cm^3)$, $8:\rho_2=1.07667(g/cm^3)$.

The governing equations are as follows:

$$\frac{\partial \xi}{\partial t} + J(\phi, \xi) = g(-\alpha T_x + \beta S_x) + \nu \nabla^2 \xi \qquad (2)$$

$$\frac{\partial T}{\partial t} + u\frac{\partial T}{\partial x} + w\frac{\partial T}{\partial z} = K_T \nabla^2 T \qquad (3)$$

$$\frac{\partial S}{\partial t} + u\frac{\partial S}{\partial x} + w\frac{\partial S}{\partial z} = K_S \nabla^2 S \qquad (4)$$

$$\xi = \frac{\partial u}{\partial z} - \frac{\partial w}{\partial x} = \nabla^2 \phi, \qquad (5)$$

where t is time and x, z are the horizontal and vertical co-ordinate, respectively. u, w represent the velocity components of x and z direction, respectively, J the Jacobian, ξ the vorticity and ϕ the stream function defined by

$$\frac{\partial \phi}{\partial z} = u \qquad , \qquad \frac{\partial \phi}{\partial x} = -w. \qquad (6)$$

ν, K_T and K_S are molecular values of viscosity, heat and salt diffusivities.

We focus on the fingering convection and parameterize the vertical fluxes of heat and salt using Stern's parameterization(Stern 1967). Thus, the equation (2) is reduced to:

$$\frac{\partial T}{\partial t} + u\frac{\partial T}{\partial x} + w\frac{\partial T}{\partial z} = K_T \frac{\partial^2 T}{\partial x^2} + \frac{\beta}{\alpha}\gamma K \frac{\partial^2 S}{\partial z^2}, \qquad (7)$$

where γ represents the density flux ratio, K the vertical eddy diffusivity of salt. Equation sets (2) and (4) to (7) are solved numerically by using the finite difference method.

Schematic view of the model is shown in Fig. 6. The dimension of the model tank is $50cm$ long and $6cm$ deep. Lighter hot-salty water is filled in the left half of the tank, and heavy cold
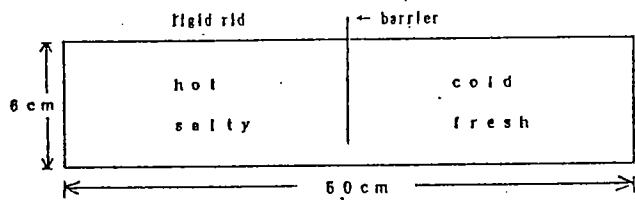
Fig. 6 Schematic view of the model for the lock exchange flow.

fresh water in the right half. The rigid rid surface is assumed. The value of the parameters used here are $K = 10^{-2}cm^2/s, K_T = 10^{-1}cm^2/s, \nu = 10^{-1}cm^2/s, \gamma = 0.56$. We calculate five cases of the initial density difference ($\Delta\rho = 0.004, 0.002, 0.001, 0.0005, 0.0002 g/cm^3$) for different three density anomalies due to salt ($\beta\Delta S = 0.0, 0.0435, 0.1$). Notice that ν, K_T and K_S are taken to be larger in order of magnitude than the usual molecular values. A typical example of numerical calculations is shown in Fig. 7. The behavior of the current shows a triangle shape which is also found in the laboratory experiment(Yoshida et al. 1987). The current speed is almost constant and is larger than that of single component case which is shown in Fig. 8. From these figures, we calculate the advancing speed of the salt head. The results are summarized in Fig. 9. As clearly shown in this figure, the double diffusive effect
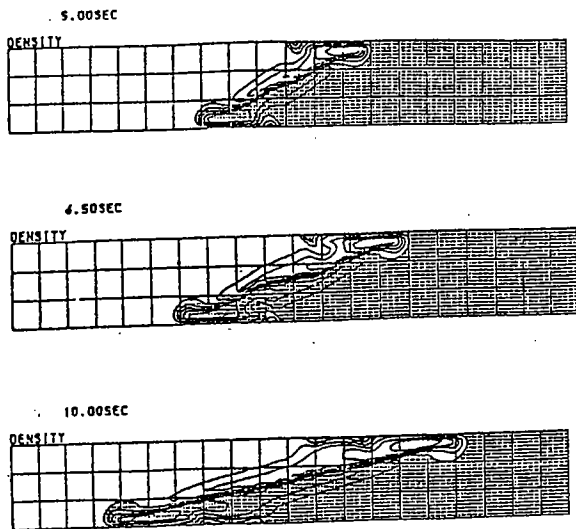
Fig. 7   A typical flow pattern of the
lock exchange flow.
$\Delta\rho = 0.002(g/cm^3), \beta\Delta S = 0.1$
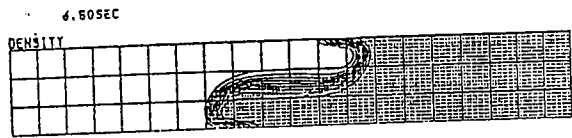
Fig. 8   A flow pattern of a single componet
case. Numerical condition is the
same as that of the middle of Fig. 7.
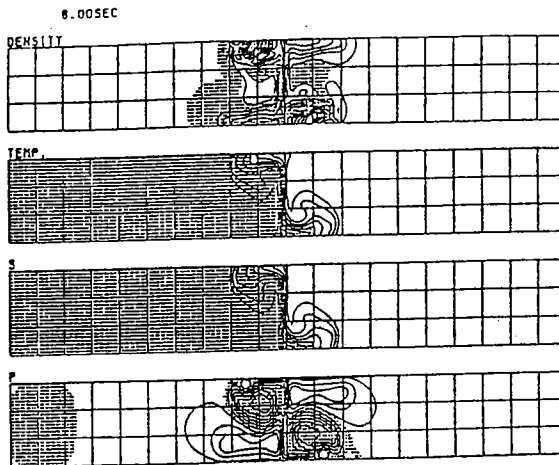
Fig. 10
A flow pattern when the initial
density difference is exactly
equal to zero. From top to
bottom, density, temperature,
salinity and flow fields are
shown.
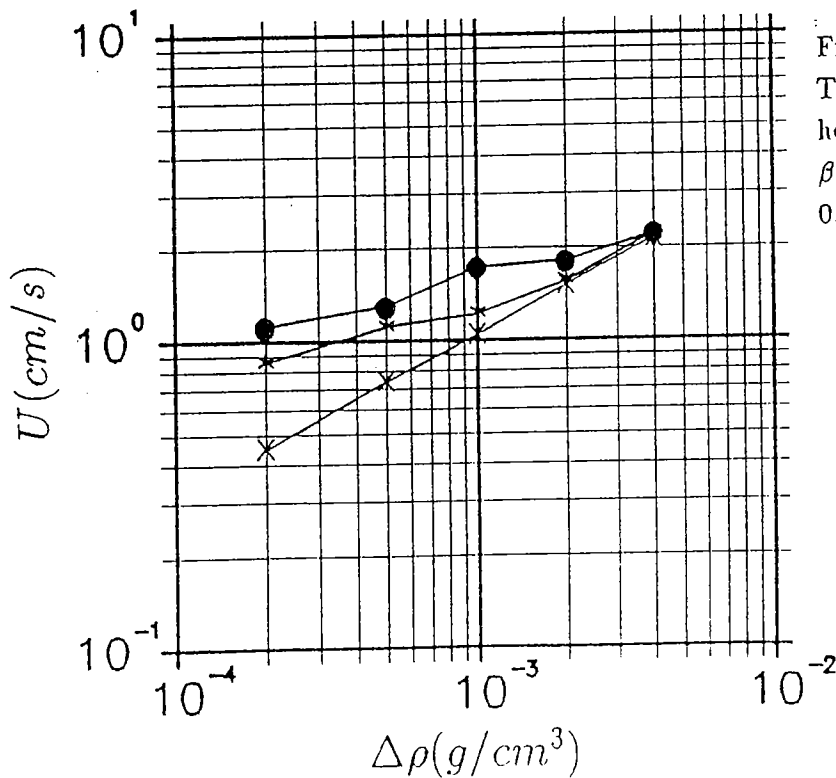
Fig. 9
The current speed of the salt
head for various $\Delta\rho$.
$\beta\Delta S$ is 0.1($\bullet$),
0.0435($*$) and 0.0($\times$).

make faster the current speed, and the larger the $\beta\Delta S$ is, the faster the current speed is. Fig. 10 is the case when $\Delta\rho$ is exactly equal to zero. The result shows that the double diffusive effect induce the density anomaly and the occurrence of the current is clearly found.

4 SUMMARY

The behavior of double diffusively induced secondary currents are investigated in laboratory experiments by discharging the sugar solution on the surface of heavier salt solution. The advancing speed of surface decreases with time and eventually current stops, but restart again after a while. The behavior of surface current is strongly affected by the secondary current which is induced by the active salt fingering convection from the surface current. There exists a maximum of the current velocity. It is found that the maximum velocity is proportional to $(-4/5)$ power of $R_\rho - 1$. The meaning of this power is rather ambiguous, however, we are now examining the meaning of this relation more precisely by numerical experiment.

The behavior of double diffusive lock-exchange flow is investigated numerically. The results shows that initial density anomaly due to salt($\beta\Delta S$) between the lock-gate have a strong influence on the behavior of current. The larger $\beta\Delta S$ is, the faster the current speed becomes. Moreover, double diffusive convection induce the current even if the density difference between the lock-gate is exactly zero. All results obtained here support quantitatively the conclusion of the laboratory experiments in Yoshida et al.(1987)

5 REFERENCES

Maxworthy, T. 1983: Dynamics of double diffusive gravity current. J. Fluid Mech., 128, 259-282.

McDougall, T.J. 1984: A model of frictionless double-diffusive gravity current on a horizontal surface. Geophys. Astrophys. Fluid Dyn., 21,

Stern, M.E. 1967: Lateral mixing of water masses. Deep-Sea Res., 14, 747-753.

Thangam, S. and C.F. Chen 1981: Salt-finger convection in the surface discharge of heated saline jets. Geophys. Astrophys. Fluid Dyn., 18, 111-146.

Yoshida, J., H. Nagashima and Wen-Ju Ma 1987: A doubled-diffusive lock exchange flow with small-density difference. Fluid Dyn. Res., 2, 205-215.

Plans for a Tracer Release Experiment
in the Eastern Subtropical North Atlantic

James R. Ledwell

Lamont-Doherty Geological Observatory of Columbia University
Palisades NY 10964

Preface

My main purpose in presenting this paper was to inform the double diffusion community of plans for a mixing experiment to take place in a low density ratio regime in 1992. Hence, the text that follows is the overview of a proposal that was submitted to the U.S. National Science Foundation in June, 1989. The funding status of this proposal is uncertain at the time of this writing, but indications are positive that there will indeed be such an experiment as scheduled. The results of a prototype experiment in Santa Monica Basin are described in Ledwell et al. (1986), and in Ledwell and Watson (1989). Further discussion of tracer release experiments, their motivation, overall strategy, and mechanics can be found in the other publications listed below.

Ledwell, J.R., A.W. Watson., and W.S. Broecker, 1986: A deliberate tracer experiment in Santa Monica Basin. *Nature, 323,* 322-324.

Ledwell, J.R., and A.J. Watson, 1988: The use of deliberately injected tracers for the study of diapycnal mixing in the ocean, from J.C.J. Nihoul and B.M. Jamart, eds., *Small scale turbulence and mixing in the ocean,* pp. 517-528, Elsevier, Amsterdam.

Ledwell, J.R., 1988: Mixing experiments. U.S. WOCE Planning Rep. No. 8, 35 pp., U.S. Planning Office for WOCE, College Station, TX.

Ledwell, J.R., 1989: A strategy for open ocean mixing experiments, from P. Muller and Diane Henderson, eds., *Parameterization of Small-Scale Mixing Processes,* Proc. Hawaiian Winter Workshop, pp. 157-164, Hawaii Inst. Geophys., U. of Hawaii, Manoa.

Ledwell, J. R., and A. J. Watson, 1989: The Santa Monica Basin Tracer Experiment: A study of diapycnal and isopycnal mixing. submitted to *J. Geophys. Res.*

Watson, A.J., and J.R. Ledwell, 1988: Purposefully released tracers, *Phil. Trans. R. Soc. Lond. A, 325,* 189-200.

NORTH ATLANTIC TRACER RELEASE EXPERIMENT: AN OVERVIEW

by James R. Ledwell

with contributions from:
Eric Kunze, James F. Price, Rolf G. Lueck,
Barry R. Ruddick, and Raymond W. Schmitt

INTRODUCTION

This package of proposals is for a direct study of diapycnal and isopycnal mixing in the main pycnocline of the North Atlantic. The idea of the experiment is to release a conservative tracer and a cluster of neutrally buoyant floats as near as possible to an isopycnal surface, and to measure their dispersion over the subsequent year. The float work will be proposed by J. Price and P. Richardson later this year (see Appendix A). Larger scale characteristics of the environment in which the mixing takes place will be monitored from the floats, from research vessels, and from moorings, both as part of this experiment and as part of the Subduction Experiment to be funded as an Accelerated Research Initiative by the Office of Naval Research (ONR). Techniques to obtain long time series of relevant finestructure from Richardson number (RiNo) floats and fine structure and microstructure from a mooring will be tried at the same time as the tracer release experiment.

The experiment will begin in the spring of 1992 in the eastern subtropical North Atlantic. Sampling of the tracer will be performed immediately after the injection, again in the fall of 1992, and finally in the spring of 1993. Thus, the tracer data will yield the diapycnal diffusivity for a summer period and a winter period. The floats will be tracked daily and thus will yield full trajectories for lateral mixing studies. Two RiNo floats will be deployed for both periods, with a recovery and redeployment during the middle tracer survey. These will yield time series of temperature gradients, salinity gradients, and shear on 1 to 5 meter vertical scale for tracks in the tracer patch for virtually the whole period. The fine- and microstructure mooring will be set in the region of the patch, and will be recovered and reset during the middle survey. It will yield temperature gradients and shears on a 5 m scale and will be a pilot attempt to obtain long time series of temperature variance and turbulent kinetic energy dissipation rates for the duration of the experiment.

The Mixing Experiment and the Subduction Experiment will be coordinated with one another for mutual benefit. A float listening array will be set up to serve both experiments simultaneously, and float manpower, logistic, and analysis resources can be combined for the two experiments. Large scale hydrographic and tracer surveys encompassing the site of the Mixing Experiment will be conducted as part of the Subduction Experiment. In particular, a full survey is planned for summer 1992, which will provide the setting on a 1000 km scale for our experiment. An array of surface moorings to measure air-sea fluxes will be maintained around the mixing experiment site for the duration of the subduction experiment, thus providing unique information on the wind forcing accompanying the mixing we observe.

We expect other U.S. scientists to ultimately propose studies of fine structure and microstructure during the experiment. Michael Gregg, of the University of Washington, plans to propose surveys with expendable current profilers during the sampling cruises to test a relation between fine scale shear and diapycnal mixing (Appendix C). Russ Davis of Scripps Institution of Oceanography and Gregg are examining the feasibility of mounting temperature microstructure probes on floats which cycle up and down through the water column. Such devices could give long time series of temperature variance dissipation rates along tracks in the patch. Ray Schmitt of WHOI plans to propose a more extensive site survey than we have included here prior to the experiment (Appendix D). He would use a free falling profiler to provide finestructure and microstructure data as well as CTD data. He and Gregg plan to propose one or more other site surveys using profilers during the experiment. Rolf Lueck may propose to measure microstructure using a towed body during the sampling surveys as well. These proposals will be submitted to the NSF or ONR Physical Oceanography Programs. The projects will enhance the experiment in that they embody different techniques to determine the diapycnal diffusion of density and heat to be compared with the diffusivity measured by the tracer.

Strong contributions to the experiment are expected from the international community. Andrew Watson of the Plymouth Marine Laboratory (PML) of the United Kingdom, and several of the PML staff, have been given a mandate to participate in the tracer release experiment. Watson will request at least 2 months use of a British research vessel for the experiment. Barry Ruddick of Dalhousie University and Neil Oakey of Bedford Institute of Oceanography have proposed to the National Science and Engineering Research Council of Canada (NSERC) to perform microstructure studies and CTD surveys with a profiler during the experiment, and to deploy a mooring which will provide a time series of the shear and the internal wave spectrum at a location within the tracer patch (Appendix B). Their mooring activity could be combined with Lueck's if both proposals are successful.

BACKGROUND AND GOALS

Diapycnal mixing has long played a central role in the oceanographer's view of the structure of the thermocline, of the deep ocean circulation, and of the flux of nutrients to the euphotic zone. The maintenance of the density struc- ture in the ocean interior is governed by a balance between upwelling and diffusion (e.g., Munk, 1966). The vertical upwelling which drives the abyssal circulation through the vorticity balance in the theory of Stommel and Arons (1960) implies a convergence of downward buoyancy flux, at least in places where isopycnal surfaces do not diverge toward the poles. Gargett (1984) has pointed out that the direction of the deep interior flow inferred from a Stommel-Arons balance can depend sensitively on how the diapycnal diffusivity varies with depth. Numerical modellers of the ocean circulation have often claimed that correct parameterization of the diapycnal diffusivity is impor- tant to their success. Bryan (1987) has shown that the meridional heat flux in a primitive equation ocean circulation model is sensitive to the value chosen for the diapycnal diffusivity.

In addition to these issues of circulation, the biological productivity of oligotrophic surface waters in the open ocean may well be limited by the

diapycnal transport of nutrients into the euphotic zone. Furthermore, the distribution of chemical species in the ocean is affected directly by the mixing, by the circulation driven by the mixing, and by the biology possibly fed by the mixing. Thus, the circulation, the biology, and the chemistry of the ocean can depend heavily on the diffusivities of heat, salt and passive tracers, and how they vary with depth. The interaction of the ocean with the atmosphere and biosphere in determining the earth's climate must then also depend on the diffusivities within the ocean.

Attempts made to measure diapycnal diffusivities for the ocean interior were summarized by Gargett (1984). The uncertainty remaining is enormous. It is fair to say that we do not know the order of magnitude of diapycnal diffusivities for most situations, let alone how they vary with environmental parameters, or under what circumstances the diffusivities for heat, salt, and passive tracers are the same, and when they differ. The situation is such that one good measurement in any representative ocean environment would advance our knowledge enormously.

The primary goal of the present experiment is to obtain a measure of the diapycnal diffusivity at one level in the pycnocline of the eastern subtropical North Atlanitc, for both a summer and a winter period. A longer term goal is to determine the physical processes governing the observed mixing, so that the results can be generalized to other systems. The program will therefore develop methods of long time-series measurements of fine structure and microstructure from which diapycnal diffusivities may be inferred, ultimately without the necessity of a tracer release.

Perhaps an explantion of this last point is in order. This project may be the first of a series of experiments to begin to explore the dependencies of the diffusivities on environmental parameters, especially those parameters that are likely to be the products of global observation programs and numerical models of the ocean circulation. The list of independent parameters that might govern diapycnal mixing in the ocean interior may be quite long. It is unlikely that it will be possible to explore the full parameter space with tracer release experiments alone in the next generation, because the technique is labor and ship-time intensive. It may also be that the diffusivity for the tracer differs from those for heat and salt. This is why we must continue to hypothesize and theorize about the physics governing the mixing, and why we must try to develop relatively inexpensive measurements from which diffusivities can be estimated via these theories.

This first experiment is a pilot experiment in a technically easy site where we can command the resources needed for a high chance of success. Granted that, it is of interest to look forward to how this experiment will fit as the first of a series of mixing experiments. The most important feature of the site in the context of diapycnal mixing is the low density ratio, R_ρ, defined as the ratio of the contribution of the temperature gradient to the negative of the contribution of the salinity gradient to the stability:

$$R_\rho = \alpha(\partial T/\partial z + \Gamma)/\{\beta \; \partial S/\partial z\}$$

where α is the thermal expansion coefficient, Γ is the adiabatic temperature gradient, and β is the derivative of density with respect to salinity.

Diapycnal diffusivities, especially that of salt, are expected to be enhanced by salt fingering for $R_\rho < 2.0$, a regime which prevails at our prospective site. In this respect the site is representative of the upper pycnocline of much of the world oceans outside of the North Pacific.

The diffusivity of the tracer should be close to that of salt, since their molecular diffusivities are similar, so the tracer release will give a good estimate of the salt diffusivity. On the other hand, one of the products of the measurements from the microstructure mooring will be an estimate of the diffusivity for heat, and both the mooring and the RiNo floats will give estimates of what the diffusivity of heat and salt would be if salt fingering were negligible. If the heat diffusivity appears much less than the tracer diffusivity, we will suspect enhancement from salt fingering.

However, since this is a pilot experiment for all of the techniques, and since it has yet to be demonstrated that the tracer and microstructure techniques will agree under any circumstances, this suspicion would have to be confirmed. For this reason, the next logical experiment to perform would be at a site which is similar to the North Atlantic site, except that it is stable with respect to salt fingering. The upper pycnocline of the North Pacific, below the salinity minimum, is the most likely prospect, and will probably be proposed as the second mixing experiment within the WOCE program. The two experiments should be viewed as a pair, and the question of whether the diffusivities of salt and nutrients are enhanced at the North Atlantic site should not be expected to be fully answered until both experiments are completed.

SITE SELECTION

The experiment will take place in the eastern North Atlantic between 20°N and 30°N, and most probably between 20°W and 30°W. The depth will be around 300 m, near the $\sigma_\theta = 26.8$ surface. We were led to these choices by both scientific and practical considerations. The participation in the experiment by Andrew Watson and the Plymouth Marine Laboratory, and the likelihood of obtaining ship time from the United Kingdom will be much greater for the North Atlantic than for any other ocean in the early 1990's. The presence of the Subduction Experiment in the Canary Basin at the same time as our experiment means that the WHOI float group, and the float listening array will be able to support both experiments efficiently. The Subduction Experiment and the Mixing Experiment will also reinforce one another through mooring deployments and hydrographic surveys, and ultimately through analysis efforts, if the Mixing Experiment is embedded within the area of the Subduction Experiment.

The specific site and depth of the experiment will be chosen with the following factors in mind:

1.) The overall diameter of the tracer patch anticipated after one year should not be larger than roughly 500 km, so the patch can be well sampled;

2.) The isopycnal surface of the tracer release must slope less than 100 m in 1000 km so that the mean vertical shear is low, and so that the RiNo floats, and other isobaric floats that may be proposed, will stay with the patch;

3.) Large scale salinity gradients on the target isopycnal surface must not be so large as to create more than a 50 m departure of an isothermal float from the target isopycnal surface over the path of the patch;

4.) The density ratio should be less than 2.0 so that the experiment will examine the low density ratio regime for study of salt fingering effects and for later comparison with a diffusively stable regime;

5.) Lateral T/S intrusions must be sufficiently rare and weak that the temperature variance dissipation can be interpreted in terms of diapycnal heat diffusivity.

These criteria are met well in the 10° x 10° region mentioned above, and also in the 10° x 10° region to the west, which was roughly the region of the Beta-Triangle experiment (Armi and Stommel, 1983). In fact, previous WOCE planning documents have mentioned the Beta-Triangle region as the likely site for the experiment (e.g., Ledwell, 1988). However, the advantages of working in the region of the Subduction Experiment are clear, and should be pursued if feasible.

The Subduction Experiment is still in the proposal stage, but one tentative mooring array is shown in Fig. 1. The moorings would be deployed for 2 years starting in the spring of 1991, and would be serviced approximately every 8 months. The mooring cruise in summer of 1992 would also be a hydrographic survey of the area defined by the moorings. A sensible site for the mixing experiment would be within the southern half of this array. We have indicated a tentative release spot at 26.5°N, 22°W in Fig. 1. The prevailing currents are believed to be around 1 cm/s to the south or southwest at this site (e.g., Thiele, 1986); and the lateral mesoscale eddy diffusivity in the upper pycno-cline in the general region has been estimated to be between 500 and 2000 m^2/s (Armi and Stommel, 1983; Jenkins, 1987; Thiele, 1986; Bauer and Siedler, 1988). With these estimates of mean advection and lateral diffusion, one would predict the tracer patch to drift into the center of the southern triangle in Fig. 1 after about 6 months and to fill the southern portion of this triangle after one year. The lateral extent of the patch would not be too large to sample with a month of ship time.

The density ratio on the σ_θ = 26.75 surface, calculated from the data of Levitus (1982) by R. Schmitt (personal communication) is shown in Fig. 2, where the tentative release site is again indicated. Given the anticipated velocities and diffusion, the tracer patch will most likely remain within the region of R_ρ = 1.8 contour for the duration of the experiment. Preliminary examination of CTD casts from the transect at 24°N during Atlantis Cruise 109 and the transect along the axis of the Canary Basin during Oceanus Cruise 202 indicate that the other criteria listed above will be met between 22°N and 28°N, and between σ_θ = 26.7 and 26.9, i.e., between about 250 and 350 m deep, in the region of the Subduction Experiment. Data presented by Bauer and Siedler (1988) also show that pressure and salinity variations on these density surfaces at 27°W in the same latitude range, and at 27.5°N right across the region, are well within the specified limits.

Figure 3 shows a typical CTD profile from the near the center of the region we expect the patch to occupy. It is clear from the CTD data that the density ratio typically increases to values at or above 2.0 more than 50 m below this

level. On the other hand, even lower density ratios can be obtained by going higher. The disadvantages of this though, are that the variations of pressure and salinity on isopycnal surfaces increase, and lateral spreading is likely to increase. On the other hand, advantages of a shallower depth are that the experiment would be more directly relevant to nutrient fluxes, tow speeds would be greater, and accessibility to ship-based acoustic doppler current profiling (ADCP) would be greater. Existing hydrographic data will have to be studied further and all these considerations weighed in the coming year before making a final decision on the site and depth.

EXPERIMENTAL PLAN

The purpose of this section is to give an overview of operations for the four components of the experiment, especially as they affect ship use. For details about the field activities and the techniques to be employed for each component, please see the individual proposals.

A site survey, float and tracer release, and mooring setting will be performed in late spring, 1992, with two cruises of about 3 weeks duration each (see Table 1 for a cruise schedule). The injection and initial sampling of the tracer patch must be performed from different ships to avoid contamination of the tracer sampling and analysis systems. The injection ship will carry the tracking floats as well as the injection equipment. The sampling ship, carrying the microstructure mooring and the RiNo floats, will arrive on site during the injection, and personnel will be transferred at sea between the two ships at the end of the injection phase. The minimum schedule to accomplish the work proposed in this package is shown in Table 2. The schedule for both ships can be lengthened to accomodate additional projects. The ships being requested for the operations are R/V Oceanus and either the RRS Darwin or RRS Discovery.

Site survey

A 5 day site survey will be performed prior to the injection by the injection ship. A 150 km square region, centered on the prospective site, will be sampled with a square grid spacing of 30 km (Fig. 4). The purpose of this survey is to provide the hydrographic setting of the injection on the eddy scale and to help chose the ultimate site of the release. The specific site for the release may be changed on the basis of this survey, if the original one is perturbed by a strong eddy, or T/S intrusion. A sixth day will be spent surveying the final site to characterize it well.

This is the minimum survey required to avoid performing the release in an awkward spot, such as in a strong eddy. Ray Schmitt plans to propose at a later date a more extensive site survey of a 500 km square area which would require a separate cruise of approximately 3 weeks duration just prior to the injection cruise (Appendix D). He would use the WHOI High Resolution Profiler (Schmitt et al., 1988) as an enhanced CTD, thus obtaining a survey of the small scale physics in the region of the experiment just before injection, including temperature variance and kinetic energy dissipation rates, and fine scale Richardson number, density ratio and overturn statistics. Such a cruise would also give a survey of the full mesoscale environment of the mixing experiment, from which it will be possible to make independent estimates of

mixing parameters from conventional hydrographic data. This will enhance the mixing experiment as a test of more conventional techniques.

Float System

   Fifteen SOFAR floats will be deployed with the tracer to track the patch and to measure lateral mixing parameters for the site. These floats will be tracked by an array of moored listening stations which will be deployed as part of the Subduction Experiment. However, since real time tracking is crucial to the tracer experiment, the injection and sampling ships will be equipped with deep hydrophones for shipboard listening, and 3 freely drifting tracking buoys will be deployed during the cruises. The floats, which are called Bobbers, are a modified version of SOFAR floats, having active ballasting to home within 0.02°C (less than 2 m in the mean gradient) of the temperature of the target isopycnal surface. They will cycle once per day to measure the layer thickness between 2 preset temperatures, about 25 m above and below the target surface. These gradient data may substantially reduce the uncertainty in the diapycnal diffusivity by keeping track of convergence of water into the area of the patch.

   The floats will also be equipped with an high frequency beacon (10 - 12 kHz) to track the floats from the ship with an accuracy of 100 m or so during the initial stages of the tracer injection and sampling. (The accuracy achievable with the SOFAR system is limited to about 5 km.) It will be worth while to recover the floats at the end of the Mixing Experiment, since the sampling ship will be in their vicinity, since the floats are relatively expensive, and since after one year of use they will still have at least a year of useful life left. The high frequency beacon will expedite their rapid recovery. Since tracking of the tracer patch is so crucial to this experiment, a backup system of simple isobaric floats that would pop up and relay their positions via satellite at the time of the sampling surveys is also proposed.

Deployment, Sampling, and Recovery Operations

   Tracer and Float Release. A series of 6 streaks will be injected in a 20 km square box pattern, as shown in Fig. 5, and the Bobber floats will be released along the tracks. Ten days are required for this phase.

   Background sampling, Microstructure Mooring and RiNo float deployment. About 5 days into the injection phase, the sampling ship will arrive to sample the background level of SF_6 in the general area surrounding the tracer patch (Fig. 4). During this survey, the microstructure mooring will be deployed in the release area. When the background survey is completed, the sampling ship will enter the area of the injection and release the RiNo floats, having performed temperature calibrations and ballasting adjustments. Subsequent to deployment, several CTD casts will be performed near the floats for in situ calibration. Five days of ship time will be required for the background survey, mooring deployment, and RiNo deployment.

   Personnel Transfer. The injection and the RiNo deployments will end at about the same time, after which personnel will be exchanged between the two ships. Tracer and float people will go over to the sampling ship to carry out the initial sampling cruise, while mooring people, RiNo people, and extra hands can board the injection ship and return to port.

Initial sampling. The locations of the Bobber floats, available once or twice a day, will guide the sampling ship to document the initial distribution of the tracer. A vertical array of integrating samplers will be towed through the patch, as located by the float positions. This sampling phase will last 8 days, during which we plan to perform at least 25 sampling tows for a total path length of at least 150 km, which should be enough to cover the patch.

Middle Sampling Cruise. A second sampling cruise will be carried out in October, 1992, guided by the float positions. An overall continuous sampling track length of 1500 km can be achieved with the integrating samplers in 28 days. This should be sufficient to sample the tracer patch well. The RiNo floats and the microstructure mooring will be recovered, serviced, and redeployed during this cruise. The length of this cruise will be about 35 days.

Final Sampling Cruise. The final survey will be performed in late spring, 1993. An overall sampling track length of 3000 km, this time with about 50% gaps, will be executed to obtain the wider coverage needed at this time. The RiNo float, the microstructure mooring, and as many of the Bobber floats as is economical, will be recovered in the course of sampling the patch. At 6 hours per float, plus the mooring, recovery will take 5 ship days. The length of this cruise will be about 42 days, perhaps on Darwin or Discovery.

PLANNING AND COORDINATION

The coordination of the experiment will be led by J. Ledwell, with continual input from the other participants. As much as possible will be done by telecommunications, but meetings will be held each winter for the following purposes:

1.) plan the core of the Mixing Experiment, proposed here;
2.) coordinate the Mixing Experiment with the Subduction Experiment;
3.) coordinate with international components;
4.) coordinate new U.S. components;
5.) facilitate data sharing and analysis, and publish results;
6.) consider the next mixing experiment.

The meeting in 1990 will start with about 15 participants, but we anticipate that the number of participants will naturally increase to about 25 by 1994. The length of the meetings will also grow, from 3 days initially to 5 days in the last two years, when there will be data to discuss, as well as plans to make. The most convenient place to have the meetings would be in Cambridge, Mass., as this is a short trip for the many participants at Woods Hole, Lamont, Baltimore, and Halifax, and an equally long trip from the west coast and the United Kingdom. Funding for the meetings is requested in the Lamont proposal.

REFERENCES

Armi, L., and H. Stommel, 1983: Four views of a portion of the North Atlantic Subtropical Gyre. *J. Phys. Oceanogr.*, *13*, 828-857.

Bauer, E., and G. Siedler, 1988: The relative contributions of advection and isopycnal and diapycnal mixing below the subtropical salinity maximum. *Deep-Sea Res.*, *35*, 811-837.

Bryan, F., 1986: Parameter sensitivity of primitive equation ocean general circulation models. J. Phys. oceanogr., 17, 970-985.

Gargett, A. E., 1984: Vertical eddy diffusivity in the ocean interior, *J. Mar. Res.*, *42*, 359-393.

Gregg, M. C., 1987: Diapycnal mixing in the thermocline: A review, *J. Geophys. Res.*, *92*, 5249-5286.

Jenkins, W. J., 1987: ^{3}H and ^{3}He in the beta triangle: Observations of gyre ventilation and oxygen utilization rates. *J. Phys. Oceanogr.*, *17*, 763-783.

Ledwell, J.R., 1988: Mixing experiments. U.S. WOCE Planning Rep. No. 8, 35 pp., U.S. Planning Office for WOCE, College Station, TX.

Levitus, S., 1982: *Cimatological Atlas of the World Ocean.* NOAA Professional Paper 13, Superintendent of Documents, U.S. Government Printing Office, Washington DC.

Munk, W.H., 1966: Abyssal recipes. *Deep-Sea Res.*, *13*, 707-730.

Schmitt, R.W., J.M. Toole, L. Koehler, C. Mellinger and K.W. Doherty, 1988: The development of a fine- and microstructure profiler. *J. Atm. Ocean. Tech.*, *5*, 484-500.

Stommel, H., and A.B. Arons, 1960: On the abyssal circulation of the world ocean - II. An idealized model of the circulation pattern and amplitude in oceanic basins. *Deep-Sea Res.*, *6*, 217-233.

Thiele, G., W. Roether, P. Schlosser, R. Kuntz, G. Siedler, and L. Stramma, 1986: Baroclinic flow and transient tracer fields in the Canary-Cape Verde Basin. *J. Phys. Oceanogr.*, *16*, 827-837.

U.S. WOCE Implementation Plan, 1989: U.S. WOCE Implementation Report No. 1, 176 pp., U.S. WOCE Office, College Station, TX.

Table 1. Cruise Calendar

Time	Activity	No. of Days
Summer 1990	Tests	5
Summer 1991	Tests	5
May-June, 1992	Survey, Injection, Bobber release	23
May-June, 1992	Deploy RiNo & Mooring, First Sampling	21
Oct., 1992	Middle sampling, recover mooring, redeploy RiNo	35
May-June, 1993	Final sampling, Bobber & RiNo recovery	42

Table 2. Cruise Schedule for Injection Cruise and First Sampling Cruise

day	Injection Ship	Sampling Ship
1	Transit	
2		
3		
4	Site survey	
5		
6		
7		
8		
9		
10	Injection and Bobber Release	Sampling Ship
11		Transit
12		
13		
14		Background survey & Set mooring
15		
16		
17		RiNo float
18		
19		
20	Transfer	Transfer
21	Transit	Sample
22		
23		
24		
25		
26		
27		
28		
29		Transit
30		
31		

Fig. 1. Prospective site for tracer and float release. The mooring
positions shown represent the tentative plan for the Subduction
Experiment (still in proposal stage). These moorings would be deployed
from the spring of 1991 until the spring of 1993. A release site has
been tentatively chosen at 26.5°N, 22°W, about 150 km north of the
southern Air-Sea Flux mooring to be deployed by WHOI as part of the
Subduction Experiment. The depth of the release would be about 300 m,
at the σ_θ = 26.8 surface. The mean velocity at this site is believed to
be about 1.0 cm/s to the south or southwest. At this speed, the center
of mass of the patch would be at the mooring after about 6 months.
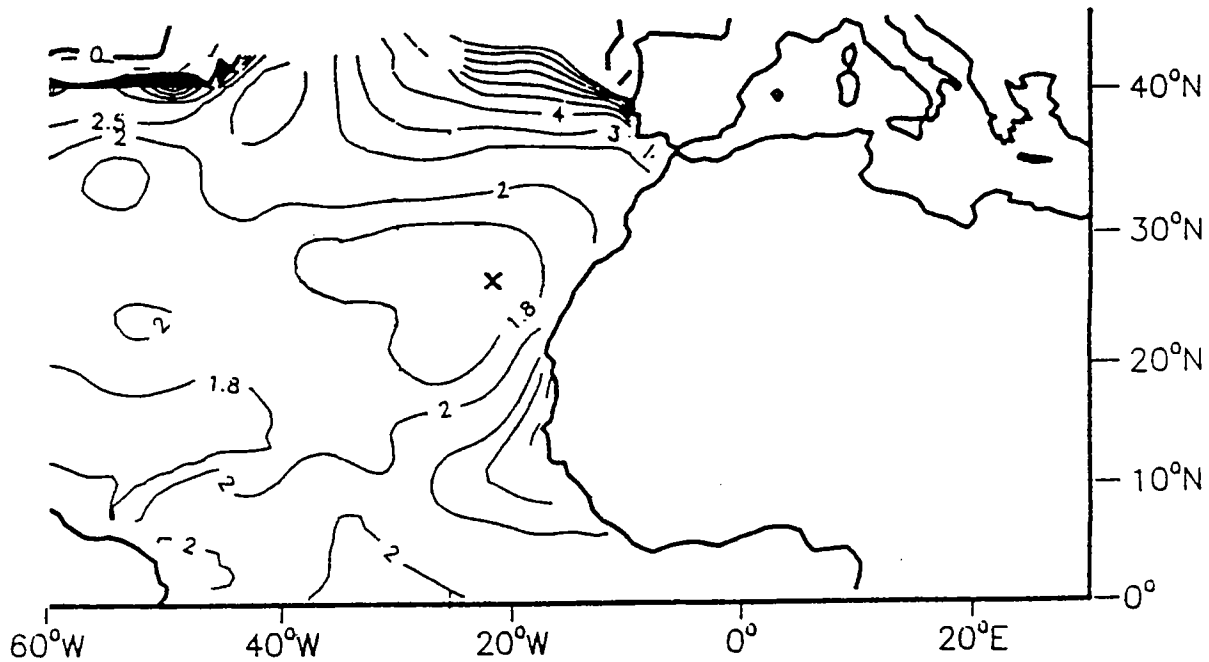
Fig. 2. Contours of the density ratio on the $\sigma_\theta = 26.75$ surface for the North Atlantic, calculated from the data of Levitus (1982). Salt fingering is expected at values below 2.0. The site indicated in Fig. 1 for the tracer release is shown as a cross, within the $R_\rho = 1.8$ contour. This figure was adapted from one provided by R. Schmitt, of WHOI.
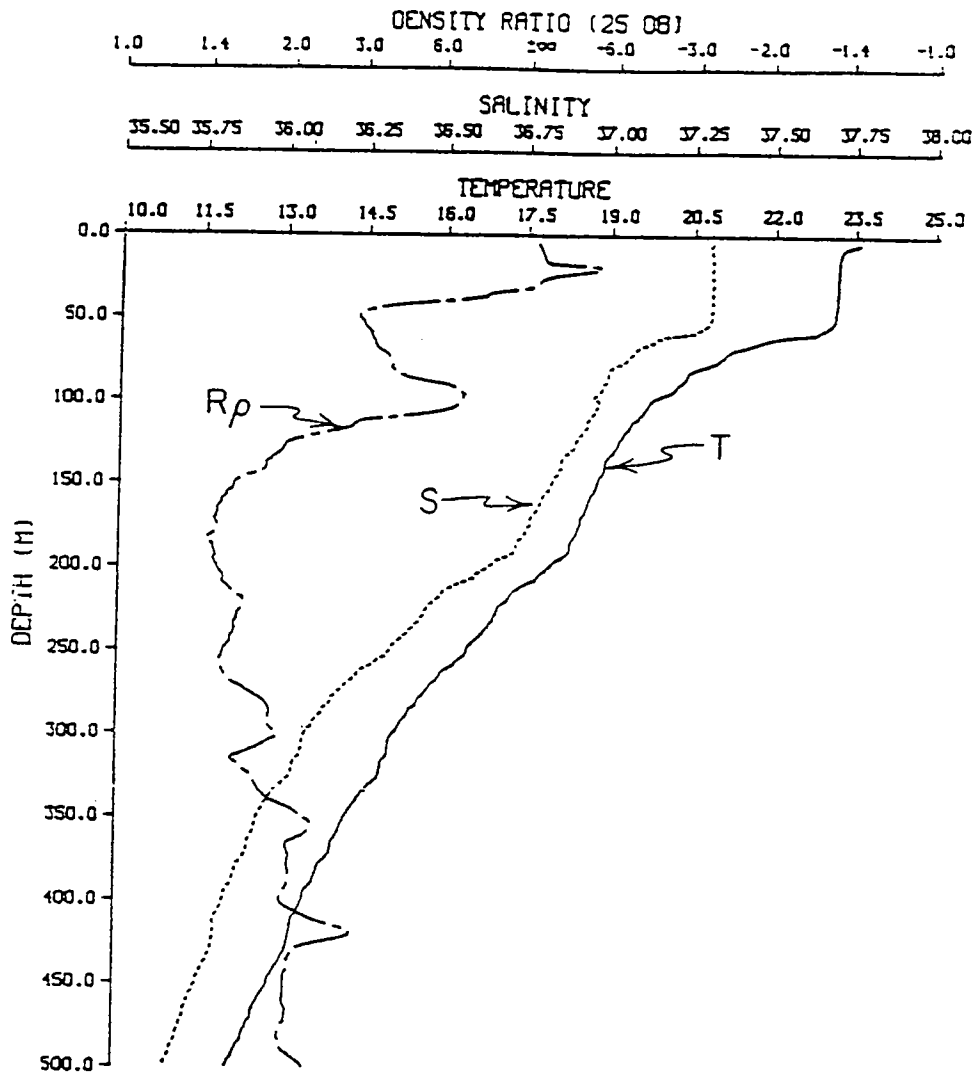
AT109 ST165 24.5N 24.3W

Fig. 3. Profiles of potential temperature, salinity, and density ratio for the station shown in Fig. 2. The level of the σ_θ = 26.8 surface, the prospective release level, is at about 300 m depth. The density ratio, calculated from 25 dbar gradients, in the neighborhood of the level is around 1.9. This figure was provided by R. Schmitt, WHOI, and is from Atlantis Cruise 109.

```
├30km┤
```


O CTD

● CTD+SF$_6$ BACKGROUND

✕ MOORING

┌ ┐
└ ┘ RELEASE SITE
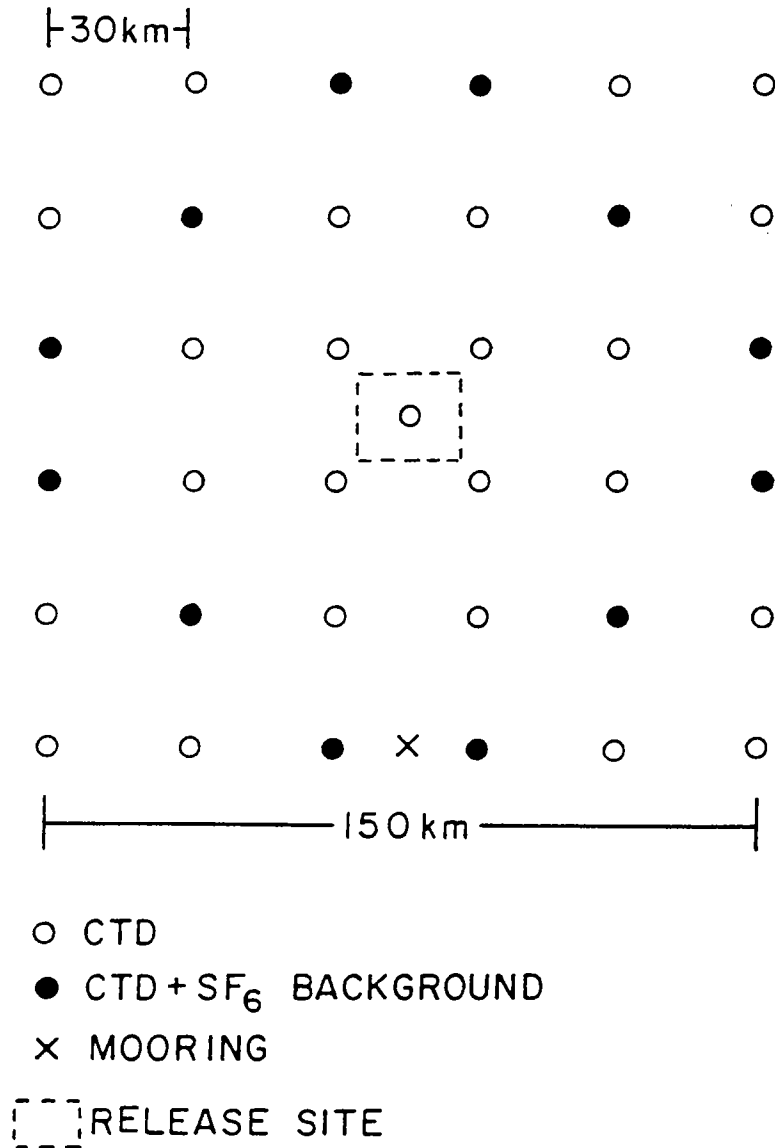
Fig. 4. Site survey plan. This survey would be performed in a "radiator pattern" by the injection ship just prior to the injection cruise. It would be centered on the prospective injection site. A 10-km resolution survey would be performed in the grid box finally chosen as the release site. During the injection operation, the sampling ship would reoccupy stations around the border of the survey area to measure background tracer concentrations, and the microstructure mooring would be deployed on the southern border of the area.

Fig. 5. Release plan. The tracer would be injected in 3 streaks to
create a 20 km x 20 km initial patch. The Bobber floats and RiNo floats
would be interspersed with the tracer injection, and the RiNo floats
would be released from the sampling ship.

Research Prospects in Oceanic Double Diffusion

The following sections on salt fingers, diffusive convection and intrusions represent summaries of topics raised during three discussion sessions at the meeting.

SALT FINGERS

Evidence for the occurrence of salt fingers can be found in a wide variety of situations: the dramatic staircases of C-SALT, the thermohaline intrusions found in all oceans, and the subtle near-surface salt fountains reported by Osborn. Since vast regions of the Central Waters may support fingering (95% of the upper kilometer of the Atlantic at 24°N is finger favorable), and the differing heat and salt transports have first order effects on thermocline structure, advancing our understanding of this ubiquitous mixing process is mandatory for the improvement of ocean models.

A variety of observational, experimental and modeling opportunities can be readily identified. If we separate these by scale, we can discuss research problems in each area.

Microstructure

One of the important outcomes of C-SALT was the realization that small dissipation rates (ϵ) are not indicative of weak mixing as is the case in stratified turbulence. That is, relatively high vertical diffusivities can be obtained because the dissipation is a small term in the energy budget compared to the potential energy exchange between the salt and heat fields. Additional problems may arise from the techniques used to estimate the dissipation within an interface. Because fingers are driven by very small-scale salt anomalies, the spectrum of the horizontal shear of the vertical velocity carries more energy at higher wavenumbers than the temperature gradient spectrum. This is completely opposite ordinary turbulence and we must be concerned that probe resolution and data analysis techniques are capable of taking proper account of the difference. Progress has been made in using spectral slope and kurtosis characteristics of temperature microstructure to distinguish salt fingers from turbulence. It would also be helpful to develop sensors for the measurement of the salinity dissipation spectrum. The structure seen by the C-SALT optical shadowgraph was roughly an order of magnitude smaller than that sensed by the temperature probes; small-scale salinity variations are the probable cause. Fiber optic refractometers may have the potential to make measurements of the smallest scales of salt variation. This is important because quite often it is the salt (or tracer) diffusivity that is of primary concern. The ability to accurately monitor temperature and salinity dissipation spectra would be very valuable in distinguishing turbulence from double diffusion. Such techniques may also be applicable to a broader range of platforms, since scalar measurements are not as vibration sensitive as shear probes. Development of acoustic or optical holographic instruments or dye techniques would be helpful in visualizing the morphology

of microstructure. Indeed, simply utilizing existing shadowgraph technology in a variety of oceanic environments would be a worthwhile contribution.

Laboratory experiments on salt fingers can still provide much useful information, as evidenced by the recent work of John Taylor. Studies of how fingers interact with shear would be particularly valuable in light of the apparent disparity between the shadowgraph observations from C-SALT and the original laboratory work of Linden (1974). There continues to be a need to establish fluxes across salt finger interfaces at low density ratio. The earlier "run-down" experiments were certainly affected to a significant degree by time dependence. Can a steady finger interface be realized using porous plates or osmotic membranes at the top and bottom of the tank to establish constant fluxes and constant T and S differences? In addition, laboratory experiments could help us to understand how internal waves interact with a salt finger interface. The varying interface thickness seen in C-SALT suggests that the interfaces are local wave guides. Is there coupling between those waves and convection in the layers?

Analytic and numerical modeling will continue to provide valuable insight to salt finger dynamics. Two dimensional numerical simulations have recently enhanced our understanding of finger spectra and the flux ratio as well as finger splitting and merging (Shen). Yet to be accomplished is the simulation of a steady finger interface interacting with adjacent deep convecting layers. This presents a formidable computational challenge, especially at realistic Prandtl and Lewis numbers, because of the difficulty of resolving the smallest scales of salinity variation. Three dimensional simulations are even more demanding of computer resources, and it is likely to be some years before problems involving the multiscale interaction of fingers with convecting layers can be attacked numerically. Analytic models which utilize stability arguments (Kunze) will continue to be helpful.

Finestructure

Many mysteries remain with regard to the most prominent form of salt-finger induced finestructure, the thermohaline staircase. As yet we have no convincing theories for the scale of the layers, how they are formed and maintained in the presence of internal waves and how they maintain lateral coherence over great distances in the presence of eddy stirring. There is evidence that the internal wave field is suppressed in the steps (Gregg, 1989) — how does this occur? The horizontal changes in layer properties are occasionally concentrated at intrusive fronts — do these intrusions help to maintain the lateral coherence? What are the sizes and structure of the intrusions? Do other staircases display lateral coherence and property changes like the C-SALT steps?

In raising such questions we must consider whether we have adequate observational tools. Obviously, much more could be done with existing profiling technology; the amount of data obtained within staircases is still quite small. Conventional CTD surveys can

certainly be of help, but it is also clear that modern towed chains (Marmorino, Mack) and Sea Soar/Batfish type instruments can provide increased resolution and/or greater survey speed. Neutrally buoyant floats, especially those equipped with instrumentation to measure local density and velocity gradients (the RiNo of Kunze, Williams and Briscoe, 1990) could be valuable in developing an understanding of the temporal evolution of steps. The step systems have a unique saw tooth structure in the vertical profile of sound speed with multiple local minima. This must have dramatic effects on horizontal sound propagation. Can acoustic propagation characteristics be used as a staircase monitoring tool? The tracer release techniques of Ledwell are also of great potential for establishing the mixing rate in a staircase. In fact, since the layers are so well defined and mixing rates expected to be high, fluorescent dyes could work well in relatively short term deployments. Monitoring the spread of a tracer or dye from layer to layer would be an unambiguous measure of mixing rate, not dependent on specific models for interpretation.

In addition to furthering our understanding of the staircases in low density ratio regions, we must address the problem of widespread fingering in the Central Waters. There is good evidence that a modest background field of salt fingers is nearly always present. It is modulated by internal wave strains and inertial wave shears; both can vary the intensity of the local vertical salt gradient (Schmitt et al, 1989). Given their high duty cycle and high efficiency and rapid growth after turbulence (Taylor), fingers could easily be as important or more important a mixing agent as shear instability (with low duty cycle and low efficiency) over vast regions of the main thermocline (Schmitt, 1990). One very promising approach to this problem is the tracer release experiment planned for the North Atlantic (Ledwell). The spread of the tracer itself will indicate the rate of mixing, and the fine- and microstructure measurements to be obtained from moorings, floats and profilers will be key to distinguishing the relative contributions of fingers and shear instability. Also useful (though challenging) would be theoretical and modeling studies of a stratified fluid with both salt fingers and internal waves present. Towed chains of microstructure sensors could provide a means of sampling significant portions of the main thermocline for the signatures of salt fingers. It is not unreasonable to consider surveying wide areas of the Central Waters with towed instrumentation for the detection of salt fingers.

Large scale

Many interesting questions arise with regard to larger scale ocean structure once the possibility of unequal heat and salt mixing rates is considered. Fingers transport salt at a greater rate than heat. Unless it is compensated for by differential advection or particular surface fluxes, this has the direct effect of increasing the slope of the $T - S$ relation, or increasing R_ρ. In the Central Waters R_ρ is remarkably constant; is it ventilation or shear which balances the finger flux in maintaining the R_ρ structure? (Schmitt, 1990). Parameterizations of salt finger mixing must be incorporated into large scale numerical models in order to develop a realistic thermohaline circulation. In situations where the

finger flux is dominant, the resulting unstable buoyancy flux can drive dynamical effects (Posmentier and Kirwan, 1985). Very little has been done to develop an understanding of how double diffusion affects oceanic thermohaline structure and global scale heat and freshwater cycles, issues raised years ago by Stern (1969, 1975). For instance, salt fingers may help to explain how the subtropical thermocline remains stable despite significant regions of unstable buoyancy flux due to evaporation (Schmitt, Bogden and Dorman, 1989).

Discussion Session on Diffusive Thermohaline Convection

Barry Ruddick
Department of Oceanography
Dalhousie University
Halifax, N.S., B3H 4J1, Canada

The science session on diffusive convection was rather small, with only three speakers. Joe Fernando described laboratory experiments on mixing and entrainment in a diffusive stratification heated from below. He modelled the process by assuming that at high Rayleigh numbers (based on layer thickness), the thickness of the layers is determined by a balance between vertical kinetic energy of the turbulent eddies and the potential energy of the stratification. Joe claims that the parameterization obtained on this basis gives good agreement with oceanic data. Ruby Krishnamurty described some extremely careful and lengthy experiments in which thermal and saline boundary conditions were imposed at the top and bottom of a small tank, slowly altered until a single finite-amplitude convection cell was established, and then reduced below the (linear) critical values to see at what point the convection stopped. Laurie Padman showed us observations of thermohaline layering in the Arctic, which appear to agree well with predictions from analytical and laboratory models. He showed us evidence that internal wave interactions with the staircase structure can be important in setting coherence scales for layers, and enhancing vertical fluxes. These presentations are summarised in more detail in this volume.

The basic questions for double-diffusing oceanographers revolve around predicting the fluxes in a given situation, and in knowing how the fluxes will change as environmental parameters change. Paradoxically, I think there has been less work in this area because we have an increased understanding of the role of diffusive convection in the ocean:

•We now have an empirical understanding of diffusive fluxes in situations where layering is observable, since the laboratory formulae for diffusive interface fluxes have been verified in-situ over a broad range of density ratios (Larson and Gregg, 1983, Osborn, 1988, Padman and Dillon, 1987). In addition, there are two current theoretical models of the diffusive interface available to be comparatively tested against available observations: Kelley, 1989, and Fernando, 1989a,b.

•The dependence of the diffusive flux on ΔS and ΔT can be recast as a dependence on layer thickness H and large-scale gradients. Thus we could parameterize the flux in terms of large-scale properties if only we could parameterize H in such terms. We have an empirical understanding of the thickness of convecting layers due to the dimensional reasoning and comparison with observations put forth by Kelley (1984). In this important paper, Kelley postulated that H is a function of buoyancy frequency N, density ratio R_ρ, and fluid properties viscosity v, thermal conductivity κ_T, and saline conductivity κ_S. He then found that, in situations where layers were observed, the diffusive layer thickness scales as $(v/N)^{1/2}$ with primary dependence on the density ratio: $H(N/v)^{1/2} = G(R_\rho)$. While Fedorov (1988) reported very close agreement between his layer-scale data and Kelley's G-scaling, Muench, Fernando and Stegen (1989) concluded that it failed in parts of a staircase in the Weddell Sea. A more detailed study of the applicability of the scaling is now clearly in order. Are there specific conditions under which the Kelley scaling fails? How is the scaling affected by background shear or turbulence? Presumably the inverse Froude number or ε/vN^2 are relevant additional dimensionless parameters.

The laboratory formulae have led to small flux estimates in most situations, and the rather pessimistic view that layers are only observed when nothing else is going on (i.e., when other process which might disrupt or dominate the layering are absent). But this leads to an important set of questions which demand that we understand the interactions between diffusive convection and the other small-scale oceanic processes: turbulence, shear, and internal waves. A zero-order hypothesis which could be tested by quantitative laboratory experiments is: "turbulent fluxes are not altered by the presence of double-diffusive stratification, even for low intensity ($\varepsilon/\nu N^2 < 15$) turbulence". Some more qualitative questions which come to mind are:

- Are layers of the thickness predicted by Kelley's (1984) $G(R_\rho)$ curve always observed? When no layers are observed, why not? Does the lack of layers mean that fluxes are greater or less than the formulation proposed by Kelley?
- What is required to form layers from a smooth gradient? Imposed fluxes? Lowered density ratio? Shear? Internal waves? Lateral T-S gradients? Which processes are most effective in forming layers?
- How are previously formed layers and the diffusive fluxes affected by shear, turbulence, or internal waves?

Interaction of internal waves and steady shear with double-diffusive convection seems to be a topic ripe for exploration. Laurie Padman described a first-order model for the interaction of internal waves with the density finestructure of diffusive layering, in which the wave energy fluxes (energy and momentum) are strongly decreased by the dissipation in the convecting layers. The energy exchange from the wave field to the turbulent convection can drive increased turbulent mixing, and lead to a change in sign of the buoyancy flux. Mike Gregg and Tom Sanford's observations of internal wave shear in C-SALT (this volume) showed decreased wave energy levels inside the layered region compared with the outside. Mike also recalled an experiment described by Steve Hurdis at the 1983 Santa Barbara conference on double diffusion, in which a varicose interfacial internal wave was found to undergo greatly enhanced dissipation in the presence of salt fingering. Ruddick (1985) described an experiment in which a standing interfacial internal wave was allowed to decay. Enhanced wave decay was found for both fingering and diffusive sense stratifications, falsely attributed to interfacial stress, but later attributed by Ruddick et al (1989) to enhanced eddy viscosity in the convecting mixed layers. This is in accord with Padman's description of wave-microstructure interactions described above. Ruddick et al (1989) used a rotating annular tank to measure the interfacial stress across a sheared convecting interface, and found the stresses to be quite weak, consistent with O(1) Prandtl number. Ruby Krishnamurti described experiments in progress in which an annular tank with a Kato and Phillips-type grid is used to study the interaction between vertical shear and diffusive convection. All of these results point to the need for a comprehensive set of laboratory experiments in which internal waves are propagated through a stratification consisting of several convecting interfaces, both finger and diffusive. The effect of the convection on the waves, and the effect of the waves on the convective layer structure and the fluxes should be observed.

Are run-down experiments the wrong way to mimic ocean processes? Perhaps fluxes should be imposed, and the evolution of the gradients and layer structure should be observed. The experimental setup described by Ruby Krishnamurti is suitable for such experiments, but would need to be much larger.

Laurie Padman closed off the discussion by noting that it should now be possible to perform a valuable field experiment in a region such as Lake Vanda, where the situation is simple enough to be completely understandable, but active enough to be relevant. Modern

instrumentation could be used to measure the suite of basic turbulence quantities, assess microscale isotropy, and measure the background shears. Surface fluxes could be easily monitored, as well as chemical measurements of geothermal source waters. As in C-SALT, it would be wise to precede the experiment with careful mesoscale surveys to determine how one-dimensional the situation is, in case lateral inhomogeneity of sources cause lateral circulation structures that may be linked with the observed layering.

Acknowledgements

References

Fedorov, K.N., 1988. Layer thicknesses and effective diffusivities in "diffusive" thermohaline convection in the ocean. In: *Small-scale Turbulence and Mixing in the Ocean,* J. Nihoul and B. Jamart (Editors), Elsevier Oceanography Series, 46, Elsevier, New York, pp. 471-480.

Fernando, H.J.S. 1989a. Buoyancy transfer across a diffusive interface. J. Fluid Mech. 209, 1-34.

Fernando, H.J.S. 1989b. Oceanographic implications of laboratory experiments on diffusive interfaces. J. Phys. Ocean. 19(11) 1787-1715.

Kelley, D.E., 1984. Effective diffusivities within ocean thermohaline staircases. *J. Geophys. Res.,* **89**, 10484-10488.

Kelley, D.E., 1989. Accuracy of 4/3 flux laws for oceanic thermohaline staircases. *J. Geophys. Res.,* submitted.

Larson, N.G., M.C. Gregg, 1983. Turbulent dissipation and shear in thermohaline intrusions. *Nature,* 306(5938), 26-32.

Muench, Fernando and Stegen 1989. Temperature and salinity staircases in the Northwestern Weddell Sea. *J. Phys. Oceanogr.,* in press.

Osborn, T.R., 1988. Signatures of doubly diffusive convection and turbulence in an intrusive regime. *J. Phys. Oceanogr.,* 18(1), 146-155.

Padman, L., T.M. Dillon, 1987. Vertical fluxes through the Beaufort Sea thermohaline staircase. *J. Geophys. Res.,* 92(10), 10799-10806.

Ruddick, B.R. 1985. Momentum transfer in thermohaline staircases. *J. Geophys. Res.,* **90**, 895-902.

Ruddick, B.R., R.W. Griffiths, G. Symonds. 1989. Frictional stress at a sheared double-diffusive interface. *J. Geophys. Res.,* in press.

THERMOHALINE INTRUSIONS

Thermohaline intrusions are found in all oceans and are particularly likely near fronts, eddies and rings. Recent observations in the tropical Pacific indicate that cross-equatorial intrusions with extraordinarily long spatial scales (hundreds of kilometers) may occur. It seems certain that they are a primary conduit for transfer of thermal and salinity variance from the mesoscale to the finescale, and thus have global significance. We need to be able to parameterize their effects on horizontal and vertical fluxes of heat and salt. However, effective modeling will require improved understanding of the fingering and diffusive processes themselves, as well as how they interact in intrusion evolution.

A number of different questions arise with respect to intrusion dynamics. For instance, what limits the amplitude of the intrusion? Is it a balance between the strength of the finger and diffusive interfaces? How important is friction and eddy straining? How do internal waves affect their evolution? Similarly, we can identify key questions for modelling their effects on larger scales: How can they best be parameterised on the mesoscale (Joyce, 1977)? How do we take account of the dynamical effects of the up-gradient density fluxes (Posmentier and Kirwan, 1985)? How do we interpret the global effect of intrusion migration across density surfaces (Garrett, 1982)?

Since the microscale measurement challenges of fingers and diffusive interfaces have been addressed before, we will focus on theoretical and observational approaches to the intrusion problem, rather than different scales.

Theory/Modelling

Theoretical work on intrusions has been done with linear stability models (Stern, 1967; Toole and Georgi, 1981; McDougall, 1986a) and slab models (Posmentier and Hibbard, 1982; McDougall, 1986b). Generally, a simple eddy diffusivity or layer to layer exchange coefficient is specified to model the double-diffusive transfers. However, it should now be possible to develop more realistic models based on flux parametizations of Kunze (1987) (fingers) and Kelly (1990) (diffusive interfaces). The dependence of mixing intensity on density ratio could be incorporated into models which calculate the effect of vertical shear on the evolution of R_ρ (Schmitt, 1990), which is a first order effect in intrusions. Very little has been done to develop numerical models of finescale ocean intrusions, and it seems an area ripe for progress. The recent discovery of very large scale intrusions spanning the equatorial Pacific (Richards and Pollard, in press) has led to an extension of the linear stability analysis to the beta plane (Richards, in press). Do these intrusions make a significant contribution to cross equatorial fluxes?

Observations

Since thermohaline fronts are nearly always density fronts as well, most intrusion observations have taken place in areas of strong dynamical activity. This poses formidable sampling problems for ship-board work, because features are advected and modified by vertical shears on time-scales short compared to ship survey times with CTD "tow-yos" etc. (Schmitt, Lueck and Joyce, 1985). However, high speed towed bodies (Batfish, Sea-Soar) are becoming more widely available for rapid finescale surveying. Also, Lagrangian floats which monitor local shear and density gradients (Kunze, Williams and Briscoe, 1990) would seem to offer new possibilities for studying the evolution of the intrusions. Such a float could monitor local conditions and serve as a water tag for the deployment of dropsondes. Similarly, the use of fluorescent dyes or trace chemicals (Ledwell, this volume) would seem to offer the opportunity to study the actual fate of water within intrusions, helping to determine the along front, across front and vertical transfer rates. Thus, a fine- and microscale field program focused on intrusion dynamics could be readily justified. Also, statistics on the global occurrence of intrusions would be well worth developing. Large field programs such as WOCE should make quality CTD data from all over the world ocean more readily available for such analysis.

A Bibliography on
Oceanic Double Diffusion

Compiled by
J. Boyd [+], *N. Fofonoff* [*]
J. Yoshida [†] *and R. Schmitt* [*]

[+] NOARL, Code 331, Stennis Space Center, MS 39529
[*] WHOI, Woods Hole, MA 02543
[†] Tokyo University of Fisheries, 4-5-7 Konan, Minato-ku, Tokyo 108 Japan

Double-Diffusion and Mixing References

June 25, 1991

1857

Jevons, W. S., 1857. On the cirrous form of cloud. *The London, Edinburgh, and Dublin Philosophical Magazine and Journal of Science*, Series 4, 14(90), 22–35.

1901

Bénard, H., 1901. Les tourbillons cellulaires dans un nappe liquide transportant de la chaleur par convection en regime permanent. *Ann. Chim. Phys.*, 23, 62–144.

1903

Boussinesq, J., 1903. *Theorie analytique de la chaleur.* 2, Paris, Gathier-Villars.

1948

Eckart, C., 1948. An analysis of the stirring and mixing processes in incompressible fluids. *Journal of Marine Research*, 7, 265–275.

1949

Stommel, H., 1949. Horizontal diffusion due to oceanic turbulence. *Journal of Marine Research*, 8, 199–225.

1954

Monin, A. S., and A. M. Obukhov, 1954. Basic laws of turbulent mixing in the ground layer of the atmosphere. *Trudy Geofiz. Inst. Akad. Nauk SSSR*, 24, 163–187.

1956

Stommel, H., A. B. Arons, and D. Blanchard, 1956. An oceanographic curiosity: the perpetual salt fountain. *Deep-Sea Research*, 3, 152–153.

1959

Groves, G. W., 1959. Flow estimate for the perpetual salt fountain. *Deep-Sea Research*, 5, 209–214.

1960

Stern, M. E., 1960. The 'salt fountain' and thermohaline convection. *Tellus*, 12, 172–175.

1962

Wilson, A. T., and H. W. Wellman, 1962. Lake Vanda: an Antarctic Lake. *Nature*, 196, 1171.

1963

Herring, J. R., 1963. Investigation of problems in thermal convection. *Journal of the Atmospheric Sciences*, 20, 325–338.

1964

Herring, J. R., 1964. Investigation of problems in thermal convection: rigid boundaries. *Journal of the Atmospheric Sciences*, **21**, 277–290.

Roden, G. I., 1964. Shallow temperature inversions in the Pacific Ocean. *Journal of Geophysical Research*, **69**(14), 2899–2914.

Turner, J. S., and H. Stommel, 1964. A new case of convection in the presence of combined vertical salinity and temperature gradients. *Proceedings of the National Academy of Sciences*, **52**, 49–53.

Walin, G., 1964. Note on the stability of water stratified by both salt and heat. *Tellus*, **16**, 389–393.

Weinburger, H., 1964. The physics of the solar pond. *Solar Energy*, **8**, 45–56.

1965

Ozmidov, R. V., 1965. On the turbulent exchange in a stably stratified ocean. *Fizika Atmos. Okeana Izv. Akad. Nauk SSSR*, **1**, 853–860.

Sani, R. L., 1965. On finite amplitude roll cell disturbances in a fluid layer subjected to a heat and mass transfer. *American Institute of Chemical Engineering Journal*, **11**, 971–980.

Swallow, J. C., and J. Crease 1965. Hot salty water at the bottom of the Red Sea. *Nature*, **205**, 165–166.

Turner, J. S., 1965. The behaviour of a stable salinity gradient heated from below. *Journal of Fluid Mechanics*, **33**, 183–200.

Turner, J. S., 1965. The coupled turbulent transports of salt and heat across a sharp density interface. *International Journal of Heat and Mass Transport*, **8**, 759–767.

Veronis, G., 1965. On finite amplitude instability in thermohaline convection. *Journal of Marine Research*, **23**, 1–17.

1966

Hoare, R. A., 1966. Problems of heat transfer in Lake Vanda, a density stratified Antarctic lake. *Nature*, **210**, 787–789.

Ingham, M. C., 1966. The salinity extrema of the world ocean. Ph.D. Dissertation, Oregon State University, Corvallis, OR.

Moore, D. W., and E. A. Spiegel, 1966. A thermally excited non-linear oscillator. *Astrophysics Journal*, **143**, 871–887.

Munk, W. H., 1966. Abyssal recipes. *Deep-Sea Research*, **13**, 707–730.

1967

Miller, L., T. H. Spurling, and E. A. Mason, 1967. Instabilities in ternary diffusion. *Physics of Fluids*, **10**, 1809–1813.

Molcard, R., 1967. A review of the stepped structure in the Tyrrhenian Sea. *Rapp. Comm. Int. Mer Medit.*, **23**, 23–24.

Nield, D. A., 1967. The thermohaline Rayleigh-Jeffries problem. *Journal of Fluid Mechanics*, **29**, 545–558.

Shirtcliffe, T.G.L, 1967. Thermosolutal convection: observation of an overstable mode. *Nature*, **213**, 489–490.

Stern, M. E., 1967. Lateral mixing of water masses. *Deep-Sea Research*, **14**, 747–753.

Stommel, H., and K. N. Federov, 1967. Small-scale structure in temperature and salinity near Timor and Mindanao. *Tellus*, **19**, 306–325.

Turner, J. S., 1967. Salt fingers across a density interface. *Deep-Sea Research*, **14**, 599–611.

1968

Cooper, J. W., and H. Stommel, 1968. Regularly spaced steps in the main thermocline near Bermuda. *Journal of Geophysical Research*, **73**, 5849–5854.

Grant, H. L., A. Moilliet, and W. M. Vogel, 1968. Some observations of the occurrence of turbulence in and above the thermocline. *Journal of Fluid Mechanics*, **34**, 443–448.

Elder, J. W., 1968. The unstable thermal interface, *Journal of Fluid Mechanics*, **32**, 69–96.

Hoare, R. A., 1968. Thermohaline convection in Lake Vanda, Antarctica. *Journal of Geophysical Research*, **73**, 607–612.

Shirtcliffe, T. G. L., and I. M. Calhaem, 1968. Measurements of temperature and electrical conductivity in Lake Vanda, Victoria Land, Antarctica. *New Zealand Journal of Geology and Geophysics*, **11**, 976–981.

Stern, M. E., 1968. T–S gradients on the micro-scale. *Deep-Sea Research*, **15**, 245–250.

Tait, R. I., and M. R. Howe, 1968. Some observations of thermohaline stratification in the deep ocean. *Deep-Sea Research*, **15**, 275–280.

Turner, J. S., 1968. The behaviour of a stable salinity gradient heated from below. *Journal of Fluid Mechanics*, **33**, 183–200.

Turner, J. S., 1968. The influence of molecular diffusivity on turbulent entrainment across a density interface. *Journal of Fluid Mechanics*, **33**, 639–656.

Veronis, G., 1968. Effect of a stabilizing gradient of solute on thermal convection. *Journal of Fluid Mechanics*, **34**, 315–336.

Woods, J. D., 1968. Wave induced shear instability in the summer thermocline. *Journal of Fluid Mechanics*, **32**, 791–800.

1969

Cox, C. S., Y. Nagata, and T. Osborn, 1969. Oceanic fine structure and internal waves. *Bull. Japan Soc. Fish. Oceanogr.*, Prof. Uda's Commemorative Paper, 67–72.

Baines, P. G., and A. E. Gill, 1969. On thermohaline convection with linear gradients. *Journal of Fluid Mechanics*, **37**, 289–306.

Degens, E. T., and D. A. Ross, 1969. *Hot Brines and Recent Heavy Metal Deposits in the Red Sea*, Springer-Verlag, New York, 599 pp.

Elder, J. W., 1969. Numerical experiments with thermohaline convection. *Physics of Fluids*, **12**, (Suppl. II), 194–197.

Gill, A. E., and J. S. Turner, 1969. Some new ideas about the formation of Antarctic Bottom Water. *Nature*, **224**, 1287–1288.

Neal, V. T., S. Neshyba, and W. Denner, 1969. Thermal stratification in the Arctic Ocean. *Science*, **166**, 373–374.

Orlanski, I., and K. Bryan 1969. Formation of the thermocline step structure by large-amplitude internal waves. *Journal of Geophysical Research*, **74**, 6975–6983.

Pingree, R. D., 1969. Small-scale structure of temperature and salinity near Station Cavall. *Deep-Sea Research*, **16**, 275–295.

Shirtcliffe, T.G.L., 1969. An experimental investigation of thermosolutal convection at marginal stability. *Journal of Fluid Mechanics*, **35**, 677–688.

Shirtcliffe, T.G.L., 1969. The development of layered thermosolutal convection. *International Journal of Heat and Mass Transfer*, **12**, 215–222.

Stern, M. E., 1969. Collective instability of salt fingers. *Journal of Fluid Mechanics*, **35**, 209–218.

Stern, M. E., 1969. Salt finger convection and the energetics of the general circulation. *Deep-Sea Research*, **16**(Suppl.), 263–267.

Stern, M. E., and J. S. Turner, 1969. Salt fingers and convecting layers. *Deep-Sea Research*, **16**, 497–511.

Thorpe, S. A., P. K. Hutt, and R. Soulsby, 1969. The effect of horizontal gradients on thermohaline convection. *Journal of Fluid Mechanics*, **38**, 375–400.

1970

Federov, K. N., 1970. On the step-like structure of temperature inversions in the ocean. *Atmospheres and Ocean Physics*, **6**, 704–709.

Hart, J. E., 1970. Thermal convection between sloping parallel boundaries. Ph.D. Dissertation, Massachusetts Institute of Technology, Cambridge, MA.

Howe, M. R., and R. I. Tait, 1970. Further observations of thermohaline stratification in the deep ocean. *Deep-Sea Research*, **17**, 963–972.

McIntyre, M. E., 1970. Diffusive destabilization of the baroclinic vortex. *Geophysical Fluid Dynamics* **1**, 19–57.

Nagata, Y. 1970, Detailed temperature cross section of the cold water belt along the northern edge of the Kuroshio, *Journal of Marine Research*, **28**, 1–14.

Shirtcliffe, T.G.L., and J. S. Turner, 1970. Observations of the cell structure of salt fingers. *Journal of Fluid Mechanics*, **41**, 707–719.

Stern, M. E., 1970. Optical measurement of salt fingers. *Tellus*, **22**, 76–81.

Turner, J. S., T.G.L. Shirtcliffe, and P. G. Brewer, 1970. Elemental variations of transport coefficients across density interfaces in multiple-diffusive systems. *Nature*, **228**, 1083–1084.

Wendt, R. P., and M. Shamim, 1970. Isothermal diffusion in the system water-magnesium chloride-sodium chloride as studied with the rotating diaphragm cell. *Journal of Physical Chemistry*, **74**, 2770–2873.

Zenk, W., 1970. On the temperature and salinity of the Mediterranean water in the northeast Atlantic. *Deep-Sea Research*, **17**, 627–632.

1971

Baker, D. J., Jr., 1971. Density gradients in a rotating stratified fluid: Experimental evidence for a new instability. *Science*, **172**, 1029–1031.

Busse, P. G., and J. A. Whitehead, 1971. Instabilities of convection rolls in a high Prandtl number fluid. *Journal of Fluid Mechanics*, **47**, 305–320.

Chen, C. F., D. G. Briggs, and R. A. Wirtz, 1971. Stability of thermal convection in a salinity gradient due to lateral heating. *International Journal of Heat and Mass Transport*, **14**, 57–65.

Escowitz, E. C., and A. F. Amos, 1971. Steps on the thermocline northeast of Barbados (abstract). *Transactions of the American Geophysical Union*, **52**, 232.

Fisher, H. B., 1971. The dilution of an undersea sewage cloud by salt fingers. *Water Research*, **5**, 909–915.

Gregg, M. C., and C. S. Cox, 1971. Measurements of the oceanic microstructure of temperature and electrical conductivity. *Deep-Sea Research*, **18**, 925–934.

Hart, J. E., 1971. Stability of the flow in a differentially heated inclined box. *Journal of Fluid Mechanics*, **47**, 547–576.

Hart, J. E., 1971. On sideways diffusive instability. *Journal of Fluid Mechanics*, **49**, 279–288.

Hart, J. E., 1971. A possible mechanism for boundary layer mixing and layer formation in a stratified fluid. *Journal of Physical Oceanography*, **1**, 258–262.

Huppert, H. E., 1971. On the stability of a series of double diffusive layers. *Deep-Sea Research*, **18**, 1005–1021.

Hurle, D.T.J., and E. Jakeman, 1971. Soret-driven thermosolutal convection. *Journal of Fluid Mechanics*, **47**, 667–687.

Lambert, R. B., 1971. Experimental studies of stratified layers. In: *Proceedings of the Joint Oceanographic Assembly*, Tokyo, 1970, 199–200.

Linden, P. F., 1971. Effect of turbulence and shear on salt fingers. Ph.D. Dissertation, University of Cambridge, Cambridge, U.K.

Linden, P. F., 1971. Salt fingers in the presence of grid-generated turbulence. *Journal of Fluid Mechanics*, **49**, 611–624.

Neshyba, S., V. T. Neal, and W. W. Denner, 1971. Temperature and conductivity measurements under Ice Island T-3. *Journal of Geophysical Research*, **76**, 8107–8120.

Neshyba, S., V. T. Neal, and W. Denner, 1971b. Internal waves and thermo-solutal microstructure. In: *Proceedings 8th U.S. Navy Symposium on Military Oceanography*, **1**, 341–348.

Pingree, R. D., 1971. Analysis of the temperature and salinity small-scale structure in the region of the Mediterranean influence in the N.E. Atlantic. *Deep-Sea Research*, **18**, 485–491.

Spencer, D. W., and P. G. Brewer, 1971. Vertical advection and redox potentials as controls on the distribution of manganese and other trace metals dissolved in waters of the Black Sea. *Journal of Geophysical Research*, **76**, 5877–5892.

Tait, R. I., and M. R. Howe, 1971. Thermohaline staircase. *Nature*, **231**, 178–179.

1972

Broughton, J. M., 1972. Experiments on steady layered convection in a doubly diffusive system. Masters Thesis, Colorado State University, Fort Collins, CO.

Delnore, V. E., and J. McHugh, 1972. BOMEX Period III Upper Ocean Soundings. Rockville, MD, National Oceanic and Atmospheric Administration/Center for Experimental Design and Data Analysis, 352 pp.

Foster, T. D., 1972. An analysis of the cabbeling instability in sea water. *Journal of Physical Oceanography*, **2**, 294–301.

Garrett, C. J. R., and W. H. Munk, 1972. Oceanic mixing by breaking internal waves. *Deep-Sea Research*, **19**, 823–832.

Gregg, M. C., and C. S. Cox, 1972. The vertical microstructure of temperature and salinity. *Deep-Sea Research*, **19**, 355–376.

Howe, M. R., and R. I. Tait, 1972. The role of temperature inversions in the mixing processes of the deep ocean. *Deep-Sea Research*, **19**, 781–791.

Huppert, H. E., and J. S. Turner, 1972. Double-diffusive convection and its implications for the temperature and salinity structure of the ocean and Lake Vanda. *Journal of Physical Oceanography*, **2**, 456–461.

Lambert, R. B., and J. W. Demenkow, 1972. On the vertical transport due to fingers in double diffusive convection. *Journal of Fluid Mechanics*, **54**, 627–640.

Neshyba, S., V. T. Neal, and W. Denner, 1972. Spectra of internal waves: In situ measurements in a multiple-layered structure. *Journal of Physical Oceanography*, **2**, 91–95.

Osborn, T., and C. S. Cox, 1972. Oceanic fine structure. *Geophysical Fluid Dynamics*, **3**, 321–345.

Pingree, R. D., 1972. Mixing in the deep stratified ocean. *Deep-Sea Research*, **19**, 549–561.

Sarsten, J. A., 1972. LNG stratification and roll-over. *Pipeline and Gas Journal*, **199**, 37–39.

Schechter, R. S., I. Prigogine, and J. R. Hamm, 1972. Thermal diffusion and convective stability. *Physics of Fluids*, **15**, 379–386.

Shirtcliffe, T.G.L., 1972. The contribution of double-diffusive processes to the vertical fluxes of salt and heat. In: R. Fraser, editor, *Oceanography of the South Pacific*. Wellington (New Zealand), New Zealand Committee for UNESCO, 137–139.

Straus, J. M., 1972. Finite amplitude doubly diffusive convection. *Journal of Fluid Mechanics*, **56**, 353–374.

Taunton, J. W., E. N. Lightfoot, and T. Green, 1972. Thermohaline instability and salt fingers in a porous medium. *Physics of Fluids*, **15**, 748–753.

Velarde, M. G., and R. S. Schechter, 1972. Thermal diffusion and convective stability. II. An analysis of the convected fluxes. *Physics of Fluids*, **15**, 1707–1714.

Wirtz, R. A., D. G. Briggs, and C. F. Chen, 1972. Physical and numerical experiments on layered convection in a density stratified fluid. *Geophysical Fluid Dynamics*, **3**, 265–288.

Woods, J. D. and R. L. Wiley, 1972. Billow turbulence and ocean microstructure, *Deep-Sea Research*, **19**, 87–121.

Yusa, Y. 1972. The re-evaluation of heat balance in Lake Vanda, Victoria Land, Antarctica. *Contrib. Geophys. Inst. Kyoto Univ.*, **12**, 87–100.

1973

Carmack, E., and K. Aagaard, 1973. On the deep water of the Greenland Sea. *Deep-Sea Research*, **20**, 687–715.

Demenkow, J. W., 1973. A study of the two layer salt finger system. Ph.D. Dissertation, University of Rhode Island, Kingston, RI.

Garrett, C.J.R., 1973. The effect of internal wave strain on vertical spectra of finestructure. *Journal of Physical Oceanography*, **3**, 83–85.

Gregg, M. C., C. S. Cox, and P. W. Hacker, 1973. Vertical microstructure measurements in the central North pacific. *Journal of Physical Oceanography*, **3**, 458–469.

Gregg, M. C., 1973. The microstructure of the ocean. *Scientific American*, 228(2), 65–77.

Linden, P. F., 1973. On the structure of salt fingers. *Deep-Sea Research*, **20**, 325–340.

Hart, J. E., 1973. Finite amplitude sideways diffusive convection. *Journal of Fluid Mechanics*, **59**, 47–64.

Huppert, H. E., and P. C. Manins, 1973. Limiting conditions for salt fingering at an interface. *Deep-Sea Research*, **20**, 315–323.

Magnell, B., 1973. Oceanic microstructure observations near Bermuda using a towed sensor. Ph.D. Dissertation. WHOI/MIT Joint Program, Woods Hole, MA.

Osborn, T. R., 1973. Temperature microstructure in Powell Lake. *Journal of Physical Oceanography*, **3**, 302–307.

Shirtcliffe, T.G.L., 1973. Transport and profile measurements of the diffusive interface in double-diffusive convection with similar diffusivities. *Journal of Fluid Mechanics*, **57**, 27–43.

Siedler, G., and W. Zenk, 1973. Variability of the thermohaline staircase. *Nature* (Physical Science), **244**(131), 11–12.

Turner, J. S., 1973. *Buoyancy Effects in Fluids*. Cambridge University Press, Cambridge, 367 pp.

1974

Chen, C. F., 1974. Onset of cellular convection in a salinity gradient due to a later temperature gradients. *Journal of Fluid Mechanics*, **63**, 563–576.

Chen, C. F., and W. W. Skok, 1974. Cellular convection in a salinity gradient along a heated inclined wall. *International Journal of Heat and Mass Transfer*, **17**, 51–60.

Chen, C. F., and S. B. Wong, 1974. Double-diffusive convection along a sloping wall. *Bulletin of the American Physical Society*, **19**, 1153.

Cortecci, G., R. Molcard, and P. Noto, 1974. Isotopic analysis of the deep staircase structure in the Tyrrhenian Sea. *Nature*, **250**, 134–136.

Elliott, A. J., M. R. Howe, and R. I. Tait, 1974. The lateral coherence of a system of thermohaline layers in the deep ocean. *Deep-Sea Research*, **21**, 95–107.

Hsu, Y. S., 1974. Double diffusive instabilities with and without a weak vertical shear. Ph.D. Dissertation, Harvard University, Cambridge, MA.

Johannessen, O. M., and O. S. Lee, 1974. Thermohaline staircase structure in the Tyrrhenian Sea. *Deep-Sea Research*, **21**, 629–639.

Linden, P. F., 1974. Salt fingers in a steady shear flow. *Geophysical Fluid Dynamics*, **6**, 1–27.

Linden, P. F., 1974. A note on the transport across a diffusive interface. *Deep-Sea Research*, **21**, 283–287.

Marmorino, G. O., 1974. Equilibrium heat and salt transport through a diffusive thermohaline interface. Master's Thesis, Oregon State University, Corvallis, Oregon.

Mazeika, P. A., 1974. Subsurface mixed layers in the northwest tropical Atlantic. *Journal of Physical Oceanography*, **4**, 446–453.

Mellberg, L. E., O. M. Johannessen, and O. S. Lee, 1974. Acoustic effect caused by a deep thermohaline stepped structure in the Mediterranean Sea. *Journal of the Acoustical Society of America*, **55**, 1081–1083.

Miller, R. R. and D. G. Browning, 1974. Thermal layering between the Galapagos Islands and South America. *Deep-Sea Research*, **21**, 669–673.

Turner, J. S., 1974. Double-diffusive phenomena. *Annual Reviews of Fluid Mechanics*, **6**, 37–56.

Turner, J. S., and C.F. Chen, 1974. Two-dimensional effects in double-diffusive convection. *Journal of Fluid Mechanics*, **63**, 577–592.

Williams, A. J., 1974. Salt fingers observed in the Mediterranean outflow. *Science*, **185**, 941–943.

1975

Carmack, E. C., and T. D. Foster, 1975. On the flow of water out of the Weddell Sea. *Deep-Sea Research*, **22**, 711–724.

Chen, C. F., 1975. Double-diffusive convection in an inclined slot. *Journal of Fluid Mechanics*, **72**, 721–729.

Crapper, P. F., 1975. Measurements across a diffusive interface. *Deep-Sea Research*, **22**, 537–545.

Evans, D. L., 1975. Large and small-scale temperature-salinity correlations in the ocean. Ph.D. Dissertation, University of Rhode Island, Kingston, RI.

Gregg, M. C., 1975. Microstructure and intrusions in the California Current. *Journal of Physical Oceanography*, **5**, 253–278.

Hayes, S. P., 1975. Preliminary measurements of the time-lagged coherence of vertical temperature profiles. *Journal Geophysical Research*, **80**, 307–311.

Hayes, S. P., T. M. Joyce, and R. C. Millard, Jr., 1975. Measurements of vertical fine structure in the Sargasso sea. *Journal of Geophysical Research*, **80**, 314–319.

Molcard, R., and A. J. Williams, 1975. Deep-stepped structure in the Tyrrhenian Sea. *Mem. Soc. Roy. des Sciences de Liege*, **6**, 191–210.

Siegmann, W. L., and L. A. Rubenfeld, 1975. A nonlinear model for double-diffusive convection. *SIAM Journal of Applied Mathematics*, **29**, 540–557.

Stern, M. E., 1975. *Ocean Circulation Physics*. Academic Press.

Voorhis, A. D., and D. L. Dorson, 1975. Thermal convection in the Atlantis II hot brine pool. *Deep-Sea Research*, **22**, 167–175.

Williams, A. J., 1975. Images of ocean microstructure. *Deep-Sea Research*, **22**, 811–829.

Yusa, Y., 1975. On the water temperature in Lake Vanda, Victoria Land, Antarctica. *Mem. Natl. Polar Res.*, Special Issue 4, 75–89.

1976

Armi, L., and R. C. Millard, 1976. The bottom boundary layer of the deep ocean. *Journal of Geophysical Research*, **81**, 4983–4990.

Chen, C. F., R. C. Paliwal, and S. B. Wong, 1976. Cellular convection in a density stratified fluid: Effect of inclination of the heated wall. *Proceedings of the 1976 Heat Transfer and Fluid Mechanics Institute*, Stanford University Press, Palo Alto, California, 18–32.

Chen, C. F., and R. D. Sandford, 1976. Sizes and shapes of salt fingers near the marginal state. *Journal of Fluid Mechanics*, **78**, 601–607.

Crapper, P. F., 1976. The transport across a diffusive interface in the presence of externally imposed turbulence. *Journal of Physical Oceanography*, **6**, 982–984.

Cussler, E. I., 1976. *Multicomponent Diffusion*. Elsevier.

Foster, T. D., and E. C. Carmack, 1976. Temperature and salinity structure in the Weddell Sea. *Journal of Physical Oceanography*, **6**, 36–44.

Gargett, A. E., 1976. An investigation of the occurrence of oceanic turbulence with respect to fine structure. *Journal of Physical Oceanography*, **6**, 139–159.

Huppert, H. E., 1976. Transitions in double-diffusive convection. *Nature*, **263**, 20–22.

Huppert, H.E., and P. F. Linden, 1976. The spectral signature of salt fingers. *Deep-Sea Research*, **23**, 909–914.

Huppert, H. E., and D. R. Moore, 1976. Nonlinear double-diffusive convection. *Journal of Fluid Mechanics*, **78**, 821–854.

Joyce, T. M., 1976. Large-scale variations in small-scale temperature/salinity fine-structure in the main thermocline of the northwest Atlantic. *Deep-Sea Research*, **23**, 1175–1186.

Linden, P. F., 1976. The formation and destruction of fine-structure by double-diffusive processes. *Deep-Sea Research*, **23**, 895–908.

Magnell, B., 1976. Salt fingers observed in the Mediterranean outflow region (34°N,11°W) using a towed sensor. *Journal of Physical Oceanography*, **6**, 511–523.

Marmorino, G. O., and D. R. Caldwell, 1976. Heat and salt transport through a diffusive thermohaline interface. *Deep-Sea Research*, **23**, 59–67.

Newman, F. C., 1976. Temperature steps in Lake Kivu: a bottom-heated saline lake. *Journal of Physical Oceanography*, **6**, 157–163.

Schmitt, R. W., 1976. On the flux ratio of salt fingers. *EOS, Transactions of the American Geophysical Union*, **57**, 261.

Stern, M. E., 1976. Maximum buoyancy flux across a salt finger interface. *Journal of Marine Research*, **34**, 95–110.

Voorhis, A. D., D. C. Webb, and R. S. Millard, 1976. Current structure and mixing in the shelf/slope water front south of New England. *Journal of Geophysical Research*, **81**, 3695–3708.

1977

Calman, J., 1977. Experiments on high Richardson number instability of a rotating stratified shear flow. *Dynamics of Atmospheres and Oceans*, **1**, 277–297.

Chen, C. F., and R. D. Sanford, 1977. Stability of time-dependent double diffusive convection in an inclined slot. *Journal of Fluid Mechanics*, **83**, 83–95.

Elliot, A. J., and R. I. Tait, 1977. On the steady-state nature of the Mediterranean Outflow step structure. A Voyage of Discovery, G. Deacon 70th Anniversary Volume, Suppl. to *Deep-Sea Research*, 213–220.

Hendricks, P. J., 1977. Finestructure and turbulence in the deep ocean. Ph.D. Dissertation. WHOI/MIT Joint Program in Ocean Engineering, Woods Hole, MA.

Joyce, T. M., 1977. A note on the lateral mixing of water masses. *Journal of Physical Oceanography*, **7**, 626–629.

Lambert, R. B., and W. Sturges, 1977. A thermohaline staircase and vertical mixing in the thermocline. *Deep-Sea Research*, **24**, 211–222.

Linden, P. F., and J. E. Weber, 1977. The formation of layers in a double diffusive system with a sloping boundary. *Journal of Fluid Mechanics*, **81**, 757–773.

Merceret, F. J., 1977. A possible manifestation of double-diffusive convection in the atmosphere. *Boundary-Layer Met.*, **11**, 121–123.

Molcard, R., and R. I. Tait, 1977. The steady state of the step structure in the Tyrrhenian Sea. *A Voyage of Discovery*, George Deacon 70th Anniversary Volume, M. V. Angel, Editor, Suppl. to *Deep-Sea Research*, 221–233.

Neshyba, S., 1977. Upwelling by icebergs. *Nature*, **267**, 507–508.

Yusa, Y., 1977. A study on the thermosolutal convection in saline lakes. *Mem. Fac. Sci., Kyoto Univ., Ser. A*, **35**, 149–183.

1978

Armi, L., 1978. Some evidence for boundary mixing in the deep ocean. *Journal of Geophysical Research*, **83**, 1971–1979.

Carmack, E. C., and P. D. Killworth, 1978. Formation and interleaving of abyssal water masses off Wilkes Land, Antarctica. *Deep-Sea Research*, **25**, 357–369.

Chen, C. F., 1978. Time-dependent double-diffusive instability in a density-stratified fluid along a heated inclined wall. *Journal of Heat Transfer*, **100**, 653–658.

Eriksen, C. C., 1978. Measurements and models of finestructure, internal gravity waves, and wave breaking in the deep ocean. *Journal of Geophysical Research*, **83**, 2989–3009.

Federov, K. N., 1978. *The thermohaline fine structure of the ocean*. Pergamon, Oxford. 170 pp.

Gargett, A. E., 1978. Microstructure and fine structure in an upper ocean frontal regime. *Journal of Geophysical Research*, **83**, 5123–5134.

Garrett, C. and E. P. W. Horne, 1978. Frontal circulation due to cabbeling and double diffusion. *Journal of Geophysical Research*, **83**, 4651–4656.

Georgi, D. T., 1978. Fine-structure in the Antarctic polar front zone: its characteristics and possible relationship to internal waves. *Journal of Geophysical Research*, **83**, 4579–4588.

Horne, E.P.W., 1978. Interleaving at the subsurface front in the slope water off Nova Scotia. *Journal of Geophysical Research*, **83**, 3659–3671.

Huppert, H. E., and J. S. Turner, 1978. On melting icebergs. *Nature*, **271**, 46–48.

Johnson, C. L., C. S. Cox, and B. Gallagher, 1978. The separation of wave-induced and intrusive oceanic microstructure. *Journal of Physical Oceanography*, **8**, 846–860.

Joyce, T. M., W. Zenk, and J. M. Toole, 1978. The anatomy of the Antarctic Polar Front in the Drake Passage. *Journal of Geophysical Research*, **83**, 6093–6113.

Linden, P. F., 1978. The formation of banded salt finger structure. *Journal of Geophysical Research*, **83**, 2902–2912.

Linden, P. F., and T.G.F. Shirtcliffe, 1978. The diffusive interface in double-diffusive convection. *Journal of Fluid Mechanics*, **87**, 417–432.

Marmorino, G. O., and D. R. Caldwell, 1978. Temperature finestructure and microstructure observations in a coastal upwelling region during a period of variable winds (Oregon, summer 1974). *Deep-Sea Research*, **25**, 1073–1106.

Masuda, A., 1978. Double diffusive convection in a rotating system. *Journal of the Oceanographic Society of Japan*, **34**, 8–16.

Posmentier, E. S., and R. W. Houghton, 1978. Fine structure instabilities induced by double diffusion in the shelf/slope water front. *Journal of Geophysical Research*, **83**, 5135–5138.

Reddy, C. S., 1978. Double-diffusive convection in an infinitely tall slot – a numerical study. *American Society of Mechanical Engineers*, ASME paper No. 78-WA/HT-8, 8 pp.

Salusti, E., 1978. Internal waves on a deep-stepped marine structure. *Deep-Sea Research*, **25**, 947–956.

Schmitt, R. W., 1978. Time-dependent and rotational effects in Salt Finger Convection. Ph.D Dissertation, University of Rhode Island.

Schmitt, R. W., and D. L. Evans, 1978. An estimate of the vertical mixing due to salt fingers based on observations in the North Atlantic Central Water. *Journal of Geophysical Research*, **83**, 2913–2919.

Sherman, F. S., J. Imberger, and G. M. Corcos, 1978. Turbulence and mixing in stably stratified waters. *Annual Review Fluid Mechanics*, **10**, 267–288.

Turner, J. S., 1978. Double-diffusive intrusions into a density gradient. *Journal of Geophysical Research*, **83**, 2887–2901.

Turner, J. S., and L. B. Gustafson, 1978. The flow of hot saline solutions from vents in the sea floor-some implications for exhalative massive sulfide and other ore deposits. *Economic Geology*, **73**, 2082–1100.

Varma, K. K., and L. V. Gangadhara Rao, 1978. Observations on fine structure in the northern Arabian Sea. *Indian Journal of Marine Sciences*, **7**, 79–83.

1979

Acheson, D. J., 1979. 'Stable' density stratification as a catalyst for instability. *Journal of Fluid Mechanics*, **96**, 723–733.

Antoranz, J. C., and M. G. Velarde, 1979. Thermal diffusion and convective stability. *Physics of Fluids*, **22**, 1038–1043.

Gregg, M. C., and M. G. Briscoe, 1979. Internal waves, finestructure, microstructure, and mixing in the ocean. *Reviews of Geophysics and Space Physics*, **17**, 1524–1548.

Gregg, M. C., and J. H. McKenzie, 1979. Thermohaline intrusions lie across isopycnals. *Nature*, **280**, 310–311.

Griffiths, R. W., 1979. The transport of multiple components through thermohaline diffusive interfaces. *Deep-Sea Research*, **26a**, 383–397.

Griffiths, R. W., 1979. The influence of a third diffusing component upon the onset of convection. *Journal of Fluid Mechanics*, **92**, 659–670.

Griffiths, R. W., 1979. A note on the formation of 'salt-finger' and 'diffusive' interfaces in three-component systems. *International Journal of Heat and Mass Transfer*, **22**, 1687–1693.

Griffiths, R. W., 1979. Transports through thermohaline interfaces in a viscous fluid and a porous medium. Ph.D. Dissertation, Australian National University, Canberra.

Herman, A. W., and K. L. Denman, 1979. Intrusions and vertical mixing at the shelf/slope water front south of Nova Scotia. *Journal of the Fisheries Research Board of Canada*, **36**, 1445–1453.

Huppert, H. E., and P. F. Linden, 1979. On heating a stable salinity gradient from below. *Journal of Fluid Mechanics*, **95**, 431–464.

McDougall, T. J, 1979. On the elimination of refractive-index variations in turbulent density-stratified liquid flows. *Journal Fluid Mechanics*, **93**, 83–96.

Neuymin, G. G., and V. A. Urdenko, 1979. Possible effects of "salt fingers" on measurements of the transparency of ocean waters. *Oceanology*, **19**, 23–26.

Paliwal, R. C., 1979. Double-diffusive convective instability in an inclined fluid layer. Ph.D. Dissertation, Department of Mechanical, Industrial and Aerospace Engineering, Rutgers University, New Brunswick, NJ.

Ruddick, B. R., and T.G.L. Shirtcliffe, 1979. Data for double diffusers: Physical properties of aqueous salt-sugar solutions. *Deep-Sea Research*, **26**, 775–787.

Ruddick, B. R., and J. S. Turner, 1979. The vertical length scale of double-diffusive intrusions. *Deep-Sea Research*, **26A**, 903–913.

Schmitt, R. W., 1979. The growth rate of super-critical salt fingers. *Deep-Sea Research*, **26A**, 23–40.

Schmitt, R. W., 1979. Flux measurements on salt fingers at an interface. *Journal of Marine Research*, **37**, 419–436.

Schmitt, R. W., and R. B. Lambert, 1979. The effects of rotation on salt fingers. *Journal of Fluid Mechanics*, **90**, 449–463.

Simpson, J. H., M. R. Howe, N.C.G. Morris, and J. Stratford, 1979. Velocity shear in the steps below the Mediterranean outflow. *Deep-Sea Research*, **26**, 1381–1386.

Turner, J. S., 1979. Laboratory models of double diffusive processes in the ocean, In: *National Academy of Sciences. Twelfth Symposium on Naval Hydrodynamics*, Washington, D.C., National Academy of Sciences, 596–606.

Zangrando, F., 1979. Observation and analysis of a full-scale experimental salt gradient solar pond. Ph.D. Dissertation, University of New Mexico, Albuquerque, NM, 131 pp.

1980

Chen, C. F., and J. S. Turner, 1980. Crystallization in double-diffusive system. *Geophysical Research*, **85**, 2573–2593.

Delnore, V. E. 1980. Numerical simulation of thermohaline convection in the upper ocean. *Journal of Fluid Mechanics*, **96**, 803–826.

Fedorov, K. N., 1980. Intrusive fine structure in frontal zones and indication of double-diffusion. In: *Marine Turbulence*, J. Nihoul, editor, New York, Elsevier, pp. 57–63.

Griffiths, R. W., and B. R. Ruddick, 1980. Accurate fluxes across a salt-sugar finger interface deduced from direct density measurements. *Journal of Fluid Mechanics*, **99**, 85–95.

Gregg, M. C., 1980a. Microstructure patches in the thermocline. *Journal of Physical Oceanography*, **10**, 915–943.

Gregg, M. C., 1980b. The three-dimensional mapping of a small thermohaline intrusion. *Journal of Physical Oceanography*, **10**, 1468–1492.

Gregg, M. C., and T. B. Sanford, 1980. Signatures of mixing from the Bermuda Slope, the Sargasso Sea and the Gulf Stream. *Journal of Physical Oceanography*, **10**, 105–127.

Griffiths, R. W., and B. R. Ruddick, 1980. Accurate fluxes across a salt-sugar interface deduced from direct density measurements. *Journal of Fluid Mechanics*, **99**, 85–95.

Horne, E.P.W., and J. M. Toole, 1980. Sensor response mismatches and lag correction techniques for temperature-salinity profilers. *Journal of Physical Oceanography*, **10**, 1122–1130.

Huppert, H. E., and J. S. Turner, 1980. Ice blocks melting into a salinity gradient. *Journal of Fluid Mechanics*, **100**, 367–384.

Huppert, H. E., and E. G. Josberger, 1980. The melting of ice in cold stratified water. *Journal of Physical Oceanography*, **10**, 953–960.

Middleton, J. H., and T. D. Foster, 1980. Finestructure measurements in a temperature-compensated halocline. *Journal of Geophysical Research*, **85**, 1107–1122.

Oakey, N. S., and J. A. Elliott, 1980. Variability of temperature gradient microstructure observed in the Denmark Strait. *Journal of Geophysical Research*, **85**, 1933–1944.

Osborn, T. R., 1980. Estimates of the local rate of vertical diffusion from dissipation measurements. *Journal of Physical Oceanography*, **10**, 83–89.

Paliwal, R. C., and C. F. Chen 1980. Double-diffusive instability in an inclined fluid layer. Part 1. Experimental investigations. *Journal of Fluid Mechanics*, **98**, 755–768.

Paliwal, R. C., and C. F. Chen 1980. Double-diffusive instability in an inclined fluid layer. Part 2. Stability analysis. *Journal of Fluid Mechanics*, 98, 769–785.

Piacsek, S. A., and J. Toomre, 1980. Nonlinear evolution and structure of salt fingers. In: *Marine Turbulence*, J.C.J. Nihoul, editor, Elsevier, New York, 193–219.

Stommel, H. M., and G. T. Csanady, 1980. A relation between the T–S curve and global heat and atmospheric water transport. *Journal of Geophysical Research*, 85, 495–501.

Toole, J. M., 1980. Wintertime convection and frontal interleaving in the Southern Ocean. Sc.D. Dissertation. WHOI/MIT Joint Program in Physical Oceanography, Woods Hole, MA.

Wiesenburg, D. A., 1980. Geochemistry of dissolved gases in the hypersaline Orca Basin. Ph.D. Dissertation, Texas A&M University, College Station, TX, 265 pp.

Williams, A. J., III, 1980. Refractive microstructure from diffusive and turbulent ocean mixing. Optical Engineering, 19, 116–121.

1981

Da Costa, L. N., E. Knobloch, and N. O. Weiss, 1981. Oscillations in double-diffusive convection. *Journal of Fluid Mechanics*, 109, 25–43.

Evans, D. L., 1981. Velocity shear in a thermohaline staircase. *Deep-Sea Research*, 28, 1409–1415.

Gordon, A. L., 1981. South Atlantic thermocline ventilation. *Deep-Sea Research*, 28, 1236–1264.

Griffiths, R. W., 1981. Layered double-diffusive convection in porous media. *Journal of Fluid Mechanics*, 102, 221–248.

Holyer, J. Y., 1981. On the collective instability of salt fingers. *Journal of Fluid Mechanics*, 110, 195–208.

Huppert, H. E., and J. S. Turner, 1981. Double diffusive convection. *Journal of Fluid Mechanics*, 106, 299–329.

Jacobs, S. S., H. E. Huppert, G. Holdsworth, and D. J. Drewry, 1981. Thermohaline steps induced by melting of the Erebus Glacier tongue. *Journal of Geophysical Research*, 86, 6547–6555.

Josberger, E. G., and S. Martin, 1981. Convection generated by vertical icewalls. *Journal of Fluid Mechanics*, 111, 439–473.

Kerr, R. A., 1981. Fingers of salt help mix the sea. *Science*, 211, 155–157.

Knobloch, E., and M.R.E. Proctor, 1981. Nonlinear periodic convection in double-diffusive systems. *Journal of Fluid Mechanics*, 108, 291–316.

Knobloch, E., and N. O. Weiss 1981: Bifurcations in a model of double diffusive convection. *Phys. Letters*, 85a, 127–130.

McDougall, T. J., 1981. Double diffusive convection with a non-linear equation of state. Part I: The accurate conservation of properties in a 2-layer system. *Progress in Oceanography*, 10, 71–89.

McDougall, T. J., 1981. Double-diffusive convection with a nonlinear equation of state. II. Laboratory experiments and their interpretation. *Progress of Oceanography*, **10**, 91–121.

McDougall, T. J., 1981. Fluxes of properties through a series of double-diffusive interfaces with a nonlinear equation of state. *Journal of Physical Oceanography*, **11**, 1294–1299.

Pearlstein, Arne J., 1981. Effect of rotation on the stability of a doubly diffusive layer. *Journal of Fluid Mechanics*, **103**, 389–412.

Poplawsky, C. J., F. P. Incropera, and R. Viskanta, 1981. Mixed-layer development in a double-diffusive, thermohaline system. Transactions of ASME, *Journal of Solar Pond Engineering*, **103**, 351–359.

Proctor, M.R.E., 1981. Steady subcritical thermohaline convection. *Journal of Fluid Mechanics*, **105**, 507–521.

Ruddick, B. R., 1981. The 'colour polarigraph' – a simple method for determining the two-dimensional distribution of sugar concentration. *Journal of Fluid Mechanics*, **109**, 277–282.

Schmitt, R. W., 1981. Form of the temperature-salinity relationship in the Central Water: evidence for double-diffusive mixing. *Journal of Physical Oceanography*, **11**, 1015–1026.

Thangam, T., and C. F., Chen 1981. Salt-finger convection in the surface discharge of heated saline jets. *Geophysical Astrophysical Fluid Dynamics*, **18**, 111–146.

Toole, J. M., 1981. Intrusion characteristics in the Antarctic Polar Front. *Journal of Physical Oceanography*, **11**, 780–793.

Toole, J. M., and D. T. Georgi, 1981. On the dynamics and effects of double-diffusively driven intrusions. *Progress in Oceanography*, **10**, 123–145.

Turner, J. S., 1981. Small-scale mixing processes. In: *The Evolution of Physical Oceanography*. MIT Press, Cambridge, MA.

Turner, J. S. and L. B. Gustafson, 1981. Fluid motions and compositional gradients produced by crystallization or melting at vertical boundaries. *Journal of Volcanology and Geothermal Research*, **11**, 93–125.

Williams, A. J., 1981. The role of double-diffusion in a Gulf Stream frontal intrusion. *Journal of Geophysical Research*, **86**, 1917–1928.

1982

Bergman, T. L., F. P. Incropera, and R. Viskanta, 1982. A multi-layer model for mixing layer development in a double-diffusive thermohaline system heated from below. *International Journal of Heat and Mass Transfer*, **25**, 1411–1418.

Castillo, J. L., and M. G. Velarde, 1982. Buoyancy-thermocapillary instability: the role of interfacial deformation in one- and two-component fluid layers heated from below and above. *Journal of Fluid Mechanics*, **125**, 463–474.

Evans, D. L., 1982. Observations of small scale shear and density structure in the ocean. *Deep-Sea Research*, **29**, 581–595.

Gargett, A. E., and R. W. Schmitt, 1982. Observations of salt fingers in the central waters of the eastern North Pacific. *Journal of Geophysical Research*, 87(C10), 8017–8029.

Garrett, C., 1982. On the parameterization of diapycnal fluxes due to double-diffusive intrusions. *Journal of Physical Oceanography*, 12, 952–959.

Gough, D. O., and J. Toomre, 1982. Single-mode theory of diffusive layers in thermohaline convection. *Journal of Fluid Mechanics*, 125, 75–97.

Joyce, T.M., 1982. Marginally unstable salt fingers: limits to growth. *Journal of Marine Research*, 40(Suppl.), 291–306.

Lambert, R. B. 1982. Lateral mixing processes in the Gulf Stream. *Journal Physical Oceanography*, 12, 851–861.

Lewis, W. T., F. P. Incropera, and R. Viskanta, 1982. Interferometric study of stable salinity gradients heated from below or cooled from above. *Journal of Fluid Mechanics*, 116, 411–430.

McDougall, T. J., and B. R. Ruddick, 1982. The effects on fine structure measurements of correcting for internal wave strain. *Journal of Physical Oceanography*, 12, 495–497.

McDougall, T. J., and J. S. Turner 1982. Influence of cross-diffusion on "finger" double-diffusive convection. *Nature*, 299, 812–814.

Mack, S. A., D. C. Wenstrand, J. Calman, and R. C. Burkhardt, 1982. Characteristics of thermal microstructure in the ocean. Johns Hopkins APL Technical Digest, 3, (1), 28–35.

Newell, T. A., and R. F. Boehm, 1982. Gradient zone constraints in a salt-stratified solar pond. Trans. ASME: *Journal of Solar Pond Engineering*, 104, 280–285.

Ozmidov, R. V., 1982. The third voyage of the scientific R/V AKADEMIK MSTISLAV KELDYSH. *Oceanology*, 22, 504–506.

Perkins, H., and K. Saunders, 1982. Physical oceanographic observations in the northwest tropical Atlantic. Tropical Ocean-Atmosphere Newsletter, September 7–9.

Posmentier, E. S., and C. B. Hibbard, 1982. The role of tilt in double diffusive interleaving. *Journal of Geophysical Research*, 87, 518–524.

Rudraiah, N., and D. Vortmeyer, 1982. The influence of permeability and of a third diffusing component upon the onset of convection in a porous media. *International Journal Heat and Mass Transfer*, 25, 457–464.

Schmitt, R. W., and D. T. Georgi, 1982. Finestructure and microstructure in the North Atlantic Current. *Journal of Marine Research*, 40 (Suppl.), 659–705.

Stern, M. E., 1982. Inequalities and variational principles in double-diffusive turbulence. *Journal of Fluid Mechanics*, 114, 105–121.

Thangam, S., A. Zebib, and C. F. Chen, 1982. Double-diffusive convection in an inclined fluid layer. *Journal of Fluid Mechanics*, 116, 363–378.

Toomre, J., D. O. Gough, and E. A. Spiegel, 1982. Time-dependent solutions of multimode convection equations. *Journal of Fluid Mechanics*, **125**, 99–122.

van Aken, H. M. 1982. The density ratio of frontal intrusions in the North Rockall Trough. *Journal Physical Oceanography*, **12**, 1318–1323.

Walton, I. C., 1982. Double-diffusive convection with large variable gradients. *Journal of Fluid Mechanics*, **125**, 123–135.

Welander, P., 1982. A simple heat-salt oscillator. *Dynamics of Atmospheres and Oceans*, **6**, 233–242.

Zeman, O., and J. L. Lumley, 1982. Modeling salt-fingering structures. *Journal of Marine Research*, **40**, 315–330.

1983

Boyd, J. D., H. T. Perkins, and K. D. Saunders, 1983. Characteristics of thermohaline step structures off the northeast coast of South America. *EOS*, **64**, 1058.

Caldwell, D. R., 1983. Small-scale physics of the ocean. U.S. Nat'l Report to the Int'l Union of Geodesy and Geophysics 1979–1982. *Reviews of Geophysics and Space Physics*, **21**, 1192–1205.

Foster, T. D., 1983. The temperature and salinity finestructure of the ocean under Ross Ice Shelf. *Geophysical Research*, **88**, 2556–2564.

Georgi, D. T. and R. W. Schmitt, 1983. Fine and microstructure observations on a hydrographic section from the Azores to the Flemish Cap. *Journal Physical Oceanography*, **13**, 632–647.

Holyer, J. Y., 1983. Double-diffusive interleaving due to horizontal gradients. *Journal of Fluid Mechanics*, **137**, 347–362.

Huppert, H. E., 1983. Multicomponent convection: turbulence in earth, sun and sea. *Nature*, **303**, 478–479.

Krishnamurti, R. and L. N. Howard, 1983. Double-diffusive instability: Measurement of heat and salt fluxes. *Bulletin American Physical Society*, **28**, 1398–1398.

Larson, N.G., and M. C. Gregg, 1983. Turbulent dissipation and shear in thermohaline intrusions. *Nature*, **306**(5938), 26–32.

Lee, S. I., 1983. Density structure associated with salt fingers. Master's Thesis, Naval Postgraduate School, Monterey, CA.

McDougall, T. J., 1983. Double-diffusive convection caused by coupled molecular diffusion. *Journal of Fluid Mechanics*, **126**, 379–397.

McDougall, T. J., 1983. Double-diffusive plumes in unconfined and confined environments. *Journal of Fluid Mechanics*, **133**, 321–343.

McDougall, T. J., 1983. Greenland Sea Bottom Water formation: a balance between advection and double-diffusion. *Deep-Sea Research*, **30**, 1109–1118.

Maxworthy, T., 1983. The dynamics of double-diffusive gravity currents. *Journal of Fluid Mechanics*, **128**, 259–282.

Moore, D. R., J. Toomre, E. Knobloch, and N. O. Weiss, 1983. Period doubling and chaos in partial differential equations for thermosolutal convection. *Nature*, **303**, 663–667.

Ruddick, Barry, 1983. A practical indicator of the stability of the water column to double-diffusive activity. *Deep-Sea Research*, **30**, 1105–1107.

Schmitt, R. W., 1983. The characteristics of salt fingers in a variety of fluid systems, including stellar interiors, liquid metals, oceans and magmas. *Physics of Fluids*, **26**, 2373–2377.

Thangam, S., A. Zeibb, and C. F. Chen, 1983. Salt finger convection in shear flow. *Physics of Fluids* 27(4), 804–811.

Tsinober, A. B., Y. Yahalom, and D. J. Shlien, 1983. A point source of heat in a stable salinity gradient. *Journal of Fluid Mechanics*, **135**, 199–217.

Worthem, S., E. Mollo-Christensen, and F. Ostapoff, 1983. Effects of rotation and shear on doubly diffusive instability. *Journal of Fluid Mechanics*, **133**, 297–319.

Zeman, O., and J. L. Lumley, 1983. Progress in modeling multi-layer salt-fingering structures. *Mathematical Modelling*, **4**, 73–85.

1984

Armi, L., and W. Zenk, 1984. Large lenses of highly saline Mediterranean water. *Journal of Physical Oceanography*, **14**, 1560–1576.

Asaeda, T., N. Tamai, and H. Ozaki, 1984. Study on the heat and mass transfer at the density interface in double-diffusive processes. *JSCE*, **342**, 135–141, (in Japanese).

Boyd, J. D., and H. T. Perkins, 1984. Estimates of vertical heat and salt fluxes in a thermohaline staircase. *EOS*, **65**, 954.

Brand, H. R., P. C. Hohenberg and V. Steinberg, 1984. Codimension-2 bifurcations for convection in binary fluid mixtures. *Physical Review A.*, **30**, 2548–2561.

Bruce, J. G., J. L. Kerling, and W. H. Beatty III, 1984. Temperature steps off Northern Brazil. *Tropical Ocean-Atmosphere Newsletter*, (23), January, 10–11.

Campbell, I. H., T. J. McDougall and J. S. Turner, 1984. A note on Fluid dynamic processes which can influence the deposition of massive sulphides. *Economic Geology*, **79**, 1905–1913.

Chen, C. F., and D. H. Johnson 1984. Double-diffusive convection: A report on an Engineering Foundation conference. *Journal of Fluid Mechanics*, **138**, 405–416.

Gordon, A. L., and B. A. Huber, 1984. Thermohaline stratification below the Southern Ocean sea ice, *Journal Geophysical Research*, **89**, 641–648

Green, T., 1984. Scales for double-diffusive fingering in porous media. *Water Resources Research*, **20**, 1225–1229.

Heinrich, J. C., 1984. A finite element model for double diffusive convection. *International Journal of Numerical Methods Engineering*, **20**, 447–464.

Holyer, J. Y., 1984. The stability of long, steady two-dimensional salt fingers. *Journal of Fluid Mechanics*, **147**, 169–185.

Huppert, H. E. and R. S. J. Sparks 1984. Double-diffusive convection due to crystallization in magmas. *Annual Reviews of Earth and Planetary Science*, **12**, 11–37.

Huppert, H. E., R. C. Kerr, and M. A. Hallworth, 1984. Heating or cooling a stable compositional gradient from side. *International Journal of Heat and Mass Transfer*.

Kaviany, M., 1984. Effect of a stabilizing solute gradient on the onset of thermal convection. *Physics of Fluids*, **27**, 1108–1113.

Kelley, D. E., 1984. Effective diffusivities within ocean thermohaline staircases. *Journal of Geophysical Research*, **89**, 10484–10488.

McDougall, T. J., 1984. Fluid dynamic implications for massive sulphide deposits of of hot saline fluid flowing into a submarine depression from below. *Deep-Sea Research*, **31**, 145–170.

McDougall, T. J., 1984. The relative roles of diapycnal and isopycnal mixing on subsurface water mass conversion. *Journal of Physical Oceanography*, **14**, 1577–1589.

McDougall, T. J., 1984. A model of a frictionless double-diffusive gravity current on a horizontal surface. *Geophysical Astrophysical Fluid Dynamics*.

McDougall, T. J., and J. R. Taylor, 1984. Flux measurements across a finger interface at low values of the stability ratio. *Journal of Marine Research*, **42**, 1–14.

McDougall, T. J., and J. A. Whitehead, Jr., 1984. Estimates of the relative roles of diapycnal, isopycnal and double-diffusive mixing in Antarctic Bottom Water in the North Atlantic. *Journal of Geophysical Research*, **89**, 10,479–10,483.

Melling, H., R. A. Lake, D. R. Topham and D. B. Fissel, 1984. Oceanic thermal structure in the western Canadian Arctic, *Continental Shelf Research*, **3**, 233–258.

Newell, T. A., 1984. Characteristics of a double-diffusive interface at high density stability ratios. *Journal of Fluid Mechanics*, **149**, 385–401.

Perkin, R. G., and E. L. Lewis, 1984. Mixing in the West Spitzbergen Current. *Journal of Physical Oceanography*, **14**, 1315–1325.

Ruddick, B., 1984. The life of a thermohaline intrusion. *Journal of Marine Research*, **42**, 831–852.

Tamai, N., T. Asaeda, and H. Ozaki 1984. Micro-structure of the mass and heat transfer near double-diffusive interface. *Proceedings of the 4th Congress-Asian and Pacific Division International Association for Hydraulic Research*. Chiang Mai, Thailand, 861–873.

Thangam, S., A. Zebib, and C. F. Chen, 1984. Salt-finger convection in shear flow. *Physics of Fluids*, **27**, 804–811.

Thangam, S., A. Zebib and C. F. Chen 1984. Double-diffusive convection in an inclined fluid layer. *Journal Fluid Mechanics*, **116**, 363–378.

Zhurbas, V. M., and R. V. Ozmidov, 1984. Forms of step-like structures of the oceanic thermocline and their generation mechanism. *Oceanology*, **24**, 153–157.

1985

Bergman, T. L., F. P. Incropera, and R. Viskanta, 1985. A differential model for salt-stratified, double-diffusive system heated from below. *Int. J. Heat Mass Trans.*, **28**, 779–788.

Holyer, J. Y., 1985. The stability of long steady three-dimensional salt fingers to long wavelength perturbations. *Journal of Fluid Mechanics*, **156**, 495–503.

Horne, E. P. W., 1985. Ice-induced vertical circulation in an Arctic Fiord. *Journal of Geophysical Research*, **90**, 1078–1086.

Jackett, D. R., and T. J. McDougall, 1985. An oceanographic variable for the characterizations of intrusions and water mass. *Deep-Sea Research*, **32**, 1195–1207.

Mack, S. A., 1985. Two-dimensional measurements of ocean microstructure: The role of double diffusion. *Journal of Physical Oceanography*, **15**, 1581–1604.

Marmorino, G. O., L. J. Rosenblum, J. P. Dugan and C. V. Shen, 1985. Temperature finestructure patchiness near an upper ocean density front. *Journal of Geophysical Research*, **90**, 11799–11810.

Maslowe, S. A. 1985. Direct resonance in double-diffusive system. *Studies in Applied Math.*, **73**, 59–74.

McDougall, T. J., 1985. Convective processes caused by a dense, hot saline source flowing into a submarine depression from above. *Deep-Sea Research*, **29**, 953–965.

McDougall, T. J., 1985. Double-diffusive interleaving. Part I: Linear stability analysis. *Journal of Physical Oceanography*, **15**, 1532–1541.

McDougall, T. J., 1985. Double-diffusive interleaving. Part II: Finite amplitude steady state interleaving. *Journal of Physical Oceanography*, **15**, 1542–1556.

Osborn, T. R., and R. G. Lueck, 1985. Turbulence measurements with a submarine. *Journal of Physical Oceanography*, **15**(C11), 1502–1520.

Posmentier, E. S., and A. D. Kirwan, 1985. The role of double diffusive interleaving in mesoscale dynamics: an hypothesis. *Journal of Marine Research*, **43**, 541–552.

Poulikakas, D., 1985. The effect of a third diffusing component on the onset of convection in a horizontal porous layer. *Physics of Fluids*, **28**, 3172–3174.

Ruddick, B. R., 1985. Momentum transport in thermohaline staircase. *Journal of Geophysical Research*, **90**, 895–902.

Ruddick, B. R. and A. S. Bennett and D. J. Lawrence, 1985. Thermohaline intrusions in the frontal zones of a ware-core ring observed by Batfish. *Journal of Geophysical Research*, **90**, 8928–8942.

Turner, J. S., 1985. Multicomponent convection. *Annual Reviews of Fluid Mechanics*, **17**, 11–44.

Tang, C. L., A. S. Bennett and D. J. Lawrence 1985: Thermohaline intrusions in the frontal zones of a ware-core ring observed by Batfish. *Journal Geophysical Research*, **90**, 8928–8942.

Yanase, S., and K. Kohno, 1985. The effect of a salinity gradient on the instability of natural convection in a vertical fluid layer. *Journal of the Physical Society of Japan*, **54**, 3747–3756.

Zangrando, F., and L. A. Bertram, 1985. The effect of variable stratification on linear doubly diffusive stability. *Journal of Fluid of Mechanics*, **151**, 55–79.

1986

Bergman, T. L., and A. Ungan, 1986. Experimental and numerical investigation of double-diffusive convection induced by a discrete heat source. *Int. J. Heat Mass Trans.*, **29**, 1695–1709.

Ahlers, G., and I. Rehbert, 1986. Convection in a binary fluid mixture heated from below. *Physics Review Letters*, **56**, 1371–1376.

Chereskin, T. K., and P. F. Linden, 1986. The effect of rotation on intrusions produced by heating a salinity gradient. *Deep-Sea Research*, **33**, 305–322.

Kawase, M., and J. L. Sarmiento, 1986. Circulation and nutrients in mid-depth Atlantic waters. *Journal of Geophysical Research*, **91**(C8), 9749–9770.

Kelley, D. E., 1986. Oceanic Thermohaline Staircases. Ph.D. Dissertation, Dalhousie University, Halifax, Nova Scotia.

Kerr, O. S., and J. Y. Holyer, 1986. The effect of rotation on double-diffusive interleaving. *Journal of Fluid Mechanics*, **162**, 23–33.

Knobloch, E. 1986. Oscillatory convection in binary mixtures. *Physical Review A*, **34**, 1538–1549.

Knobloch, E. *et al.* 1986. Transitions to chaos in two-dimensional double-diffusive convection. *Journal of Fluid Mechanics*, **166**, 409–448.

McDougall, T. J., 1986. Oceanic intrusions: Some limitations of the Ruddick and Turner (1979) mechanism. *Deep-Sea Research*, **33**, 1653–1664.

Miller, D. G., and V. Vitagliano, 1986. Experimental test of McDougall's theory for the onset of convective instability in isothermal ternary systems. *Journal of Physical Chemistry*, **90**, 1706–1717.

Moses, E., and V. Steinberg, 1986. Flow patterns and nonlinear behavior of traveling waves in a convective binary fluid. *Physics Review*, A, **34**, 693–700.

Moses, E., and V. Steinberg, 1986. Competing patterns in a convective binary fluid. *Physical Review Letters*, 2018–2021.

Niino, H., 1986. A linear stability theory of double-diffusive horizontal intrusions in a temperature-salinity front. *Journal of Fluid Mechanics*, **171**, 71–100.

Proctor, M.R.E., and J. Y. Holyer, 1986. Planform selection in salt fingers. *Journal of Fluid Mechanics*, **168**, 241–253.

Schmitt, R. W., R. G. Lueck, and T. M. Joyce, 1986. Fine- and micro-structure at the edge of a warm core ring. *Deep-Sea Research*, **33**, 1665–1689.

Taylor J., and G. Veronis, 1986. Experiments on salt fingers in a Hele-Shaw cell. *Science*, **231**, 39–41.

Wells, J. D., 1986. Solvent fluxes, coupled diffusion, and convection in concentrated ternary solutions. *Journal of Physical Chemistry*, **90**, 2433-2440.

Woods, J. D., R. Onken, and J. Fischer, 1986. Thermohaline intrusions created isopycnally at oceanic fronts are inclined to isopycnals. *Nature*, **322**, 446-449.

Yanase, S. 1986. The effect of time-periodic heating on the stability of a horizontal double-diffusive fluid layer. *Journal of the Physical Society of Japan*, **55**, 1130-1138.

1987

Boyd, J. D., and H. Perkins, 1987. Characteristics of thermohaline steps off the northeast coast of South America, July 1983. *Deep-Sea Research*, **34**, (3), 337-364.

Gregg, M. C., 1987. Diapycnal Mixing in the Thermocline: A Review. *Journal of Geophysical Research*, **92**(C5), 5249-5286.

Gregg, M. C., and T. Sanford, 1987. Shear and turbulence in a thermohaline staircase. *Deep-Sea Research*, **34**(10), 1689-1696.

Holyer, J. Y., T. J. Jones, M. G. Priestly, and N. J. Williams, 1987. The effect of vertical temperature and salinity gradients on double-diffusive interleaving. *Deep-Sea Research*, **34**, 517-530.

Holloway, G., and A. Gargett, 1987. The inference of salt fingering from towed microstructure observations. *Journal of Geophysical Research*, **11**, 1963-1965.

Howard, L. N., and G. Veronis, 1987. The salt finger zone. *Journal of Fluid Mechanics*, **183**, 1-24.

Kelley, D. E., 1987. Interface migration in thermohaline staircases. *Journal of Physical Oceanography*, **17**, 1633-1639.

Kelly, D. 1987. The influence of planetary rotation on oceanic double-diffusive system. *Journal Marine Research*, **45**, 829-841.

Kunze, E., A. J. Williams III, and R. W. Schmitt, 1987. Optical microstructure in the thermohaline staircase east of Barbados. *Deep-Sea Research*, **34**(10), 1697-1704.

Kunze E., 1987. Limits on growing, finite length salt fingers: a Richardson number constraint. *Journal of Marine Research*, **45**, 533-556.

Lueck, R., 1987. Microstructure measurements in a thermohaline staircase. *Deep-Sea Research*, **34**(10), 1677-1688.

Marmorino, G. O., W. K. Brown, and W. D Morris, 1987. Two-dimensional temperature structure in the C-SALT thermohaline staircase. *Deep-Sea Research*, **23**, (10), 1667-1675.

Marmorino, G. O. 1987. Observations of small-scale mixing processes in the seasonal thermocline. Part I: Salt fingering. *Journal of Physical Oceanography*, **17**, 1339-1347.

McDougall, T. J. and A. B. Giles 1987. Migration of intrusions across isopycnals, with examples from the Tasman Sea. *Deep-Sea Research*, **34**, 1851-1866.

McDougall, T. J. 1987. Neutral surfaces. *Journal of Physical Oceanography*, **17**, 1950–1964.

McDougall, T. J. 1987. Thermobaricity, cabbeling, and water-mass conversion. *Journal of Geophysical Research*, **92**, 5448–5464.

Neilson, D. G., and F. P. Incropera, 1987. Double-diffusive flow and heat transfer for a cylinderical source submerged in a salt-stratified solution. *Int. J. Heat Mass Trans.*, **30**, 2559–2570.

Ochoa, J. 1987. Two limiting types of oceanic finestructure. *Journal of Physical Oceanography*, **17**, 1539–1545.

Padman, L., and T. M. Dillon, 1987. Vertical fluxes through the Beaufort sea thermohaline staircase. *Journal of Geophysical Research*, **92**, 10799–10806.

Schmitt, R. W., 1987. The Caribbean Sheets And Layers Transects (C-SALT) Program. *EOS, Transactions of the American Geophysical Union*, **68**(5), 57–60.

Schmitt, R. W., H. Perkins, J. D. Boyd, and M. C. Stalcup, 1987. C-SALT: an investigation of the thermohaline staircase in the western tropical North Atlantic. *Deep-Sea Research*, **34**, (10), 1697–1704.

Veronis, G., 1987. The role of the buoyancy layer in determining the structure of salt fingers. *Journal of Fluid Mechanics*, **180**, 327–342.

Washburn, L., and R. H. Käse, 1987. Double diffusion and the distribution of the density ratio in the Mediterranean water from southeast of the Azores. *Journal of Physical Oceanography*, **17**, 12–25.

Yanase, S. and N. Gotoh, 1987. Super-critical state of double-diffusive convection under time-periodic heating. *Journal of the Physical Society of Japan*, **56**, 2387–2395.

Yoshida, J., H. Nagashima, and Wen-Ju Ma, 1987. A double-diffusive lock-exchange flow with small density difference. *Fluid Dynamics Research*, **2**, 205–215.

1988

Bauer, E., and G. Siedler, 1988. The relative contributions of advection and isopycnal and diapycnal mixing below the subtropical salinity maximum, *Deep-Sea Research*, **35**, 811–837.

Bergman, T. L., and A. Ungan, 1988. A note on lateral heating in a double-diffusive system. *Journal of Fluid Mechanics*, **194**, 175–186.

Chen, F., and C. F. Chen, 1988. Onset of finger convection in a porous layer underlying a fluid layer. *Trans. ASMEC C: Journal of Heat Transfer*, **110**, 403–409.

Federov, K. N., 1988. Layer thicknesses and effective diffusivities in "diffusive" thermohaline convection in the ocean. In: *Small-Scale Turbulence and Mixing in the Ocean*, J. Nihoul and B. Jamart, editors, Elsevier Oceanography Series, 46, Elsevier, New York, pp. 471–480.

Gargett, A. E., 1988. The scaling of turbulence in the presence of stable stratification. *Journal of Geophysical Research*, **93**, 5021–5036.

Gregg, M. C., 1988. Mixing in the thermohaline staircase east of Barbados. In: *Small-Scale Turbulence and Mixing in the Ocean*, J. Nihoul and B. Jamart, editors, Elsevier Oceanography Series, 46, Elsevier, New York, pp. 453–470.

Hebert, D., 1988. Estimates of salt-finger fluxes. *Deep-Sea Research*, **35**, 1887–1901.

Hebert, D., 1988. A Mediterranean Salt Lens, Ph.D. Thesis, Dalhousie University, Halifax, N. S.

Kelley, D. E., 1988. Explaining effective diffusivities within diffusive staircases. In: *Small-Scale Turbulence and Mixing in the Ocean*, J. Nihoul and B. Jamart, editors, Elsevier Oceanography Series, 46, Elsevier, New York, pp. 481–502.

Ledwell, J. R. and A. J. Watson, 1988. The use of deliberately injected tracers for the study of diapycnal mixing in the ocean. In: *Small-Scale Turbulence and Mixing in the Ocean*, J. Nihoul and B. Jamart, editors, Elsevier Oceanography Series, 46, Elsevier, New York, pp. 11–20.

McDougall, T. J., 1988. Some implications of ocean mixing for ocean modelling. In: *Small-Scale Turbulence and Mixing in the Ocean*, J. Nihoul and B. Jamart, editors, Elsevier Oceanography Series, 46, Elsevier, New York, pp. 21–36.

Oakey, N. S., 1988. Estimates of mixing inferred from temperature and velocity microstructure. In: *Small-Scale Turbulence and Mixing in the Ocean*, J. Nihoul and B. Jamart, editors, Elsevier Oceanography Series, 46, Elsevier, New York, pp. 239–248.

Osborn, T. R., 1988. Signatures of doubly diffusive convection and turbulence in an intrusive regime. *Journal of Physical Oceanography*, 18(1), 146–155.

Padman, L., and T. J. Dillon, 1988. On the horizontal extent of the Canada Basin thermohaline steps. *Journal of Physical Oceanography*, 18, 1458–1462.

Piacsek, S. A., N. H. Brummell, and B. E. McDonald, 1988. Numerical experiments on thermohaline convective motions across interfaces of intrusions. In: *Small-Scale Turbulence and Mixing in the Ocean*, J. Nihoul and B. Jamart, editors, Elsevier Oceanography Series, 46, Elsevier, New York, pp. 503–516.

Ruddick, B., and D. Hebert, 1988. The mixing of Meddy "Sharon." In: *Small-Scale Turbulence and Mixing in the Ocean*, J. Nihoul and B. Jamart, editors, Elsevier Oceanography Series, 46, Elsevier, New York, pp. 249–262.

Schmitt, R. W., 1988. Mixing in a thermohaline staircase. In: *Small-Scale Turbulence and Mixing in the Ocean*, J. Nihoul and B. Jamart, editors, Elsevier Oceanography Series, 46, Elsevier, New York, pp. 435–452.

SCOR Working Group 69, 1988. Small-scale turbulence and mixing in the ocean: A glossary. In: *Small-Scale Turbulence and Mixing in the Ocean*, C. J. Nihoul and B. M. Jamart, editors, Elsevier Oceanography Series, 46, Elsevier, New York, pp. 3–10, Elsevier.

Tanny, J., and A. B. Tsinober, 1988. The dynamics and structure of double-diffusive layers in sidewall-heating experiments. *Journal of Fluid Mechanics*, 196, 135–156.

Taylor, J., 1988. The fluxes across a diffusive interface at low values of the density ratio. *Deep-Sea Research*, **35**, 555–567.

Yanase, S., 1988. Chaos in double-diffusive convections. *J. Japan Soc. Fluid Mech.*, 7, 3–14.

1989

Boyd, J. D. 1989. Properties of thermal staircase off the northeast coast of South America, Spring and Fall 1985. *Journal of Geophysical Research*, **94**, 8303–8312.

Churchill, J. H., P. C. Cornillon, and P. Hamilton, 1989. Velocity and hydrographic structure of subsurface shelf waters at the Gulf Stream's edge. *Journal of Geophysical Research*, **94**(C8), 10,791–10,800.

Dean, A. E., E. Knobloch, and J. Toomre, 1989. Traveling waves and chaos in thermosolution convection. *Physics Review A*, **36**(6), 2862–2869.

Deane, A. E., E. Knobloch, and J. Toomre, 1989. Traveling waves in large-aspect-ratio thermosolutal convection. *Physics Review A*, **37** (5), 1817–1820.

Gargett, A. E., 1989. Ocean Turbulence. *Ann. Rev. Fluid Mech.*, **21**, 419–451.

Gregg, M. C., 1989. Scaling turbulent dissipation in the thermocline. *Journal of Geophysical Research*, **94**, (C7), 9686–9698.

Hamilton, J. M., M. R. Lewis, and B. R. Ruddick, 1989. Vertical fluxes of nitrate associated with salt fingers in the world's oceans. *Journal of Geophysical Research*, **94**(C2), 2137–2145.

Hosoyamada, T., and H. Honji, 1989. A thermohaline-diffusion tank with a movable plate. *Experiments in Fluids*, **7**, 208–210.

Hyun, J. M., and H. S. Kwak, 1989. Flow of a double-diffusive stratified fluid in a differentially-rotating cylinder. *Geophysical and Astrophysical Fluid Dynamics*, **46**, 203–220.

Käse, R. H., A. Beckmann, and H.-H. Hinrichsen, 1989. Observational evidence of salt lens formation in the Iberian Basin. *Journal of Geophysical Research*, **94**(C4), 4905–4912.

Kazmierczak, M., and D. Poulikakos, 1989. Transient double-diffusive experiments in a horizontal fluid layer extending over a bed of spheres. *Phys. Fluids*, **A1**, 480–489.

Leibovich, S., S. K. Lele, and I. M. Moroz, 1989. Nonlinear dynamics in Langmuir circulations and in thermosolutal convection. *Journal of Fluid Mechanics*, **198**, 471–511.

Mack, S. A., 1989. Towed chain measurement of ocean microstructure. *Journal of Physical Oceanography*, **19**(8), 1108–1129.

Marmorino, G.O., 1989. Substructure of oceanic salt finger interfaces. *Journal of Geophysical Research*, **94**(C4), 4891–4904.

Murray, B. T., and C. F. Chen, 1989. Double-diffusive convection in a porous medium. *Journal of Fluid Mechanics*, **201**, 147–166.

Padman, L., and T. M. Dillon, 1989. Thermal microstructure and internal waves in the Canada Basin diffusive staircase. *Deep-Sea Research*, **36**, 531–542.

Pearlstein, A. J., R. M. Harris, and G. Terrones, 1989. The onset of convective instability in a triply diffusive fluid layer. *Journal of Fluid Mechanics*, **202**, 443–465.

Ruddick, B. R., R. W. Griffiths, and G. Symonds, 1989. Frictional stress at a sheared double-diffusive interface. *Journal of Geophysical Research*, **94**, 18,161–18,173.

Ruddick, B., and L. Zhang, 1989. The mythical thermohaline oscillator? *Journal of Marine Research*, **47**(4), 717–746.

Schmitt, R. W., K. L. Polzin, and J. M. Toole, 1989. Shear and Salt Fingers. Proceedings: Hawaiian winter workshop on Parameterization of small scale Processes. University of Hawaii, January 17–20, 1989. pp. 127–144.

Shen, C. Y., 1989. The evolution the double-diffusive instability: salt fingers. *Physics of Fluids*, **A1**(5), 829–844.

Taylor, J., and P. Bucens, 1989. Laboratory experiments on the structure of salt fingers. *Deep-Sea Research*, **36**(11), 1675–1704.

Welander, P., 1989. A new type of double-diffusive instability. *Tellus*, **41A**, 66–72.

Whitfield, D.W.A., G. Holloway, and J. Y. Holyer, 1989. Spectral transform simulations of finite amplitude double-diffusive instabilities in two dimensions, *Journal of Marine Research*, **47**, 241–265.

Yoshida, J., H. Nagashima, and H. Niino, 1989. The behavior of double-diffusive intrusion in a rotating system. *Journal of Geophysical Research*, **94**(C4), 4923–4938.

1990

Clarke, R. A., S. H. Swift, J. L. Reid, and K. P. Koltermann, 1990. The formation of Greenland Sea Deep Water: Double-diffusion or deep convection? *Deep-Sea Research*, **37**(9A), 1385–1424.

Federiuk, J. M., and R. W. Schmitt, 1990. Advection and diffusion estimates in a thermohaline staircase region. *Deep-Sea Research*, submitted.

Fleury, M., and R. G. Lueck, 1990. Fluxes across a thermohaline staircase. *Deep-Sea Research*, submitted.

Gosink, J. P., and G. C. Baker, 1990. Salt fingering in subsea permafrost: Some stability and and energy considerations. *Journal of Geophysical Research*, **95**(C6), 9575–9584.

Kelley, D. E., 1990. Fluxes through diffusive staircases: A new formulation. *Journal of Geophysical Research*, **95**, 3365–3371.

Lillibridge, J. L., G. Hitchcock, T. Rossby, E. Lessard, M. Mark, and L. Golmer, 1990. Entrainment of mixing of shelf/slope waters in the near-surface Gulf Stream. *Journal of Geophysical Research*, **95**(C8), 13,065–13,087.

Marmorino, G. O., 1990. "Turbulent mixing" in a salt-finger staircase. *Journal of Geophysical Research*, **95**, 12,983–12,994.

McDougall, T. J., and Y. You, 1990. Implications of the nonlinear Equation of State for upwelling in the ocean interior. *Journal of Geophysical Research*, **95**(C8), 13,263–13,276.

Muench, R. D., H.J.S. Fernando, and G. R. Stegan, 1990. Temperature and salinity staircases in the northwestern Weddell Sea. *Journal of Physical Oceanography*, **20**, 295–306.

Schmitt, R. W. 1990. On the density ratio balance in the Central Water. *Journal of Physical Oceanography*, **20**(6), 900–906.

Taylor, J., 1990. Laboratory experiments on the formation of salt fingers after the decay of turbulence. *Journal of Geophysical Research*, in press.

You, Y., and T. J. McDougall, 1990. Neutral surfaces and potential vorticity in the world's oceans. *Journal of Geophysical Research*, **95**(C8), 13,235–13,261.

1991

Lee, J. H., and G. Veronis, 1991. On the difference between tracer and geostrophic velocities obtained from C-SALT data. *Deep-Sea Research*, **38**(5A), 555–568.

McDougall, T. J., 1991. Interfacial advection in the thermohaline staircase east of Barbados. *Deep-Sea Research*, **38**(3), 357–370.

DOCUMENT LIBRARY

March 11, 1991

Distribution List for Technical Report Exchange

Attn: Stella Sanchez-Wade
Documents Section
Scripps Institution of Oceanography
Library, Mail Code C-075C
La Jolla, CA 92093

Hancock Library of Biology &
  Oceanography
Alan Hancock Laboratory
University of Southern California
University Park
Los Angeles, CA 90089-0371

Gifts & Exchanges
Library
Bedford Institute of Oceanography
P.O. Box 1006
Dartmouth, NS, B2Y 4A2, CANADA

Office of the International
  Ice Patrol
c/o Coast Guard R & D Center
Avery Point
Groton, CT 06340

NOAA/EDIS Miami Library Center
4301 Rickenbacker Causeway
Miami, FL 33149

Library
Skidaway Institute of Oceanography
P.O. Box 13687
Savannah, GA 31416

Institute of Geophysics
University of Hawaii
Library Room 252
2525 Correa Road
Honolulu, HI 96822

Marine Resources Information Center
Building E38-320
MIT
Cambridge, MA 02139

Library
Lamont-Doherty Geological
  Observatory
Colombia University
Palisades, NY 10964

Library
Serials Department
Oregon State University
Corvallis, OR 97331-5503

Pell Marine Science Library
University of Rhode Island
Narragansett Bay Campus
Narragansett, RI 02882

Working Collection
Texas A&M University
Dept. of Oceanography
College Station, TX 77843

Library
Virginia Institute of Marine Science
Gloucester Point, VA 23062

Fisheries-Oceanography Library
151 Oceanography Teaching Bldg.
University of Washington
Seattle, WA 98195

Library
R.S.M.A.S.
University of Miami
4600 Rickenbacker Causeway
Miami, FL 33149

Maury Oceanographic Library
Naval Oceanographic Office
Stennis Space Center
NSTL, MS 39522-5001

Marine Sciences Collection
Mayaguez Campus Library
University of Puerto Rico
Mayagues, Puerto Rico 00708

Library
Institute of Oceanographic Sciences
Deacon Laboratory
Wormley, Godalming
Surrey GU8 5UB
UNITED KINGDOM

The Librarian
CSIRO Marine Laboratories
G.P.O. Box 1538
Hobart, Tasmania
AUSTRALIA 7001

Library
Proudman Oceanographic Laboratory
Bidston Observatory
Birkenhead
Merseyside L43 7 RA
UNITED KINGDOM

Mac 90-32

50272-101

REPORT DOCUMENTATION PAGE	1. REPORT NO. WHOI-91-20	2.	3. Recipient's Accession No.

4. Title and Subtitle	5. Report Date
Double Diffusion in Oceanography: Proceedings of a Meeting September 26-29, 1989	July 1991
	6.

7. Author(s) Raymond W. Schmitt	8. Performing Organization Rept. No. WHOI-91-20

9. Performing Organization Name and Address	10. Project/Task/Work Unit No.
Woods Hole Oceanographic Institution Woods Hole, Massachusetts 02543	11. Contract(C) or Grant(G) No. (C) OCE 88-13060 (G)

12. Sponsoring Organization Name and Address	13. Type of Report & Period Covered
National Science Foundation	Technical Report
	14.

15. Supplementary Notes

This report should be cited as: Woods Hole Oceanog. Inst. Tech. Rept., WHOI-91-20.

16. Abstract (Limit: 200 words)

A meeting to review research progress on double-diffusive phenomena in the ocean was held September 26-29, 1989, at the Woods Hole Oceanographic Institution. Twenty-five oral presentations were made and a number of discussion sessions were held. This report contains manuscripts provided by meeting participants, summaries of the discussion sessions and an extensive bibliography on oceanic double-diffusion. Since double-diffusive processes appear to play an important role in ocean mixing, further research in this field should have high priority. It is hoped that this update on the status of our current understanding will facilitate planning of additional research.

17. Document Analysis a. Descriptors

mixing
double-diffusion
salt-fingers

b. Identifiers/Open-Ended Terms

c. COSATI Field/Group

18. Availability Statement	19. Security Class (This Report)	21. No. of Pages 259
Approved for public release; distribution unlimited.	20. Security Class (This Page)	22. Price

(See ANSI-Z39.18)　　　　　See Instructions on Reverse　　　　　OPTIONAL FORM 272 (4-77)
(Formerly NTIS-35)
Department of Commerce